

# **GRAVITY WAVE DAMPING BY STRATIFIED POROUS STRUCTURES**

Thesis

submitted in partial fulfillment of the requirements for the degree of

**DOCTOR OF PHILOSOPHY**

by

**V. VENKATESWARLU**  
(165065 AM16F13)

Under the guidance of

**Dr. DEBABRATA KARMAKAR**  
Assistant Professor



**DEPARTMENT OF WATER RESOURCES AND OCEAN ENGINEERING  
NATIONAL INSTITUTE OF TECHNOLOGY KARNATAKA  
SURATHKAL, MANGALORE - 575 025, INDIA**

**AUGUST, 2020**



## DECLARATION

I hereby declare that the Ph.D. Thesis entitled “**GRAVITY WAVE DAMPING BY STRATIFIED POROUS STRUCTURES**” which is being submitted to **National Institute of Technology Karnataka, Surathkal**, for the partial fulfillment of the requirement for the award of degree of **Doctor of Philosophy** in the **Department of Water Resources and Ocean Engineering**, is a bonafide report of the work carried out by me. The material contained in this Ph.D. Thesis has not been submitted to any university or Institution for the award of any degree.

.....  
**V. VENKATESWARLU (165065 AM16F13)**  
Department of Applied Mechanics and Hydraulics  
National Institute of Technology Karnataka, Surathkal

Place: NITK, SURATHKAL.

Date: 19<sup>th</sup> AUGUST 2020



## **CERTIFICATE**

This is to certify that the Ph.D. Thesis entitled “**GRAVITY WAVE DAMPING BY STRATIFIED POROUS STRUCTURES**” submitted by **V. VENKATESWARLU (165065 AM16F13)**, as the record of the work carried out by him, is accepted as the Ph.D. Thesis submission in partial fulfillment of the requirements for the award of the degree of **Doctor of Philosophy** in the **Department of Water Resources and Ocean Engineering, National Institute of Technology Karnataka, Surathkal**, is a bonafide work carried out by him under my supervision and guidance.

.....  
**Dr. DEBABRATA KARMAKAR**

Assistant Professor

Department of Applied Mechanics and Hydraulics  
National Institute of Technology Karnataka, Surathkal

.....  
**Chairman - DRPC**

Department of Applied Mechanics and Hydraulics  
National Institute of Technology Karnataka, Surathkal



## ACKNOWLEDGEMENT

I take this opportunity to express my sincere gratitude and profound thanks to my guide **Dr. D. Karmakar**, Assistant Professor, Department of Water Resources and Ocean Engineering, National Institute of Technology Karnataka, Surathkal for his advice, expert guidance, constant encouragement and reference material provided throughout my research work.

I acknowledge my sincere thanks to **Prof. Arkal Vittal Hegde**, **Dr. K. Subrahmanya** and **Dr. Manu** Department of Water Resources and Ocean Engineering, and **Dr. Bibhuti Bhusan Das**, Department of Civil Engineering for being the members of Research Progress Assessment Committee (RPAC) and giving valuable suggestions and encouragement at various stages of this work.

I would like to express my sincere gratitude towards **Prof. G.S Dwarakish** and **Prof. Amai Mahesha**, former Heads of the Department of Water Resources and Ocean Engineering and **Prof. Amba Shetty**, Head of the Department of Water Resources and Ocean Engineering, NITK Surathkal for providing necessary facilities and sincere co-operation throughout my stay at the NITK campus. I also extend my heartfelt gratitude to all the faculty members of the Department of Water Resources and Ocean Engineering, and also Department of Civil Engineering, NITK Surathkal.

My special thanks to Mr. Balakrishna, Mr. B. Jagadish, Asst. Executive Engineer (Rtd.) and Mr. Seetharam, Department of Water Resources and Ocean Engineering for their help in all the departmental works. I would also like to thank all the non-teaching staff of the Department of Water Resources and Ocean Engineering, National Institute of Technology Karnataka, Surathkal for their co-operation and help during the project work.

I thank Mr. Praveen K.M. for his valuable contribution in the preparation of my thesis. The informal support and encouragement of many friends has been indispensable. I also acknowledge the good company and help received from the research scholar of NITK, Surathkal.

I express my heartfelt gratitude to the authors of research articles which have been refereed in preparing this thesis. I also express my gratitude to the reviewers of my research articles for their invaluable suggestions in improving this work.

I am very much grateful to my father Sri. Valliboina Hazarathaiah and mother Smt. Valliboina Hazarathamma who provided me the best education and encouraged me in all my endeavors. Above all, I thank Lord, the almighty for his grace throughout the research work.

**V. VENKATESWARLU (AM16F13)**

Department of Applied Mechanics and Hydraulics  
National Institute of Technology Karnataka, Surathkal



## ABSTRACT

In the present study, wave transformation due to multiple porous structures in the presence and absence of vertical rigid wall, barrier-rock breakwaters of various configurations, multiple horizontally stratified porous absorbers, vertically stratified porous structure lying on flat seabed, elevated seabed and stepped seabed is analysed under the oblique wave incidence. The eigenfunction expansion method using the continuity of pressure and velocity along with mode-coupling relation is adopted based on linearized wave theory. The direct analytical relations are derived for finding the wave reflection and transmission coefficients due to porous breakwaters of various structural configurations. In the preliminary stage, the analytical results are validated with numerical and physical model results available in the literature. As a special case, a comparative study is performed between the vertical rigid wall, permeable wall and stepped wall away from the double horizontally stratified wave absorbers. The vertical and stepped wall shows almost similar values of wave reflection at each of the resonating crests, but minimal values of the resonating trough in wave reflection is obtained from the stepped wall.

A comparative study is performed between single and multiple porous structures of fixed structural width and depth. The 42% reduction in wave transmission is achieved with double porous structures as compared with single porous structure for uniform structural width, which may be due to wave damping in the free spacing available between the two structures. The distribution of incident wave energy in the form of wave reflection and transmission is effective in the case of horizontally stratified porous structure as compared with other structures. The vertically stratified porous structures performance is partially dependent upon structural width. Higher structural width effectively reduces the wave transmission as compared with conventional porous structures. The effect of each layer porosity, friction factor, structural width, incident wavelength, number of structures, angle of incidence, free spacing and trapping chamber effect on wave reflection, transmission damping, fluid force on seaward/leeward sides of breakwater and force on vertical wall is analysed for various types of porous structures. The critical angle due to standing waves, fluid resonance in the free spacing and clapotis has an efficient role in the design of porous structures.

*Keywords: Multi-layered porous structure; stratification, wave reflection; energy dissipation; friction factor; step-type seabed.*



## NOMENCLATURE

$A_m$	added mass coefficient
$a_j$	depth of each porous and rigid layers
$b_N$	positions of the energy absorbing structure
$C_f$	turbulent resistant coefficient
$d_j$	width of each energy absorbing structure
$d$	cumulative structural width
$d_{s(l)}$	width of seaside(leeside) vertical thin wall
$f_j$	linearized friction factor in each of the porous layer
$f_{jn}$	vertical eigenfunction in each of the region
$f_{s(l)}$	friction factor due to of seaside(leeside) vertical thin wall
$g$	acceleration due to gravity
$G$	porous effect parameter
$h_j$	water depth in each region
$I_{10}$	incident wave amplitude
$i$	imaginary number
$K_d$	energy dissipation
$K_{fb}$	wave force on leeside of the porous structure
$K_{fs}$	wave force on seaside of the porous structure
$K_{fw}$	wave force on vertical rigid wall
$K_{ip}$	intrinsic permeability
$K_r$	reflection coefficient
$K_t$	transmission coefficient
$k_{jn}$	wave number in the x-direction
$l$	wave number in z-direction
$L$	spacing between the porous structure and rigid wall
$M$	truncated number
$N$	number of energy absorbing structures
$q$	instantaneous Eulerian velocity vector at any point
$R_{10}$	complex amplitude of reflected wave
$s_j$	inertial force in each of the porous layer

$S_{s(l)}$	inertia coefficient due to of seaside(leeside) vertical thin wall
$T_{30}$	complex amplitude of transmitted wave
$t$	time
$T$	wave period
$V$	volume of the structure
$w$	spacing between the periodic porous structures
$\zeta_j$	free surface wave elevation
$\rho$	density of water
$\omega$	wave frequency
$\lambda$	wavelength
$\phi$	velocity potential
$\delta_{mn}$	Kronecker delta
$\theta$	angle of contact
$\gamma_{jn}$	wave number in y-direction
$\varepsilon_j$	porosity in each of the porous layer
$\varepsilon_{s(l)}$	porosity of seaside(leeside) vertical thin wall
$\nu$	kinematic viscosity

## **ABBREVIATIONS**

BVP	-	Boundary Value Problem
KFSBC	-	Kinematic Free Surface Boundary Condition
DFSBC	-	Dynamic Free Surface Boundary Condition
FEM	-	Finite Element Method
FDM	-	Finite Difference Method
BEM	-	Boundary Element Method
VLFS	-	Very Large Floating Structures



## LIST OF FIGURES & TABLES

Figure 1.1	Porous structures are protecting the island and coasts from high wave attack at (a) Mangalore, India and (b) Dongying city, China.	4
Figure 1.2	Schematic diagram for wave propagation.	24
Figure 1.3	Wave motion through barrier-rock porous structure	29
Figure 1.4	Wave motion through horizontally stratified porous structure	29
Figure 2.1	Schematic diagram of multiple porous structures with (a) leeward unbounded region and (b) leeward wall/leeward confined region.	39
Figure 2.2	Comparative study on (a) $K_d$ due to three layered structure compared (Twu and Chieu, 2000) and (b) the $K_r$ due to the porous structure with back wall (Mallayachari and Sundar, 1994).	48
Figure 2.3	Variation in (a) $K_r$ (b) $K_t$ and (c) $K_d$ versus $\gamma_{10}d$ for different values of porosity considering $\theta = 0^0$ and $f = 1$ .	49
Figure 2.4	Variation in (a) $K_r$ (b) $K_t$ and (c) $K_d$ versus $\gamma_{10}d$ for different values of porosity of the structure considering $\theta = 0^0$ , $w/h = 1$ and $f = 1$ .	50
Figure 2.5	Variation in (a) $K_r$ (b) $K_t$ and (c) $K_d$ versus $\gamma_{10}d$ for different values of friction factor considering $\theta = 0^0$ and $\varepsilon = 0.4$ .	52
Figure 2.6	Variation in (a) $K_r$ (b) $K_t$ and (c) $K_d$ versus $\gamma_{10}d$ for different values of friction factor considering $w/h = 1$ , $\theta = 0^0$ and $\varepsilon = 0.4$ .	53
Figure 2.7	Variation in (a) $K_r$ and (b) $K_t$ versus $\theta$ for different values of $\gamma_{10}h$ for triple porous structure considering $d/h = 2$ , $w/h = 0.5$ and $f = 2$ .	54
Figure 2.8	Variation in (a) $K_r$ , (b) $K_t$ and (c) $K_d$ versus $\gamma_{10}h$ with variation in $w/h$ considering $d/h = 0.25$ , $\theta = 0^0$ , $f = 0.25$ and $\varepsilon = 0.4$ .	55

Figure 2.9	Variation in $K_r$ and $K_t$ versus $w/h$ with variation in porosity for four porous structures considering $d/h=1$ , $f=0.5$ , (a) $\gamma_{10}h=0.5$ and (b) $\gamma_{10}h=1$ .	56
Figure 2.10	Variation in (a) $K_r$ and (b) $K_t$ versus $\theta$ with increase in the number of porous structures for $f=1$ , $\varepsilon=0.4$ , $\gamma_{10}h=1$ , $w/h=1$ and $d/h=2$ .	57
Figure 2.11	Variation in $K_{fw}$ versus $L/h$ for (a) single (b) double (c) triple and (d) four porous structures considering $\gamma_{10}h=1$ , $f=1$ , $\theta=0^0$ , $d/h=1$ and $w/h=1$ .	59
Figure 2.12	Variation in $K_{fw}$ versus $\theta$ with increase in the number of porous structures for $\gamma_{10}h=0.75$ , $f=1$ , $w/h=1$ , $d/h=3$ , $L/h=1$ , $\varepsilon=0.3$ and (b) $\varepsilon=0.6$ .	60
Figure 2.13	Variation in (a) $K_r$ and (b) $K_t$ versus $\gamma_{10}w$ for various values of porosities considering four porous blocks kept on multi-step rigid bottom for $\gamma_{10}h_1=2$ , $\theta=0^0$ and $f=2$ .	61
Figure 2.14	Variation in $K_r$ versus $d/h_1$ due to double porous blocks for (a) different step heights (b) dimensionless wave length considering $\theta=0^0$ , $w/h_1=1$ and $L/h_1=1$ .	62
Figure 2.15	Variation in $K_r$ and $K_t$ versus $\theta$ for different values of $d/h_1$ for $\gamma_{10}h_1=0.5$ , $h_2/h_1=0.9$ , $w/h_1=1$ , $f=0.5$ , $d_1=d_2=d/2$ with (a) $\varepsilon=0.4$ and (b) $\varepsilon=0.8$ .	64
Figure 2.16	Variation in $K_r$ versus $d/h_1$ due to triple porous blocks placed on one-step seabed considering $w/h_1=1$ , $\gamma_{10}h_1=2$ , $L/h_1=1$ , (a) $\varepsilon=0.4$ , $f=0.5$ and (b) $\varepsilon=0.7$ , $f=2$ .	64
Figure 2.17	Comparative study between the multiple structures in (a) $K_r$ and (b) $K_{fw}$ versus $L/h_1$ with $\gamma_{10}h_1=0.5$ , $\varepsilon=0.4$ , $f=0.5$ , $\theta=0^0$ , $d/h_1=2$ , $w/h_1=1$ and $h_2/h_1=0.8$ .	65
Figure 3.1	Schematic diagram for (a) barrier-rock porous structure of finite thickness (b) structure away from rigid wall (c) structure backed by rigid wall and (d) structure of semi-infinite thickness placed on step-bottom.	71



Figure 3.2	Comparative study with (a) Dalrymple et al. (1991) (b) Liu and Li (2013) (c) Mallayachari and Sundar (1994) and (d) Zhu and Chwang (2001) for several structural configurations	84
Figure 3.3	Variation of (a) $K_r$ (b) $K_t$ and $K_d$ versus $d/h_1$ for various values of structural porosity considering $\gamma_{10}h_1 = 0.5$ and $\theta = 15^\circ$ .	84
Figure 3.4	Variation of (a) $K_r$ (b) $K_t$ and $K_d$ versus $d/h_1$ for various values of friction factor considering $\gamma_{10}h_1 = 0.5$ and $\theta = 15^\circ$ .	85
Figure 3.5	Variation of (a) $K_r$ (b) $K_t$ and $K_d$ versus $\theta$ for various values of $\gamma_{10}h_1$ considering $h_2/h_1 = 0.8$ and $d/h_1 = 2$ .	86
Figure 3.6	Variation of $K_r$ , $K_t$ and $K_d$ versus $d/h_1$ for seaward barrier porosity (a) $\varepsilon_1 = 0.3$ and (b) $\varepsilon_1 = 0.6$ considering $\gamma_{10}h_1 = 0.5$ and $\theta = 15^\circ$ .	86
Figure 3.7	Variation of (a) $K_r$ (b) $K_{fw}$ (c) $K_{fs}$ and (d) $K_{fb}$ versus $d/h_1$ for various values of trapping chamber length $L/h_1$ considering $\gamma_{10}h_1 = 1$ and $\theta = 15^\circ$ .	87
Figure 3.8	Variation of (a) $K_r$ (b) $K_{fw}$ (c) $K_{fs}$ and (d) $K_{fb}$ versus $L/h_1$ for various values of porosity $\varepsilon_b$ considering $\gamma_{10}h_1 = 1$ and $\theta = 15^\circ$ .	89
Figure 3.9	Variation of $K_r$ versus $d/h_1$ for various values of (a) porosity $\varepsilon_b$ (b) friction factor $f_b$ (c) angle of incidence $\theta$ and (d) dimensionless wave number $\gamma_{10}h_1$ considering $\varepsilon_1 = 0.3$ and $f_1 = 2$ .	90
Figure 3.10	Variation of $K_r$ versus angle of incidence $\theta$ for various values of (a) porosity $\varepsilon_b$ (b) friction factor $f_b$ considering $h_2/h_1 = 0.8$ and $\gamma_{10}h_1 = 0.5$ .	92
Figure 3.11	Variation of $K_r$ versus angle of incidence $\theta$ for various values of structural porosity $\varepsilon_b$ considering $f_b = 1$ and $\gamma_{10}h_1 = 0.5$ for (a) full solution and (b) long-wave approximation.	92

Figure 3.12	(a) Variation of skin depth versus angle of incidence, (b) comparative study of four types of barrier-rock porous structures.	93
Figure 4.1	Schematic diagram for multiple fully-extended energy absorbing structures.	99
Figure 4.2	(a) Convergence in wave transformation for multiple structures for different evanescent wave modes and (b) validation of present study results with Liu and Li (2013) for long-wave approximation and full solution.	112
Figure 4.3	Variation of (a) $K_r$ , (b) $K_t$ and $K_d$ versus $d/h_1$ due to single structure for variable $a_1/h_2$ and $a_2/h_2$ composed of double porous layers considering $h_1/\lambda = 0.1$ and $\theta = 20^\circ$ .	114
Figure 4.4	Variation of (a) $K_r$ , (b) $K_t$ and $K_d$ versus $d/h_1$ due to single structure for variable $\varepsilon_1$ and $f_1$ composed of double porous layers considering $h_1/\lambda = 0.1$ and $\theta = 20^\circ$ .	114
Figure 4.5	Variation of $K_r$ and $K_t$ versus $\theta$ due to two structures for variable $\varepsilon_1$ and $f_1$ composed of double porous layers for $h_1/\lambda = 0.1$ , $w/h_1 = 5$ , considering (a) $d/h_1 = 1$ and (b) $d/h_1 = 2$ .	115
Figure 4.6	Variation of $K_r$ and $K_t$ versus $w/h_1$ due to two structures for variable $a_1/h_1$ composed of double porous layers considering $h_1/\lambda = 0.1$ (a) $\theta = 0^\circ$ and (b) $\theta = 30^\circ$ .	116
Figure 4.7	Variation of (a) $K_r$ , (b) $K_t$ and $K_d$ versus $w/h_1$ due to two structures for variable $a_1/h_1$ composed of double porous layers considering $h_1/\lambda = 0.2$ and $d/h_1 = 2$ .	118
Figure 4.8	Variation of (a) $K_r$ , (b) $K_t$ and $K_d$ versus $w/h_1$ due to three structures for variable $\varepsilon_1$ and $f_1$ composed of double porous layers considering $h_1/\lambda = 0.2$ and $\theta = 30^\circ$ .	119
Figure 4.9	Variation of (a) $K_r$ and (b) $K_t$ versus $w/h_1$ due to four structures for variable $a_1/h_2$ composed of double porous layers considering $h_1/\lambda = 0.1$ and $\theta = 20^\circ$ .	120

Figure 4.10	Variation of (a) $K_r$ , (b) $K_t$ and $K_d$ due to single and multiple structures composed of double porous layers considering $h_1/\lambda=0.1$ and $\theta=15^\circ$ .	121
Figure 4.11	Variation of (a) $K_r$ , (b) $K_t$ and $K_d$ versus $d/h_1$ due to single structure for variable $a_3/h_1$ composed of triple porous layers considering $h_1/\lambda=0.1$ and $\theta=20^\circ$ .	123
Figure 4.12	Variation of (a) $K_r$ and (b) $K_t$ versus $\theta$ due to single structure for variable $a_1/h_2$ and $a_2/h_2$ composed of triple porous layers considering $h_1/\lambda=0.1$ and $d/h_1=4$ .	124
Figure 4.13	Variation of (a) $K_r$ , (b) $K_t$ and $K_d$ versus $\gamma_{10}d$ due to two structures for variable $a_3/h_1$ composed of triple porous layers considering $h_1/\lambda=0.1$ and $\theta=20^\circ$ .	125
Figure 4.14	Variation of (a) $K_r$ and (b) $K_t$ versus $w/h_1$ due to two structures for variable $a_3/h_1$ composed of triple porous layers considering $h_1/\lambda=0.1$ and $d/h_1=2$ .	125
Figure 4.15	Variation of (a) $K_r$ , (b) $K_t$ and $K_d$ versus $w/h_1$ due to three structures for variable $a_3/h_1$ composed of triple porous layers considering $h_1/\lambda=0.2$ and $\theta=20^\circ$ .	126
Figure 4.16	Variation of (a) $K_r$ and $K_t$ , (b) $K_d$ versus $\theta$ due to four structures for variable $\varepsilon_1$ and $f_1$ composed of triple porous layers considering $h_1/\lambda=0.1$ and $a_3/h_1=0.1$ .	127
Figure 4.17	Variation of (a) $K_r$ , (b) $K_t$ and $K_d$ due to single and multiple structures composed of triple porous layers considering $h_1/\lambda=0.2$ and $a_3/h_1=0.2$ .	128
Figure 4.18	Variation of $K_r$ and $K_t$ versus $d/h_1$ due to single submerged structure for variable $h_2/h_1$ composed of double porous layers for $h_1/\lambda=0.1$ , $\theta=20^\circ$ considering (a) $\varepsilon_2=0.8$ , $f_2=0.4$ and (b) $\varepsilon_2=0.5$ , $f_2=1.0$ .	130
Figure 4.19	Variation of $K_r$ and $K_t$ versus (a) $\theta$ for variable $d/h_1$ and (b) $w/h_1$ for variable $a_3/h_1$ due to two submerged structures	131

composed of double porous layers considering  $h_1 / \lambda = 0.1$ .

- Figure 4.20 Variation of (a)  $K_r$  and (b)  $K_t$  versus  $\gamma_{10}d$  for variable  $\varepsilon_2$  and  $f_2$  due to three submerged structures composed of double porous layers considering  $h_1 / \lambda = 0.2$  and  $\theta = 20^\circ$ . 132
- Figure 4.21 Variation of (a)  $K_r$  and (b)  $K_t$  versus  $w/h_1$  for variable  $\theta$  due to four submerged structures composed of double porous layers considering  $h_1 / \lambda = 0.1$  and  $a_3 / h_1 = 0.3$ . 133
- Figure 4.22 Variation of  $K_r$ ,  $K_t$  and  $K_d$  due to single and two submerged energy absorbing structures for (a) uniform width, (b) variable width considering  $h_1 / \lambda = 0.2$  and  $\theta = 30^\circ$ . 134
- Figure 5.1 Oblique wave transport through series of stratified wave absorbers away from the (a) vertical wall (b) permeable wall and (c) stepped wall. 140
- Figure 5.2 Convergence study in wave reflection coefficient  $K_r$  due to multiple structures away from vertical wall, permeable wall and stepped wall considering  $h_1 / \lambda = 0.1$  and  $h_1 / \lambda = 0.2$ . 152
- Figure 5.3 Comparative study between the present study analytical results, previous experimental results of (a) Dattatri et al., (1978) and (b) Twu and Chieu (2000). 152
- Figure 5.4 The  $K_r$  versus (a) dimensionless width  $\gamma_{10}d$  and (b) angle of contact  $\theta$  considering horizontal variable porosity  $\varepsilon_1$  for  $d/h_1 = 1$  and  $\omega^2 h_1 / g = 1$ . 153
- Figure 5.5 The  $K_r$  versus  $L/h_1$  for various values of (a)  $\varepsilon_1, f_1$ , (b)  $a_1/h_1, a_2/h_1$ , (c)  $\theta$  and (d)  $d/h_1$  considering  $h_1 / \lambda = 0.1$  and  $N = 1$ . 154
- Figure 5.6 The  $K_{fv}$  versus  $L/h_1$  for various values of (a)  $\varepsilon_1, f_1$ , (b)  $a_1/h_1, a_2/h_1$ , (c)  $\theta$  and (d)  $d/h_1$  considering  $h_1 / \lambda = 0.1$  and  $N = 1$ . 155
- Figure 5.7 The  $K_r$  versus  $w/h_1$  for various values of (a)  $\varepsilon_1, f_1$ , (b)  $a_1/h_1, a_2/h_1$ , (c)  $\theta$  and (d)  $d/h_1$  considering  $h_1 / \lambda = 0.2$  and 156

$N = 2$ .

- Figure 5.8 The  $K_{fw}$  versus  $w/h_1$  for various values of (a)  $\varepsilon_1, f_1$ , (b)  $a_1/h_1, a_2/h_1$ , (c)  $\theta$  and (d)  $d/h_1$  considering  $h_1/\lambda = 0.2$  and  $N = 2$ . 157
- Figure 5.9 The  $K_r$  versus  $d/h_1$  for various values of (a)  $a_1/h_1, a_2/h_1$  and (b)  $L/h_1$  considering  $h_1/\lambda = 0.1$  and  $N = 3$ . 158
- Figure 5.10 The  $K_r$  versus  $\theta$  for various values of  $L/h_1$ , (a)  $d/h_1 = 2$  and (b)  $d/h_1 = 4$  considering  $h_1/\lambda = 0.1$  and  $N = 4$ . 159
- Figure 5.11 Comparative study of (a,c)  $K_r$  and (b,d)  $K_{fw}$  versus  $L/h_1$  for single and multiple structures with uniform structural width considering (a,b)  $h_1/\lambda = 0.1$  and (c,d)  $h_1/\lambda = 0.2$ . 160
- Figure 5.12 Comparative study of (a,c)  $K_r$  and (b,d)  $K_{fw}$  versus  $L/h_1$  for single and multiple structures with variable structural width considering (a,b)  $h_1/\lambda = 0.1$  and (c,d)  $h_1/\lambda = 0.2$ . 161
- Figure 5.13 The  $K_r$  versus  $d/h_1$  for various values of  $a_1/h_1, a_2/h_1, a_3/h_1$  considering (a)  $h_1/\lambda = 0.1$ , (b)  $h_1/\lambda = 0.2$  and  $N = 2$ . 162
- Figure 5.14 The  $K_r$  versus  $w/h_1$  for various values of  $a_1/h_1, a_2/h_1, a_3/h_1$  considering (a)  $d = 0.25w$ , (b)  $d = 0.5w$  and  $N = 3$ . 162
- Figure 5.15 Comparative study of  $K_r$  due to various structural configurations considering (a)  $N = 1$  (b)  $N = 2$  (c)  $N = 3$  and (d)  $N = 4$ . 165
- Figure 5.16 Comparative study of  $K_{fw}$  due to various structural configurations considering (a)  $N = 1$  (b)  $N = 2$  (c)  $N = 3$  and (d)  $N = 4$ . 165
- Figure 5.17 The  $K_r$  versus  $d/h_1$  for various values of (a)  $a_1/h_1, a_2/h_1, a_3/h_1$  (b)  $\theta$  considering  $h_1/\lambda = 0.2$  and  $N = 2$ . 166
- Figure 5.18 The  $K_r$  versus  $w/h_1$  for various values of  $\theta$  in the presence of (a) two-layered and (b) submerged absorber away from 168

permeable wall considering  $h_1 / \lambda = 0.2$  and  $N = 2$ .

Figure 5.19	The $K_r$ versus (a) $d / h_1$ and (b) $\theta$ considering various structural configurations in the presence of permeable wall.	168
Figure 5.20	The $K_r$ due to triple-layered wave absorber with change in (a) $\varepsilon_1, f_1$ (b) $\theta$ (c) $d / h_1$ and (d) $L_s / h_1$ considering $h_1 / \lambda = 0.2$ and $N = 2$ .	170
Figure 5.21	The $K_r$ due to (a) triple-layered and (b) submerged wave absorbers in the presence of vertical wall, stepped wall and permeable wall considering $h_1 / \lambda = 0.2$ .	171
Figure 6.1	Stratified porous block placed on varying seabed with leeward wall.	176
Figure 6.2	Comparison of the experimental data (Twu and Chieu, 2000) and the present study for the wave energy damping due to (a) two-layered porous structure and (b) three layered porous structure in the absence of seawall.	186
Figure 6.3	Effect of the seabed variation on (a) $K_r$ (b) $K_t$ and (c) $K_d$ versus $\theta$ for $f = 1$ , $\varepsilon = 0.4$ , $d / h_1 = 1$ and $\omega^2 h_1 / g = 0.2012$ .	189
Figure 6.4	Variation in $K_r$ and $K_t$ due to multi-layered porous structure for (a) $f = 0.5$ and (b) $f = 1.0$ in the presence of different types of seabed considering $\gamma_{10} h_1 = 1.0$ , $\varepsilon = 0.4$ and $d / h_1 = 0.5$ .	190
Figure 6.5	Effect of structural porosity on (a) $K_r$ (b) $K_t$ and (c) $K_d$ versus $\gamma_{10} d$ in the presence of uniform seabed for $f = 1$ , $\theta = 0^\circ$ and $\gamma_{10} h_1 = 0.5$ .	192
Figure 6.6	Variation in $K_r$ and $K_t$ due to multi-layered porous structure placed on elevated seabed for various values of (a) friction factor with $d / h_1 = 1$ and (b) structural width with $f = 0.5$ considering $\gamma_{10} h_1 = 0.5$ .	193
Figure 6.7	The $K_r$ versus $\gamma_{10} d$ for different (a) porosity with $f = 1$ and	195

(b) friction factor with  $\varepsilon = 0.5$  considering  $\omega = 0.3630$ .

- Figure 6.8 The  $K_r$  and  $K_{fs}$  versus  $d/\lambda$  for varying structural porosity on uniform seabed for (a)  $\gamma_{10}h_1 = 1.0$  and (b)  $\gamma_{10}h_1 = 1.5$  considering  $f = 0.25$  and  $\theta = 30^\circ$ . 197
- Figure 6.9 The  $K_r$  versus  $\theta$  for varying seabed characteristics in the case of (a)  $d/h_1 = 2$  and (b)  $d/h_1 = 4$  considering  $\gamma_{10}h_1 = 0.75$ . 198
- Figure 6.10 The  $K_r$  versus  $\gamma_{10}h_1$  for varying seabed characteristics in the case of (a)  $\theta = 0^\circ$  and (b)  $\theta = 45^\circ$  considering  $f = 1$  and  $d/h_1 = 1$ . 199
- Figure 6.11 The  $K_r$  versus  $L/h_1$  for various values of structural porosity placed on uniform seabed for (a)  $\gamma_{10}h_1 = 0.5$  and (b)  $\gamma_{10}h_1 = 1.0$  considering  $f = 0.25$ ,  $d/h_1 = 4$  and  $\theta = 0^\circ$ . 200
- Figure 6.12 The  $K_r$  versus  $\theta$  for various values of structural porosity placed on uniform seabed for (a)  $\gamma_{10}h_1 = 0.5$  and (b)  $\gamma_{10}h_1 = 1.0$  considering  $f = 0.5$ ,  $L/h_1 = 1$  and  $\theta = 0^\circ$ . 201
- Figure 6.13 The  $K_r$  versus  $\theta$  for various seabed conditions with multiple porosities in the case of (a)  $\theta = 0^\circ$  and (b)  $\theta = 30^\circ$  considering  $f = 0.5$ ,  $\gamma_{10}h_1 = 0.5$  and  $d/h_1 = 4$ . 202
- Figure 6.14 The  $K_r$  and  $K_{fv}$  versus  $\theta$  for varying seabed condition with multiple porosities for (a) finite water depth and (b) long-wave approximation considering  $d/h_1 = 2$ ,  $L/h_1 = 2$ ,  $\gamma_{10}h_1 = 0.5$  and  $f = 1$ . 203
- Figure 6.15 (a)  $K_r$  and (b)  $K_r$  and  $K_d$  versus  $d/h_1$  for varying bottom rigid bar height in the absence of the porous structure considering  $f_1 = 0$ ,  $\varepsilon_1 = 1$ ,  $\gamma_{10}h_1 = 1$  and  $\theta = 30^\circ$ . 204
- Figure 6.16 (a)  $K_r$  versus  $d/h_1$  for varying bottom leeward step height without porous structure considering  $\gamma_{10}h_1 = 1.5$ , (b) the  $K_r$ ,  $K_r$  and  $K_d$  versus  $\gamma_{10}d$  for permeable and impermeable 206

submerged bars considering  $\gamma_{10}h_1 = 0.4$  and  $\theta = 30^\circ$ .

Table 1.1	Roots of the two-layered ( $\varepsilon_1 = 0.8$ , $f_1 = 0.4$ ) and submerged two-layered ( $\varepsilon_1 = 1$ , $f_1 = 0$ ) dispersion relation considering $a_1/h_2 = 0.5$ , $a_2/h_2 = 0.5$ , $a_3/h_1 = 0.2$ , $\varepsilon_2 = 0.5$ , $f_2 = 1$ , $S_1 = S_2 = 1$ , $\theta = 20^\circ$ and $h_1/\lambda = 0.1$ .	35
Table 2.1	Table 2.1: Convergence in reflection and transmission coefficients considering $d/h = 1$ , $w/h = 1$ , $\gamma_{10}h = 0.5$ , $f = 0.5$ , $\theta = 0^\circ$ and $\varepsilon = 0.4$ .	47
Table 3.1	Convergence of $K_r$ and $K_t$ for four-types of barrier-rock porous structures considering $\gamma_{10}h = 0.5$ , $B/h = 3$ , $h_b/h = 0.7$ , $\theta = 15^\circ$ , $\varepsilon_b = 0.4$ and $f_b = 1$ .	82
Table 4.1	Roots of the two-layered ( $\varepsilon_1 = 0.8$ , $f_1 = 0.4$ ) and submerged two-layered ( $\varepsilon_1 = 1$ , $f_1 = 0$ ) dispersion relation considering $a_1/h_2 = 0.5$ , $a_2/h_2 = 0.5$ , $a_3/h_1 = 0.2$ , $\varepsilon_2 = 0.5$ , $f_2 = 1$ , $S_1 = S_2 = 1$ , $\theta = 20^\circ$ and $h_1/\lambda = 0.1$ .	111
Table 5.1	Various types of wave absorber configurations for comparative study.	163
Table 6.1	Convergence in $K_r$ and $K_t$ of a multi-layered porous structure considering $\omega = 0.3367$ , $\theta = 30^\circ$ , $d/h_1 = 2$ , $f_j = 0.5$ $\varepsilon_j = 0.5$ for $j=1,2$ and 3.	187
Table 6.2	Multiple porosities and friction factors with different model configuration.	191



# TABLE OF CONTENTS

DECLARATION	
CERTIFICATE	
ACKNOWLEDGEMENT	i
ABSTRACT	iii
NOMENCLATURE	v
ABBREVIATION	vii
LIST OF FIGURES & TABLES	ix
TABLE OF CONTENTS	xix
<b>CHAPTER 1</b>	
<b>GENERAL INTRODUCTION</b>	<b>1</b>
1.1 PERMEABLE	1
1.1.1 Wave interaction with breakwaters	3
1.1.2 Coastal protection through porous structures and seawalls	3
1.2 MOTIVATION	5
1.3 AIM AND OBJECTIVES	5
1.3.1 Objective of the study	5
1.3.2 Scope of the work	7
1.4 GRAVITY WAVE DISSIPATION BY POROUS STRUCTURES	7
1.4.1 Wave scattering by porous structures with changes in seabed	8
1.4.2 Wave interaction with multiple porous structures	12
1.4.3 Effect of seawalls on wave transformation	14
1.4.4 Wave damping by vertically stratified porous structures	15
1.4.5 Wave damping by horizontally stratified porous structures	17
1.5 CRITICAL REVIEW	18
1.6 BRIEF OVERVIEW OF THESIS	18
1.7 LIST OF PUBLICATIONS FROM THE RESEARCH WORK	21
1.8 FUNDAMENTALS OF WAVES AND POROUS STRUCTURES	23

1.8.1	Basic equations of wave motion	23
1.8.2	Kinematic Free Surface Boundary Condition (KFSBC)	24
1.8.3	Dynamic Free Surface Boundary Condition (DFSBC)	25
1.8.4	Velocity potential, surface elevation and dispersion relation	27
1.8.5	Far-field boundary condition	28
1.8.6	Basic structure equations	28
1.8.7	Dispersion relations in the open water and porous structure regions	32
1.8.8	Perturbation method	33
1.8.9	Solution approach for finding the roots of dispersion relation	34
1.9	CLOSURE	36

## **CHAPTER 2**

	<b>WAVE DISSIPATING PERFORMANCE OF MULTIPLE POROUS STRUCTURES</b>	<b>37</b>
2.1	GENERAL INTRODUCTION	37
2.2	MATHEMATICAL FORMULATION	38
2.3	METHOD OF SOLUTION	41
2.3.1	Wave transformation by multiple structures	41
2.3.2	Wave trapping by multiple structures	43
2.3.3	Wave transformation for single porous structure	44
2.3.4	Wave transformation for single porous block considering leeward wall	45
2.4	NUMERICAL RESULTS AND DISCUSSION	47
2.4.1	Multiple porous structures with leeward unbounded region	48
2.4.2	Multiple structures with leeward confined region/ leeward wall	58
2.4.3	Multiple structures placed on step-type rigid bottom	61
2.5	CLOSURE	66

## **CHAPTER 3**

	<b>WAVE DAMPING BY BARRIER-ROCK POROUS STRUCTURES</b>	<b>69</b>
--	---	-----------

3.1	GENERAL INTRODUCTION	69
3.2	MATHEMATICAL FORMULATION	70
3.3	METHOD OF SOLUTION	74
3.3.1	Barrier-rock porous structure	74
3.3.2	Barrier-rock porous structure away from rigid wall	77
3.3.3	Barrier-rock porous structure backed by rigid wall	79
3.3.4	Barrier-rock porous structure of semi-infinite thickness	80
3.4	RESULTS AND DISCUSSION	82
3.4.1	Barrier-rock porous structure	83
3.4.2	Barrier-rock porous structure away from rigid wall	87
3.4.3	Barrier-rock porous structure backed by rigid wall	89
3.4.4	Barrier-rock porous structure of semi-infinite thickness	91
3.4.5	Comparative study of various barrier-rock porous structures	93
3.5	CLOSURE	94

## **CHAPTER 4**

### **WAVE DAMPING BY MULTIPLE HORIZONTALLY STRATIFIED POROUS STRUCTURES 97**

4.1	GENERAL INTRODUCTION	97
4.2	THEORETICAL FORMULATION	98
4.3	METHOD OF SOLUTION	102
4.3.1	Multiple wave absorbing structures	103
4.3.2	Fully extended two-layered energy absorbing structure	106
4.3.3	Fully extended three-layered energy absorbing structure	107
4.3.4	Two-layered submerged energy absorbing structure	108
4.3.5	Solution approach for finding the roots of dispersion relation	110
4.4	RESULTS AND DISCUSSION	111
4.4.1	Two-layered fully extended multiple energy absorbing structures	113
4.4.2	Three-layered fully extended multiple energy absorbing structures	122

4.4.3	Submerged two-layered multiple energy absorbing structures	129
4.5	CLOSURE	135

## **CHAPTER 5**

### **WAVE TRAPPING BY HORIZONTALLY STRATIFIED POROUS STRUCTURE WITH END WALL 137**

5.1	GENERAL INTRODUCTION	137
5.2	MATHEMATICAL FORMULATION	138
5.3	METHOD OF SOLUTION	143
5.3.1	Multiple wave absorbers away from vertical wall	143
5.3.2	Three-layered stratified wave absorber away from the vertical wall	146
5.3.3	Series of stratified wave absorbers away from semi-infinite permeable wall	148
5.3.4	Series of stratified wave absorbers away from stepped wall	149
5.3.5	Solution approach for finding the roots of dispersion relation	149
5.4	RESULTS AND DISCUSSIONS	150
5.4.1	Effect of vertical wall with porous absorbers on wave trapping	151
5.4.2	Effect of semi-infinite permeable wall with porous absorbers on wave trapping	167
5.4.3	Effect of stepped wall with porous absorbers on wave trapping	169
5.4.4	Comparative study between vertical, permeable and stepped wall	170
5.5	CLOSURE	171

## **CHAPTER 6**

### **WAVE TRANSFORMATION DUE TO VERTICALLY STRATIFIED POROUS BLOCK 173**

6.1	GENERAL INTRODUCTION	173
6.2	MATHEMATICAL FORMULATION	175
6.3	METHOD OF SOLUTION	178

6.3.1	Porous structure in the absence of leeward wall	179
6.3.2	Porous structure backed by leeward wall	182
6.3.3	Porous structure away from leeward wall	184
6.4	<b>RESULTS AND DISCUSSION</b>	186
6.4.1	Porous structure in the absence of leeward wall with variation in seabed	187
6.4.2	Porous structure backed by leeward wall with variation in seabed	194
6.4.3	Porous structure away from the leeward wall with variation in seabed	200
6.4.4	Wave motion over elevated/stepped bottom in the absence of porous block	204
6.5	<b>CLOSURE</b>	207
<b>CHAPTER 7</b>		
<b>CONCLUDING REMARKS AND FUTURE WORK</b>		<b>209</b>
7.1	<b>GENERAL INTRODUCTION</b>	209
7.2	<b>SUMMARY OF THE RESEARCH WORK</b>	209
7.2.1	Wave damping by multiple porous structures	209
7.2.2	Wave scattering by barrier-rock porous structures	210
7.2.3	Wave damping by horizontally stratified porous structures	210
7.2.4	Wave trapping by horizontally stratified porous structures	211
7.2.5	Wave damping and trapping by vertically stratified porous structures	211
7.3	<b>SIGNIFICANT CONTRIBUTION FROM THE RESEARCH WORK</b>	212
7.4	<b>FUTURE SCOPE OF RESEARCH</b>	213
 <b>REFERENCES</b>		 215
 <b>AUTHORS RESUME</b>		 223



# CHAPTER 1

## GENERAL INTRODUCTION

### 1.1 PERMEABLE

The survivability of marine infrastructure is partially/fully depends upon the coastal structures. Various types of breakwaters such as trapezoidal, semi-circular, thin/thick vertical breakwaters, and a group of piles are constructed in the offshore regions to establish a calm wave environment in the shoreward regions. The optimal aim of breakwaters is to have high wave damping and wave breaking. However, the available breakwaters are unable to meet the requirements in most of the situations, and the effect of incoming wave energy is observed to be high on shoreward regions due to global warming and sea-level rise. Numerous coastal structures get damaged due to extreme wave attacks and create a situation to reconstruct the structures. Catastrophic storms and tremendous wave attack on the breakwaters are some of the primary reasons for the failure of the structures. The entire structure displacement, foundation failures, erosion at the toe, and failures from weak points at the structure are significant failures causing over maintained and reconstruction of the breakwaters. The necessity of increasing the life span of the breakwater is mandatory for protecting the natural resources and creating job opportunities from the ocean. Some studies (Karmakar and Guedes Soares, 2014; 2015) demonstrated that the rigid breakwaters are controlling the coastal erosion in the parent coast and enhance the severe erosion in their adjacent beaches (Pondicherry, India). The particular reason behind the coastal erosion in the adjacent coasts is that the breakwaters divert the wave energy from one coast to its nearby coast, which increases the coastal erosion in the adjacent coasts. Numerous researchers demonstrated that the locations, where the rigid breakwaters could not able to provide satisfying results (Behera and Sahoo, 2014). In those locations, the submerged and fully-extended thick and thin porous structures are one of the perfect solutions to control the incoming waves as well as creates tranquillity wave climate at ports and harbours.

The majority of the world population are residing near the coastal areas. The natural resources and cargo handling in ports and harbours are the primary reason for the high

population near the coastline. The ports and harbours are identified as the most common coastal infrastructures, which must be protected from high wave impact for safe cargo handling (Vijay et al., 2019). Coastal erosion, sea-level rise, unprecedented incoming waves and seawater intrusion, loading, and unloading of the cargo are also some of the significant problems, which dictate the life span of coastal infrastructure and the country's growth. To overcome the aforementioned practical problems, coastal engineers proposed several types of innovative techniques in the construction of coastal structures.

The coastal protection can be performed using a hard engineering technique and soft engineering technique. The hard engineering technique demonstrates the protection of the shore with coastal structures like offshore breakwaters, artificial headlands, jetties, groins, submerged, and emerged porous or non-porous breakwaters. On the other hand, the soft engineering technique which is also called as non-structural management techniques that cover the artificial vegetation, dune building, and feeding. These methods are implemented as coastal remedial measures for protecting the coast from tremendous wave trains. The submerged rigid breakwaters have been used as one of the feasible solutions for the protection of coasts. Several studies (Behera and Sahoo, 2014; Karmakar and Guedes Soares, 2014; 2015) demonstrated that the submerged rigid breakwaters can protect the coast from erosion and at the same time these structures are diverting the wave energy towards the adjacent coasts, which causes the severe erosion in the adjacent coasts. Due to the erosion taking place on the adjacent coast, the government authorities started implementing the submerged and fully-extended porous structure of different shapes such as rectangular, trapezoidal, and semi-circular breakwaters for moderate wave reflection, minimal wave transmission and considerable wave energy absorption. Very recently, the pile-rock porous structures (rock-fill between two-row of piles) are constructed to overcome the structural failures due to weak seabed conditions (Liu and Li, 2015; Li et al., 2017). The structural porosity and friction factor due to porous breakwater enhance the wave damping. Moreover, the seawalls such as the vertical wall, stepped seawall and curved walls are also constructed in several locations to reduce the wave impact on the offshore facilities. The optimal aim of a porous structure is to have considerable wave damping with minimal wave reflection and transmission (Twu and Chieu, 2000).



### **1.1.1 Wave interaction with breakwaters**

Wave interaction with submerged and fully extended structures (structure constructed till free surface) is a subject of great interest. In the past few decades, the thick/thin vertical and sloping breakwaters are proposed to control the incoming wave trains in ports and harbours. The rubble mound breakwaters are the most common structures and most capable of decreasing the wave elevation at leeward regions. In literature, most of the studies are performed using physical modelling to analyse the performance characteristics of a breakwater. The numerical and analytical models are used for validating the data set obtained using laboratory measurements. In recent years, the numerical and analytical models have received more attention for analysing the breakwaters due to its advantage in the accuracy of the numerical results.

### **1.1.2 Coastal protection through porous structures and seawalls**

The permeable porous breakwaters are used to protect the shoreline from wave trains around the ports and harbours. Figure 1.1 illustrates the porous structures constructed in some of the locations for regulating the incident wave attack. The porosity, inertia coefficient and friction factor of the porous structures are taken into account. The structural porosity can transform turbulent flow into the laminar flow to protect the coast from a high wave attack. The researchers and scientists (Yu and Chwang, 1994; Lin et al., 2018) are working on multi-layered porous structures to obtain minimal wave reflection, minimal wave transmission, and maximal energy damping. The minimum wave reflection and minimal wave transmission cause the minimal fluid force experienced by the seaward and leeward interfaces of the breakwater, which enhances the life span of the porous structure due to the free flow of the incident waves through porous breakwaters. In the case of the multi-layered structure, the width and depth of the porous structure are divided into multiple layers. Each porous layer consists of individual porosity and friction factor. In a horizontal two-layered structure, the minimal porosity is considered in the bottom layer to protect the breakwater from the failures and high porosity is considered at upper layers for better wave absorption. Similarly, in the case of the vertically multi-layered breakwater, the high porosity in the seaside and minimal porosity in the leeside layer is suggested (Twu et al., 2002) for higher wave damping.

Seawalls are the most common coastal protecting structures from tremendous wave attack. Various types of sea walls are constructed to mitigate coastal erosion as well as over flooding due to high wave attack. Different kinds of seawalls such as vertical sea walls, curved walls, stepped seawalls and permeable walls are developed in several locations. Very recently, an innovative pile-rock structure is constructed in the Dongying bay China (Liu and Li, 2014) for the protection of coastal infrastructure. The pile-rock breakwater consists of two-rows of piles placed with finite free spacing and the free spacing is filled with rocks for wave damping (Figure 1.1b). The two-rows of piles are useful for protecting the rock-fill from vertical or horizontal displacement. The new Kelsey bay, Canada constructed a leeside rigid wall away from a thin porous barrier. Further, the spacing between the thin barrier and rigid wall is filled with rocks (Isaacson et al., 2000). In general, the thin barriers are useful for the protection of rock-fill from vertical and horizontal displacements due to high wave attack.

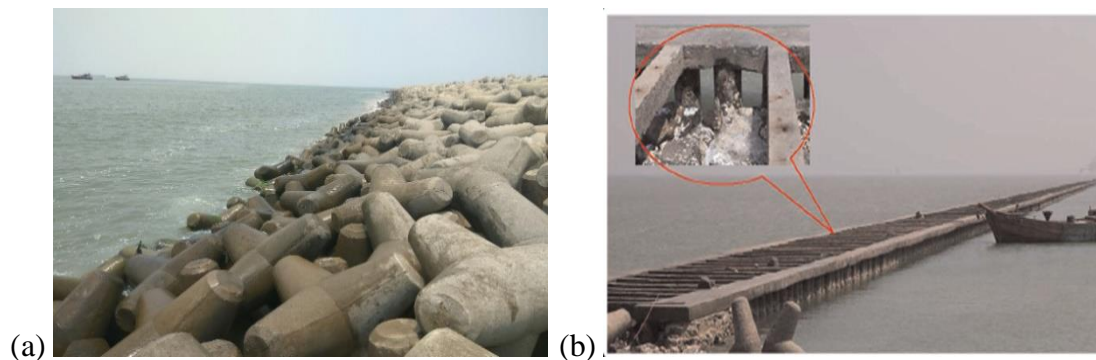


Figure 1.1: Porous structures are protecting the island and coasts from high wave attack at (a) Mangalore, India and (b) Dongying city, China.

The innovative idea is developed recently by the scientists and engineers for wave energy absorption with the installation of inclined plates, flexible membranes, multiple solid and porous plate type breakwaters to reduce the capital construction cost and maintenance cost (Vijay and Sahoo, 2019). Porous plates and solid plates are frequently used as a breakwater for better wave reflection in the ports and harbours as temporary protection. The significant advantages of the porous and solid plates are that this type of breakwaters occupies less space and it never affects the beach aesthetic. The floating plate type porous plates can effectively work as a wave energy absorbers and can overcome the foundation related problems arising during construction. In deep water, these floating plates are one of the solutions to regulate the high wave trains.

## 1.2 MOTIVATION

The coastal structures such as sea walls, fully-extended porous structures, submerged wave absorbers, group piles, porous and solid plates are constructed in several port and harbours. The advantages of porous structures compared to conventional breakwaters are as follows:

- The high incident waves can be attenuated with the use of permeable breakwaters, which can create tranquillity conditions at ports and harbours through wave damping.
- The submerged wave absorbers do not affect the coastal aesthetic and marine transportation.
- The deeply submerged wave energy absorbers are eco-friendly and seawater level rise does not damage the structures.
- The conventional rigid breakwaters are effective in reflecting the incident waves and also diverts less wave energy to its adjacent coasts in some locations. In those locations, the porous structures can control tremendous waves through high wave energy absorption.
- The vertical and horizontal displacements of breakwaters are quite common in recent years, and these problems can be solved using the concept of barrier-rock porous breakwaters.
- The seawalls such as vertical seawall, stepped seawall and permeable walls are one of the better options in several locations, where the coastline is very near to the mainlands.

## 1.3 AIM AND OBJECTIVES

The present study is focused on the wave interaction with porous structures, seawalls, two-layered porous structures, and vertical permeable barriers. The study aims to analyse vertical breakwater with suitable porosity, friction factor, structural width, and angle of incidence for coastal protection.

### 1.3.1 The objective of the study

The following objectives are framed for the determination of minimal wave reflection coefficient, transmission coefficient and high wave damping.

- The wave interaction with multiple porous structures is performed
  - ✓ To study the wave damping and wave trapping phenomenon by multiple structures placed on the horizontal rigid seabed.
  - ✓ To study the effect of the rigid elevated bottom on wave damping and wave trapping in the presence of multiple porous structures.
  - ✓ To analyse the performance of single and multiple breakwaters considering identical structural width.
- Analysis of barrier-rock porous structure is performed
  - ✓ To propose the direct analytical relations for finding the wave reflection and wave transmission by barrier-rock porous structures placed on the flat seabed and elevated seabed.
  - ✓ To study the wave scattering performance of four types of barrier-rock porous breakwaters such as the structure of finite width, structure away from seawall, backed by a seawall, and semi-infinite breakwater.
- The performance of the horizontal two-layered porous structures is analysed
  - ✓ To examine the wave damping and wave trapping performance of multiple horizontal two-layered porous breakwater.
  - ✓ To investigate the effect of various seawalls such as vertical seawall, stepped seawall, and permeable seawall in the presence of two-layered porous structures.
  - ✓ To examine the seabed change impact on wave damping and wave trapping by multiple horizontally stratified porous breakwaters.
- The performance of the vertically stratified porous structures are analysed
  - ✓ To study the hydraulic characteristics through vertically stratified porous structures in the presence of uniform seabed, elevated seabed, and stepped seabed.
  - ✓ To propose direct analytical relations for finding the wave reflection by two-layer and three-layer porous front wall.
  - ✓ To analyse the wave action through stratified porous structures with and without trapping chamber.

### **1.3.2 Scope of the work**

A substantial contribution to water wave mechanics is made more than a century ago developed by Airy in 1845. After that higher-order wave theory by Stokes in 1847, a long-wave approach by Boussinesq in 1872 and limiting wave heights by Michell in 1893 and McCowan in 1894 was developed and studied. The water wave motion through a porous structure is initiated by Sollitt and Cross (1972) and thereafter, Dalrymple et al. (1991) examined the effect of oblique wave motion through the porous structure. In the last few decades, notable studies on different configurations of porous structures are performed by researchers. The present study is focused on the multiple porous structures, barrier-rock porous structures, and stratified porous structures with various types of seawall based on suggestions made by notable authors.

The scope of research work includes normalized values and realistic assumptions in the analysis of the wave structure interaction. The wave interaction with single and multiple porous structures of different configurations such as vertically stratified porous structures, horizontally stratified porous structures, and barrier-rock breakwaters are considered. The merits and demerits of the structure as breakwater are proposed in terms of scattering coefficients. Various types of seawalls such as the porous wall, vertical wall, and stepped seawalls in the presence of various breakwaters are also examined. The direct analytical relations for determining the wave scattering and wave trapping is obtained and validated with the available relations. The basic structural configurations such as porous structures, porous structure away from the wall, backed by a wall, semi-infinite porous structures are examined and validated with the available literature. The bottom topography is considered to be flat, elevated, and varied stepped for sloping type sea bottom profile. The seaward and leeward thin walls are proposed to reduce the vertical and horizontal displacements of the rock core.

## **1.4 GRAVITY WAVE DISSIPATION BY POROUS STRUCTURES**

In order to protect the shore, single and multiple porous structures are built to mitigate the effect of wave action. Though there exist different types of breakwaters but almost 80% of the coasts are protected by means of conventional breakwaters (i.e. rubble-mound or rock dumps). The gravity wave action over the bottom fixed impermeable/permeable structures is a subject of great interest due to its continuous application in

the construction of breakwaters. The selection of proper breakwater configuration is site dependent and is governed by the most prominent wave height in the nearshore region. The major challenges for scientists/ coastal engineers are to realign the eroded beaches and to protect the marine amenities such as coastal infrastructure and commercial activities from the destructive incident waves. The breakwaters are broadly classified as floating and deeply submerged/bottom founded structures. In the case of bottom founded thick structures, there exist several structural shapes such as rectangular, trapezoidal, semi-trapezoidal, triangular, semi-circular and quarter-circular structures. In the case of multiple submerged breakwaters, the effect of structural porosity and free spacing available between any two-consecutive permeable and impermeable structures plays a major role in damping the unwanted wave oscillations and mitigates the standing wave formation.

In the present section, the detailed review of the literature is presented on the wave scattering performance of porous structures, vertical barriers, and sea walls. The hydrodynamic characteristics of the wave interaction with the porous structure are one of the influencing factors in the design of coastal structures. Several studies addressed wave reflection, wave transmission, energy damping, wave run-up, wave elevation, the fluid force experienced by barriers and force on seawalls in the presence of various types of breakwaters using least-squares approximation, eigenfunction expansion method, Boundary Element Method (BEM) and Finite Element Method (FEM). In most of the studies, the numerical results are validated with available numerical and experimental results. Several researchers used the eigenfunction expansion method for predicting the wave behaviour in the presence of wave energy absorbers of conventional shapes. Orthogonal mode-coupling relation, matching equations based on continuity of velocity and pressure are used at interfaces of open water and porous structure regions. The system of equations is developed for finding the wave scattering performance of breakwaters. The energy loss coefficient by porous structure is calculated based on the law of conservation of energy. A brief literature review is presented on wave interaction with various types of coastal structures, seawalls, two-layered porous structures, and porous screens. Various physical changes in porous structures, changes in seawalls, and changes in bottom topography in the presence of different types of breakwaters are discussed in the following subsections.

### **1.4.1 Wave scattering by porous structures with changes in seabed**

Valuable information in the field of wave structure interaction with changes in the ocean bathymetry is available in the literature and the bottom topography changes are considered to be an influencing parameter in wave scattering problems. In the recent scenario, the sloping beaches are developed for tourism purposes and flat bottom topography is utilized for ports and harbours. A lot of studies are performed on wave reflection and transmission due to submerged porous structures, porous barriers, porous bars, solid plates, porous plates, and very large floating structures with changes in bathymetry. Apart from the analysis of various structures, numerical models are developed for analysing the wave behaviour in the presence of elevated bottom, stepped bottom, sloping bottom, and abrupt changes in bathymetry. Wave propagation with variations in bottom topography is one of the prominent research areas for understanding the wave behaviour. Newman (1965a) performed wave reflection and transmission due to long obstacles by considering the wave diffraction. Further, Newman (1965b) presented a numerical model for understanding the wave propagation over infinite step and compared with the experimental results. Davies (1982) performed wave propagation over undulation ocean bathymetry using perturbation theory.

A significant study has been performed by various researchers to develop new methods and techniques to reduce the computational difficulties in the analysis of the wave structure interaction problems. Sollitt and Cross (1972) proposed a complex dispersion relation to analyse the wave motion inside the porous structure. The porous structure of finite width placed in the finite depth is analysed using the eigenfunction expansion approach. The wave reflection and transmission due to the porous structure are investigated and validated with the laboratory measurements. Several researchers conducted hydraulic tests to study the performance of breakwaters in various physical configurations. Sloping type breakwaters are constructed in several locations for smooth wave breaking. Dattatri et al. (1978) tested the scattering performance of impermeable and permeable structures with various shapes using laboratory measurements. The wave transmission by trapezoidal, rectangular, semi-trapezoidal, and vertical barrier type breakwaters are reported and studied. The 16.5 mm and 43.4 mm aggregates with porosities of 41% and 42% are used for analysing wave behaviour in the presence of various shapes of permeable and impermeable breakwaters. Variation

in wave transmission from the vertical and trapezoidal breakwaters are compared. The reflection coefficient is observed to be higher from vertical breakwater as compared with a trapezoidal breakwater. In both cases, wave transmission is found to be similar and energy loss is maximum from trapezoidal breakwater compared to a vertical breakwater. The study concluded that the shape of the breakwater is an influencing factor for altering wave reflection and energy loss. Finally, the experimental outcomes concluded that the semi-trapezoidal breakwater shows better performance in the wave blocking compared with the other physical configurations. Sulisz (1985) investigated the wave scattering performance of rubble mound breakwater using BEM and the results are validated with experimental outcomes. The comparative study concluded that the numerical and experimental results show a pretty acceptable correlation in the case of wave transmission. Still, a little high estimation is obtained in the wave reflection for BEM results compared with experimental results. The study pointed out that the high estimation in the wave reflection may be due to ignoring the added mass coefficient. Thereafter, Dalrymple et al. (1991) introduced the effect of incident wave angle on hydrodynamic coefficients such as wave reflection by porous structure using matched eigenfunction expansion method. The direct analytical relations for finding the wave reflection and transmission by porous structure, structure backed by the wall and semi-infinite structure are derived and reported. The study reported a comparative study between long-wave reflection and plane-wave reflection along with the effect of evanescent waves on hydrodynamic coefficients by a porous structure. The study concluded that the evanescent waves have a significant role in the design of offshore breakwaters.

Trapezoidal permeable and impermeable structures are the most common coastal structures used to protect the leeward regions. The exact reason for constructing the trapezoidal breakwaters is that the stability of the structure due to the existing slope in the seaward and leeward edges. The slope existing in the structure causes the smooth wave breaking, which results in the maximum wave energy dissipation. The wave reflection is minimum compared with caisson breakwaters, but the stability of the structure is comparatively better for trapezoidal breakwaters. Cox and Clark (1992) analysed a new physical model that consists of a conventional rubble mound breakwater along with a submerged reef operating in tandem. The spacing between the two



breakwaters is referred to as a wave damping zone and suggested for the southern end of Lake Michigan, USA. Reddy and Neelamani (2004) performed a study on wave forces acting on submerged offshore breakwater using an experimental approach. The physical properties of the low crested breakwater are kept constant and water depth is varied considering the tidal rages at that particular location. Rambabu and Mani (2005) addressed the wave transmission in the presence of submerged trapezoidal permeable and impermeable breakwater using the boundary element approach. The effect of crest width, submergence depth of the structure, and effective spacing between the two submerged trapezoidal breakwaters on wave transmission characteristics is presented. Further, the study explored the significance of porosity on wave damping. The independent numerical model is developed for finding the wave transmission through the permeable submerged trapezoidal structure and compared with the impermeable trapezoidal structure. The minimum transmission coefficient is achieved in the case of permeable breakwater compared with impermeable structure due to wave damping. Mani (2009) conducted a series of experiments for finding the reflection, transmission characteristics, and wave forces acting on zig-zag porous screen breakwater. The correctness of the experimental results is tested with numerical results and better agreement is observed between the numerical and experimental results.

Recently Liu and Li (2013) developed an analytical method to reduce the complexity in the formulation and study neglected the porous structure dispersion relation for the analysis of the porous structures. The newly developed analytical study is validated with the results of Yu and Chwang (1994) and Madsen (1983) and a better correlation is obtained between the new analytical method and available results. Some of the studies reported the direct analytical equations to reduce the problems pertaining to wave scattering analysis of different types of breakwaters. The simplified analytical relations for finding the wave reflection and transmission coefficients by the finite permeable wall (Madsen, 1983), finite and semi-infinite porous structure (Darlymple et al., 1991; Liu and Li, 2013) are proposed for long-wave and plane-wave approximation (neglecting evanescent waves). Porous structures of vertical edges placed on the rigid seabed are studied in detail using numerical and experimental methods and the previous studies performed by various researchers can be extended for the multiple structures of different shapes considering multiple wave trapping regions.

Very recently, the semi-circular breakwater is proposed for the successful wave blocking to create the tranquillity wave climate in the beaches and harbours. The Weihai city, China developed the semi-circular permeable breakwater (Liu and Li, 2013) to protect the leeward locations from the high wave impact. To propose a better breakwater configuration, Liu and Li (2013) investigated the submerged permeable semi-circular structure under oblique wave action. The study developed the semi-analytical technique using eigenfunction and multipole expansions. The minimum estimation in the wave reflection and transmission is achieved with the semi-circular structure for the  $45^{\circ} - 60^{\circ}$  angle of incidence. Thereafter, Koley and Sahoo (2017) employed the coupled eigenfunction and BEM approach to examine the semi-circular permeable breakwater placed on the porous bottom and rigid bottom backed by sloping seawall under oblique wave impinging. The study reported that 70% - 90% wave energy can be attenuated with a semi-circular permeable breakwater. The porosity and the radius of the structure play an immense role in the wave energy damping. In the previous studies, the semi-circular breakwater is widely reported for the uniform seabed, and it is noted that the studies on semi-circular breakwater can be extended for the seaward undulating bottom.

#### **1.4.2 Wave interaction with multiple porous structures**

The permeable wall is an effective solution to prevent the free passage of incident waves. Dieppe in France (Belorgey et al., 2003) and Dalian Chemical Production Terminal in the Republic of China (Huang et al., 2011) constructed multiple permeable walls to dissipate the incident waves. Recently, coastal engineers focused on the multiple permeable barriers for better wave energy trapping due to the presence of the multiple confined regions. Several researchers examined the wave damping and wave trapping performance of different types of porous and non-porous breakwaters using analytical, numerical, and experimental methods (Rajendra et al., 2017). Most of the studies focused on wave damping and wave trapping by multiple wave absorbers due to its wide application. Twu and Lin (1990) examined the multiple thin porous plates using long flume and the study reported that the optimal spacing between two porous plates is 0.88 times of water depth for variable wavelength. Losada et al. (1993) analysed multiple porous screens as an effective wave damper with the rigid leeward

wall using the analytical method. The occurrences of Bragg resonance are observed by multiple periodic screens. The increase in the number of porous screens shows an effective decrease in wave reflection and an increase in resonating patterns.

The wave damping characteristics by an array of porous structures are performed by Twu and Liu (2004) using the matched eigenfunction expansion approach. The effect of geometric properties on reflection, transmission, and energy dissipation is presented. It is observed that the porosity, structural height, width of the bars and number of porous bars play a key role in altering the wave reflection and transmission. The significant variation is observed in wave reflection between the permeable and impermeable bars. The study concluded that the permeable bars are capable of dissipating the maximum wave energy and the increase in porosity causes a decrease in the reflection coefficient and an increase in energy absorption. Sankarbabu et al. (2007) examined the significance of a group of cylinders consisting of the outer porous layer and a rigid inner layer. The study focused on the wave force acting on the cylinder using the analytical method and study results are validated with the laboratory measurements. The study stated that the wave force impact on the cylinder is reduced with the increase in width between the cylinders. Afterward, Sankarbabu et al. (2008) extended the study for the analysis of double cylindrical caisson structures using the eigenfunction expansion technique. Finally, the study showed an impressive performance of hydrodynamic characteristics with the double cylindrical system considering the doughnut chamber width 0.5 (ratio of the rigid inner cylinder to the outer porous layer).

The perforated caisson with three wave damping chambers is constructed in Porto Torres industrial harbor, Italy (Franco, 1994). Similarly, the perforated caisson breakwater having five damping chambers is being constructed at Dalian Chemical Production Terminal, China (Huang et al., 2011; Liu et al., 2007). The wave scattering by thin barriers of various configurations such as, multiple surface piercing barriers (Karmakar et al., 2013), multiple bottom-standing barriers (Karmakar and Guedes Soares 2014, 2015) are reported in the literature using eigenfunction expansion and least square approximation. Overall, the surface piercing barriers increase the magnitude of wave oscillations as compared with other types of barriers. Zhao et al. (2017) extensively studied wave reflection and transmission by an impermeable wall protected by multiple submerged porous bars in series using the boundary element

method and eigenfunction expansion method. The study proposed that the performance of submerged porous bars can be accelerated with the increase in bars for fixed structural width. The width between the porous bar and the leeward wall has a significant role in creating the tranquillity condition in the leeward region. To reduce the construction area required for developing the sloping breakwaters, multiple slotted walls are introduced and are extensively analysed by Neelamani et al. (2017). Thereafter, Vijay et al. (2019) reported the wave trapping by multiple slotted walls using a numerical method and validated with the experimental results. The studies concluded that the triple walls with 30%-40% porosity are sufficient to reduce the wave reflection and fluid oscillations in the harbour regions. Behera and Ng (2017), Kaligatla et al. (2018) reported the wave scattering by multiple barriers in the presence of seabed variation using the eigenfunction expansion technique. Various seabed configurations are studied using the mild-slope equation. The study suggests that the wave trapping can be achieved with the variation in the seabed characteristics and multiple confined regions due to the presence of multiple barriers. The double porous boxes are proposed as an effective breakwater system by Vijay and Sahoo (2019) and the study discussed the formation of clapotis due to the free spacing available between the double porous boxes.

### **1.4.3 Effect of seawalls on wave transformation**

In the present sub-section, the wave damping and wave trapping by permeable wall breakwaters are discussed. The permeable wall breakwater consists of a thick/thin permeable structure placed very near or far away from the rigid seawall. The oblique wave damping by the porous structure with a solid wall is essential for the practical engineering design of coastal structures. Madsen (1983) presented the wave reflection coefficient due to vertical homogenous wave absorber backed by a rigid wall. Matched eigenfunction expansion method is used and the numerical results are compared with the experimental result performed by Abbott et al. (1981). The effect of absorber porosity on the wave reflection is discussed. The study proposed a novel method to solve the friction factor offered by the porous absorber.

Numerous researchers extended the study as presented in Madsen (1983) and proposed permeable coastal structures with the leeward wall for the protection of marine

facilities. Mallayachari and Sundar (1994) examined vertical and seaside sloping permeable block backed by wall placed on the uniform seabed and sloping seabed using the analytical method. The study reported that the minimum wave reflection is achieved with a porous structure placed on sloping seabed compared with the uniform seabed. Thereafter, Zhu and Chwang (2001) extended the study as in Mallayachari and Sundar (1994) considering the finite spacing/trapping region between the porous structure and rear wall. The performance of the absorber is analysed using the eigenfunction expansions and Finite Difference Method. Finally, the study stated that the change in the trapping region would minimize wave reflection and increases energy damping. Chen et al. (2006) performed wave reflection from the submerged bottom-mounted porous structures with end wall using mild-slope approximation. The time-dependent mild-slope equation involves the major influencing parameters such as friction factor, inertia, and porosity existing in the structure. The study is performed for the analysis of wave behaviour in the presence of vertical breakwater protected with porous structures on the impermeable flat bottom. Various shapes of the porous structures are examined and wave reflection from the rectangular, triangular, and trapezoidal porous structures is presented. Numerical results are compared with analytical results and a better agreement is observed. The study is extended for sloping bottom and variation in reflection coefficient in the finite water and shallow water depth are compared. The maximum wave reflection is observed for the porous structure placed in finite water depth.

The porous structure placed upon elevated seabed with the back wall is analysed by Das and Bora (2014a,b) with and without trapping chamber using the eigenfunction expansion method. The study showed that the increase in rigid step height enhances the wave reflection due to zero flow near the rigid step. Das and Bora (2014c,d) predicted wave reflection from the submerged porous structure with the end wall. The sloping ocean bathymetry is approximated into multiple rigid steps. Each of the rigid steps consists of a vertical porous layer. Hence, the wave reflection due to the porous structure placed on the stepped bottom is analysed using the eigenfunction expansion method. A number of two and seven rigid steps are considered. A very minimal variation in the wave reflection is observed by porous structure placed on two-step bottom and seven-step bottom. Very recently, Koley et al. (2015) used the matched

eigenfunction expansion and BEM approach to investigate the submerged and surface piercing porous structures away from the wall. The wave reflection, wave force on the seaward, leeward side of the submerged porous block, and wave force impact on the leeward wall with variation in the structural height is presented. The study mainly concentrated on the wave transformation due to the porous structure with uniform porosity and friction factor. Zhao et al. (2017) examined the single submerged porous bars in the presence of partially reflecting sidewalls. The wave reflection is presented using the matched eigenfunction expansion method and the boundary element method. The distance between the porous bar and lee side wall is observed to play a significant role in the oscillatory wave reflection.

#### **1.4.4 Wave damping by vertically stratified porous structures**

An ideal structure must perform low wave reflection, low wave transmission, and high energy damping. Thus, it is a challenge for the coastal engineers to design a suitable breakwater which can perform low wave reflection and transmission coefficients. It is observed that the fully extended porous blocks with uniform porosity are a better option, but the performance needs to be improved with new techniques to dissipate the wave energy. If the porous structure allows minimum wave transmission, then the structure is considered to enable high wave reflection. If the structure is allowing high wave reflection, the foundation failure may result while the dissipation of wave energy through the structure, and in this process the structure will be incapable of protecting the leeside facilities. Hence, the stratification concept is introduced. The porous structure consists of multiple porosities and friction factors, which can allow more waves in the seaside layer due to high porosity. The leeside porous layer consists of minimal porosity and it will be useful for wave blocking. The high wave energy damping due to progressive wave absorber is introduced by Le Méhauté (1972) and the analysis is performed using the numerical approach considering the multiple porosities. The theoretical outcomes are validated with the experimental results and a better agreement is obtained between both the study outcomes.

An attempt was made by Twu and Chieu (2000) to adopt multiple porosities in a single porous structure placed on the uniform seabed to dissipate the maximum wave energy, and the analytical study using matched eigenfunctions is validated with the laboratory

measurements. Two-layered and three-layered porous structures are thoroughly analysed using the hydraulic tests in the presence of the multiple porosities and friction factors. Finally, the higher porosity in the seaward layer and low porosity in the leeward layer is suggested for better wave damping. Meanwhile, Twu et al. (2001) extended the study for deeply submerged porous bars with multiple porous slices. The study stated that the relevance of the energy damping and multiple porosities in a single submerged porous bar can dissipate the 50% more wave energy as compared with a single submerged porous bar with uniform porosity. The multi-layered porous structure could be constructed for partial shelter to the shores from high wave attack and the application of the multiple porosities provides more emphasis on the wave blocking. Afterward, Twu et al. (2002) extended the analytical study considering the multiple friction factors in a single porous structure placed over flat seabed for oblique wave action. The reduction in the wave reflection and increase in the energy damping shows the influence of the multiple porosities and friction factors on the wave blocking. The performance of the multi-layered porous structure is useful to achieve high wave energy damping. The present concept helps in the reduction of the space required for the construction of porous structure due to the increase in the performance (Twu et al., 2002). It is also observed that the correlation between the experimental and theoretical results is acceptable and the study is useful in the attenuation of the incoming waves. However, the previous studies strongly suggested the multi-layered concept for better wave blocking and the variation in the seabed characteristics and impact of the rear wall in the presence of the stratified porous structure is still far from complete.

#### **1.4.5 Wave damping by horizontally stratified porous structures**

The competence of a porous structure is evaluated based on the scattering coefficients namely the wave reflection, transmission, and energy damping coefficients. Most of the studies reported that the minimum values of wave reflection, transmission, and higher values of wave damping is acceptable to reduce the structural failures from storm surges. The vertical and horizontal displacements of emerged structures and underwater rock dumps are one of the severe problems experienced by various coasts due to extreme wave impact. Hence, the coastal engineers have focused on the stratification concept for the wave-induced flow through breakwaters. Yu and Chwang (1994) addressed the wave motion upon the porous seabed in the presence of the porous block.

The porous block is assumed to be horizontal two-layered and analysis is performed using the eigenfunction expansion technique. A complex dispersion relation is solved for finding the wave number in the two-layered porous structure. Finally, the study reported that the large porosity and less dissipative medium with the high structural thickness could perform better values in the transmission coefficient.

The Kelsey Bay, Canada is a live example of the porous breakwater with seaward vertical barrier and the leeward impermeable wall (Isaacson et al., 2000). Isaacson et al. (2000) examined the breakwater configuration as in Kelsey Bay, Canada, which is a porous structure protected with seaward permeable wall and leeward impermeable wall using the matched eigenfunction expansion method. The wave force impact on the structure is reported in detail and reduction in the wave force is observed for higher values of porosity and structural width due to the increase in the wave damping. Further, Liu et al. (2007) investigated the breakwater configuration as in Kelsey Bay, Canada on considering the two horizontal porous layers. The wave reflection and force on the structure are reported for a two-layered rock-fill porous structure with the back wall. The matched eigenfunction expansion method is adopted for solving the boundary value problem. The wavenumber is calculated with a complex dispersion relation in the two-layered porous structure region and solved based on the step approach method. Numerical results are compared with results available in the literature and better agreement is observed. The study demonstrates the effect of porosity, non-dimensional width, and friction factor on wave reflection and non-dimensional wave forces on the structure.

Very recently, Lin et al. (2018) proposed a submerged two-layered porous structure to protect the coast from extreme incident waves. The wave scattering by two-layer porous structure is reported using the matched eigenfunction expansion method. The inner product technique is used to reduce the difficulties in the analysis of porous breakwater. Thereafter, Hu et al. (2019) examined a new-type of breakwater, which is divided into multiple horizontal layers in the horizontal direction. The scattering coefficients by multi-layer breakwater are presented using the semi-analytical solution based on the continuity of velocity and pressure. Different structural configurations such as floating thick plates, thin plates, and floating breakwaters are examined using the newly developed analytical solution.



#### **1.4.6 Incident wave damping by floating porous structures**

The persistent problems such as coastal erosion, level of protection in the ports and harbours due to constant gravity wave interaction served as incentives for the development of novel breakwaters. The floating and submerged membranes are regularly referred to as versatile mobile breakwaters for temporary protection of sophisticated oilfields, amphibious military operations, assault landing and construction of marine infrastructure. In general, the flexible membranes are inexpensive, easily handled, lightweight, effectively reusable and liberated from water depth (Kim and Kee, 1996). On the other hand, the vertical seawalls are also recognized as viable coastal structures, which avoid wave transmission due to the effective return flow. However, the seawalls are exposed to high wave impact due to zero-porosity, thus the partially reflecting harbour walls are introduced, which adequately controls the incident waves of high frequencies through partial wave damping (Isaacson and Qu, 1990). The concept of the easily transportable tethered floating breakwater was initially introduced by Prof. John Isaacs, Scripps Institution of Oceanography (Essoglou et al., 1975) for temporary protection in the offshore regions through wave damping. In the hydraulic viewpoint, viscous drag created by relative velocity available between the floating breakwater and fluid particle motion dissipates the incident wave energy. The wave damping efficiency and practical significance of floating breakwaters (Isaacson and Byres, 1988) and partially reflecting harbour walls (Elchahal et al, 2008) are well discussed in the literature. Some of the scientists suggested the inclined plate to secure the available very large floating structures (Cheng et al., 2016) and fully developed concrete structures. Huang and Wang (2017) conducted a comparative study on the wave damping efficiency of the inclined plate, cross plates, submerged and surface floating horizontal plate for the protection of Three Gorges Dam, China from impulse wave generated due to occurrences of landslides. The study results concluded that the cross plates show a larger quantity of wave decay and multi-rows of large plates can increase the wave decay.

The U.S navy Civil Engineer Corps Bulletin (1948) tested the functional efficiency of the sloping breakwater (50 X 175 feet) placed in different levels of submergence with several angle of inclinations (Patrick, 1951). Thereafter, several scientists examined the inclined plate in different physical configurations such as bottom

mounted inclined plate (Bayram, 2000), moored sloping plate breakwater (Kharaghani and Lee, 1986) using the experimental and numerical methods. The laboratory measurements of the submerged inclined plate suggest that the strong turbulence wave pattern is identified in the shoreward side of the inclined plate (Murakami et al., 1994). Nallayarasu et al. (1994) developed a finite element model for the investigation of the submerged inclined plate and numerical results recommended that the optimal value of breakwater inclination varies within  $30^{\circ}$  to  $60^{\circ}$  which displays minimal horizontal force on inclined plate. The wave action over the single inclined flexible membrane (Cho and Kim, 2000), multiple inclined plates (Cho and Kim, 2008) and dual submerged porous plates (Cho et al., 2013) is examined using the multi-domain BEM solution. A set of experiments also conducted for finding the wave reflection and transmission coefficients by inclined plates. As a special case, the horizontal flexible membrane is formulated using the matched eigenfunction expansion method and validated. Finally, the study suggests that the optimal angle of inclination varies within  $10^{\circ}$  to  $20^{\circ}$  and the wave damping performance of the lower plate is not appreciable as compared with the upper plate.

## **1.5 CRITICAL REVIEW**

The literature review suggests that very few studies are performed on wave scattering by vertically and horizontally stratified porous structures. Most of the studies reported the wave damping by multiple porous structures, but the wave trapping by multiple porous structures in the presence of different types of seawalls has more impact on the protection of nearshore regions. In order to protect the breakwater from vertical and horizontal displacements, the vertical barriers (New Kelsey bay Canada) and piles (Dongying bay China) are considered, which must be analysed for further design and development of novel breakwater system.

## **1.6 BRIEF OVERVIEW OF THESIS**

The content of the thesis is divided into seven Chapters depending on the physical problem investigated and the solution approach considered in the problem formulation. The detail description of the Chapters are as follows:

In Chapter 1, the introduction and the motivation behind the present work are discussed along with the detailed fundamental theory of oblique wave transport through porous

breakwaters. The boundary conditions associated with the wave structure interaction problems using matched eigenfunction expansion method in the finite and shallow water depths are presented. The detailed review of literature relevant to the wave interaction with single submerged and fully-extended porous structure, multiple porous structures, submerged, surface piercing barriers, vertically and horizontally stratified porous structures, various types of seawalls, pile/barrier-rock porous structures are discussed thoroughly. Further, the research gaps based on the literature review are discussed followed by a brief introduction to the research work pursued in the thesis.

Chapter 2 describes the study on wave propagation through multiple fully extended porous structures placed on flat/elevated seabed with the leeside unbounded region and confined region/leeward wall using the eigenfunction expansion method. The analytical results obtained in the present study are validated with the available results for specific structural configurations. Further, the wave scattering and trapping by multiple porous structures are presented. The significance of porous structure considering various ranges of porosity, friction factor, the finite spacing between multiple structures, structural thickness, and angle of incidence are discussed and analysed. A comparative study is performed between single and multiple porous structures for fixed structural width.

In Chapter 3, the four types of barrier-rock porous structures are examined using the eigenfunction expansion method and analytical results are validated with previous results for several structural configurations. Thereafter, the straight analytical relations are proposed for finding the wave reflection/transmission characteristics for plane-wave approximation. The effect of physical parameters of breakwater and incident wave properties on wave scattering and wave trapping is presented. The skin depth for the semi-infinite barrier-rock porous structure is presented in the presence of a step-bottom. Finally, the comparative study is performed between four different types of porous structures in the presence of step-bottom considering variable breakwater porosity.

In Chapter 4, the wave reflection, transmission, and energy damping due to single and multiple porous structures are examined considering horizontal variable porosity using the eigenfunction expansion method. Initially, the series of horizontal two-layer porous

structures are examined considering the finite spacing between the structures. Further, the study is extended for three-layer horizontal porous media, and the bottom layer is considered as impermeable, which replaces the natural seabed variation and also regarded as an artificial impermeable layer. Thereafter, the submerged two-layered porous structure is investigated considering free surface wave motion along with the porous layer placed on the bottom impermeable layer. The dispersion relation is solved for the two-layered fully-extended/submerged porous structure. The effect of multiple porosities, porous layer depth, angle of contact, bottom layer height, the free spacing between the multiple structures, structural width, number of structures, and dimensionless wave number on wave scattering is presented. The number of porous structures is limited to five (in the case of two-layered and three-layered structure) and a comparative study is performed between the single and multiple structures. Finally, the wave transformation is reported for single and two submerged two-layered structures for fixed and variable structural width.

In Chapter 5, the wave trapping by various seawalls away from horizontal two-layer and three-layer porous structures are examined. Three types of seawalls such as (a) vertical wall (b) semi-infinite permeable wall and (c) stepped seawall are considered and analysed. The wave reflection, transmission, and wave damping by various types of porous structures are analysed and validated with the available experimental and theoretical results. The harmonic peaks and troughs in wave transformation due to the presence of a series of porous structures and wave trapping in free spacing is reported in detail. The effect of the generation of clapotis due to fluid resonance is also discussed. The effective wave trapping points, cushion effect, critical angle, critical width is discussed for the design and development of stratified porous structures.

In Chapter 6, the vertically stratified porous structure placed on the uniform seabed, elevated seabed, and stepped seabed conditions are examined. The stratified porous structure is examined for three different configurations such as (a) stratified porous structure with finite thickness (b) porous structure backed by the rigid wall and (c) porous structure placed far away from the rigid wall. The study is performed for nine different conditions (three different structures placed on three different seabed characteristics) based on linearized wave theory using finite water depth and long-wave

approximation. The closed-form solution is presented for the stratified porous structure and it is used for all the individual structural configurations. The direct analytical relations are presented for two-layer and three-layer stratified porous structures in the presence of a leeward wall. As a special case, the wave scattering by submerged stepped and elevated seabed is presented and compared with the porous structure. The study results are validated with experimental results available in the literature. Finally, the significance of multiple porosities, friction factors, angle of incidence, structural width and trapping chamber length on wave scattering and wave trapping is investigated in the presence of vertically stratified porous structure lying on the uniform, elevated and stepped seabed conditions.

Finally, Chapter 7 summarizes the work performed in the thesis followed by the future scope of research. Major contributions made in the thesis are also highlighted.

## **1.7 FUNDAMENTALS OF WAVES AND POROUS STRUCTURES**

In order to analyze the fluid-structure interaction problem, certain physical assumptions are made to formulate the mathematical model of the physical problem. In this Section, the basic equation for the wave theory and the basic equations for the porous structure along with the boundary conditions related to the present research work is discussed in brief.

### **1.7.1 Basic equations of wave motion**

The fluid is considered to be irrotational motion, inviscid and incompressible which is bounded above the free surface and is under the action of gravity and constant atmospheric pressure. The monochromatic wave is assumed to act along the positive  $x$ -axis. A 3D Cartesian coordinate system is considered, which has a longitudinal  $x$ -axis and the  $y$ -axis is vertically downwards positive. The fluid is bounded below by the smooth rigid bottom surface of uniform depth  $h$  in the case of finite and shallow water depth and the fluid is of infinite horizontal extent in both the cases. The fluid occupies the infinite strip  $-\infty < x, z < \infty$ ,  $0 < y < h$  in both the cases of fluid of finite and shallow depth as in Figure 1.2. Under the assumption of the fluid to be irrotational motion, inviscid and incompressible as mentioned above, we have the existence of a velocity potential  $\Phi(x, y, z, t)$  which satisfies the Laplace equation given by

$$\frac{\partial^2 \Phi_j}{\partial x^2} + \frac{\partial^2 \Phi_j}{\partial y^2} + \frac{\partial^2 \Phi_j}{\partial z^2} = 0 \text{ at } -\infty < x, z < \infty, 0 < y < h. \quad (1.1)$$

In the wave structure interaction problems, the governing equation is the two/three-dimensional Laplace equation as mentioned above. Next, we will discuss the various types of boundary conditions which arise in the wave structure interaction problems.

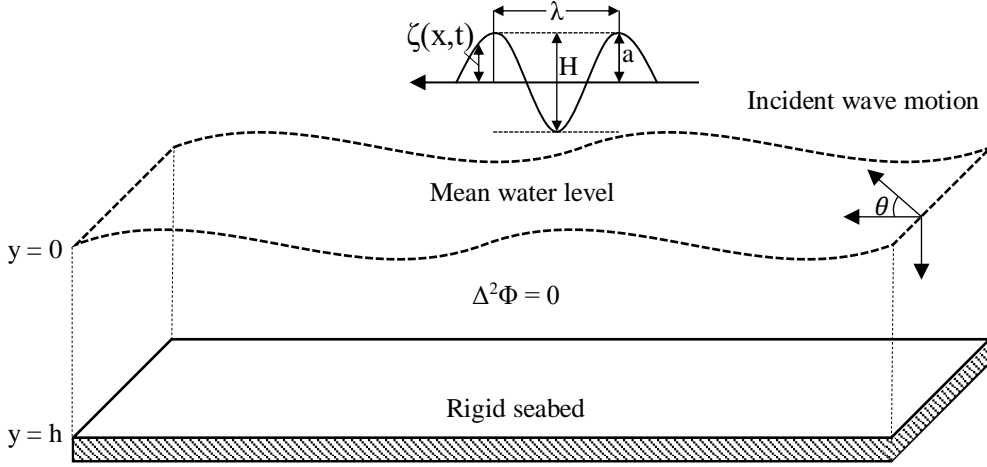


Figure 1.2: Schematic diagram for incident wave propagation.

### 1.7.2 Kinematic Free Surface Boundary Condition (KFSBC)

Let us consider  $F(x, y, z, t) = 0$  to be the surface that constitutes a fixed or moving boundary. Then, the kinematic boundary condition is derived based on the assumption that there is no gap across the surface/interface, which yields

$$\frac{DF}{Dt} = 0, \quad (1.2)$$

where  $D/Dt$  represents the material derivative, which is a combination of time and space derivatives and is given by

$$\frac{D}{Dt} \equiv \partial_t + u\partial_x + v\partial_y + w\partial_z, \quad (1.3)$$

where  $u, v$  and  $w$  being the  $x, y$  and  $z$ -components of the fluid velocity  $V$ . In the context of water waves, we have two surfaces namely (i) the bottom surface and (ii) the free surface. In general, the bottom boundary surface is described as  $y = h(x, z, t)$ , where the origin is at the mean free surface  $y = 0$  and  $h(x, z, t)$  represents the water

depth. In the context of the present work, the bottom surface is assumed to be impermeable and is given by  $F(x, y, z, t) = y - h(x, z, t)$ . Thus, a similar assumption that there is no gap between the bottom surface and the fluid at  $y = h(x, z, t)$  yields

$$\{\partial_t + u\partial_x + w\partial_z\}h - v = 0. \quad (1.4)$$

On the other hand, in the case of water of finite depth, i.e., for  $y = h$ , the bottom boundary condition is given by

$$\frac{\partial\Phi}{\partial y} = 0 \text{ at } y = h. \quad (1.5)$$

Similarly, the free surface of a wave can be described as  $F(x, y, z, t) = y - \zeta(x, z, t)$ , where  $\zeta(x, z, t)$  is the vertical displacement of the free surface about the horizontal plane  $y = 0$  (referred to as the mean free surface). Thus, from the condition (1.2), the kinematic condition on the free surface becomes

$$\zeta_t + \Phi_x \zeta_x + \Phi_z \zeta_z = \Phi_y \text{ on } y = \zeta(x, z, t). \quad (1.6)$$

Next, using the Taylor series expansion, we expand the terms present in the Eq. (1.6) with respect to the mean free surface  $y = 0$ , which yield

$$\left(\Phi_y - \zeta_t - \Phi_x \zeta_x - \Phi_z \zeta_z\right)\Big|_{y=0} + \zeta \partial_y \left(\Phi_y - \zeta_t - \Phi_x \zeta_x - \Phi_z \zeta_z\right)\Big|_{y=0} + \dots = 0. \quad (1.7)$$

Under the assumptions of the linearized theory of water waves, the velocity of the water particles, the free surface elevation  $\zeta(x, z, t)$  and their derivatives are small quantities, which yield that the product and square terms of  $\zeta$  and  $\Phi$  are very small. Hence, neglecting the product, square and higher powers of the dependent variables  $\zeta$  and  $\Phi$ , the linearized kinematic condition on the mean free surface  $y = 0$  is obtained as

$$\zeta_t = \Phi_y \text{ on } y = 0. \quad (1.8)$$

### 1.7.3 Dynamic free surface boundary condition (DFSBC)

A fixed surface like rigid bottom topography can support the pressure variation, whereas the free surface like the air-water interface cannot support the variations in pressure. Thus, a second boundary condition is required to describe the pressure

distribution on the free surface boundary, which is called the dynamic free surface boundary condition. The dynamic free surface boundary condition is derived under the assumption that on the free surface  $y = \zeta(x, z, t)$ , the hydrodynamic pressure is the same as the atmospheric pressure. Thus, from Bernoulli's equation, we have

$$\Phi_t + \left\{ \Phi_x^2 + \Phi_y^2 + \Phi_z^2 \right\} - gy - \frac{P}{\rho}, \text{ on } y = \zeta(x, z, t), \quad (1.9)$$

where  $P$  is the atmospheric pressure, which is assumed to be constant and is taken as  $P = 0$  without loss of generality. It may be noted that in the dynamic condition on the free surface, the effect of surface tension is neglected. Proceeding in a similar manner as in Eq. (1.6), the Taylor series expansion of the terms present in Eq. (1.8) with respect to the mean free surface  $y = 0$  yields

$$\left[ \Phi_t + \frac{1}{2} \left\{ \Phi_x^2 + \Phi_y^2 + \Phi_z^2 \right\} - gy \right]_{y=0} + \zeta \partial_y \left[ \Phi_t + \frac{1}{2} \left\{ \Phi_x^2 + \Phi_y^2 + \Phi_z^2 \right\} - gy \right]_{y=0} + \dots = 0. \quad (1.10)$$

Proceeding with similar assumption as in case of the kinematic condition (1.6), here also we neglect the product, square and higher powers of the dependent variables  $\zeta$  and  $\Phi$ , to obtain the linearized dynamic free surface condition on the mean free surface  $y = 0$  as given by

$$\Phi_t = g\zeta \text{ on } y = 0. \quad (1.11)$$

It may be noted that these linearized forms in Eqs. (1.7) and (1.9) can also be obtained by using a perturbation series expansion for  $\zeta$  and  $\Phi$ , as in Stoker (1957). Eliminating  $\zeta$  from the Eqs. (1.7) and (1.9), we arrive at the boundary condition on the mean free surface as given by

$$\Phi_{tt} = g\Phi_y \text{ on } y = 0. \quad (1.12)$$

Once,  $\Phi$  is obtained,  $\zeta(x, z, t)$  can be computed from any one of the Eqs. (1.8) and (1.11). Assuming that the fluid motion is simple harmonic in time with angular frequency  $\omega$ , the velocity potential  $\Phi(x, y, z, t)$  and the surface elevation  $\zeta(x, z, t)$  can be written in the form  $\Phi(x, y, z, t) = \text{Re} \left\{ \phi(x, y, z) e^{-i\omega t} \right\}$  and  $\zeta(x, z, t) = \text{Re} \left\{ \eta(x, z) e^{-i\omega t} \right\}$



Thus, the spatial velocity potential  $\phi(x, y, z)$  satisfies the Laplace Eq. (1.1) and the bottom boundary condition (1.5). However, the linearized free surface boundary condition (1.11) yields

$$\phi_y + K\phi = 0 \text{ at } y = 0, \quad (1.13)$$

where  $K = \omega^2/g$ . The condition (1.11) represents the free surface condition in the absence of surface tension in the linearized theory of surface water waves of homogeneous density having a free surface.

#### 1.7.4 Velocity potential, surface elevation and dispersion relation

In the case of obliquely incident surface waves, the water surface profile associated with a monochromatic progressive wave is in general given by

$$\zeta(x, z, t) = \frac{H}{2} \cos\{k_x x + k_z z - \omega t\}, \quad (1.14)$$

where  $H$  is water depth,  $k$  ( $k = 2\pi/\lambda$ ) is wavenumber,  $\lambda$  is wavelength,  $\omega$  ( $= 2\pi/T$ ) is angular frequency,  $T$  is wave period,  $k_x = k \cos \theta$  and  $k_z = k \sin \theta$  with  $\theta$  being the angle made by the wave with the positive  $x$ -axis. The corresponding velocity potential is  $\Phi(x, y, z, t)$  satisfying the governing Eq. (1.1) along with the bottom boundary condition (1.5a) and the linearized free surface condition (1.11) is expressed as

$$\Phi(x, y, z, t) = \frac{H}{2} \frac{g}{\omega} \frac{\cosh k(h-y)}{\cosh kh} \sin\{(k_x)x + (k_z)z - \omega t\}, \quad (1.15)$$

where  $k$  and  $\omega$  are related by the dispersion relation given by

$$\omega^2 = gk \tanh kh. \quad (1.16)$$

Now we make a note on wave classification which is based on relative water depth  $h/\lambda$ . The waves are called shallow-water waves or long waves if  $h/\lambda < 1/20$  and for  $h/\lambda > 1/2$ , the waves are called deep water waves. In the intermediate range  $1/20 < h/\lambda < 1/2$ , the waves are termed as the intermediate depth waves. The dispersion relation for shallow water reduces to  $\omega^2 = gk^2 h$  and in case of deep water waves, it is given by  $\omega^2 = gk$ .

### 1.7.5 Far-field boundary condition

In the case of a BVP defined in an infinite/semi-infinite domain, the uniqueness of the solution demands the behaviour of the function at the far-field. In the case of water wave problems, often the fluid domains are either the half/quarter-planes or infinite/semi-infinite strips depending on whether the problem is considered in the water of infinite or finite depths. Without going into theoretical details, we will prescribe the far-field boundary conditions in the case of plane progressive waves as given by

$$\Phi(x, y, z, t) \sim \left\{ Ae^{i(k_x x + k_z z - \omega t)} + Be^{-i(k_x x + k_z z + \omega t)} \right\} \frac{\cosh k(h-y)}{\cosh kh}, \quad x, z \rightarrow \pm\infty, \quad (1.17)$$

in the case of finite depth and

$$\Phi(x, y, z, t) \sim \left\{ Ae^{i(k_x x + k_z z - \omega t)} + Be^{-i(k_x x + k_z z + \omega t)} \right\}, \quad x, z \rightarrow \pm\infty, \quad (1.18)$$

in the case of shallow depth.

In the above conditions,  $A$  and  $B$  are constants associated with the wave amplitudes at the far-field and depend upon the physical nature of the problem.

### 1.7.6 Wave action analysis of porous structures

The oblique wave transport through porous breakwater in the form of boundary conditions associated with the open water region and breakwater occupied regions are discussed. Figures 1.3 and 1.4 show the wave motion through barrier-rock porous structure and horizontally stratified porous structure. In each of the fluid region, the linearized free surface boundary condition at still water level for  $j = 1, 2, 3$  is given by

$$\frac{\partial \phi_j(x, y)}{\partial y} + K_j \phi_j(x, y) = 0 \quad \text{at } y = 0, \quad (1.19)$$

where  $K_{1,3} = \omega^2/g$  in the case of open water region and  $K_2 = \omega^2(S + if)/g$  in the case of porous structure region. The bottom boundary condition is given by

$$\frac{\partial \phi_j(x, y)}{\partial y} = 0 \quad \text{at } y = h_j \text{ for } j = 1, 2, 3. \quad (1.20)$$

The flow of fluid is partially obstructed due to the presence of a porous structure. Thus there exists a pressure difference between the porous structure and open water regions.

The permeability of porous structure plays a significant role in the pressure difference between the two subsequent regions. The celerity of fluid through the porous structure is a function of the dynamic pressure difference between the subsequent regions and dynamic pressure is a function of velocity potential.

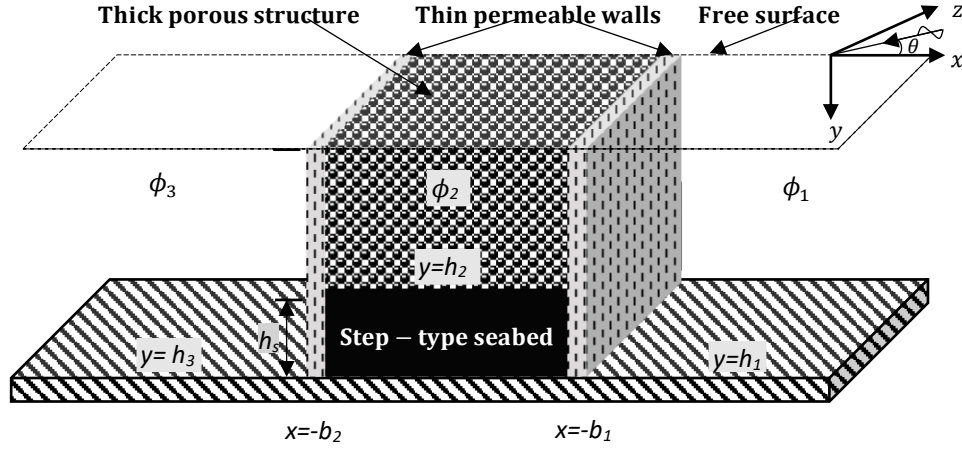


Figure 1.3: Wave motion through the barrier-rock porous structure.

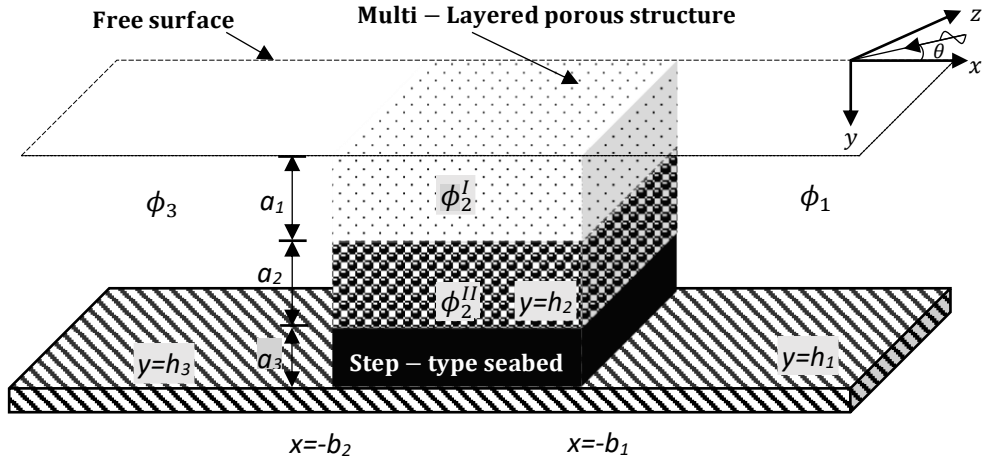


Figure 1.4: Wave motion through a horizontally stratified porous structure.

The ideal condition is employed to satisfy the continuity of dynamic pressure and mass flux at the common boundaries and is given by

$$\phi_1(x, y) = G\phi_2(x, y) \quad \text{and} \quad \phi_{1x}(x, y) = \varepsilon\phi_{2x}(x, y) \quad \text{at} \quad x = -b_1, \quad 0 < y < h_2, \quad (1.21)$$

$$G\phi_2(x, y) = \phi_3(x, y) \quad \text{and} \quad \varepsilon\phi_{2x}(x, y) = \phi_{3x}(x, y) \quad \text{at} \quad x = -b_2, \quad 0 < y < h_2, \quad (1.22)$$

where  $\varepsilon$  is the porosity of the structure,  $G = S + if$  is the impedance of the porous medium,  $f$  is the linearized friction factor,  $i$  imaginary number and  $S$  is the medium reactance. It may be noted that in the case of porosity of the structure  $\varepsilon = 1$  and friction factor  $f = 0$ , the porous structure region changes into the open water region. Hence, all the boundary conditions, dispersion relation pertaining to porous structure automatically satisfy the open water wave motion. In the case of barrier-rock porous structure (Figure 1.3), the continuity of dynamic pressure and mass flux at the common boundaries (Isaacson et al., 2000; Karmakar et al., 2013; Karmakar and Guedes Soares 2014, 2015) are given by

$$\frac{\partial \phi_1(x, y)}{\partial x} = \varepsilon_b \frac{\partial \phi_2(x, y)}{\partial x} = i\gamma_{10} G_1 [(S_b - if_b)\phi_2(x, y) - \phi_1(x, y)] \quad \text{at } x = -a_1 \quad (1.23)$$

$$\frac{\partial \phi_3(x, y)}{\partial x} = \varepsilon_b \frac{\partial \phi_2(x, y)}{\partial x} = i\gamma_{30} G_2 [\phi_3(x, y) - (S_b - if_b)\phi_2(x, y)] \quad \text{at } x = -a_2 \quad (1.24)$$

where  $\varepsilon_b$  breakwater porosity,  $G_j$  for  $j = 1, 2$  is porous effect parameter of seaward and leeward vertical porous barriers respectively of the form

$$G_j = \frac{\varepsilon_{a(b)}}{\gamma_{10} d_{a(b)} (f_{a(b)} - iS_{a(b)})} \quad (1.25)$$

where  $d_{a(b)}$  is thickness  $\varepsilon_{a(b)}$  is porosity,  $f_{a(b)}$  is resistance and  $S_{a(b)}$  is the reactance of seaward and leeward barriers respectively.

In the case horizontally stratified porous structure (Figure 1.4), there exists a flow within the multiple porous layers ( $j = 2, 4, \dots, 2N$ ) in the vertical direction (Losada et al., 1996; Liu et al., 2007), which is defined as

$$(S_1 + if_1)\phi_2^I(x, y) = (S_2 + if_2)\phi_2^{II}(x, y) \quad \text{on } y = a_1, \quad (1.26)$$

$$\varepsilon_1 \frac{\partial \phi_2^I(x, y)}{\partial y} = \varepsilon_2 \frac{\partial \phi_2^{II}(x, y)}{\partial y} \quad \text{on } y = a_1. \quad (1.27)$$

To model the continuity of pressure and continuity velocity due to the existence of the two-layer and three-layer porous breakwaters (Figure 1.4), the boundary conditions are given by

$$\phi_1(x, y) = \begin{cases} (S_1 + if_1)\phi_2'(x, y) \\ (S_2 + if_2)\phi_2''(x, y) \end{cases} \text{ and } \frac{\partial \phi_1(x, y)}{\partial x} = \begin{cases} \varepsilon_1 \frac{\partial \phi_2'(x, y)}{\partial x} \\ \varepsilon_2 \frac{\partial \phi_2''(x, y)}{\partial x} \end{cases} \text{ on } x = -b_1, \quad (1.28)$$

$$\phi_3(x, y) = \begin{cases} (S_1 + if_1)\phi_2'(x, y) \\ (S_2 + if_2)\phi_2''(x, y) \end{cases} \text{ and } \frac{\partial \phi_3(x, y)}{\partial x} = \begin{cases} \varepsilon_1 \frac{\partial \phi_2'(x, y)}{\partial x} \\ \varepsilon_2 \frac{\partial \phi_2''(x, y)}{\partial x} \end{cases} \text{ on } x = -b_2, \quad (1.29)$$

where  $\varepsilon_1, \varepsilon_2$  are the surface and bottom layer porosity,  $f_1, f_2$  are the surface and bottom layer friction factors,  $S_1, S_2$  are the surface and bottom layer inertia effect. In the case of the submerged two-layered porous structure, the  $\varepsilon_1 = 1$  and  $f_1 = 0$  due to the absence of the surface porous layer, which is treated as a free surface region. The velocity near to the elevated step is given by

$$\phi_{1x}(x, y) = 0 \text{ at } x = -b_1, h_2 < y < h_1, \quad (1.30)$$

$$\phi_{3x}(x, y) = 0 \text{ at } x = -b_2, h_2 < y < h_3. \quad (1.31)$$

The partial wave reflection due to the presence of the rear wall (Isaacson and Qu, 1990, Elchahal et al., 2008) is given by

$$\frac{\partial \phi_j(x, y)}{\partial x} = i \left( \frac{1 - C_R}{1 + C_R} \right) k_{j0} \phi_j(x, y) \text{ at } x = -b_j, j = 2, 3. \quad (1.32)$$

where  $\phi_j$  implies the velocity potential near to the vertical wall,  $C_R$  is the reflection coefficient due to the wall varying within  $0 \leq C_R \leq 1$ . In the case of  $C_R = 0$  suggests that, the complete wave energy is dissipated due to the rear wall and  $C_R = 1$  suggests the zero velocity at the wall as in Dalrymple et al. (1991), Das and Bora (2014d). The no-flow condition due to the presence of impermeable wall is given by

$$\frac{\partial \phi_j(x, y)}{\partial x} = 0 \text{ at } x = -b_j, 0 < y < h_j \text{ for } j = 2, 3. \quad (1.33)$$

The medium reactance and resistance representing the inertial effect and friction factor of the porous medium (Sollitt and Cross, 1972; Chwang and Chan, 1998) is given by

$$S = 1 + A_m \left[ \frac{1 - \varepsilon}{\varepsilon} \right], \quad (1.34)$$

$$f = \frac{1}{\omega} \left\{ \frac{\int_V dV \int_t^{t+T} \varepsilon^2 \left( \frac{\nu q^2}{K_p} + \frac{C_f \varepsilon}{\sqrt{K_p}} |q|^3 \right) dt}{\int_V dV \int_t^{t+T} \varepsilon q^2 dt} \right\}, \quad (1.35)$$

where  $A_m$  is added mass coefficient in the surface and bottom porous layers,  $\omega$  is wave frequency,  $K_{ip}$  is intrinsic permeability having  $K_{ip} / h_1^2 = 0.95 * 10^{-6}$ ,  $0.22 * 10^{-5}$  and  $0.345 * 10^{-5}$  (Twu and Liu, 2004)  $q_i$  is instantaneous Eulerian velocity vector,  $C_f = 0.228$  is a turbulent resistant coefficient (Twu and Liu, 2004),  $\nu$  is the kinematic viscosity,  $V$  is the volume and  $T$  is the wave period. The inertia effect is kept fixed  $s_1 = s_2 = 1$  throughout the analytical study (Sollitt and Cross, 1972; Yu and Chwang, 1994; Liu and Li, 2013) the friction factor, layer porosity and wavelength are similar as in Twu and Liu (2004).

### 1.7.7 Dispersion relations in the open water and porous structure regions

The wavenumber  $\gamma_{j0}$  for  $j=1,3$  is the positive real roots satisfies the conventional dispersion relation given by

$$\omega^2 = g \gamma_{j0} \tanh \gamma_{j0} h_j. \quad (1.36)$$

The wavenumber  $\gamma_{20}$  satisfy the porous structure dispersion relation given by

$$\omega^2 (S + if) = g \gamma_{20} \tanh \gamma_{20} h_2. \quad (1.37)$$

In the case of the long-wave approximation, the dispersion relations (Dalrymple et al., 1991) are given by

$$\omega^2 = g \gamma_{j0}^2 h_j \text{ for } j=1,3 \text{ and } \omega^2 (S + if) = g \gamma_{20}^2 h_2. \quad (1.38)$$

where  $\omega$  is wave frequency,  $g$  is the acceleration due to gravity,  $\gamma_{j0}$  is progressive wave number and  $h_j$  for  $j=1,2,3$  is the water depth in open water and porous structure regions. The wavenumber  $\gamma_{j0}$  for  $j=1,3$ , in the free surface region and the wavenumber  $\gamma_{20}$  in the two/three-layered (Figure 1.4) porous structure region satisfies the dispersion relations given by

$$\omega^2 = g\gamma_{j0} \tanh \gamma_{j0} h_j, \text{ for } j=1,3, \quad (1.39)$$

$$(S_1 + if_1)\omega^2 - g\gamma_{j0} \tanh \gamma_{j0} h_j = P_n \left[ (S_1 + if_1)\omega^2 \tanh \gamma_{j0} h_j - g\gamma_{j0} \right], \quad (1.40)$$

where  $P_n = \left[ \left( 1 - \frac{\varepsilon_2(S_1 + if_1)}{\varepsilon_1(S_2 + if_2)} \right) \tanh \gamma_{20} a_2 \right] / \left[ 1 - \frac{\varepsilon_2(S_1 + if_1)}{\varepsilon_1(S_2 + if_2)} \tanh^2 \gamma_{20} a_2 \right]$ . In the case

of the two-layered submerged porous structure, the surface layer behaves as open water region by considering the surface porosity  $\varepsilon_1 = 1$  and friction factor  $f_1 = 0$ . The dispersion relation for the submerged two-layer porous structure region (submerged porous layer placed on the elevated rigid layer) is given by

$$\omega^2 - g\gamma_{j0} \tanh \gamma_{j0} h_j = P_n \left[ \omega^2 \tanh \gamma_{j0} h_j - g\gamma_{j0} \right], \quad (1.41)$$

where  $P_n = \left[ \left( 1 - \frac{\varepsilon_2}{(S_2 + if_2)} \right) \tanh \gamma_{20} a_2 \right] / \left[ 1 - \frac{\varepsilon_2}{(S_2 + if_2)} \tanh^2 \gamma_{20} a_2 \right]$ , which is similar

as in Losada et al. (1996) and Koley et al. (2014).

### 1.7.8 Perturbation method

The roots of the dispersion relation play a significant role in the analysis of wave damping by porous breakwaters. In general, the dispersion relations for various structural configurations such as fully-extended porous structure, horizontally stratified porous structure, and submerged porous structure are different due to change in free surface boundary conditions. The solving procedure of open water region dispersion relation is well reported in the literature using the Newton-Raphson method (Das and Bora, 2014a). The perturbation scheme given by Mendez and Losada (2004) is used to find the root of the porous structure dispersion relation given by

$$F(K, \psi) = \psi \Gamma \tanh \Gamma - Kh_2 = 0 \quad (1.42)$$

where  $\psi = \frac{1}{S + if}$ ,  $K = \frac{\omega^2}{g}$ , and  $\Gamma = \gamma_2 h_2$ .

According to the perturbation approach, a little perturbation  $\delta\psi$  in  $\psi$  will result in a small change in  $\delta\Gamma$  in the dimensionless wavenumber  $\Gamma$ . The explicit form of  $\delta\Gamma$  is given by

$$\delta\Gamma = -\delta\psi \frac{(\partial F/\partial\psi)}{(\partial F/\partial\Gamma)} \quad (1.43)$$

The following iterative method is used to find  $\Gamma$  for the given  $\psi$  :

- The  $\delta\psi = (\psi - \psi_0)/N_1$  where  $N_1$  is the number of steps.
- Calculate  $\delta\Gamma_i$  using Eq. (1.43) as a function of  $\Gamma_{i-1}$ ,  $\psi_{i-1}$  and  $\delta\psi$ .
- Find the  $\Gamma_i$  using  $\Gamma_i = \Gamma_{i-1} + \delta\Gamma_i$ .
- Repeat the procedure to determine the  $\psi = \psi_{N_1} = \psi_{N_1-1} + \delta\psi$ .

A number of  $N_1 = 40$  iterations were suggested by Mendez and Losada (2004), Das and Bora (2014a,b) to minimize the error to find the accurate roots of the porous structure dispersion relation.

In the present study, the final values given by the perturbation scheme are used as the initial guess for finding the roots of dispersion for submerged porous structures and two-layered porous structures using Newton-Raphson method to achieve very accurate roots with negligible error. If  $\psi_0 = 1$ , which transforms the porous structure dispersion relation into open water dispersion relation. The Newton-Raphson method is used for finding the roots of the dispersion relation.

### 1.7.9 Solution approach for finding the roots of dispersion relation

In general, the root-finding process for the two-layered porous structure is complicated due to the presence of imaginary values. The dispersion relation for the two-layered porous structure is given by

$$(S_1 + if_1)\omega^2 - g\gamma_{2n} \tanh \gamma_{2n} h_2 = P_n \left[ (S_1 + if_1)\omega^2 \tanh \gamma_{2n} h_2 - g\gamma_{2n} \right] \quad (1.44)$$

where  $P_n = \left[ \left( 1 - \frac{\varepsilon_2 (S_1 + if_1)}{\varepsilon_1 (S_2 + if_2)} \right) \tanh \gamma_{jn} a_2 \right] / \left[ 1 - \frac{\varepsilon_2 (S_1 + if_1)}{\varepsilon_1 (S_2 + if_2)} \tanh^2 \gamma_{jn} a_2 \right]$ .

In addition, the dispersion relation for the two-layered porous structure is simplified in the following form given by

$$(S_1 + if_1)\Delta - \Upsilon \tanh \beta\Upsilon = \varphi \left[ \Upsilon - (S_1 + if_1)\Delta \tanh \beta\Upsilon \right] \tanh \alpha\Upsilon, \quad (1.45)$$



where  $\Delta = \frac{\omega^2 h_2}{g}$ ,  $\beta = \frac{a_2}{h_2}$ ,  $\alpha = \frac{a_1}{h_2}$ ,  $\Upsilon = \gamma_{2n} h_2$ ,  $\varphi = \frac{\varepsilon_2 (S_1 + if_1)}{\varepsilon_1 (S_2 + if_2)}$ . In the case of the single-layer porous structure, the  $\varepsilon_1 = \varepsilon_2 = \varepsilon$ ,  $S_1 = S_2 = S$  and  $f_1 = f_2 = f$ . Hence, the two-layered porous structure dispersion relation reduces to the complex single-layered porous structure dispersion relation given by

$$\omega^2 (S + if) = g \gamma_{jn} \tanh \gamma_{jn} h_j \quad (1.46)$$

On considering the surface layer porosity  $\varepsilon_1 = 1$  and friction factor  $f_1 = 0$  in Eq. (1.45), the two-layered fully-extended porous structure dispersion relation reduces to submerged porous structure dispersion relation.

Table. 1.1: Roots of the two-layered ( $\varepsilon_1 = 0.8, f_1 = 0.4$ ) and submerged two-layered ( $\varepsilon_1 = 1, f_1 = 0$ ) dispersion relation considering  $a_1 / h_2 = 0.5$ ,  $a_2 / h_2 = 0.5$ ,  $a_3 / h_1 = 0.2$ ,  $\varepsilon_2 = 0.5$ ,  $f_2 = 1$ ,  $S_1 = S_2 = 1$ ,  $\theta = 20^\circ$  and  $h_1 / \lambda = 0.1$ .

Evanescent waves	Two and three-layer porous structure		Submerged two-layer porous structure	
	Root	Error	Root	Error
$M = 0$	0.0810 + 0.0221i	3.4792*10 <sup>-17</sup>	0.0854 + 0.0078i	1.8440*10 <sup>-17</sup>
$M = 1$	0.0041 + 0.7781i	8.0531*10 <sup>-16</sup>	0.0018 + 0.7767i	1.7743*10 <sup>-16</sup>
$M = 2$	0.0020 + 1.5672i	5.5612*10 <sup>-15</sup>	0.0009 + 1.5665i	4.9881*10 <sup>-15</sup>
$M = 3$	0.0014 + 2.3538i	1.1422*10 <sup>-14</sup>	0.0006 + 2.3533i	3.2745*10 <sup>-16</sup>
$M = 4$	0.0010 + 3.1398i	5.7771*10 <sup>-15</sup>	0.0004 + 3.1394i	2.0345*10 <sup>-14</sup>
$M = 5$	0.0008 + 3.9255i	2.1287*10 <sup>-14</sup>	0.0003 + 3.9253i	2.5881*10 <sup>-14</sup>
$M = 6$	0.0007 + 4.7112i	9.2078*10 <sup>-14</sup>	0.0003 + 4.7110i	5.1238*10 <sup>-14</sup>
$M = 7$	0.0006 + 5.4968i	3.4792*10 <sup>-17</sup>	0.0002 + 5.4966i	1.7347*10 <sup>-17</sup>

In the previous studies, numerous authors reported various methods such as Newton-Raphson method, perturbation scheme and contour plots (Sollitt and Cross, 1972; Dalrymple et al., 1991; Yu and Chwang, 1994; Mendez and Losada, 2004; Liu et al., 2007; Behera and Sahoo, 2014; Das and Bora, 2014; Zhao et al., 2017) for finding multiple roots of the complex dispersion relation. In the present study, the Newton-Raphson method is used for finding the roots of the two-layered porous structure dispersion relation and the perturbation scheme as in Mendez and Losada (2004) is used for finding the initial values for fast convergence. The multiple roots for the two-layered

fully-extended and the submerged porous structure are given in Table 1.1 for a specific structural configuration.

## **1.8 CLOSURE**

In this chapter, a brief introduction to wave scattering and wave trapping by barrier-rock porous structure and the stratified porous structure is presented. The importance and need of a porous structure in the offshore and nearshore regions are discussed in detail. A detailed review of literature is performed for wave scattering and wave trapping by porous structures and seawalls. The research gaps and necessity of the stratification concept in the porous structure are reviewed. The basic theory of water waves along with the wave motion through porous structures using matching equations associated edge conditions is presented. The solving procedure of complex dispersion relation is reported. The perturbation method and Newton-Raphson methods used for finding the roots of the fully-extended, submerged and two-layer porous structure dispersion relations are discussed in detail.

## CHAPTER 2

# WAVE DISSIPATING PERFORMANCE OF MULTIPLE POROUS STRUCTURES

### 2.1 GENERAL INTRODUCTION

Coastal protection is an essential phenomenon for the country's growth and development. In most of the situations, the unprecedented gravity waves cause huge losses to the coastline and offshore facilities. To protect the coastline and coastal facilities from gravity wave action, coastal regions require coastal defences like porous plates, thin barriers, permeable and impermeable breakwaters. The porous structure can be one of the better solutions for wave energy dissipation and widely used in the coastal areas to protect the harbours, wharfs, coastal cliffs, mainlands, islands and beaches from wave trains. Porous structures are easy to construct without affecting the coastal aesthetic and allows the incident waves to get transmitted through the structure, which causes the energy dissipation. So, the porosity decreases the resultant force impact acting on the structure and reduces the wave energy on the leeward side. Various countries such as India, Japan, the United States, China, Canada, Australia, and European countries implemented permeable breakwaters for providing better sheltering to the mainlands from the action of gravity waves. Gudong and Zhuangxi Sea Dike in the Shengli Oilfield at Republic of China (Zhao et al., 2017) developed submerged porous structures. Dieppe in France (Belorgey et al., 2003) and Dalian Chemical Production Terminal in the Republic of China (Huang et al., 2011) constructed the permeable wall to regulate the wave action.

The study on wave motion through the bottom-mounted porous structures and porous screens with leeside wall are well documented in the literature, but the very limited study on wave propagation through multiple fully extended porous structures placed on flat/elevated seabed with leeside unbounded region and confined region/leeward wall is performed. The present study elaborates on the oblique wave scattering due to multiple fully-extended porous structures considering the leeward unbounded region and confined region using matched eigenfunction expansion method. Further, the wave

scattering and trapping are presented for multiple porous structures placed on the single and multi-step impermeable bottom. The significance of porous structure considering various ranges of porosity, friction factor, the finite spacing between the structures, structural thickness, and angle of wave incidence are discussed and analysed.

## 2.2 MATHEMATICAL FORMULATION

The oblique wave propagation through multiple fully-extended porous structures considering leeward unbounded and confined region placed at finite water depth is examined under the assumption of linearized wave theory. A three-dimensional coordinate system is considered in the analysis with  $x - z$  being a horizontal plane and  $y -$  axis being vertically downward positive. The  $2N$  number of porous structures are placed at  $x = -b_j$  for  $j = 1, 2, \dots, 2N$  considering the leeward unbounded region and leeward wall as in Figure 2.1(a,b). The series of porous structures are placed to reduce the wave force impact on the shore and leeward wall. The fluid is assumed to occupy the region  $\bigcup_{j=1}^{2N+1} I_j$  with  $I_j \equiv (-b_j < x < -b_{j-1}, 0 < y < h)$  for  $j = 2, 3, \dots, 2N$  and  $I_1 \equiv (-b_1 < x < \infty, 0 < y < h)$ ,  $I_{2N+1} \equiv (-\infty < x < -b_{2N}, 0 < y < h)$  with  $z \in (-\infty, \infty)$  for all  $I_j$ . The fluid is considered to be inviscid, incompressible, motion is irrotational and simple harmonic in time with angular frequency  $\omega$ . Thus, there exists the velocity potential  $\Phi_j(x, y, z, t)$  and the free surface deflection  $\zeta_j(x, z, t)$  which can be written as  $\Phi_j(x, y, z, t) = \text{Re}\{\phi_j(x, y)e^{ilz - i\omega t}\}$  and  $\zeta_j(x, z, t) = \text{Re}\{\eta_j(x)e^{ilz - i\omega t}\}$  where  $\text{Re}$  is the real part and  $l = \gamma_{10} \sin \theta$  is the component of wave number along the  $z -$  direction,  $\theta$  is the angle of incident on the porous structure at  $x = -b_1$ . The spatial velocity potential,  $\phi_j(x, y)$  for  $j = 1, 2, \dots, (2N + 1)$  satisfies the partial differential equation given by

$$\frac{\partial^2 \phi_j(x, y)}{\partial x^2} + \frac{\partial^2 \phi_j(x, y)}{\partial y^2} - l^2 \phi_j(x, y) = 0, \quad \text{for } 0 < y < h. \quad (2.1)$$

The linearized free surface boundary condition in each of the regions  $I_j$  for  $j = 1, 2, \dots, (2N + 1)$  is given by

$$\frac{\partial \phi_j(x, y)}{\partial y} + K_j \phi_j(x, y) = 0 \quad \text{at } y = 0, \quad (2.2)$$

where  $K_j = \frac{\omega^2}{g}$  for  $j=1,3,\dots,(2N+1)$  in the case of open water region and  $K_j = \frac{\omega^2(S+if)}{g}$  for  $j=2,4,\dots,2N$  in the case of porous structure region.

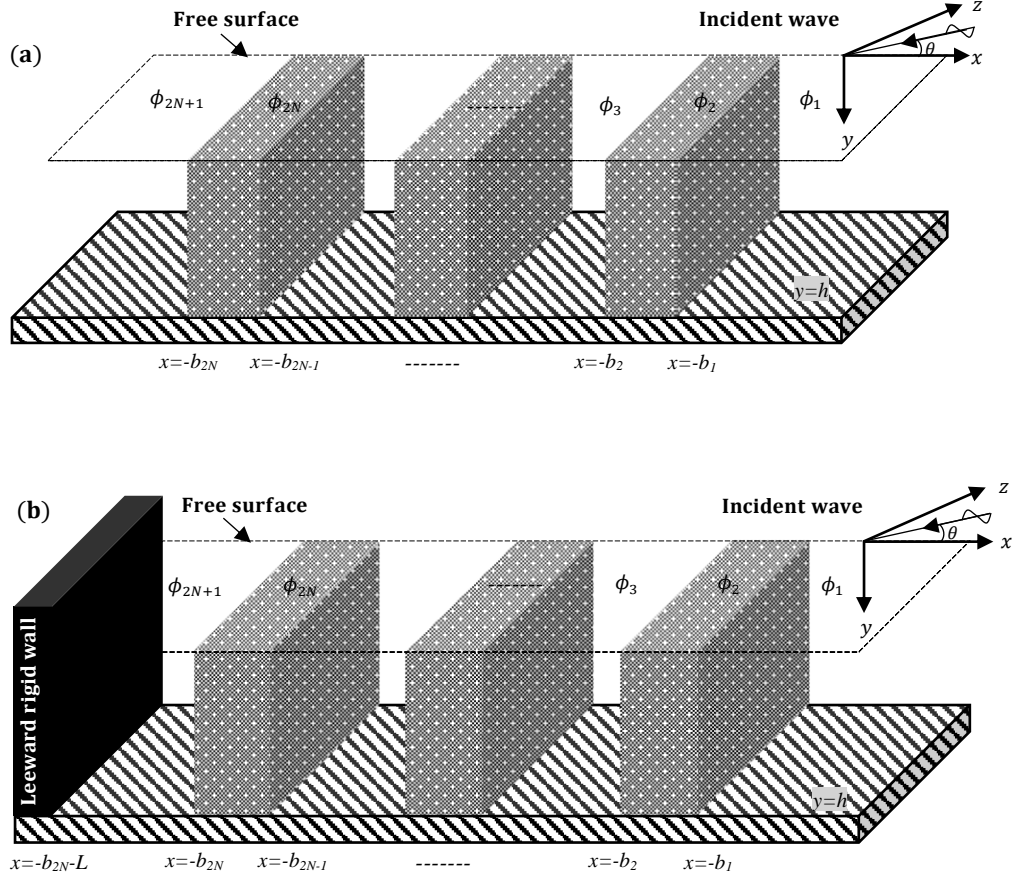


Figure 2.1: Schematic diagram of multiple porous structures with (a) leeward unbounded region and (b) leeward wall/leeward confined region.

The fluid flow over rigid bottom condition is given by

$$\frac{\partial \phi_j(x, y)}{\partial y} = 0 \quad \text{at } y = h. \quad (2.3)$$

The continuity of velocity and pressure at each of the interfaces along the horizontal  $x$  – direction is given by

$$\phi_j(x, y) = G\phi_{(j+1)}(x, y) \quad \text{and} \quad \phi_{jx}(x, y) = \varepsilon\phi_{(j+1)x}(x, y) \quad \text{at } x = -b_j, \quad (2.4a)$$

for  $j = 1, 3, \dots, (2N - 1),$

$$G\phi_j(x, y) = \phi_{(j+1)}(x, y) \quad \text{and} \quad \varepsilon\phi_{jx}(x, y) = \phi_{(j+1)x}(x, y) \quad \text{at } x = -b_j, \quad (2.4b)$$

for  $j = 2, 4, \dots, 2N,$

where  $\varepsilon$  is structural porosity,  $G = S + if$  is the impedance of the porous medium,  $S$  is the inertia coefficient and  $f$  is friction factor (Sollitt and Cross, 1972; Twu and Chieu, 2000), which are computed using the relations given by

$$S = 1 + A_m \left[ \frac{1 - \varepsilon}{\varepsilon} \right], \quad (2.5a)$$

$$f = \frac{\frac{1}{V} \int_V dV \int_t^{t+T} \varepsilon^2 \left( \frac{\nu q^2}{K_p} + \frac{C_f \varepsilon}{\sqrt{K_p}} |q|^3 \right) dt}{\omega \int_V dV \int_t^{t+T} \varepsilon q^2 dt}, \quad (2.5b)$$

where  $A_m$  is a virtual added mass coefficient due to wave impinging on porous structure,  $\nu$  is kinematic viscosity,  $q$  is instantaneous Eulerian velocity vector at any point,  $K_p$  is intrinsic permeability,  $V$  is volume,  $C_f$  is a dimensionless turbulent resistant coefficient and  $T$  is wave period. The medium reactance is usually treated as unity due to the negligible added mass coefficient (Sollitt and Cross, 1972; Liu and Li, 2013) as the structure is in a fixed position. The far-field radiation condition in the absence of leeward wall is of the form

$$\phi_j(x) = \begin{cases} \left( I_{10} e^{-ik_{10}x} + R_{10} e^{ik_{10}x} \right) f_{10}(y) & \text{as } x \rightarrow \infty, \\ \left( T_{(2N+1)0} e^{-ik_{(2N+1)0}x} \right) f_{(2N+1)0}(y) & \text{as } x \rightarrow -\infty, \end{cases} \quad (2.6)$$

with  $I_{10}$  is the incident wave,  $R_{10}$  and  $T_{(2N+1)0}$  are the unknown coefficients explaining reflected and transmitted wave amplitudes.

The wavenumber  $\gamma_{j0}$  satisfy the open water dispersion relation is given by

$$\omega^2 = g \gamma_{j0} \tanh \gamma_{j0} h \quad \text{for } j = 1, 3, \dots, (2N+1). \quad (2.7a)$$

The wavenumber  $\gamma_{j0}$  satisfy the porous structure dispersion relation is given by

$$\omega^2 (S + if) = g \gamma_{j0} \tanh \gamma_{j0} h \quad \text{for } j = 2, 4, \dots, 2N. \quad (2.7b)$$

where  $\omega$  is wave frequency,  $g$  is the acceleration due to gravity,  $\gamma_{j0}$  is a progressive wavenumber in each region at water depth  $h$ . Newton–Raphson method and perturbation technique proposed by Mendez and Losada (2004) are used to solve the dispersion relation for open water and porous structure regions. The no-flow condition near the leeward rigid wall is given by

$$\frac{\partial \phi_{j+1}(x, y)}{\partial x} = 0 \quad \text{at } x = -(b_j + L), \quad j = 2N, \quad (2.8)$$

where  $\phi_{j+1}$  denotes the leeside open water region.

## 2.3 METHOD OF SOLUTION

The oblique wave impinging on multiple porous structures is studied using the eigenfunction expansion approach for the determination of unknown parameters. The study is performed to analyse the multiple fully-extended porous structures considering leeward unbounded and confined regions.

### 2.3.1 Wave transformation by multiple porous structures

The multiple porous structures are often used to provide efficient sheltering to the coastline, ports, and harbours. In the case of multiple fully-extended porous structures, the velocity potentials for open water and porous structure regions are given by

$$\phi_1(x, y) = \left\{ I_{10} e^{-ik_{10}(x+b_1)} + R_{10} e^{ik_{10}(x+b_1)} \right\} f_{10}(y) + \sum_{n=1}^{\infty} \left\{ R_{1n} e^{-\kappa_{1n}(x+b_1)} \right\} f_{1n}(y), \quad (2.9a)$$

for  $-b_1 < x < \infty$ ,

$$\phi_j(x, y) = \sum_{n=0}^{\infty} \left\{ A_{jn} e^{-ik_{jn}(x+b_{j-1})} + B_{jn} e^{ik_{jn}(x+b_j)} \right\} f_{jn}(y) \quad (2.9b)$$

for  $-b_j < x < -b_{j-1}$ ,  $j = 2, 3, \dots, 2N$ ,

$$\phi_{2N+1}(x, y) = \left\{ T_{(2N+1)0} e^{-ik_{(2N+1)0}(x+b_{2N})} \right\} f_{(2N+1)0}(y) + \sum_{n=1}^{\infty} \left\{ T_{(2N+1)n} e^{\kappa_{(2N+1)n}(x+b_{2N})} \right\} f_{(2N+1)n}(y) \quad (2.9c)$$

for  $-\infty < x < -b_{2N}$ ,

where,  $I_{10}$  is the incident wave,  $R_{1n}, A_{jn}, B_{jn}$  and  $T_{(2N+1)n}$  for  $n = 0, 1, 2, 3, \dots$  and  $j = 1, 2, 3, \dots, 2N$  are the unknown constants to be determined,  $d = -(b_{j+1} - b_j)$  for  $j = 1, 2, 3, \dots, 2N$  is the thickness of the porous structure. The eigenfunctions  $f_{jn}(y)$  for the open water and fully-extended porous structure regions are given by

$$f_{jn}(y) = \frac{\cosh \gamma_{jn}(h-y)}{\cosh \gamma_{jn} h} \quad \text{for } n = 0, 1, \dots \quad (2.10)$$

where  $\gamma_{jn}$  for  $j = 1, 2, 3, \dots, (2N+1)$ . The eigenvalues satisfy the open water and porous structure dispersion relations given by

$$\omega^2 = g \gamma_{jn} \tanh \gamma_{jn} h \quad \text{for } j = 1, 3, \dots, (2N+1), \quad n = 0, \quad (2.11a)$$

$$\omega^2 (S + if) = g\gamma_{jn} \tanh \gamma_{jn} h \quad \text{for } j = 2, 4, \dots, 2N, \quad n = 0, 1, 2, \dots \quad (2.11b)$$

with  $\gamma_{jn} = i\gamma_{jn}$  for  $n = 1, 2, 3, \dots$  for open water region. The roots of the dispersion relation for  $j = 1, 2, 3, \dots, (2N + 1)$  satisfying  $\gamma_{jn}^2 = k_{jn}^2 + l^2$ ,  $n = 0$  with  $l = \gamma_{10} \sin \theta$ ,  $\theta$  is the angle of incidence,  $k_{jn}$  being the component of wavenumber in  $x$ -direction and  $\gamma_{jn}$  is the wavenumber in  $y$ -direction. In addition, there are purely imaginary roots  $\gamma_{jn}$  with  $\gamma_{jn}^2 = k_{jn}^2 - l^2$  for  $n = 1, 2, 3, \dots$ . The eigenfunctions in each of the regions  $f_{jm}(y)$ ,  $j = 1, 2, 3, \dots, (2N + 1)$  that satisfy the orthogonality relation of the form

$$\langle f_{jm}, f_{jm} \rangle_{j=1,3,\dots,(2N+1)} = \begin{cases} 0 & \text{for } m \neq n, \\ C'_n & \text{for } m = n, \end{cases} \quad \text{and} \quad \langle f_{jm}, f_{jm} \rangle_{j=2,4,\dots,2N} = \begin{cases} 0 & \text{for } m \neq n, \\ C''_n & \text{for } m = n, \end{cases} \quad (2.12)$$

with respect to the orthogonal mode-coupling relation defined by

$$\langle f_{jm}, f_{jn} \rangle_{j=1,2,3,\dots,(2N+1)} = \int_0^h f_{jm}(y) f_{jn}(y) dy, \quad (2.13)$$

where  $C'_n|_{j=1,3,\dots,(2N+1)} = \left\{ \frac{2\gamma_{jn}h + \sinh 2\gamma_{jn}h}{4\gamma_{jn} \cosh^2 \gamma_{jn}h} \right\}$  and  $C''_n|_{j=2,4,\dots,2N} = \left\{ \frac{2\gamma_{jn}h + \sinh 2\gamma_{jn}h}{4\gamma_{jn} \cosh^2 \gamma_{jn}h} \right\}$ .

(2.14)

with  $C'_n|_{j=1,3,\dots,(2N+1)}$  for  $n = 1, 2, 3, \dots$  are obtained by substituting  $\gamma_{jn} = i\gamma_{jn}$  in the case of the open water region. To find the unknown coefficients, the mode-coupling relation (2.13) is employed on the velocity potential  $\phi_j(x, y)$  and  $\phi_{jx}(x, y)$  with the eigenfunction  $f_{jm}(y)$  along with continuity of pressure and velocity as in Equation (2.4a,b) across the vertical interface  $x = -b_j, 0 < y < h$  for  $j = 1, 3, \dots, (2N - 1)$  to obtain

$$\langle \phi_j(x, y), f_{jm}(y) \rangle = \int_0^h \phi_j(x, y) f_{jm}(y) dy = G \int_0^h \phi_{(j+1)}(x, y) f_{jm}(y) dy, \quad (2.15)$$

for  $m = 0, 1, 2, \dots$  and  $j = 1, 3, \dots, (2N - 1)$ ,

$$\langle \phi_{jx}(x, y), f_{jm}(y) \rangle = \int_0^h \phi_{jx}(x, y) f_{jm}(y) dy = \varepsilon \int_0^h \phi_{(j+1)x}(x, y) f_{jm}(y) dy, \quad (2.16)$$

for  $m = 0, 1, 2, \dots$  and  $j = 1, 3, \dots, (2N - 1)$ .

Again, the mode-coupling relation (2.13) is employed on velocity potential  $\phi_{j+1}(x, y)$  and  $\phi_{(j+1)x}(x, y)$  with the eigenfunction  $f_{(j+1)m}(y)$  along with continuity of pressure



and continuity velocity as in Equation (2.4a,b) across the vertical interface  $x = -b_j$ ,  $0 < y < h$  to obtain the system of linear equations

$$\langle \phi_{j+1}(x, y), f_{(j+1)m}(y) \rangle = \int_0^h \phi_{j+1}(x, y) f_{(j+1)m}(y) dy = G \int_0^h \phi_j(x, y) f_{(j+1)m}(y) dy \quad (2.17)$$

for  $m = 0, 1, 2, \dots$  and  $j = 2, 4, \dots, 2N$ ,

$$\langle \phi_{(j+1)x}(x, y), f_{(j+1)m}(y) \rangle = \int_0^h \phi_{(j+1)x}(x, y) f_{(j+1)m}(y) dy = \varepsilon \int_0^h \phi_{jx}(x, y) f_{(j+1)m}(y) dy, \quad (2.18)$$

for  $m = 0, 1, 2, \dots$  and  $j = 2, 4, \dots, 2N$ .

The infinite sums presented in Equation (2.15), (2.16), (2.17) and (2.18) are truncated upto finite  $M$  terms to obtain a linear system of  $4j(M+1)$  for  $j = 1, 2, \dots, 2N$  algebraic equations for the determination of  $4j(M+1)$  unknowns and the wave reflection and transmission due to the porous structure obtained as

$$K_r = \left| \frac{R_{10}}{I_{10}} \right| \quad \text{and} \quad K_t = \left| \frac{T_{(2N+1)0}}{I_{10}} \right|. \quad (2.19a)$$

Due to the existence of porous structures, the energy dissipation (Chwang and Chan, 1998) is represented as

$$K_d = 1 - K_r^2 - K_t^2. \quad (2.19b)$$

### 2.3.2 Wave trapping by multiple porous structures

The wave interaction with multiple porous structures in the presence of the leeward wall is investigated to analyse the wave transformation mechanism. The velocity potentials are similar as explained in Section 2.3.1, except for the leeward region. The velocity potential in the leeward open water region is obtained based on the wave transmission from the structure and full-wave reflection from the leeward wall given by

$$\phi_1(x, y) = \left\{ I_{10} e^{-ik_{10}(x+b_1)} + R_{10} e^{ik_{10}(x+b_1)} \right\} f_{10}(y) + \sum_{n=1}^{\infty} \left\{ R_{1n} e^{-\kappa_{1n}(x+b_1)} \right\} f_{1n}(y), \quad (2.20a)$$

for  $-b_1 < x < \infty$ ,

$$\phi_j(x, y) = \sum_{n=0}^{\infty} \left\{ A_{jn} e^{-ik_{jn}(x+b_{j-1})} + B_{jn} e^{ik_{jn}(x+b_j)} \right\} f_{jn}(y) \quad (2.20b)$$

for  $-b_j < x < -b_{j-1}$ ,  $j = 2, 3, \dots, 2N$ ,

$$\begin{aligned} \phi_{2N+1}(x, y) = & \left\{ T_{(2N+1)0} e^{-ik_{(2N+1)0}(x+b_{2N})} + D_{(2N+1)0} e^{ik_{(2N+1)0}(x+b_{2N}+L)} \right\} f_{(2N+1)0}(y) \\ & + \sum_{n=1}^{\infty} \left\{ T_{(2N+1)n} e^{k_{(2N+1)n}(x+b_{2N})} + D_{(2N+1)n} e^{-k_{(2N+1)n}(x+b_{2N}+L)} \right\} f_{(2N+1)n}(y) \quad (2.20c) \\ & \text{for } -(b_{2N} + L) < x < -b_{2N}, \end{aligned}$$

where  $k_{jn} = i\kappa_{jn}$  for  $n = 1, 2, 3, \dots$ ,  $D_{(2N+1)n} = T_{(2N+1)n} e^{ik_{(2N+1)n}L}$  is found using the no-flow condition due to the wall as in Equation (2.8) and  $L$  is the width between the leeward wall and leeward structure. The system of equations is obtained using orthogonal mode-coupling relation, and it is similar as described in Section 2.3.1 for porous structures in series with the leeward confined region. The infinite sums in the equations are truncated upto finite  $M$  terms to obtain a linear system of  $4j(M+1)$  for  $j = 1, 2, \dots, 2N$  algebraic equations for the analysis of  $4j(M+1)$  unknowns.

The wave force impact acting on the leeward wall  $K_{fw}$  is given by

$$K_{fw} = \frac{F_w}{2\rho gh I_{10}}, \quad (2.21a)$$

$$\text{and } F_w = i\rho\omega \int_0^h \phi_{(2j+1)}(x, y) dy \quad \text{at } x = -\{(b_{2j} - b_1) + L\}, \quad \text{for } j = 1, 2, \dots, N, \quad (2.21b)$$

where  $I_{10}$  is the amplitude of the incident wave potential considered to be unity.

### 2.3.3 Wave transformation by a single porous structure

In the case of oblique wave scattering due to single porous structure, the fluid domain is divided into three sub-domains such as seaward open water ( $-b_1 < x < \infty$ ,  $0 < y < h$ ), porous structure ( $-b_2 < x < -b_1$ ,  $0 < y < h$ ) and leeward open water region ( $-\infty < x < -b_2$ ,  $0 < y < h$ ). The velocity potentials  $\phi_j(x, y)$  for  $j = 1, 2, 3$  satisfying the governing equations and boundary conditions Equations (2.2) – (2.3) is given by

$$\begin{aligned} \phi_1(x, y) = & \left\{ I_{10} e^{-ik_{10}(x+b_1)} + R_{10} e^{ik_{10}(x+b_1)} \right\} f_{10}(y) + \sum_{n=1}^{\infty} \left\{ R_{1n} e^{-\kappa_{1n}(x+b_1)} \right\} f_{1n}(y), \quad (2.22a) \\ & \text{for } -b_1 < x < \infty, \end{aligned}$$

$$\phi_2(x, y) = \sum_{n=0}^{\infty} \left\{ A_{2n} e^{-ik_{2n}(x+b_1)} + B_{2n} e^{ik_{2n}(x+b_2)} \right\} f_{2n}(y) \quad \text{for } -b_2 < x < -b_1, \quad (2.22b)$$

$$\phi_3(x, y) = \left\{ T_{30} e^{-ik_{30}(x+b_2)} \right\} f_{30}(y) + \sum_{n=1}^{\infty} \left\{ T_{3n} e^{k_{3n}(x+b_2)} \right\} f_{3n}(y), \quad \text{for } -\infty < x < -b_2, \quad (2.22c)$$

where,  $R_{1n}, A_{2n}, B_{2n}$  and  $T_{3n}$  for  $n = 0, 1, 2, 3, \dots$  are unknowns. The general formulation as in Section 2.3.1 is applied on Equation (2.22a-2.22c) using the continuity of velocity and pressure as in Equation (2.4a,b) and mode-coupling relation as in Equation (2.13) across the vertical interface at  $x = -b_j, 0 < y < h$  for  $j = 1, 2$  to obtain the system of equations given by

$$\left\{ I_{10} \delta_{nm} + R_{1m} \right\} \langle f_{1n}(y), f_{1m}(y) \rangle = G \left[ \sum_{n=0}^{\infty} \left\{ A_{2n} + B_{2n} e^{-ik_{2n}d} \right\} \int_0^h f_{2n}(y) f_{1m}(y) dy \right], \quad (2.23)$$

$$-ik_{1n} \left\{ I_{10} \delta_{nm} - R_{1m} \right\} \langle f_{1n}(y), f_{1m}(y) \rangle = \varepsilon \left[ \sum_{n=0}^{\infty} -ik_{2n} \left\{ A_{2n} - B_{2n} e^{-ik_{2n}d} \right\} \int_0^h f_{2n}(y) f_{1m}(y) dy \right] , \quad (2.24)$$

$$G \left[ \sum_{n=0}^{\infty} \left\{ A_{2n} e^{-ik_{2n}d} + B_{2n} \right\} \int_0^h f_{2n}(y) f_{3m}(y) dy \right] = T_{3n} \langle f_{3n}(y), f_{3m}(y) \rangle, \quad (2.25)$$

$$\varepsilon \left[ \sum_{n=0}^{\infty} -ik_{2n} \left\{ A_{2n} e^{-ik_{2n}d} - B_{2n} \right\} \int_0^h f_{2n}(y) f_{3m}(y) dy \right] = -ik_{3n} T_{3n} \langle f_{3n}(y), f_{3m}(y) \rangle \quad (2.26)$$

where,  $\delta_{nm} = \begin{cases} 1 & \text{for } m = n = 0, \\ 0 & \text{for } m = n = 1, 2, \dots, \end{cases} \quad d = -(b_2 - b_1), \quad n = 1, 2, 3, \dots \text{ and } m = 0, 1, 2, \dots$

The infinite sums presented in the Equations (2.23), (2.24), (2.25) and (2.26) are truncated for finite  $M$  terms, and a linear system of  $4(M+1)$  equations is obtained for the determination of  $4(M+1)$  unknowns. The unknown constants  $R_{1n}, T_{3n}, A_{2n}, B_{2n}$ , for  $n = 0, 1, 2, \dots, M$  are evaluated and the wave reflection and transmission due to a single porous structure is obtained as

$$K_r = \left| \frac{R_{10}}{I_{10}} \right| \quad \text{and} \quad K_t = \left| \frac{T_{30}}{I_{10}} \right|. \quad (2.27)$$

### 2.3.4 Wave transformation by a single porous structure with leeward wall

In this section, the necessity of the leeward wall on wave transformation is discussed. The velocity potentials in seaward open water region and porous structure regions remain the same as in Section 2.3.3, but the velocity potential in the leeward open water

region is considered in terms of wave transmission from structure and wave reflection due to leeward wall. The velocity potentials in each of the three regions are given by

$$\phi_1(x, y) = \left\{ I_{10} e^{-ik_{10}(x+b_1)} + R_{10} e^{ik_{10}(x+b_1)} \right\} f_{10}(y) + \sum_{n=1}^{\infty} \left\{ R_{1n} e^{-\kappa_{1n}(x+b_1)} \right\} f_{1n}(y), \quad (2.28a)$$

for  $-b_1 < x < \infty$ ,

$$\phi_2(x, y) = \sum_{n=0}^{\infty} \left\{ A_{2n} e^{-ik_{2n}(x+b_1)} + B_{2n} e^{ik_{2n}(x+b_2)} \right\} f_{2n}(y) \quad \text{for } -b_2 < x < -b_1, \quad (2.28b)$$

$$\phi_3(x, y) = \left\{ T_{30} e^{-ik_{30}(x+b_2)} + D_{30} e^{ik_{30}(x+b_2+L)} \right\} f_{30}(y) + \sum_{n=1}^{\infty} \left\{ T_{3n} e^{\kappa_{3n}(x+b_2)} + D_{3n} e^{-\kappa_{3n}(x+b_2+L)} \right\} f_{3n}(y) \quad \text{for } -(b_2 + L) < x < -b_2, \quad (2.28c)$$

where  $D_{3n} = T_{3n} e^{ik_{3n}L}$  is found using the no-flow condition as in Equation (2.8).

The general formulation in Section 2.3.2 is applied on Equation (2.28a-2.28c) using the continuity of velocity and pressure as in Equation (2.4a,b) and mode-coupling relation as in Equation (2.13) across the vertical interface at  $x = -b_j, 0 < y < h$  for  $j = 1, 2$  to obtain the system of equations given by

$$\left\{ I_{10} \delta_{nm} + R_{1m} \right\} \langle f_{1n}(y), f_{1m}(y) \rangle = G \left[ \sum_{n=0}^{\infty} \left\{ A_{2n} + B_{2n} e^{-ik_{2n}d} \right\} \int_0^h f_{2n}(y) f_{1m}(y) dy \right], \quad (2.29)$$

$$-ik_{1n} \left\{ I_{10} \delta_{nm} - R_{1m} \right\} \langle f_{1n}(y), f_{1m}(y) \rangle = \varepsilon \left[ \sum_{n=0}^{\infty} -ik_{2n} \left\{ A_{2n} - B_{2n} e^{-ik_{2n}d} \right\} \int_0^h f_{2n}(y) f_{1m}(y) dy \right], \quad (2.30)$$

$$G \left[ \sum_{n=0}^{\infty} \left\{ A_{2n} e^{-ik_{2n}d} + B_{2n} \right\} \int_0^h f_{2n}(y) f_{3m}(y) dy \right] = \left\{ T_{3n} + D_{3n} e^{ik_{3n}L} \right\} \langle f_{3n}(y), f_{3m}(y) \rangle, \quad (2.31)$$

$$\varepsilon \left[ \sum_{n=0}^{\infty} -ik_{2n} \left\{ A_{2n} e^{-ik_{2n}d} - B_{2n} \right\} \int_0^h f_{2n}(y) f_{3m}(y) dy \right] = -ik_{3n} \left\{ T_{3n} - D_{3n} e^{ik_{3n}L} \right\} \langle f_{3n}(y), f_{3m}(y) \rangle, \quad (2.32)$$

where  $D_{3n} = T_{3n} e^{ik_{3n}L}$ ,  $m = 0, 1, 2, \dots$ ,  $k_{jn} = i\kappa_{jn}$  for  $n = 1, 2, 3, \dots$  and  $L$  is width between the leeward wall and porous structure. The infinite sums presented in the above equations are limited for finite  $M$  terms and a linear system of  $4(M + 1)$  equations is obtained for the determination of  $4(M + 1)$  unknowns. The wave reflection due to the porous structure is obtained using Equation (2.27).

## 2.4 RESULTS AND DISCUSSION

The numerical investigation is performed to examine the wave scattering for porous structures in series considering various values of porosity  $\varepsilon$ , linearized friction factor  $f$ , angle of incidence  $\theta$ , finite spacing between the structures  $w/h$  and water chamber length  $L/h$ . The wave reflection  $K_r$ , transmission  $K_t$ , energy dissipation  $K_d$  and the wave force on the leeward wall  $K_{fw}$  is plotted to understand the behaviour of porous structure as an effective absorber. The parameters that were kept constant are  $\rho = 1000 \text{ kg/m}^3$ ,  $g = 9.81 \text{ m/s}^2$  and  $S = 1$  throughout the computation. Initially, the convergence of scattering coefficients is examined and the accuracy of the numerical results is obtained by increasing the evanescent waves for single, double, triple, and four structures in series. Table 2.1 presents the effect of the evanescent waves on wave scattering considering  $d/h = 1$ ,  $w/h = 1$ ,  $\gamma_{10}h = 0.5$ ,  $f = 0.5$ ,  $\theta = 0^\circ$  and  $\varepsilon = 0.4$  for single and multiple structures. The convergence of the scattering coefficients is obtained for evanescent modes  $M \geq 15$  upto five decimal places.

Table 2.1: Convergence of reflection and transmission coefficients considering  $d/h = 1$ ,  $w/h = 1$ ,  $\gamma_{10}h = 0.5$ ,  $f = 0.5$ ,  $\theta = 0^\circ$  and  $\varepsilon = 0.4$ .

$M$	Single structure		Double structure		Triple structure		Four structures	
	$K_r$	$K_t$	$K_r$	$K_t$	$K_r$	$K_t$	$K_r$	$K_t$
0	0.41850	0.71591	0.31155	0.75535	0.19930	0.76786	0.09538	0.76601
1	0.41841	0.71582	0.31113	0.75520	0.19910	0.76760	0.09529	0.76498
5	0.41849	0.71585	0.31110	0.75518	0.19913	0.76758	0.09520	0.76525
10	0.41850	0.71592	0.31109	0.75514	0.19915	0.76756	0.09517	0.76579
15	0.41850	0.71592	0.31109	0.75514	0.19915	0.76756	0.09511	0.76575
20	0.41850	0.71592	0.31109	0.75514	0.19915	0.76756	0.09511	0.76575
30	0.41850	0.71592	0.31109	0.75514	0.19915	0.76756	0.09511	0.76575

In Figures 2.2(a,b), the validation of the numerical result is performed for porous structure kept at finite water depth with the experimental and theoretical results available in the literature. The wave damping  $K_d$  by the three-layer porous structure in the absence of the finite spacing is reported and also validated with the experimental results of Twu and Chieu (2000). An acceptable agreement for the wave energy

damping  $K_d$  versus  $h/\lambda$  is observed in comparison with Twu and Chieu (2000) experimental results. Mallayachari and Sundar (1994) evaluated the wave reflection  $K_r$  due to the permeable wall as in Figure 2.2(b). The correlation between the previous theoretical outcomes and present study outcomes are acceptable. Afterward, the present study is extended to analyse the porous structures in series considering leeward unbounded and confined regions placed on the flat and step-type seabed. The single structure width  $d/h$  is separated into equal multiple structures and the width between the two porous structures is identical throughout the simulation.

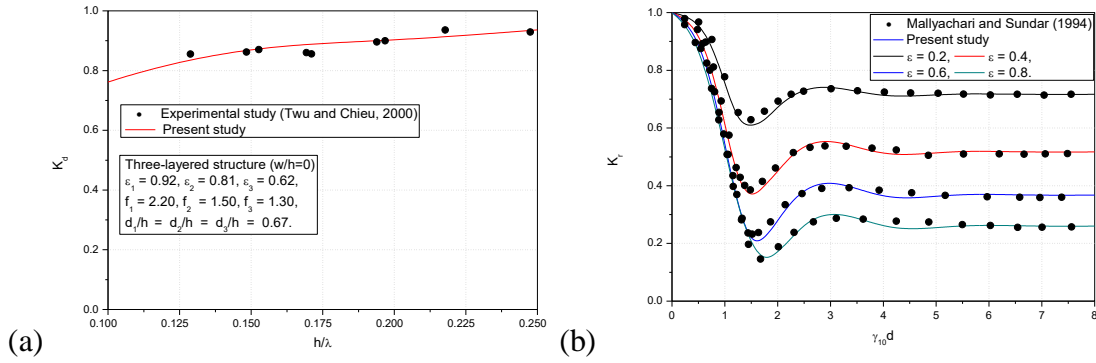


Figure 2.2: Validation of (a)  $K_d$  by three-layered structure (Twu and Chieu, 2000) and (b)  $K_r$  due to the porous structure with the back wall (Mallayachari and Sundar, 1994).

#### 2.4.1 Multiple porous structures with leeward unbounded region

In the present subsection, a detailed investigation on wave scattering due to fully extended multiple porous structures in the absence of a vertical wall is presented.

##### 2.4.1.1 Effect of structural porosity

The structural porosity and friction factor are interrelated as in Equation (2.5b). However, in the previous studies, structural porosity is varied and friction factor is kept fixed for simplicity (Madsen, 1983; Mallayachari and Sundar, 1994; Zhu, 2001; Das and Bora, 2014a). A similar method is adopted in the analysis of single and multiple porous structures placed on the flat seabed. In Figures 2.3(a-c), the structural porosity is varied within  $0.3 < \varepsilon < 0.7$  for the determination of  $K_r$ ,  $K_t$  and  $K_d$  due to a single porous structure. The sharp rise in  $K_r$  is obtained within  $0.01 < \gamma_{10}d < 1.5$  for all the values of porosity within  $0.3 < \varepsilon < 0.7$  presented as in Figure 2.3(a) and it is found that with the increase of  $\varepsilon$  the  $K_r$  is observed to be decreasing. The variation in wave

transformation is analysed and it is observed that maximum wave reflection  $K_r$  occurs at  $\gamma_{10}d = 1.25$  for  $\varepsilon = 0.3$ . Similar pattern in  $K_r$  is observed with the change in porosity but a reduction of 15% in  $K_r$  for  $\varepsilon = 0.4$ , 27% reduction in  $K_r$  for  $\varepsilon = 0.5$ , 39% reduction in  $K_r$  for  $\varepsilon = 0.6$  and 50% reduction in  $K_r$  for  $\varepsilon = 0.7$  in comparison with structural porosity  $\varepsilon = 0.3$  at  $\gamma_{10}d = 1.25$  is noticed. In Figure 2.3(b),  $K_t$  decreases with increase in non-dimensional structural width  $\gamma_{10}d$  and with the increase in porosity  $\varepsilon$ . The  $K_t$  is observed to be increasing but the percentage of change due to the change in porosity is not so significant as observed in the case of  $K_r$ .

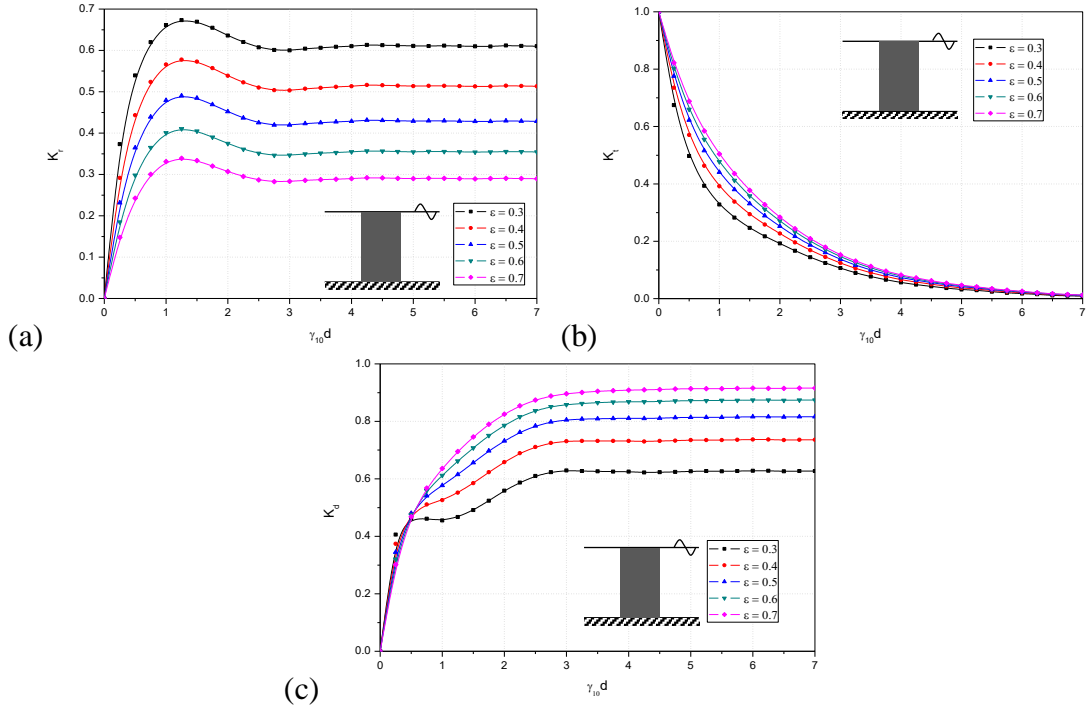


Figure 2.3: Variation in (a)  $K_r$  (b)  $K_t$  and (c)  $K_d$  versus  $\gamma_{10}d$  for different values of porosity considering  $\theta = 0^\circ$  and  $f = 1$ .

The change in the  $K_r$  and  $K_t$  due to an increase in porosity may be due to an increase in energy dissipation  $K_d$  as observed in Figure 2.3(c). In the case of minimum porosity, the flow of the fluid particle within the structure is less as compared to high porosity. So, the energy dissipation  $K_d$  is maximal for higher structural porosity and almost 91.5% wave damping is observed due to the presence of a single structure for  $\varepsilon = 0.7$  within  $2 < \gamma_{10}d < 7$  which shows that the increase in  $\gamma_{10}d$  shows the high interaction

between the incident wave and porous media for  $\varepsilon = 0.7$ . The study reveals that the wave energy dissipation is low for minimum porosity, and for higher porosity the wave energy gets absorbed due to porous structure.

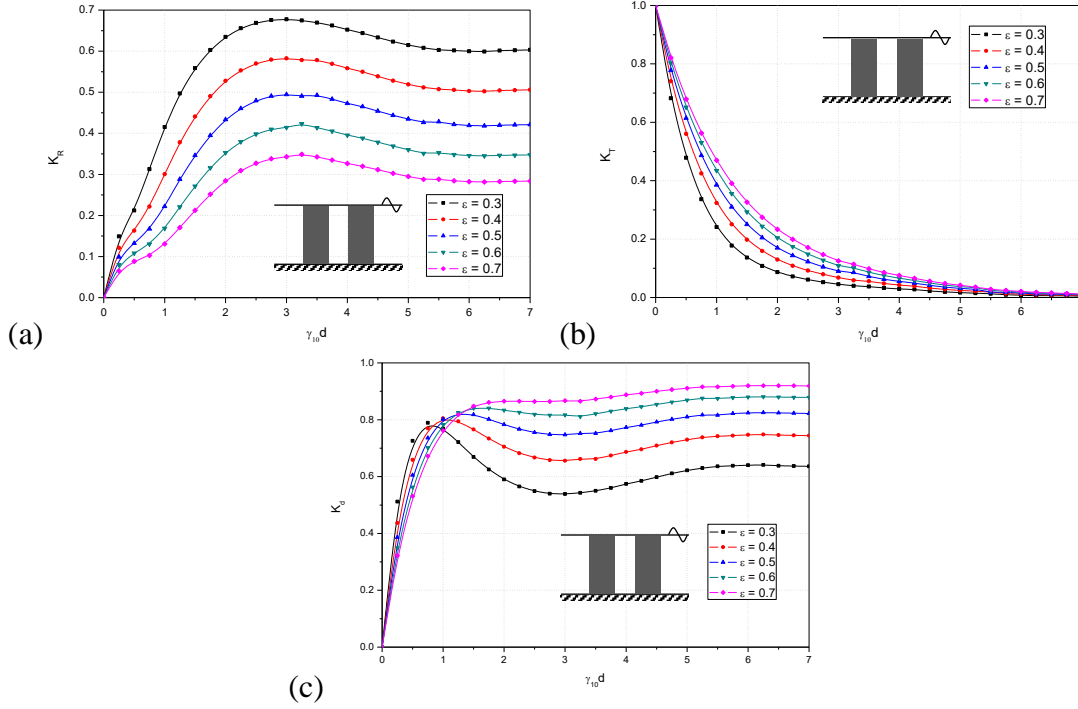


Figure 2.4: Variation in (a)  $K_r$  (b)  $K_t$  and (c)  $K_d$  versus  $\gamma_{10}d$  for different values of porosity of the structure considering  $\theta = 0^0$ ,  $w/h = 1$  and  $f = 1$ .

In Figures 2.4(a-c), the wave reflection  $K_r$ , transmission  $K_t$ , and energy dissipation  $K_d$  are analysed for double porous structures. The resonating trend in the  $K_r$  is observed varying with non-dimensional structural width  $\gamma_{10}d$ , which may be due to the trapping of waves between the two porous structures observed in Figure 2.4(a). The  $K_r$  decreases with the increase in the porosity within  $0.01 \leq \gamma_{10}d \leq 2$  and the  $K_t$  (Figure 2.4b) increases with the increase in the structural porosity. The presence of the double porous structures shows that the wave reflection is little higher as compared to the single porous structure and the wave attenuation is achieved with the increase in the porous structures in series. A similar, decreasing pattern with an increase in  $\gamma_{10}d$  is observed in  $K_t$  (Figure 2.4b) for all the values of porosity. The minimum in the wave transmission is observed for the non-dimensional thickness within  $2 < \gamma_{10}d < 7$  for all the values of porosity and almost zero  $K_t$  is observed with increase in the  $\gamma_{10}d$ .



Resonating pattern in the energy dissipation  $K_d$  disappears with the increase in the structural porosity and it is observed that almost 92% energy damping  $K_d$  is achieved for  $\varepsilon = 0.7$  in the presence of double porous structures within  $1.5 < \gamma_{10}d < 7$  (Figure 2.4c). The comparison between the wave scattering in the presence of single and double porous structures is discussed. It is noted that the performance of the double porous structure is significant within  $1 < \gamma_{10}d < 3$ . Particularly, 12% increase in the energy damping is obtained with the double porous structure as compared with single porous structure at  $\gamma_{10}d = 1.5$ . Which is due to the wave trapping in the finite spacing and increase in  $K_r$  may be due to the existence of second porous structure.

#### 2.4.1.2 Effect of friction factor

In Figures 2.5(a-c), the  $K_r$  (Figure 2.5a),  $K_t$  (Figure 2.5b) and  $K_d$  (Figure 2.5c) versus  $\gamma_{10}d$  for single porous structure is analysed on varying the linearized friction factor  $f$ . The reduction in  $K_r$  is observed with increase in  $f$  for  $\gamma_{10}d < 2.5$  but the opposite trend in  $K_r$  is observed for  $\gamma_{10}d > 2.5$ . The variation in  $K_t$  (Figure 2.5b) is significant with an increase in friction factor and the high oscillating pattern is observed for  $f = 0.25$  within  $0.1 < \gamma_{10}d < 4$ . The 47% reduction in  $K_t$  for  $f = 0.5$ , 71% reduction in  $K_t$  for  $f = 0.75$  and 85% reduction in  $K_t$  for  $f = 1$  is noted as compared with  $f = 0.25$  at  $\gamma_{10}d > 4$ . The reason behind the reduction in the  $K_t$  is only due to the high resistance offered by the structure which causes high wave energy damping. Further, the  $K_d$  (Figure 2.5c) is found to be increasing with the increase in  $f$  and the variation in  $K_d$  is significant within  $0.1 < \gamma_{10}d < 3$ . Thereafter, a uniform result in  $K_d$  is noted within  $0.5 \leq f \leq 1.0$  for  $\gamma_{10}d > 3$ . Thus, the study reveals that the wave energy gets absorbed inside the porous structure for the higher value of  $f = 1$ .

In Figures 2.6(a-c), the variation in wave scattering with the effect of friction factor is examined for a pair of porous structures as a function of  $\gamma_{10}d$ . The resonating pattern in  $K_r$  (Figure 2.6a) is observed and maximum value of  $K_r = 0.73$  is noticed for  $f = 0.25$  at  $\gamma_{10}d = 3.5$ . The 14% reduction in  $K_r$  is observed for  $f = 0.5$ , 20% reduction in  $K_r$  for  $f = 0.75$  and 22% reduction in  $K_r$  is achieved for  $f = 1$ . Thus the

reduction in  $K_r$  is observed with increase in  $f$  for double porous structures due to the constructive seaside interferences for  $\gamma_{10}d > 5$ .

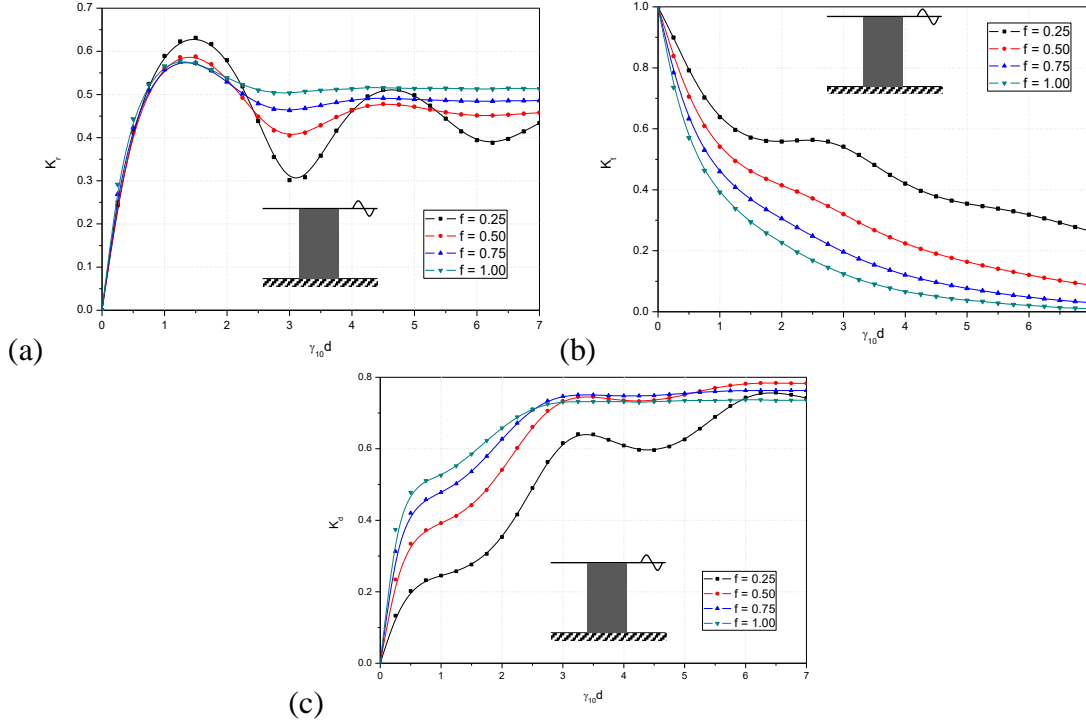


Figure 2.5: Variation in (a)  $K_r$  (b)  $K_t$  and (c)  $K_d$  versus  $\gamma_{10}d$  for different values of friction factor considering  $\theta = 0^\circ$  and  $\varepsilon = 0.4$ .

Wave transmission  $K_t$  (Figure 2.6b) also decreases with an increase in friction factor  $f$  and a considerable decrease in  $K_t$  is observed with an increase in  $f$  due to wave trapping between the two porous structures. A sharp reduction pattern in the long-wave regime and almost identical values of  $K_t$  for shorter waves is observed, which is due to the wave decay by massive structural width. The  $K_d$  (Figure 2.6c) increases with the increase in  $f$  and minimum  $K_d$  is observed for  $f = 0.25$  due to the minimum friction offered by the porous material. The 4% decrease in  $K_d$  for  $f = 0.75$ , 13% decrease in  $K_d$  for  $f = 0.5$  and 40% of the decrease in  $K_d$  for  $f = 0.25$  is observed compared with  $f = 1$  at  $\gamma_{10}d = 3.5$ . The variation between single and double porous structures is clearly observed in the  $K_t$  within  $1 < \gamma_{10}d < 3$  and the performance of the double porous structure is far better than the single porous structure for trapping of incoming waves in the confined region provided between the two porous structures.

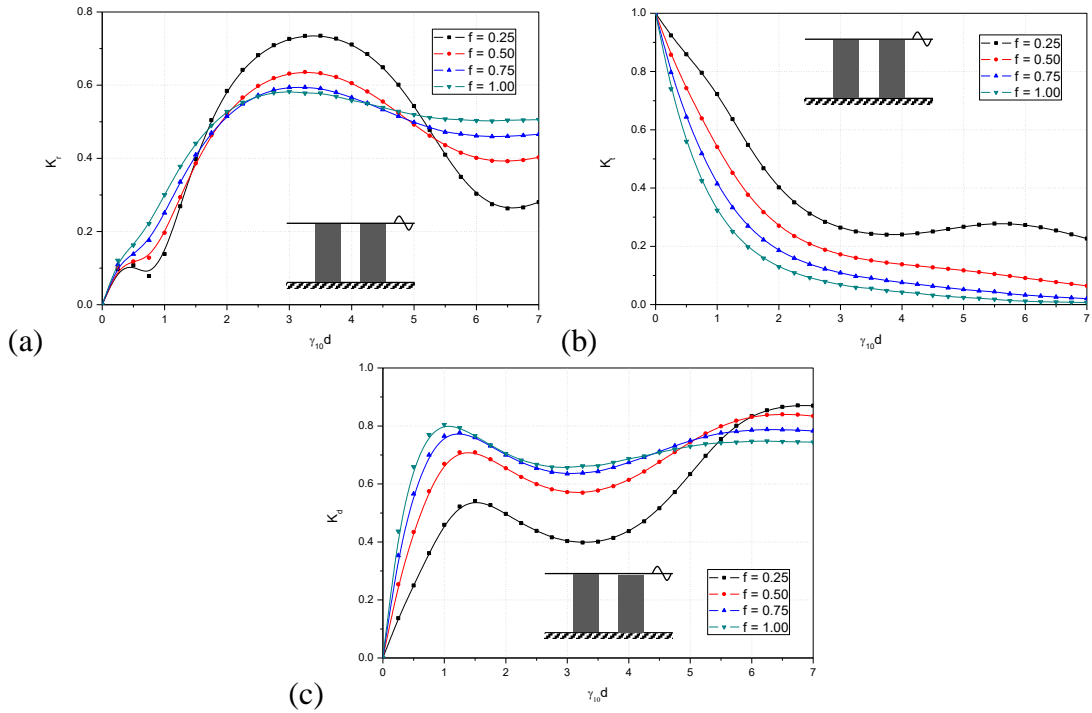


Figure 2.6: Variation in (a)  $K_r$  (b)  $K_t$  and (c)  $K_d$  versus  $\gamma_{10}d$  for different values of friction factor considering  $w/h=1$ ,  $\theta=0^\circ$  and  $\varepsilon=0.4$ .

#### 2.4.1.3 Effect of angle of incidence

In Figures 2.7(a,b), the wave reflection and transmission due to the presence of the triple porous structure are analysed as a function of angle of incidence  $\theta$  for different values of  $\gamma_{10}h$ . The minimal increase in  $K_r$  (Figure 2.7a) is observed with increase in  $\gamma_{10}h$  for normal angle of incidence  $\theta$ . Thereafter, the increase in  $\theta$  shows the decrease in  $K_r$  within  $0^\circ < \theta < 80^\circ$  for  $\varepsilon=0.3$  and  $0^\circ < \theta < 64^\circ$  for  $\varepsilon=0.7$ . The minimal  $K_r$  is observed at  $\theta=80^\circ$  for  $\varepsilon=0.3$  and  $\theta=64^\circ$  for  $\varepsilon=0.7$  due to the formation of standing waves and it is regarded as the critical angle. Afterward, a sharp rise in  $K_r$  is obtained for  $\varepsilon=0.3$  and  $\varepsilon=0.7$  and  $K_r$  approaches to unity. This is an unsuitable angle of impinging for the construction of the porous structure, which may lead to structural collapse. The increase in  $\gamma_{10}h$  shows neither increase nor decrease in the  $K_r$  and it is negligible in the design of offshore structures. The drastic decrease in  $K_t$  (Figure 2.7b) is noticed with the increase in  $\gamma_{10}h$  for  $\varepsilon=0.3$  and  $\varepsilon=0.7$ . In the case of normal wave interaction, the  $K_t$  is observed to be minimal compared with oblique wave incidence for  $\varepsilon=0.3$  and uniform pattern in the  $K_t$  is observed for  $\varepsilon=0.7$ .

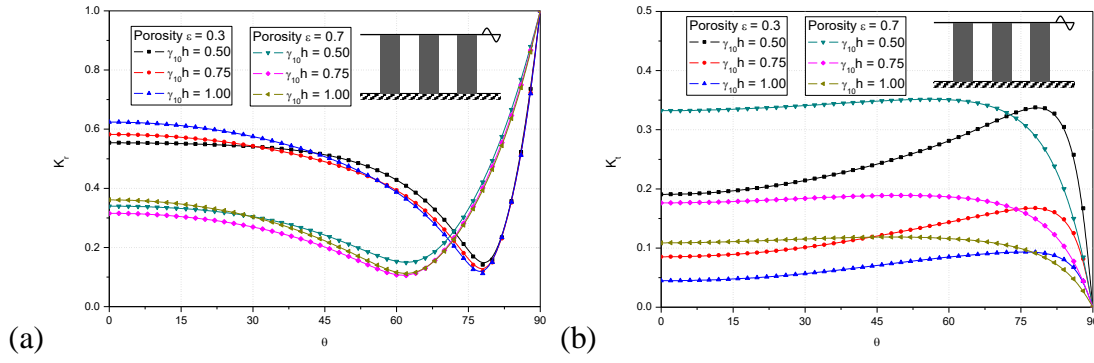


Figure 2.7: Variation in (a)  $K_r$  and (b)  $K_t$  versus  $\theta$  for different values of  $\gamma_{10}h$  for triple porous structure considering  $d/h = 2$ ,  $w/h = 0.5$  and  $f = 2$ .

A sharp rise in  $K_t$  is noticed for the triple porous structure within  $0.5 < \gamma_{10}h < 1$  for  $\varepsilon = 0.3$  and the peak in  $K_t$  is obtained at a critical angle  $\theta = 80^\circ$ . The critical angle for  $K_r$  and  $K_t$  is same for  $\varepsilon = 0.3$ , but almost uniform values is noticed in the  $K_t$  for  $\varepsilon = 0.7$ . However, it is important to notice that, the critical angle (resonating trough in  $K_r$  and resonating peak in  $K_t$ ) is observed for minimum porosity  $\varepsilon = 0.3$  due to the interaction between the incident and reflected waves. But in the case of high porosity  $\varepsilon = 0.7$  the critical angle presents the minimal impact on the hydraulic characteristics due to the high energy damping. The lower porosity  $\varepsilon = 0.3$  is effective in creating the resonating pattern in  $K_r$  and  $K_t$  but higher porosity  $\varepsilon = 0.7$  is significant in reducing the  $K_r$ , which leads to high energy damping by the triple porous structure with finite confined regions.

#### 2.4.1.4 Effect of width between the multiple structures

In the case of multiple structures, the width between two porous structures  $w/h$  shows the significant role in wave trapping. The different values of spacing between the double porous structures is considered to examine the variation in wave scattering for  $\gamma_{10}h$ . In Figures 2.8(a-c), the  $K_r$  (Figure 2.8a),  $K_t$  (Figure 2.8b) and  $K_d$  (Figure 2.8c) versus  $\gamma_{10}h$  is analysed varying the  $w/h$ . The periodic local maxima and local minima are observed in  $K_r$  (Figure 2.8a) for different values of  $w/h$  within  $0.01 < \gamma_{10}h < 7$  may be due to the destructive interferences. The increase in  $w/h$  increases resonating peaks and troughs in  $K_r$  due to constructive interferences. A similar trend is obtained

in  $K_r$  (Figure 2.8b) as aforementioned, the increase in  $w/h$  and  $\gamma_{10}h$  shows the increase in resonating trend in  $K_r$ . The resonating trend is obtained may be due to trapping of incident waves by the finite spacing between structures. The  $K_d$  (Figure 2.8c) is observed to be varying with the increase in  $w/h$  in an oscillating manner. The variation between  $w/h=0.25$  and  $0.75 < w/h < 1$  is significant in the design of double porous structures for protecting the beaches. From the present case, it is observed that the local maxima in the energy damping  $K_d$  show a significant role in the analysis of double porous structures and it is observed that the  $w/h=1$  show higher energy damping and minimum wave reflection  $K_r$  and wave transmission  $K_t$  in the oscillatory pattern.

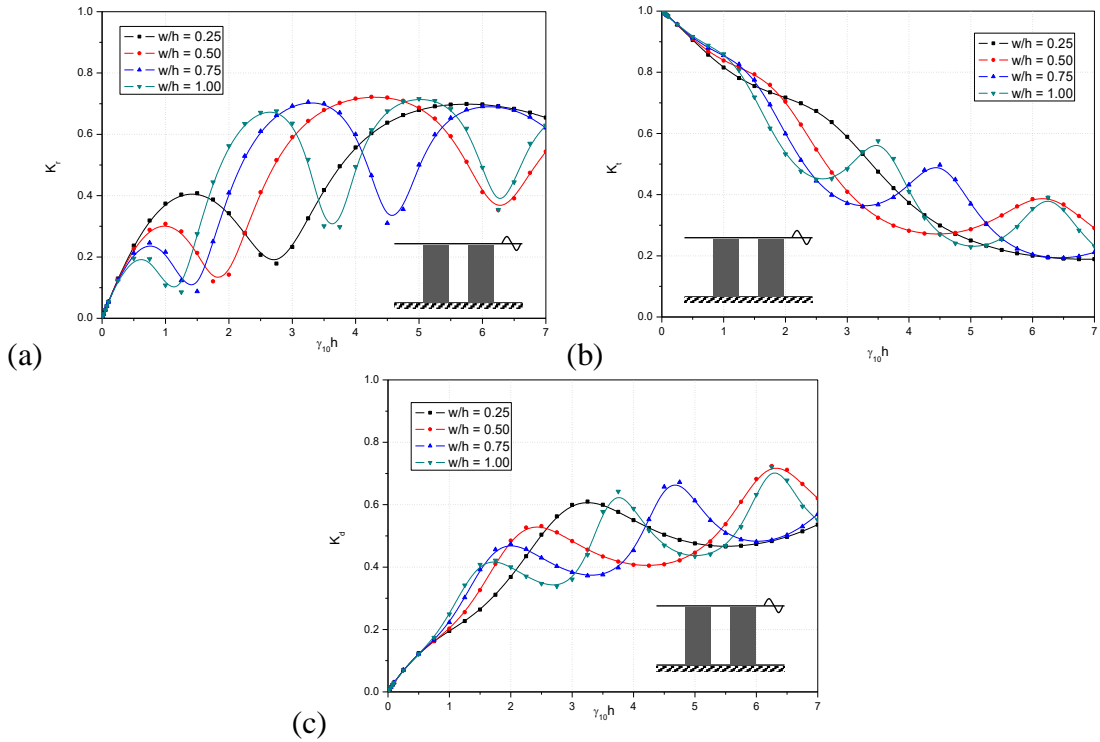


Figure 2.8: Variation in (a)  $K_r$ , (b)  $K_t$  and (c)  $K_d$  versus  $\gamma_{10}h$  with variation in  $w/h$  considering  $d/h=0.25$ ,  $\theta=0^0$ ,  $f=0.25$  and  $\varepsilon=0.4$ .

In Figures 2.9(a,b), the  $K_r$  and  $K_t$  due to four porous structures with multiple confined regions are presented considering  $\gamma_{10}h=0.5$  (Figure 2.9a) and  $\gamma_{10}h=1$  (Figure 2.9b) for porosity within  $0.3 < \varepsilon < 0.7$  with variation in  $w/h$ . The resonating peaks and sub-peaks in  $K_r$  along with uniform estimation in  $K_t$  is noticed with the increase in the  $w/h$  within  $0.3 < \varepsilon < 0.7$  for  $\gamma_{10}h=0.5$  (Figure 2.9a). It is also noticed that the

secondary resonating peaks are observed in between the primary resonating peaks, which may be due to trapping of incident waves in the multiple confined regions  $w/h$ . The increase in porosity of four structures shows the small decrease in  $K_r$ , little increase in  $K_t$  and the variation is due to increase in energy damping by four structures. The primary and secondary resonating peaks is higher for minimum porosity  $\varepsilon = 0.3$  and less for higher porosity  $\varepsilon = 0.7$ , which may be due to high wave motion through the multiple porous structures which leads to high energy damping for  $\varepsilon = 0.7$ .

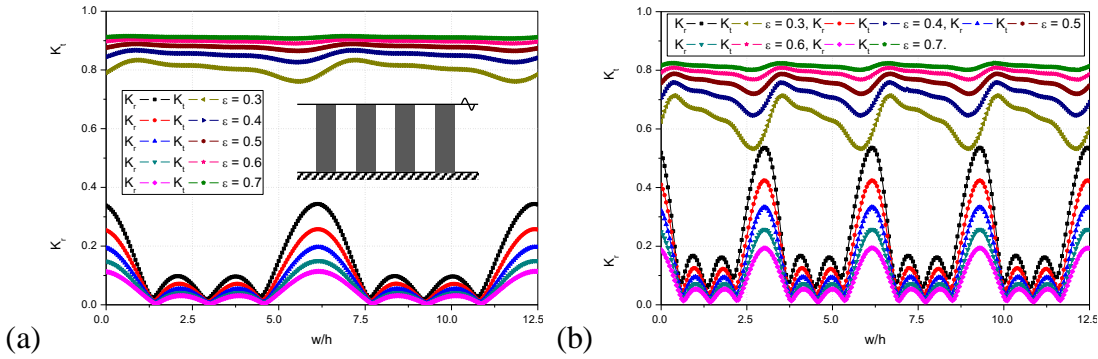


Figure 2.9: Variation in  $K_r$  and  $K_t$  versus  $w/h$  with variation in porosity for four porous structures considering  $d/h = 1$ ,  $f = 0.5$ , (a)  $\gamma_{10}h = 0.5$  and (b)  $\gamma_{10}h = 1$ .

The increase in the  $\gamma_{10}h = 1$  (Figure 2.9b) shows the decrease in  $K_r$  and also broadens the resonating primary and secondary peaks in  $K_r$ , as compared with  $\gamma_{10}h = 0.5$  (Figure 2.9a). The resonating peaks in  $K_r$  and resonating troughs in  $K_t$  is observed at the same intervals of  $w/h$  may be due to the trapping of incident waves by multiple confined regions and also the oscillatory pattern in  $K_t$  vanishes with the increase in porosity of four structures. The  $K_t$  is observed to be higher for  $\gamma_{10}h = 0.5$  (Figure 2.9a) and  $\gamma_{10}h = 1$  (Figure 2.9b) due to the minimum structural width  $d/h = 1$  (each structure width is  $d_j/h = 0.25$  for  $j = 1, 2, 3$  and 4) and hydrodynamic performance can be improved with the increase in structural width for damping the waves of higher wavelength. However, the variation in  $K_r$  and  $K_t$  with variation in  $\gamma_{10}h$  is significant in the design of the offshore structures and the increase in the  $w/h$  shows the significant role in decreasing the  $K_r$ . Particularly, the resonating troughs are obtained in  $K_t$  (at the point of resonating crests in  $K_r$ ), which suggests that the point of

secondary resonating peaks play an evident role in the effective distribution of incident waves in the form of wave reflection, transmission, and energy damping.

#### 2.4.1.5 Comparative study between multiple porous structures

The comparative study is performed between the multiple porous structures of  $N = 5$  for the case of plane-wave approximation (neglecting the evanescent wave modes). The width of the single porous structure  $d/h = 1$  is divided into multiple structures having equal width in each case and the width between any two porous structures  $w/h = 1$  is kept constant to compare the performance of multiple porous structures. The identical friction factor  $f = 1$  and porosity  $\varepsilon = 0.4$  is considered to compare the performance of multiple structures for  $\gamma_{10}h = 1$  as in Figures 2.10(a,b).

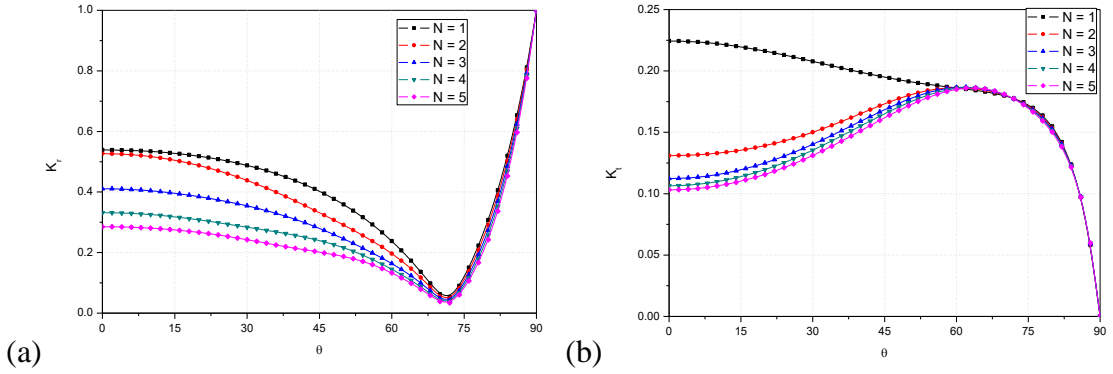


Figure 2.10: Variation in (a)  $K_r$  and (b)  $K_t$  versus  $\theta$  with increase in the number of porous structures for  $f = 1$ ,  $\varepsilon = 0.4$ ,  $\gamma_{10}h = 1$ ,  $w/h = 1$  and  $d/h = 2$ .

The variation in the wave reflection coefficient (Figure 2.10a) is acceptable for single and multiple porous structures and the decreasing trend is obtained in the  $K_r$  with the increase in the multiple structures due to increase in confined regions  $w/h$ . The minimum values in  $K_r$  is observed at  $\theta = 72^\circ$  (critical angle) for the single and multiple structures due to the formation of standing waves. Similarly, in the case of transmission coefficient  $K_t$  (Figure 2.10b) the variation between single and double porous structure is significant and a 42% decrease in  $K_t$  is obtained with double porous structure as compared with a single porous structure. Afterward, the variation between multiple structures within  $3 \leq N \leq 5$  is negligible due to the fixed structural width and the performance of multiple structures within  $3 \leq N \leq 5$  can be accelerated with an increase

in dimensionless width. However, in the presence of  $\theta = 90^\circ$ , the  $K_r$  is observed to be higher and  $K_t$  is observed to be zero for single and multiple structures. The porous structures should have minimum wave reflection, minimum wave transmission and high energy damping (Twu and Chieu, 2000) for the better service life of the structure. From the present study, it is observed that the higher number of porous structures is a better option to distribute the incident waves of higher wavelengths  $\gamma_{10}h \geq 1$  in the form of  $K_r$ ,  $K_t$  and  $K_d$  due to the presence of multiple confined regions.

#### **2.4.2 Multiple porous structures with leeward confined region**

The necessity of the leeward wall with a porous structure is helpful to protect the offshore facilities from high wave attack. The wave reflection due to multiple porous screens, slotted permeable barriers and deeply submerged bars backed by wall is studied in detail using the analytical solution (Losada et al., 1993), experimental approach (Neelamani et al., 2017) and boundary element method (Zhao et al., 2017). The previous studies were focused on the significance of trapping chamber/ water chamber length (width between leeward wall and porous structures) on wave trapping and numerical prediction shows that the resonating trend in the  $K_r$  is reduced with an increase in the number of structures. Hence, the present study is focused on wave force on the leeward wall in the presence of single and multiple structures with variation in trapping chamber considering porosity as influencing parameter. Further, the comparative study between single and multiple structures is briefly discussed in detail.

##### **2.4.2.1 Effect of water chamber length**

In Figures 2.11(a-d), the wave force impact on the leeward wall  $K_{fw}$  is analysed in the presence of single (Figure 2.11a), double (Figure 2.11b), triple (Figure 2.11c) and four porous structures (Figure 2.11d) versus trapping chamber  $L/h$  for different porosities within  $0.3 < \varepsilon < 0.7$ . In the case of a single structure (Figure 2.11a) with the leeward wall, the increase in  $\varepsilon$  shows the decrease in  $K_{fw}$  at each resonating peak and increase in  $K_{fw}$  at each resonating troughs. But, in the case of multiple porous structures as in Figure 2.11(b-d), the increase in  $\varepsilon$  shows the preferable increase in  $K_{fw}$  at each resonating peaks and troughs which suggests that the higher porosity allows the more



wave energy to pass through the porous structure and perform more wave transmission causing high wave force impact on the leeward wall. In the case of a single porous structure (Figure 2.11a), the resonating peaks are observed to be higher compared with double porous structure (Figure 2.11b). This is only due to the wave trapping in the finite spacing between the structures  $w/h$  and it shows the efficiency of the double structure as compared with a single structure in decreasing the hydraulic characteristics for fixed structural width. Thereafter, the performance of triple structure (Figure 2.11c) and four structures (Figure 2.11d) is significant in reducing the  $K_{fw}$  at each of the resonating peaks as compared with double structure.

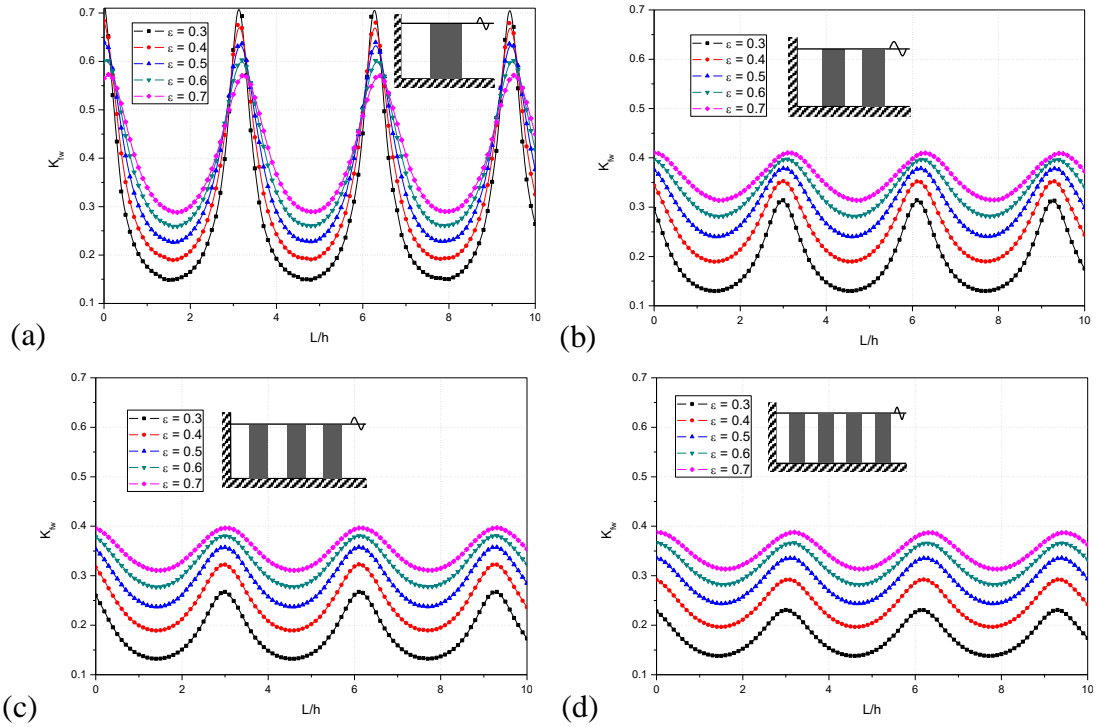


Figure 2.11: Variation in  $K_{fw}$  versus  $L/h$  for (a) single (b) double (c) triple and (d) four porous structures considering  $\gamma_{10}h=1$ ,  $f=1$ ,  $\theta=0^0$ ,  $d/h=1$  and  $w/h=1$ .

The variation between the double, triple and four structures are clearly seen in the  $K_{fw}$  for  $0.3 \leq \epsilon \leq 0.4$  at each of the resonating peaks. The 56%, 62%, 68% decrease in the  $K_{fw}$  is achieved with the double, triple and four structures as compared with the single porous structure at  $L/h=3$  for  $\epsilon=0.3$ . The increase in porosity of double, triple and four porous structures shows almost uniform values in  $K_{fw}$  due to fixed structural width (single porous structure width  $d/h=1$  is equally separated into double, triple and four

structures). However, the higher wavelength has minimum impact on porous structures and maximum impact on the leeward wall for higher porosity  $\varepsilon = 0.7$ . Thus, the study suggests that the double and triple porous structures with moderate porosity can perform well in reducing the  $K_{fw}$ .

#### 2.4.2.2 Comparative study between multiple structures considering leeward wall

The significance of the oblique wave damping by multiple fully extended porous structures with the leeward wall is analysed under the assumption of plane-wave approximation. Figures 2.12(a,b) shows the wave force impact on the leeward wall  $K_{fw}$  considering  $\varepsilon = 0.3$  (Figure 2.12a) and  $\varepsilon = 0.6$  (Figure 2.12b). It is found that the increase in the number of structures  $N$  shows a significant decrease in wave force impact acting on the leeward wall  $K_{fw}$ . The variation between single and double porous structures is clearly seen for  $\varepsilon = 0.3$  and  $\varepsilon = 0.6$ . Almost 58% (Figure 2.12a) and 34% (Figure 2.12b) reduction in the  $K_{fw}$  is achieved with two porous structures as compared with the single porous structure for normal wave incidence. Thereafter, the increase in the number of structures shows a minimum variation in  $K_{fw}$  due to fixed structural width. In the presence of minimum porosity  $\varepsilon = 0.3$  (Figure 2.12a), the resonating crest is observed and it gets disappeared with the increase in the porosity  $\varepsilon = 0.6$  (Figure 2.12b). However, minimum porosity shows the minimum wave force on the leeward wall  $K_{fw}$  and it is a suitable option for better performance of the multiple structures under oblique wave impinging.

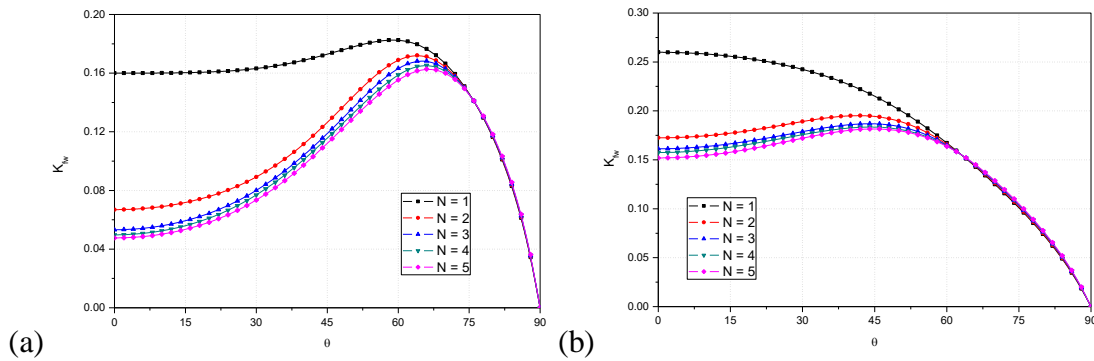


Figure 2.12: Variation in  $K_{fw}$  versus  $\theta$  with increase in the number of porous structures for  $\gamma_{10}h = 0.75$ ,  $f = 1$ ,  $w/h = 1$ ,  $d/h = 3$ ,  $L/h = 1$ , (a)  $\varepsilon = 0.3$  and (b)  $\varepsilon = 0.6$ .

### 2.4.3 Multiple porous structures placed on the step-type rigid bottom

The continental shelves, natural and artificial sand bars are most common in the offshore region and it is cumbersome to identify the uniform sea bottom (Behera et al., 2016). To consider the artificial and natural seabed variation, the changes in the seabed are approximated into rigid steps. The multiple fully extended porous structures are placed on the single and multi-step rigid seabed with multiple confined regions considering leeside unbounded region and confined region.

#### 2.4.3.1 Effect of width between the two structures

The multiple porous structures with multiple confined regions (spacing between the porous structures without the leeward wall) are having a considerable role in the wave damping. In the present case, each of the open water depth is uniform and the porous structure is placed on a rigid step and the step height is considered around 10% in the open water depth. Four porous structures upon multi-step rigid seabed (four rigid steps) with leeward unbounded regions is examined with variation in  $\gamma_{10}w$  for the porosities within  $0.2 \leq \varepsilon \leq 0.8$ . The resonating peaks and troughs are observed in the  $K_r$  (Figure 2.13a) with the increase in the length of the confined regions within  $0.01 \leq \gamma_{10}w \leq 20$ .

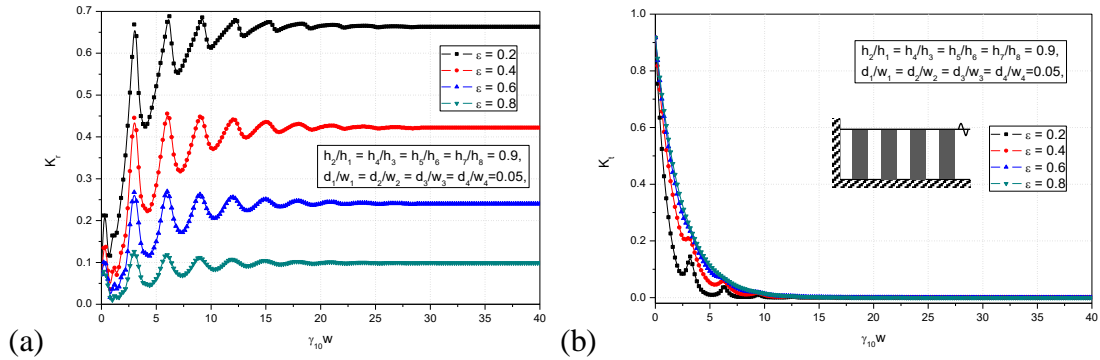


Figure 2.13: Variation in (a)  $K_r$  and (b)  $K_t$  versus  $\gamma_{10}w$  for various values of porosities considering four porous structures kept on the multi-step rigid bottom for  $\gamma_{10}h_1 = 2$ ,  $\theta = 0^\circ$  and  $f = 2$ .

Thereafter uniform estimation is obtained in the  $K_r$  within  $20 \leq \gamma_{10}w \leq 40$ . A sharp decrease in the  $K_t$  (Figure 2.13b) is observed with an increase in the  $\gamma_{10}w$  and minor estimation in the  $K_t$  is achieved due to the presence of the multiple structures with multiple confined regions. The increase in structural porosity shows the decrease in  $K_r$ ,

and little variation in  $K_t$  due to an increase of energy damping. The oscillation pattern is observed to be decreasing with an increase in the porosity within  $0.2 \leq \varepsilon \leq 0.8$ . Hence, it is evident that the multiple confined regions are effective in wave trapping and porous structures on step bottom are useful in the wave damping.

### 2.4.3.2 Effect of step height

In Figure 2.14(a) the wave reflection  $K_r$  due to double porous structures kept on the step-type seabed with the leeward wall is examined. The seaside and leeside open water depths are kept fixed ( $h_1/h_5 = 1$ ) and the two porous structures are placed on the step-type seabed ( $h_2 = h_3 = h_4$ ) and it is varied within  $0.5 \leq h_2/h_1 \leq 1$ . The oscillatory trend is observed in the  $K_r$  within  $0.1 \leq d/h_1 \leq 10$ , afterward oscillatory pattern gets disappeared with the increase in  $d/h_1$ . The increase in the step height shows the increase in  $K_r$  at each of the resonating peak due to wave interaction with rigid bodies (step-type seabed) which causes high wave reflection. It may be noted that the higher values in  $K_r$  are obtained within  $0.1 \leq d/h_1 \leq 2$  due to the full-wave reflection  $K_r = 1$  by the leeward wall. The oscillations can be reduced with the increase in the porosity and friction factor. However, the minimum step-type seabed height shows minimum values in  $K_r$  and encourages wave damping. The increase in step height shows the increase in  $K_r$  at each of the resonating peaks, which can reduce the wave force impact on the leeward wall. Thus, moderate step height is suggested for further development of coastal structures for optimal wave damping.

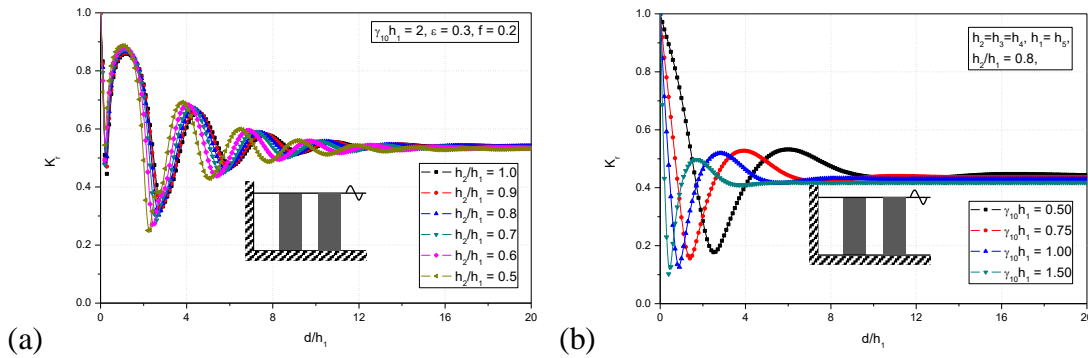


Figure 2.14: Variation in  $K_r$  versus  $d/h_1$  due to double porous structures for (a) step heights (b) dimensionless wave length considering  $\theta = 0^0$ ,  $w/h_1 = 1$  and  $L/h_1 = 1$ .

### 2.4.3.3 Effect of dimensionless wavelength

The variation in wave reflection  $K_r$  with variation in dimensionless wavelength  $\gamma_{10}h_1$  for the double porous structures upon step-type seabed with the leeward wall is presented in Figure 2.14(b). A sharp decrease in  $K_r$  is obtained with an increase in  $d/h_1$  and  $K_r$  approaches to the minimum value. Thereafter  $K_r$  increases to a peak value and remains uniform within  $0.5 < \gamma_{10}h_1 < 1.5$ . The increase in  $\gamma_{10}h_1$  shows significant variation in  $K_r$  within  $0.01 < d/h_1 < 10$  for all the combinations of  $\gamma_{10}h_1$ . Afterward, uniform values in  $K_r$  is achieved within  $10 < d/h_1 < 20$  for all the combinations of  $\gamma_{10}h_1$  due to the increase in the energy damping. It is concluded that the minimum  $\gamma_{10}h_1$  requires higher dimensionless structural width  $d/h_1$  to achieve the required energy damping and the wave force impact on the leeward wall can reduce with the increase in the dimensionless structural width  $d/h_1$ .

### 2.4.3.4 Effect of angle of incidence

The angle of incidence and structural width are the essential phenomena for the wave blocking, especially the waves of higher wavelength can be attenuated with significant structural width. The present condition elaborates on the effect of the non-dimensional structural width  $d/h_1$  on wave scattering for a double porous structure placed on the elevated bottom. In Figures 2.15(a,b), the  $K_r$  and  $K_t$  versus angle of incidence  $\theta$  is presented with variation in the  $d/h_1$  for  $\varepsilon = 0.4$  (Figure 2.15a) and  $\varepsilon = 0.8$  (Figure 2.15b). The increase in the  $d/h_1$  shows the increase in the  $K_r$  and minimum  $K_r$  from the structure is observed at  $\theta = 74^\circ$  (Figure 2.15a) and  $\theta = 54^\circ$  (Figure 2.15b) for all non-dimensional structural width within  $0.25 < d/h_1 < 2$ . The minimum  $K_r$  at  $\theta = 74^\circ$  (Figure 2.15a) and  $\theta = 54^\circ$  (Figure 2.15b) is due to the formation of standing waves at that particular angle of incidence, which may be termed as the critical angle. However, the increase in the  $d/h_1$  illustrates significant reduction in the  $K_t$  for  $\varepsilon = 0.4$  (Figure 2.15b) and  $\varepsilon = 0.8$  (Figure 2.15b). It may be noted that for  $d/h_1 = 2$  the variation in  $K_r$  and  $K_t$  is more as compared to other non-dimensional widths of the structure. High wave reflection is observed for all the combinations of structural width  $d/h_1$  at  $\varepsilon = 0.4$

as compared with  $\varepsilon = 0.8$  but the transmission coefficient is almost similar for  $\varepsilon = 0.4$  and  $\varepsilon = 0.8$ . This shows that the increase in the  $\varepsilon$  presents a preferable decrease in the wave reflection and less variation in wave transmission is noted between  $\varepsilon = 0.4$  and  $\varepsilon = 0.8$  due to the increase in the energy damping by fluid and porous structure interaction. However, the zero  $K_t$  can achieve with the increase in the structural width.

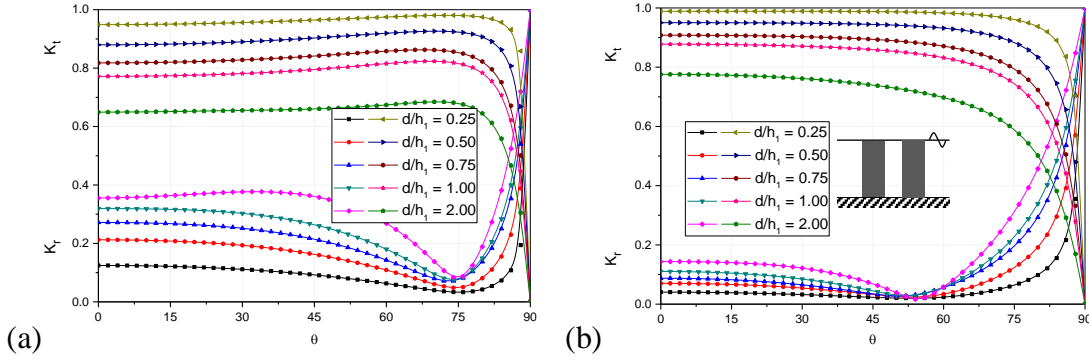


Figure 2.15: Variation in  $K_r$  and  $K_t$  versus  $\theta$  for different values of  $d/h_1$  for  $\gamma_{10}h_1 = 0.5$ ,  $h_2/h_1 = 0.9$ ,  $w/h_1 = 1$ ,  $f = 0.5$ ,  $d_1 = d_2 = d/2$  with (a)  $\varepsilon = 0.4$  and (b)  $\varepsilon = 0.8$ .

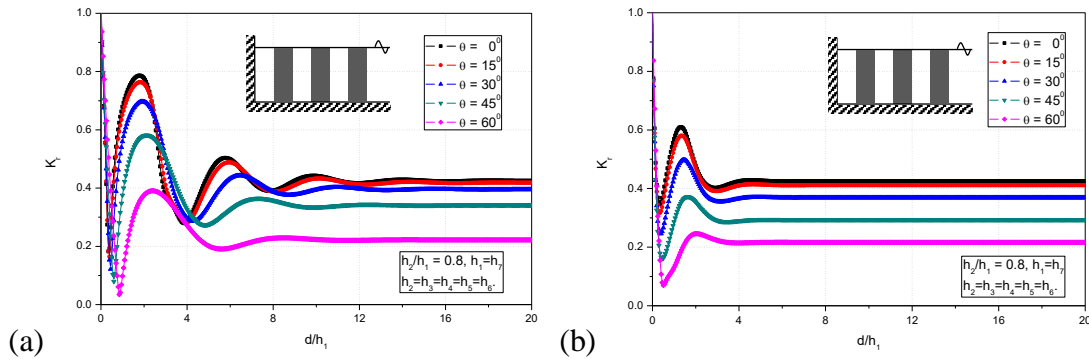


Figure 2.16: Variation in  $K_r$  versus  $d/h_1$  due to triple porous structures placed on one-step seabed considering  $w/h_1 = 1$ ,  $\gamma_{10}h_1 = 2$ ,  $L/h_1 = 1$ , (a)  $\varepsilon = 0.4$ ,  $f = 0.5$  and (b)  $\varepsilon = 0.7$ ,  $f = 2$ .

The triple porous structures placed on the one-step seabed with finite spacing away from the leeward wall are studied for a long-wave solution. Figures 2.16(a,b) present the  $K_r$  due to triple porous structures with variation in structural width for oblique waves. The trend of the  $K_r$  is unchanged and it is similar to previous solutions. The oscillatory pattern for lower friction factor (Figure 2.16a) and almost uniform values of  $K_r$  for higher friction factor (Figure 2.16b) is obtained. The variation in the width of

the three structure shows an immense role in reducing the oscillatory pattern in  $K_r$  within  $8 \leq d/h_1 \leq 20$  due to the increase in energy damping. The structural porosity plays a significant role in reducing the  $K_r$  within  $1 \leq d/h_1 \leq 8$  due to an increase in energy damping. The reduction in  $K_r$  is significant with an increase in the angle of incidence and minimum estimation in  $K_r$  is obtained for  $\theta = 60^\circ$  which may be due to the formation of standing waves.

#### 2.4.3.5 Comparative study of multiple porous structures with leeside wall

To study the significance of the multiple porous structures with leeside wall for wave trapping, a comparative study is performed by an increase in the number of porous structures under the assumption of plane-wave approximation. The numerical parameters  $\gamma_{10}h_1 = 0.5$ ,  $\varepsilon = 0.4$ ,  $f = 0.5$ ,  $\theta = 0^\circ$ ,  $w/h_1 = 1$  and  $h_2/h_1 = 0.8$  are kept fixed. The width of a single porous structure is considered as  $d/h_1 = 2$ . Afterwards, the  $d/h_1$  is separated into equal multiple structures for the purpose of comparison. Figure 2.17 (a,b) shows the variation in the  $K_r$  (Figure 2.17a) and  $K_{fv}$  (Figure 2.17b) due to single and multiple structures with variation in trapping chamber length  $L/h_1$ .

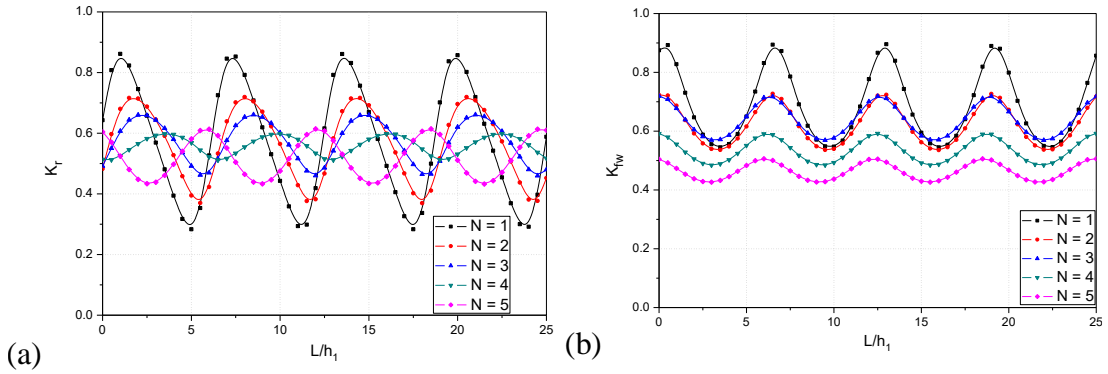


Figure 2.17: Comparative study between the multiple structures in (a)  $K_r$  and (b)  $K_{fv}$  versus  $L/h_1$  with  $\gamma_{10}h_1 = 0.5$ ,  $\varepsilon = 0.4$ ,  $f = 0.5$ ,  $\theta = 0^\circ$ ,  $d/h_1 = 2$ ,  $w/h_1 = 1$  and  $h_2/h_1 = 0.8$ .

The resonating peaks are clear in the case of the single porous structure as compared with the multiple porous structures and the resonating peaks and troughs in the  $K_r$  (Figure 2.17a) is observed decreasing for the higher number of porous structures lying

on the elevated bottom which may be due to the increase in the confined regions  $w/h_1$  and the transmitted wave from the first porous structure reflected by the subsequent porous structure and interacting with the incoming waves. Similarly, the  $K_{fw}$  (Figure 2.17b) is noted decreasing with the increase in the multiple structures, and the resonating peaks and troughs are observed to be high for  $N=1$  and these resonating peaks and troughs decrease with the increase in the multiple porous structures. The increase in the confined regions is the major reason behind the decrease in the  $K_{fw}$ . The present study suggests that the multiple structures are the better solution for the wave blocking and the magnitude of resonating peaks and troughs in the wave reflection  $K_r$  and wave force on the leeside wall  $K_{fw}$  can be reduced through wave damping. The resonating troughs are observed in the  $K_{fw}$  at particular intervals, and the resonating troughs also encourage the formation of clapotis (Twu and Lin, 1990). These clapotis nodes are helpful in the design of coastal structures to find the optimum water chamber length for the construction of the porous structure away from the leeward wall to achieve the better wave trapping in practice.

## **2.5 CLOSURE**

The wave dissipating performance of multiple fully-extended porous structures considering the leeward unbounded region and confined region/leeward wall is examined. The following conclusions are drawn from the present study:

- 91.5% energy damping is observed for a single structure within  $3 < \gamma_{10}d < 7$  and 12% increase in energy damping is achieved with double structures compared with a single structure within  $1 < \gamma_{10}d < 3$ .
- The lower values of the friction factor show the oscillating pattern in the wave reflection and transmission, whereas higher values of the friction factor show the uniform values of wave reflection and transmission.
- The resonating trend in the  $K_r$  and  $K_t$  is observed to be increasing with the increase in width between the structures  $w/h$  and the  $w/h=1$  is effective in increasing wave energy damping.



- The resonating peaks become higher for minimal porosity and broadens with the increase in  $\gamma_{10}h$  and  $w/h$  in the presence of four porous structures with finite spacing.
- The 42% decrease in  $K_t$  is achieved with a pair of porous structures as compared with a single porous structure. Afterward, the uniform estimation in  $K_t$  is obtained with an increase in multiple structures within  $3 \leq N \leq 5$  for fixed structural thickness.
- The presence of double porous structures shows a drastic variation in reducing the wave force impact on the leeward wall compared with a single structure. The triple porous structure showed a considerable decrease in  $K_{fw}$  compared with double porous structures for minimum porosity within  $0.3 \leq \varepsilon \leq 0.4$  at each resonating peak.
- The performance of triple and four porous structures are almost similar in reducing the  $K_{fw}$  for fixed structural width.
- The increase in step height shows an increase in  $K_r$  along with the increase in resonating trend in  $K_r$  within  $0.1 \leq d/h_1 \leq 2$ . The increase in the angle of incidence shows the decrease in  $K_r$  due to multiple structures upon step-type seabed with the leeward wall.
- Overall, the higher porosity is suitable for increasing the energy damping (in the absence of leeward wall) and lower porosity is suitable in decreasing the wave force impact on the leeward wall in the presence of double and triple structures.



## CHAPTER 3

# WAVE DAMPING BY BARRIER-ROCK POROUS STRUCTURES

### 3.1 GENERAL INTRODUCTION

The fully-extended permeable breakwaters are identified as the most common structures for dissipating the fluid oscillations, which can create gentle wave action over the leeward locations and also allows the exchange of seawater for safe loading and unloading of goods. The traditional rigid breakwaters require a huge quantity of construction material and the process of construction is cumbersome. In many cases, conventional rigid structures are subjected to high wave impact and collapsed in various locations. In particular situations, it is a complicated phenomenon for coastal engineers/specialists to suggest a breakwater configuration for effective oblique wave attenuation. Hence, researchers have introduced the porosity/permeability concept, which directly reduces the construction material, construction cost and indirectly helps in enhancing wave damping. In general, a porous structure usually permits the maximum number of waves to pass through pore spaces and the interaction between incident waves and pores spaces enhances the wave decay. In the present study, a novel breakwater configuration titled barrier-rock porous structure is suggested for wave blocking. The barrier-rock porous structure consists of seaward and leeward vertical thin barriers with a rock-fill between two barriers. The barrier-rock porous structure can be considered as suitable options in different locations, where there is a significant seabed scour and weak geological faults/conditions (Liu and Li, 2014). In general, a barrier-rock porous structure can be developed in different structural configurations such as (a) barrier-rock porous structure (b) structure away from rigid wall (c) structure backed by the rigid wall and (d) structure of semi-infinite thickness placed on uniform/step-bottom.

In general, the life of a porous structure can be improved by reducing the wave impact on the seaward structural interface (Twu and Chieu, 2000). In those situations, the barrier-rock porous structures can perform significantly in reducing the fluid force on

the rock-core. Moreover, seaward and leeward thin barriers can work as protective structures of the breakwater in the presence of high wave action (Liu and Li, 2014). In the present study, four types of barrier-rock structures are examined using the eigenfunction expansion method and analytical results are validated with previous results for several structural configurations. Thereafter, the straight analytical relations are proposed for the determination of wave reflection and transmission using plane-wave approximation. The effect of structural porosity, friction factor, incident wave angle, breakwater thickness and trapping chamber length on wave scattering/trapping is presented for various types of barrier-rock porous structures. The skin depth for the semi-infinite barrier-rock porous structure is presented considering step-bottom. Finally, the comparative study is performed between four different structural configurations in the presence of step-bottom considering variable breakwater porosity.

### **3.2 MATHEMATICAL FORMULATION**

The wave motion through the idealized barrier-rock porous structure of various structural configurations is shown in Figure 3.1(a-d). In general, vertical breakwater with barriers can be designed in four possible cases such as barrier-rock porous structure (Figure 3.1a), structure away from the rigid wall (Figure 3.1b) backed by a rigid wall (Figure 3.1c) and structure of semi-infinite thickness (Figure 3.1d). The linearized wave theory is used to examine the wave scattering and wave trapping by the barrier-rock porous structure. The 3D Cartesian co-ordinate system is considered having x-axis being perpendicular to the structure, y-axis being positive downward and z-axis is parallel to the breakwater. The angle of incidence on the barrier-rock porous structure is denoted as  $\theta$  which varies within  $0^\circ \leq \theta \leq 90^\circ$  at water depth  $h_j$ . The seaward and leeward thin barriers are examined by adopting the barrier condition as in Yu (1995) and rock-core placed between the two thin porous barriers is analysed using the classical method proposed by Sollitt and Cross (1972) for wave-induced flow through porous blocks on assuming homogeneous porosity. The fluid is assumed to be incompressible, inviscid and fluid motion is irrotational with simple harmonic in time and angular frequency  $\omega$ .

In addition, the incident wave is assumed to be impinging on the porous breakwater at an angle  $\theta$ . Thus, there exist velocity potentials  $\phi_j(x, y, z, t)$  and free surface deflection

$\zeta_j(x, z, t)$  given in the form of  $\zeta_j(x, z, t) = \text{Re}\{\eta_j(x)e^{i(\lambda z - \omega t)}\}$ , where  $\text{Re}$  being real part and  $\lambda = \gamma_{10} \sin \theta$  is the wave-number component in the  $z$ -direction,  $\theta$  is the angle of impinging which varies within  $0^\circ \leq \theta \leq 90^\circ$ . The porous barriers width is minimal as compared to the wavelength of incident waves (Sahoo et al., 2000; Huang et al., 2011). So, the whole fluid domain is divided into upstream/downstream open water regions and porous structure region. The spatial velocity potentials  $\phi_j(x, y)$  satisfy the Helmholtz relation in each fluid region given by

$$\frac{\partial^2 \phi_j(x, y)}{\partial x^2} + \frac{\partial^2 \phi_j(x, y)}{\partial y^2} - l^2 \phi_j(x, y) = 0, \quad \text{for } j=1,2,3 \quad (3.1)$$

where  $j=1,2,3$  shows the velocity potentials in free water and barrier-rock porous structure occupied regions.

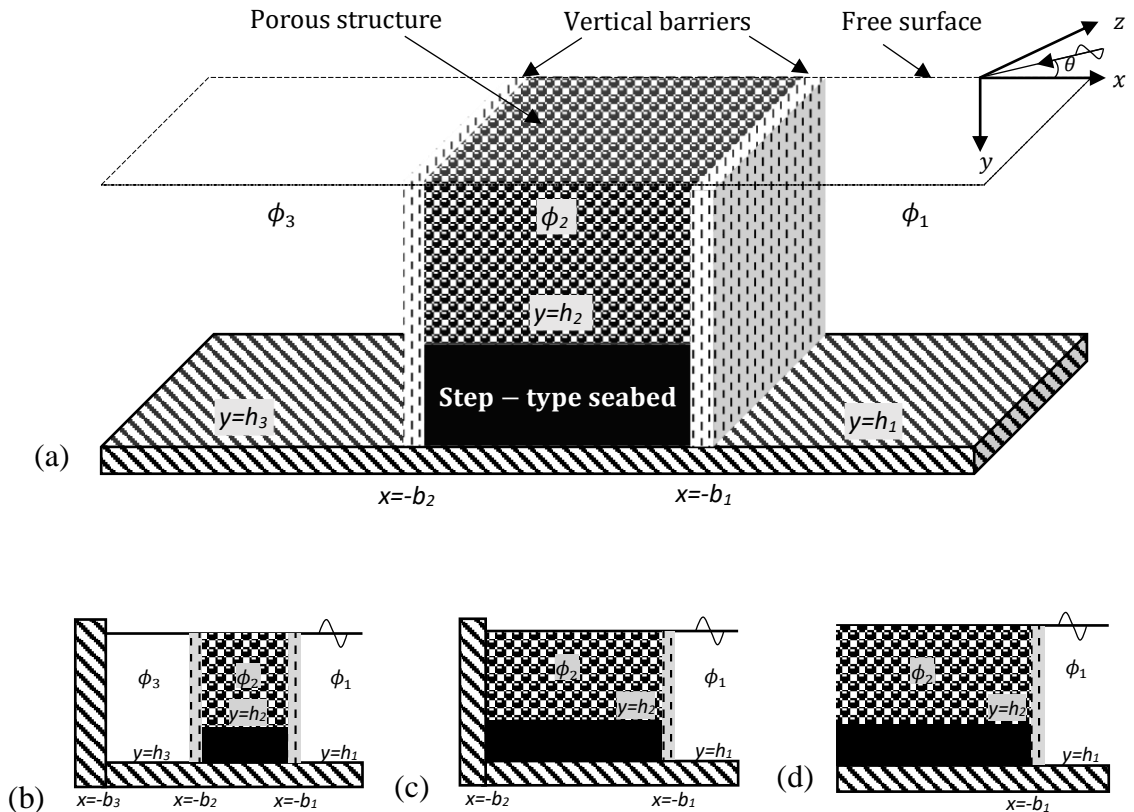


Figure 3.1: Schematic diagram for (a) barrier-rock porous structure of finite thickness (b) structure away from rigid wall (c) structure backed by the rigid wall and (d) structure of semi-infinite thickness placed on step-bottom.

The linearized free surface condition for free-water and structure regions is given by

$$\frac{\partial \phi_j(x, y)}{\partial y} + \Gamma_j \phi_j(x, y) = 0 \quad \text{on } y = 0, \quad (3.2)$$

where  $\Gamma_{1,3} = \omega^2/g$  and  $\Gamma_2 = \omega^2(S_b + if_b)/g$  for free-water regions and porous structure region respectively, the  $S_b$  and  $f_b$  are reactance and resistance coefficients of the porous breakwater and  $i = \sqrt{-1}$  is the imaginary number. The wave motion upon impermeable seabed is given by

$$\frac{\partial \phi_j(x, y)}{\partial y} = 0 \quad \text{on } y = h_j \quad \text{for } j = 1, 2, 3 \quad (3.3)$$

where  $h_j$  for  $j = 1, 3$  is water depth in upstream/downstream free-water regions and  $h_2$  is water depth in barrier-rock porous structure region. However, the fluid pressure and velocity must be continuous across the seaward and leeward structural interfaces within  $0 \leq y \leq h_2$ , the matching condition at the structural interfaces (Isaacson et al., 2000; Karmakar et al., 2013; Karmakar and Guedes Soares 2014, 2015) are given by

$$\frac{\partial \phi_1(x, y)}{\partial x} = \varepsilon_b \frac{\partial \phi_2(x, y)}{\partial x} = i\gamma_{10} G_1 [(S_b + if_b)\phi_2(x, y) - \phi_1(x, y)] \quad \text{at } x = -b_1 \quad (3.4a)$$

$$\frac{\partial \phi_3(x, y)}{\partial x} = \varepsilon_b \frac{\partial \phi_2(x, y)}{\partial x} = i\gamma_{30} G_2 [\phi_3(x, y) - (S_b + if_b)\phi_2(x, y)] \quad \text{at } x = -b_2 \quad (3.4b)$$

where  $\varepsilon_b$  breakwater porosity,  $G_j, j = 1, 2$  is porous effect parameter of seaward and leeward vertical porous barriers respectively of the form

$$G_{1(2)} = \frac{\varepsilon_{s(l)}}{\gamma_{10} d_{s(l)} (f_{s(l)} - iS_{s(l)})} \quad (3.5)$$

where  $d_{s(l)}$  is thickness  $\varepsilon_{s(l)}$  is porosity,  $f_{s(l)}$  is resistance and  $S_{s(l)}$  is the reactance of seaward and leeward barriers respectively. The no-flow condition near the rigid step-bottom is given by

$$\frac{\partial \phi_1(x, y)}{\partial x} = 0 \quad \text{on } x = -b_1, \quad \text{for } h_2 \leq y \leq h_1, \quad (3.6a)$$

$$\frac{\partial \phi_3(x, y)}{\partial x} = 0 \quad \text{on } x = -b_2, \quad \text{for } h_2 \leq y \leq h_3. \quad (3.6b)$$

The barrier-rock structure is placed near/far away from the seawall. Hence, the no-flow condition at the seawall is given by

$$\frac{\partial \phi_2(x, y)}{\partial x} = 0 \text{ on } x = -b_2, 0 \leq y \leq h_2, \quad (3.6c)$$

$$\frac{\partial \phi_3(x, y)}{\partial x} = 0 \text{ on } x = -b_3, 0 \leq y \leq h_3, \quad (3.6d)$$

The linearized resistance  $f_b$  and reactance coefficients  $S_b$  (Sollitt and Cross, 1972) due to the presence of porous rock-fill is determined on solving the relation given by

$$S_b = 1 + C_m \left[ \frac{1 - \varepsilon_b}{\varepsilon_b} \right] \quad (3.7a)$$

$$f_b = \frac{1}{\omega} \left\{ \frac{\int_V dV \int_t^{t+T} \varepsilon_b^2 \left( \frac{\nu q^2}{K_p} + \frac{C_f \varepsilon_b}{\sqrt{K_p}} |q|^3 \right) dt}{\int_V dV \int_t^{t+T} \varepsilon_b q^2 dt} \right\}, \quad (3.7b)$$

where  $C_m$  is the coefficient of added mass considered to be very minimal/zero (Sollitt and Cross, 1972), thus  $S_b = 1$  is kept fixed throughout the study. The  $K_p$  is intrinsic permeability,  $q$  is instantaneous Eulerian velocity vector,  $\nu$  is kinematic viscosity,  $V$  is volume,  $C_f$  is a turbulent resistant coefficient and  $T$  is wave period. In the case of seaward and leeward porous barriers, the reactance  $S_{s(l)} = 1$ , resistance  $f_{s(l)} = 2$ , and barrier thickness  $d_{s(l)} / h_1 = 0.04$  for  $j = 1, 2$  is kept fixed (Suh et al., 2011; Liu and Li, 2014).

The wavenumber in upstream/downstream free-water region  $\gamma_{jn}$  for  $j = 1, 3$  and barrier-rock porous structure region  $\gamma_{2n}$  satisfies the dispersion relation for finite and shallow water depth is given by

$$\omega^2 = \begin{cases} g\gamma_{j0} \tanh \gamma_{j0} h_j & \text{for } n = 0 \\ -g\gamma_{jn} \tan \gamma_{jn} h_j & \text{for } n = 1, 2, \dots \end{cases} \text{ for } j = 1, 3 \quad (3.8a)$$

$$\omega^2 (S_b + if_b) = \begin{cases} g\gamma_{20} \tanh \gamma_{20} h_2 & \text{for } n = 0 \\ g\gamma_{2n} \tanh \gamma_{2n} h_2 & \text{for } n = 1, 2, \dots \end{cases} \quad (3.8b)$$

$$\omega^2 = g\gamma_{j0}^2 h_j \text{ for } j = 1, 3 \quad (3.9a)$$

$$\omega^2 (S_b + if_b) = g\gamma_{20}^2 h_2 \quad (3.9b)$$

where  $\omega$  is wave frequency and  $g$  is acceleration due to gravity.

In the far-field region, the radiation conditions in the presence of barrier-rock porous structure are given by

$$\phi_j(x) = \begin{cases} (I_{10}e^{-ik_{10}x} + R_{10}e^{ik_{10}x})f_{10}(y) & \text{as } x \rightarrow \infty, \\ (T_{30}e^{-ik_{30}x})f_{30}(y) & \text{as } x \rightarrow -\infty, \end{cases} \quad (3.10)$$

where  $I_{10}$ ,  $R_{10}$  and  $T_{30}$  are the complex amplitude of incident, reflected and transmitted waves respectively. However, the monochromatic incident wave amplitude  $I_{10}$  is considered as unity.

### 3.3 METHOD OF SOLUTION

The barrier-rock porous structure in various structural configurations is examined using the eigenfunction expansion method. The method of solution for each of the structural configurations is presented in as subsections.

#### 3.3.1 Barrier-rock porous structure of finite thickness

The barrier-rock porous structure configuration is designed and constructed at Dongying bay, China (Liu and Li, 2014) to dissipate the incident waves. In the case of the barrier-rock porous structure, the fluid domain is divided into seaward and leeward free water regions along with a barrier-rock porous structure occupied region. The velocity potentials  $\phi_j(x, y)$  for  $j=1, 2, 3$  representing each of the regions is given by

$$\phi_1(x, y) = \left\{ I_{10}e^{-ik_{10}(x+b_1)} + R_{10}e^{ik_{10}(x+b_1)} \right\} f_{10}(y) + \sum_{n=1}^{\infty} R_{1n}e^{-\kappa_{1n}(x+b_1)} f_{1n}(y), \quad (3.11a)$$

for  $-b_1 < x < \infty$ ,  $0 < y < h_1$ ,

$$\phi_2(x, y) = \sum_{n=0}^{\infty} \left\{ A_{2n}e^{-ik_{2n}(x+b_1)} + B_{2n}e^{ik_{2n}(x+b_2)} \right\} f_{2n}(y) \quad \text{for } -b_2 < x < -b_1, \quad 0 < y < h_2, \quad (3.11b)$$

$$\phi_3(x, y) = T_{30}e^{-ik_{30}(x+b_2)} f_{30}(y) + \sum_{n=1}^{\infty} T_{3n}e^{\kappa_{3n}(x+b_2)} f_{3n}(y), \quad (3.11c)$$

for  $-\infty < x < -b_2$ ,  $0 < y < h_3$ .

where  $f_{j0} = \frac{\cosh \gamma_{jn}(h_j - y)}{\cosh \gamma_{jn}h_j}$  for  $j=1, 3$ ,  $f_{20} = \frac{\cosh \gamma_{2n}(h_2 - y)}{\cosh \gamma_{2n}h_2}$ ,  $\gamma_{j0}$ ,  $\gamma_{jn}$  are

wavenumbers in the y-direction,  $k_{j0} = \sqrt{\gamma_{j0}^2 - l^2}$ ,  $k_{jn} = \sqrt{\gamma_{jn}^2 - l^2}$  are wavenumbers in the x-direction, and  $l = \gamma_{10} \sin \theta$  is wavenumber in the z-direction. Moreover, the



$\gamma_{j0} = i\gamma_{jn}$  for  $j=1,3$  and  $n=1,2,\dots$ . It may be noted that the eigenfunction  $f_{jn}(y)$ ,  $j=1,2$  and 3 satisfy the orthogonal relation given by

$$\langle f_{jn}, f_{jm} \rangle_{j=1,3} = \begin{cases} 0 & \text{for } m \neq n, \\ C'_n & \text{for } m = n, \end{cases} \quad \text{and} \quad \langle f_{jn}, f_{jm} \rangle_{j=2} = \begin{cases} 0 & \text{for } m \neq n, \\ C''_n & \text{for } m = n, \end{cases} \quad (3.12a)$$

with respect to the orthogonal mode-coupling relation defined by

$$\langle f_{jm}, f_{jn} \rangle_{j=1,3} = \int_0^{h_j} f_{jm}(y) f_{jn}(y) dy, \quad \text{and} \quad \langle f_{jm}, f_{jn} \rangle_{j=2} = \int_0^{h_2} f_{jm}(y) f_{jn}(y) dy, \quad (3.12b)$$

where  $C'_n|_{j=1,3} = \left\{ \frac{2\gamma_{jn}h_j + \sinh 2\gamma_{jn}h_j}{4\gamma_{jn} \cosh^2 \gamma_{jn}h_j} \right\}$  and  $C''_n|_{j=2} = \left\{ \frac{2\gamma_{jn}h_j + \sinh 2\gamma_{jn}h_j}{4\gamma_{jn} \cosh^2 \gamma_{jn}h_j} \right\}$  for

$n=0,1,\dots$  with  $C'_n|_{j=1,3}$  for  $n=1,2,\dots$  are obtained by substituting  $\gamma_{jn} = i\gamma_{jn}$  for free water region.

### 3.3.1.1 Full solution

The hydrodynamic performance of the barrier-rock porous structure is examined on applying the mode-coupling relation as in Equation (3.12a,b) along with the velocity potentials as in Equation (3.11a) – (3.11c), matching conditions as in Equation (3.4a,b) and no-flow conditions at rigid-step as in Equation (3.6a,b). Using the mode-coupling relation, the system of equations is given by

$$\left[ I_{10} \delta_{nm} (i\gamma_{10} G_1 - ik_{10}) + \sum_{n=0}^{\infty} (i\gamma_{10} G_1 + ik_{1n}) R_{1n} \right] \int_0^{h_2} f_{1n}(y) f_{1m}(y) dy = \sum_{n=0}^{\infty} i\gamma_{10} G_1 (S_b + if_b) [A_{2n} + B_{2n} e^{-ik_{2n}d}] \int_0^{h_2} f_{2n}(y) f_{1m}(y) dy, \quad (3.13a)$$

$$-ik_{1n} \{ I_{10} \delta_{nm} - R_{1m} \} \langle f_{1n}(y), f_{1m}(y) \rangle = \varepsilon_b \left[ \sum_{n=0}^{\infty} -ik_{2n} \{ A_{2n} - B_{2n} e^{-ik_{2n}d} \} \int_0^{h_2} f_{2n}(y) f_{1m}(y) dy \right], \quad (3.13b)$$

$$i\gamma_{30} G_2 \left[ (S_b + if_b) \sum_{n=0}^{\infty} \{ A_{2n} e^{-ik_{2n}d} + B_{2n} \} \int_0^{h_2} f_{2n}(y) f_{3m}(y) dy \right] = \sum_{n=0}^{\infty} (i\gamma_{30} G_2 + ik_{3n}) T_{3n} \int_0^{h_2} f_{3n}(y) f_{3m}(y) dy, \quad (3.13c)$$

$$\varepsilon_b \left[ \sum_{n=0}^{\infty} -ik_{2n} \{ A_{2n} e^{-ik_{2n}d} - B_{2n} \} \int_0^{h_2} f_{2n}(y) f_{3m}(y) dy \right] = -ik_{3n} T_{3n} \langle f_{3n}(y), f_{3m}(y) \rangle. \quad (3.13d)$$

where  $\delta_{nm} = \begin{cases} 1 & \text{for } m = n = 0, \\ 0 & \text{for } m = n = 1, 2, \dots, \end{cases}$   $d = -(b_2 - b_1)$ ,  $n = 0, 1, 2, \dots$  and  $m = 0, 1, 2, \dots$

The infinite series sums presented in Equation (3.13a) - (3.13d) are truncated for a finite term  $M$  to obtain the linear system of  $4(M + 1)$  equations to determine  $4(M + 1)$  unknown coefficients such as  $R_{1n}$ ,  $A_{2n}$ ,  $B_{2n}$  and  $T_{3n}$ . The oblique wave reflection, transmission and damping coefficients due to the barrier-rock porous structure is determined using the relation given by

$$K_r = \left| \frac{R_{10}}{I_{10}} \right|, \quad K_t = \left| \frac{T_{30}}{I_{10}} \right| \quad \text{and} \quad K_d = 1 - (K_r^2 + K_t^2). \quad (3.14)$$

### 3.3.1.2 Plane-wave approximation

The straight analytical relations for finding the  $K_r$  and  $K_t$  due to barrier-rock porous structure placed on step-type bottom are presented for progressive plane wave given by

$$K_r = \left| \frac{R_{10}}{I_{10}} \right| = \frac{i \tan k_{20} d (X^2 - M_b^2 Q_L Q_L) + M_b X (Q_L - Q_L)}{i \tan k_{20} d (X^2 + M_b^2 Q_S Q_L) + M_b X (Q_L + Q_S)}, \quad (3.15a)$$

$$K_t = \left| \frac{T_{30}}{I_{10}} \right| = \frac{2EM_b \{(1 - R_{10})(X - ik_{10}) - i\gamma_{10}G_1(1 + R_{10})\}}{(M_b Q_L + X)(M_b - i\gamma_{10}G_1) - (M_b Q_L - X)(M_b + i\gamma_{10}G_1)E^2}, \quad (3.15b)$$

where  $M_b = \frac{\varepsilon_b}{G_b} \left[ \frac{k_{20}}{k_{10}} \right] = \frac{\varepsilon_b}{G_b} \left[ \frac{k_{20}}{k_{30}} \right]$ ,  $G_b = S_b + if_b$ ,  $k_{20} = (\gamma_{20}^2 - l^2)^{1/2}$ ,  $k_{10} = (\gamma_{10}^2 - l^2)^{1/2}$ ,

$$l = \gamma_{10} \sin \theta, \quad E = e^{ik_{20}d}, \quad Q_l = \frac{i\gamma_{10}G_1 - ik_{10}}{i\gamma_{10}G_1}, \quad Q_s = \frac{i\gamma_{10}G_1 + ik_{10}}{i\gamma_{10}G_1}, \quad Q_L = \frac{i\gamma_{30}G_2 + ik_{30}}{i\gamma_{30}G_2},$$

$$d = -(b_2 - b_1), \quad X = \frac{U}{V}, \quad \Lambda = \frac{V}{W}, \quad W = \int_0^{h_2} f_{20}(y)f_{10}(y)dy = \int_0^{h_2} f_{20}(y)f_{30}(y)dy,$$

$$U = \int_0^{h_1} f_{10}(y)f_{10}(y)dy = \int_0^{h_3} f_{30}(y)f_{30}(y)dy \quad \text{and} \quad V = \int_0^{h_2} f_{10}(y)f_{10}(y)dy = \int_0^{h_2} f_{30}(y)f_{30}(y)dy.$$

The analytical equations as in Equation (3.15a,b) can be used for several structural configurations such as

- $h_2/h_1 = 1$ , shows the barrier-rock porous structure placed on a uniform bottom
- $\varepsilon_b = 1$  and  $f_b = 0$ , shows the wave scattering by two permeable barriers without porous structure

- $G_1 = G_2 = 0$  shows the porous structure with seaward/leeward rigid barriers
- The  $G_1 = G_2 \rightarrow \infty$  shows a porous structure without barriers ( $G_1 = G_2 = 10^{10}$  is suggested by Liu and Li, 2014).

The wave reflection/transmission due to porous structure without barriers placed on step-bottom on considering  $G_1 = G_2 \rightarrow \infty$  is given by

$$K_r = \left| \frac{R_{10}}{I_{10}} \right| = \frac{i \tan k_{20} d (X^2 - M_b^2)}{i \tan k_{20} d (X^2 + M_b^2) + 2M_b X}, \quad (3.15c)$$

$$K_t = \left| \frac{T_{30}}{I_{10}} \right| = \frac{\{-R_{10}(X+1) + (X-1)\} M_b}{i(M_b^2 - X) \sin k_{20} B + (X_b - 1) M_b \cos k_{20} B}. \quad (3.15d)$$

The analytical relations as in Equation (3.15c,d) can be used for the uniform bottom on considering  $X = U/V = 1$ .

### 3.3.2 Barrier-rock porous structure placed away from a rigid wall

The present subsection shows the wave trapping by a barrier-rock porous structure placed far away from the rigid wall as in Figure 3.1(b). The velocity potentials in each of the region for the wave interaction with the barrier-rock porous structure placed far away from the rigid wall is given by

$$\phi_1(x, y) = \left\{ I_{10} e^{-ik_{10}(x+b_1)} + R_{10} e^{ik_{10}(x+b_1)} \right\} f_{10}(y) + \sum_{n=1}^{\infty} R_{1n} e^{-\kappa_{1n}(x+b_1)} f_{1n}(y), \quad (3.16a)$$

for  $-b_1 < x < \infty, 0 < y < h_1$ ,

$$\phi_2(x, y) = \sum_{n=0}^{\infty} \left\{ A_{2n} e^{-ik_{2n}(x+b_1)} + B_{2n} e^{ik_{2n}(x+b_2)} \right\} f_{2n}(y) \quad \text{for } -b_2 < x < -b_1, 0 < y < h_2, \quad (3.16b)$$

$$\phi_3(x, y) = T_{30} \left\{ e^{-ik_{30}(x+b_2)} + e^{ik_{30}(x+b_3+L)} \right\} f_{30}(y) + \sum_{n=1}^{\infty} T_{3n} \left\{ e^{\kappa_{3n}(x+b_2)} + e^{-\kappa_{3n}(x+b_3+L)} \right\} f_{3n}(y)$$

for  $-a_3 < x < -a_2, 0 < y < h_3$ .

(3.16c)

where  $L$  is the spacing between structure and rigid wall.

#### 3.3.2.1 Full solution

The mode-coupling relation as in Equation (3.12a,b) is utilized along with the velocity potentials as in Equation (3.16a) – (3.16c), matching conditions in Equation (3.4a,b)

and no-flow conditions as in Equation (3.6a,b) to obtain the system of linear equations given by

$$\left[ I_{10} \delta_{nm} (i\gamma_{10} G_1 - ik_{10}) + \sum_{n=0}^{\infty} (i\gamma_{10} G_1 + ik_{1n}) R_{1n} \right] \int_0^{h_2} f_{1n}(y) f_{1m}(y) dy = \sum_{n=0}^{\infty} i\gamma_{10} G_1 (S_b + if_b) \left[ A_{2n} + B_{2n} e^{-ik_{2n}d} \right] \int_0^{h_2} f_{2n}(y) f_{1m}(y) dy, \quad (3.17a)$$

$$-ik_{1n} \{ I_{10} \delta_{nm} - R_{1m} \} \langle f_{1n}(y), f_{1m}(y) \rangle = \varepsilon_b \left[ \sum_{n=0}^{\infty} -ik_{2n} \{ A_{2n} - B_{2n} e^{-ik_{2n}d} \} \int_0^{h_2} f_{2n}(y) f_{1m}(y) dy \right], \quad (3.17b)$$

$$i\gamma_{30} G_2 \left[ (S_b + if_b) \sum_{n=0}^{\infty} \{ A_{2n} e^{-ik_{2n}d} + B_{2n} \} \int_0^{h_2} f_{2n}(y) f_{3m}(y) dy \right] = \sum_{n=0}^{\infty} T_{3n} \left[ i\gamma_{30} G_2 \{ 1 + e^{2ik_{3n}L} \} + ik_{3n} \{ 1 - e^{2ik_{3n}L} \} \right] \int_0^{h_2} f_{3n}(y) f_{3m}(y) dy, \quad (3.17c)$$

$$\varepsilon_b \left[ \sum_{n=0}^{\infty} -ik_{2n} \{ A_{2n} e^{-ik_{2n}d} - B_{2n} \} \int_0^{h_2} f_{2n}(y) f_{3m}(y) dy \right] = -ik_{3n} T_{3n} (1 - e^{2ik_{3n}L}) \langle f_{3n}(y), f_{3m}(y) \rangle. \quad (3.17d)$$

The infinite series sums presented in Equation (3.17a) – (3.17d) are truncated for a finite term  $M$  to obtain  $4(M+1)$  linear equations for determination of  $4(M+1)$  unknown coefficients and  $K_r$ , due to the barrier-rock porous structure away from the rigid wall is computed using Equation (3.14).

### 3.3.2.2 Plane-wave approximation

The analytical relation for  $K_r$ , due to a barrier-rock porous structure placed far away from the rigid wall in the case of a progressive plane wave is given by

$$K_r = \left| \frac{R_{10}}{I_{10}} \right| = \frac{i \tan k_{20}d (X^2 - M_b^2 Q_I Z_L) + M_b X (Z_L - Q_I)}{i \tan k_{20}d (X^2 + M_b^2 Q_S Z_L) + M_b X (Z_L + Q_S)}, \quad (3.18a)$$

where  $L = (b_3 - b_2)$  and  $Z_L = \frac{\gamma_{30} G_2 + ik_{30} \tan k_{30} L}{i\gamma_{30} G_2 \tan k_{30} L}$ .

If the  $G_1 = G_2 \rightarrow \infty$ , then the relation for  $K_r$ , presented in Equation (3.18a) reduces for wave propagation through the porous structure without barriers and is given by

$$K_r = \left| \frac{R_{10}}{I_{10}} \right| = \frac{i \tan k_{20} d (iX^2 \tan k_{30} L - M_b^2) + M_b X (1 - i \tan k_{30} L)}{i \tan k_{20} d (iX^2 \tan k_{30} L + M_b^2) + M_b X (1 + i \tan k_{30} L)}. \quad (3.18b)$$

### 3.3.3 Barrier-rock porous structure backed by a rigid wall

In the case of barrier-rock porous structure backed by a rigid wall, the rock-fill is placed within the seaward barrier and rigid leeward wall (Figure 3.1c). The application of the present case can be found in Kelsey Bay, Canada (Isaacson et al., 2000). The velocity potentials for seaward free-water and porous structure occupied regions are given by

$$\phi_1(x, y) = \left\{ I_{10} e^{-ik_{10}(x+b_1)} + R_{10} e^{ik_{10}(x+b_1)} \right\} f_{10}(y) + \sum_{n=1}^{\infty} R_{1n} e^{-\kappa_{1n}(x+b_1)} f_{1n}(y), \quad (3.19a)$$

for  $-a_1 < x < \infty$ ,  $0 < y < h_1$ ,

$$\phi_2(x, y) = \sum_{n=0}^{\infty} A_{2n} \cos k_{2n}(x+b_2) f_{2n}(y) \quad \text{for } -a_2 < x < -a_1, 0 < y < h_2. \quad (3.19b)$$

#### 3.3.3.1 Full solution

The full solution for the barrier-rock porous structure backed by a rigid wall is obtained using orthogonal mode-coupling relation, and on solving the system of linear equations are given by

$$I_{10} \delta_{nm} (i\gamma_{10} G_1 - ik_{10}) \int_0^{h_2} f_{1n}(y) f_{1m}(y) dy + \sum_{n=0}^{\infty} (i\gamma_{10} G_1 + ik_{1n}) R_{1n} \int_0^{h_2} f_{1n}(y) f_{1m}(y) dy =$$

$$(S_b + if_b) \sum_{n=0}^{\infty} i\gamma_{10} G_1 A_{2n} \cos(k_{2n} d) \int_0^{h_2} f_{2n}(y) f_{1m}(y) dy, \quad (3.20a)$$

$$-ik_{1n} \{ I_{10} \delta_{nm} - R_{1m} \} \langle f_{1n}(y), f_{1m}(y) \rangle = \varepsilon_b \sum_{n=0}^{\infty} -k_{2n} A_{2n} \sin(k_{2n} d) \int_0^{h_2} f_{2n}(y) f_{1m}(y) dy. \quad (3.20b)$$

The infinite series sums presented in Equation (3.20a,b) are truncated for a finite term  $M$  to obtain  $2(M+1)$  linear equations to compute the  $K_r$  due to barrier-rock structure backed by wall using Equation (3.14).

#### 3.3.3.2 Plane-wave approximation

The analytical relation for finding the  $K_r$  due to barrier-rock porous structure backed by a rigid wall is given by

$$K_r = \left| \frac{R_{10}}{I_{10}} \right| = \frac{X - (i\gamma_{10} G_1 - ik_{10}) M_b \tan k_{20} d}{X + (i\gamma_{10} G_1 + ik_{10}) M_b \tan k_{20} d}. \quad (3.21a)$$

where  $M_b = \frac{\varepsilon_b}{i\gamma_{10}G_1(S_b - if_b)} \left[ \frac{k_{20}}{k_{10}} \right]$ . It may be noted that, if  $G_1 \rightarrow \infty$ , then the relation

for  $K_r$  presented in Equation (3.21a) reduces for wave propagation through the porous structure without barrier and is given by

$$K_r = \left| \frac{R_{10}}{I_{10}} \right| = \frac{X - M_b \tan k_{20}d}{X + M_b \tan k_{20}d}. \quad (3.21b)$$

### 3.3.4 Barrier-rock porous structure of semi-infinite thickness

In the present case, barrier-rock porous structure width is considered to be infinite, which suggests that the whole leeward region is occupied by the porous structure. As the gravity waves enter through barrier-rock porous structure at the seaward interface, then the oblique wave amplitudes are subjected to wave decay due to semi-infinite structural thickness. The velocity potentials for the semi-infinite barrier-rock porous structure are given by

$$\phi_1(x, y) = \left\{ I_{10}e^{-ik_{10}(x+b_1)} + R_{10}e^{ik_{10}(x+b_1)} \right\} f_{10}(y) + \sum_{n=1}^{\infty} R_{1n}e^{-\kappa_{1n}(x+b_1)} f_{1n}(y), \quad (3.22a)$$

for  $-b_1 < x < \infty$ ,  $0 < y < h_1$ ,

$$\phi_2(x, y) = \sum_{n=0}^{\infty} A_{2n}e^{-ik_{2n}(x+b_1)} f_{2n}(y), \quad \text{for } -\infty < x < -b_1, 0 < y < h_2. \quad (3.22b)$$

#### 3.3.4.1 Full solution

The system of linear equations on applying the orthogonal mode-coupling relation along with the matching conditions are given by

$$I_{10}\delta_{nm} (i\gamma_{10}G_1 - ik_{10}) \int_0^{h_2} f_{1n}(y)f_{1m}(y)dy + \sum_{n=0}^{\infty} (i\gamma_{10}G_1 + ik_{1n})R_{1n} \int_0^{h_2} f_{1n}(y)f_{1m}(y)dy =$$

$$(S_b + if_b) \sum_{n=0}^{\infty} i\gamma_{10}G_1 A_{2n} \int_0^{h_2} f_{2n}(y)f_{1m}(y)dy, \quad (3.23a)$$

$$-ik_{1n} \{ I_{10}\delta_{nm} - R_{1m} \} \langle f_{1n}(y), f_{1m}(y) \rangle = \varepsilon_b \sum_{n=0}^{\infty} -ik_{2n} A_{2n} \int_0^{h_2} f_{2n}(y)f_{1m}(y)dy. \quad (3.23b)$$

The infinite series sums presented in Equation (3.23a,b) are truncated for a finite term  $M$  to obtain  $2(M+1)$  a system of linear equations for the determination of  $K_r$  due to barrier-rock porous structure of semi-infinite thickness using Equation (3.14).

### 3.3.4.2 Plane-wave approximation

The analytical relation for finding the  $K_r$  due to the barrier-rock structure of semi-infinite thickness using plane-wave approximation is given by

$$K_r = \left| \frac{R_{10}}{I_{10}} \right| = \frac{X - (i\gamma_{10}G_1 - ik_{10})M_b}{X + (i\gamma_{10}G_1 + ik_{10})M_b}. \quad (3.24a)$$

Further, in the case of  $G_1 \rightarrow \infty$ , the relation for  $K_r$  presented in Equation (3.24a) reduces for wave motion through the porous structure without barrier and is given by

$$K_r = \left| \frac{R_{10}}{I_{10}} \right| = \frac{X - M_b}{X + M_b}. \quad (3.24b)$$

The analytical relation for finding the  $K_r$  and  $K_t$  due to porous structure in the absence of vertical barriers considering various structural configurations such as finite structure (Equation 3.15c,d), structure away from the rigid wall (Equation 3.18b), structure backed by rigid wall (Equation 3.21b) and structure of semi-infinite thickness (Equation 3.24b) can be validated with analytical relations proposed by Madsen (1983) and Dalrymple et al. (1991) on considering the uniform bottom  $X = U/V = 1$ .

The wave force on the seaward side  $K_{fs}$  and leeward side  $K_{fb}$  of the barrier-rock porous structure is obtained as

$$K_{fs} = \frac{F_s}{2\rho ghI_{10}} \quad \text{and} \quad K_{fb} = \frac{F_b}{2\rho ghI_{10}}, \quad (3.25a)$$

with  $F_s = i\rho\omega \int_0^h (\phi_1 - \phi_2) dy$  at  $x = -b_1$  and  $F_b = i\rho\omega \int_0^h (\phi_2 - \phi_3) dy$  at  $x = -b_2$ .

The wave force experienced by a rigid vertical wall  $K_{fw}$  is obtained as

$$K_{fw} = \frac{F_w}{2\rho ghI_{10}}, \quad (3.25b)$$

where  $F_w = i\rho\omega \int_0^h \phi_3(x, y) dy$   $x = -b_3$  with the leeward confined region and  $\rho$  is the fluid density. The oblique wave dissipation due to semi-infinite barrier-rock porous structure is measured using the skin depth  $K_{sd}$  (Dalrymple et al., 1991) given by

$$K_{sd} = \frac{\gamma_{10}}{(\gamma_{20}^2 - l^2)^{1/2}}. \quad (3.26)$$

### 3.4 RESULTS AND DISCUSSION

The convergence of hydrodynamic characteristics is presented on increasing the number of evanescent wave modes  $M$  in Table 3.1 for four different types of barrier-rock porous structures. The  $K_r$  and  $K_t$  shows considerable variation between the plane-wave assumption and full solution for all the types of barrier-rock porous structures in the presence of step-bottom as compared with the uniform bottom. However, an enhance in the number of evanescent wave modes  $M \geq 15$  illustrates the convergence in the hydrodynamic characteristics upto four decimal places (Dalrymple et al., 1991; Twu and Chieu, 2000). So, the evanescent wave modes are truncated upto finite number  $M = 15$ , and kept fixed throughout the study.

Table 3.1. The convergence of  $K_r$  and  $K_t$  for four-types of barrier-rock porous structures considering  $\gamma_{10}h = 0.5$ ,  $B/h = 3$ ,  $h_b/h = 0.7$ ,  $\theta = 15^\circ$ ,  $\varepsilon_b = 0.4$  and  $f_b = 1$ .

Number of evanescent wave modes $M$	Barrier-rock porous structure of finite thickness		Barrier-rock structure away from rigid wall	Barrier-rock structure backed by rigid wall	Barrier-rock structure of semi-infinite thickness
	$K_r$	$K_t$	$K_r$	$K_r$	$K_r$
$M = 0$	0.55184	0.31011	0.58012	0.34512	0.50435
$M = 1$	0.55211	0.30382	0.58899	0.35131	0.50511
$M = 5$	0.55301	0.30401	0.58961	0.35142	0.50520
$M = 10$	0.55303	0.30407	0.58966	0.35147	0.50524
$M = 15$	0.55303	0.30400	0.58966	0.35147	0.50524
$M = 20$	0.55303	0.30400	0.58966	0.35147	0.50524

The results obtained in the present study are compared with the available numerical/analytical results reported by a few of the researchers. The wave reflection  $K_r$  versus angle of incidence  $\theta$  is computed for variable friction factor  $f_b$  and compared with Dalrymple et al. (1991) in Figure 3.2(a). The study noted that the increase in  $f_b$  maximizes  $K_r$  and the zeros in  $K_r$  is obtained at  $\theta = 74^\circ$ . The  $K_r$  and  $K_t$  versus dimensionless structural width  $\gamma_{10}d$  is presented for the full solution (on considering evanescent waves) and long-wave assumption in Figure 3.2(b), and compared with Liu



and Li (2013). The increase in  $\gamma_{10}h_1$  shows a little reduction in  $K_r$  and  $K_t$ . Mallayachari and Sundar (1994) examined the  $K_r$  due to porous breakwater backed by a rigid wall for variable structural porosity (Figure 3.2c) using a numerical approach. The study noted that the lower structural porosity maximizes the  $K_r$  and higher structural porosity minimizes  $K_r$  due to enhance in damping coefficient. Zhu and Chwang (2001) presented  $K_r$  versus  $\theta$  (Figure 3.2d) for a thick porous barrier away from the rigid seawall. The minimum  $K_r$  is obtained for  $\theta = 66^\circ$  due to the formation of standing waves. Figures 3.2(a-d) show that the present analytical results agree well with available analytical/ numerical results. Thus, the present study examined the wave scattering/ trapping by (a) barrier-rock porous structure, (b) structure away from rigid wall (c) structure backed by the rigid wall and (d) structure of semi-infinite thickness placed on the uniform and step bottom.

### 3.4.1 Barrier-rock porous structure of finite thickness

The wave reflection  $K_r$ , transmission  $K_t$  and damping coefficient  $K_d$  due to barrier-rock porous structure consisting of two permeable vertical thin walls along with a rockfill within the two barriers as shown in Figure 3.1(a) is examined using eigenfunction expansion method.

#### 3.4.1.1 Role of structural porosity

Figure 3.3(a-b) depicts the  $K_r$ ,  $K_t$  and  $K_d$  versus dimensionless width  $d/h_1$  for various values of structural porosity within  $0.2 \leq \varepsilon_b \leq 0.8$ . Minimal porosity  $\varepsilon_b = 0.2$  shows the maximum  $K_r$  (Figure 3.3a), minimum  $K_t$  and  $K_d$  (Figure 3.3b) as compared with other combinations of  $\varepsilon_b$ . However, increase in the  $\varepsilon_b$  maximizes  $K_t$ ,  $K_d$  and minimizes the  $K_r$ . The increase in  $d/h_1$  shows a resonating crest at  $d/h_1 = 2.5$  and thereafter uniform values in  $K_r$  is obtained due to the seaward constructive interference. The high porosity allows more oblique incident waves through porous structure and enhances the wave decay. Similarly,  $K_t$  is observed to reduces monotonously with enhance in structural width. However, optimal values in  $K_r$ ,  $K_t$  and  $K_d$  are observed at  $d/h = 5$  for all the combinations of porosity within

$0.2 \leq \varepsilon_b \leq 0.8$ . The dimensionless width  $d/h_1$  within  $5 \leq d/h_1 \leq 10$  shows almost uniform values in  $K_r$  and  $K_d$  along with a slight reduction in  $K_t$ . The increase in  $d/h_1$  enhances the capital cost of breakwater but the performance is limited after achieving the optimal values in wave scattering. Hence, the wave decay due to  $d/h_1 = 5$  is evident for optimal wave damping by the barrier-rock porous structure.

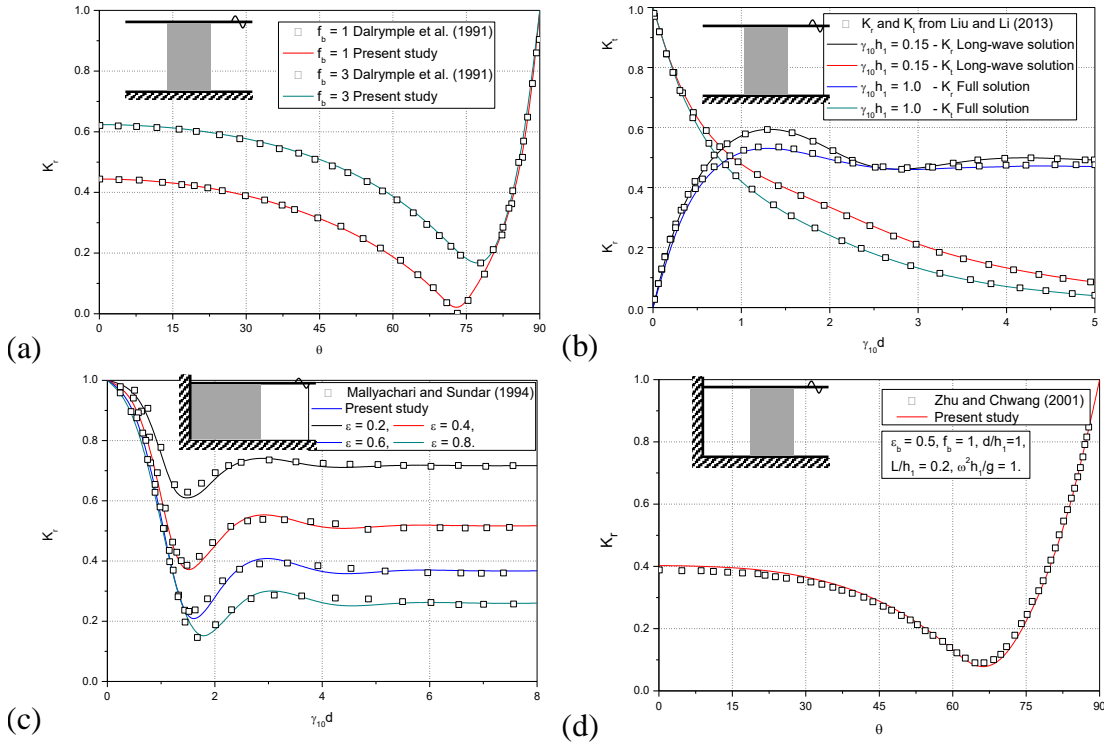


Figure 3.2. Comparative study of present study results with (a) Dalrymple et al. (1991) (b) Liu and Li (2013) (c) Mallayachari and Sundar (1994) and (d) Zhu and Chwang (2001) for several structural configurations.

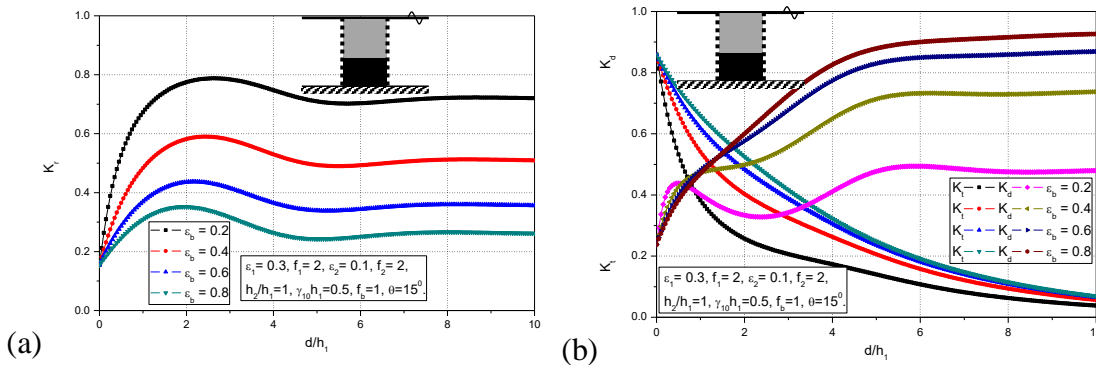


Figure 3.3. Variation of (a)  $K_r$  (b)  $K_t$  and  $K_d$  versus  $d/h_1$  for various values of structural porosity considering  $\gamma_{10}h_1 = 0.5$  and  $\theta = 15^\circ$ .

### 3.4.1.2 Role of friction factor

Figure 3.4(a-b) shows  $K_r$ ,  $K_t$  and  $K_d$  versus dimensionless structural width  $d/h_1$  for variable friction factor within  $0.25 \leq f_b \leq 1$ . The minimal friction factor  $f_b = 0.25$  shows more oscillations in  $K_r$  (Figure 3.4a) and maximum  $f_b = 1$  shows almost uniform values in  $K_r$  after achieving the resonating peak at  $d/h_1 = 2$ . The decreasing pattern in  $K_t$  and increasing trend in  $K_d$  (Figure 3.4b) is obtained with an increase in structural width  $d/h_1$ . The study shows that the friction factor plays a significant role in reducing the  $K_t$  due to the enhancement in  $K_d$ .

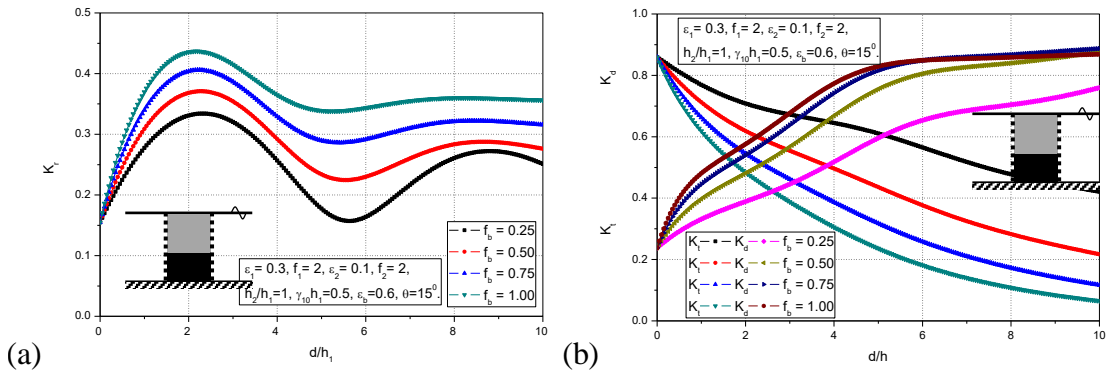


Figure 3.4. Variation of (a)  $K_r$  (b)  $K_t$  and  $K_d$  versus  $d/h_1$  for various values of friction factor considering  $\gamma_{10}h_1 = 0.5$  and  $\theta = 15^\circ$ .

### 3.4.1.3 Role of the angle of incidence

Figure 3.5(a-b) depicts the  $K_r$ ,  $K_t$  and  $K_d$  versus angle of attack  $\theta$  for variable dimensionless wave number  $\gamma_{10}h_1$  within  $0.5 \leq \gamma_{10}h_1 \leq 2$ . The higher values of  $\gamma_{10}h_1$  shows the resonating phenomena along with a slight reducing pattern in  $K_r$  (Figure 3.5a), decreasing trend in  $K_t$  (Figure 3.5b) and increasing pattern in  $K_d$  (Figure 3.5b) within  $0^\circ \leq \theta \leq 65^\circ$ . Thereafter, a sudden surge in  $K_r$ , a drastic reduction in  $K_t$  and  $K_d$  is obtained. The minimal values of  $K_r$  is obtained within  $45^\circ \leq \theta \leq 65^\circ$  for variable  $\gamma_{10}h_1$  due to the dominance of standing waves. Specifically, very minimal values in  $K_r$ ,  $K_t$  and more than 90% of  $K_d$  is achieved for  $\gamma_{10}h_1 = 1.5$  and  $\gamma_{10}h = 2$  within  $0^\circ \leq \theta \leq 60^\circ$  for  $d/h_1 = 2$ .

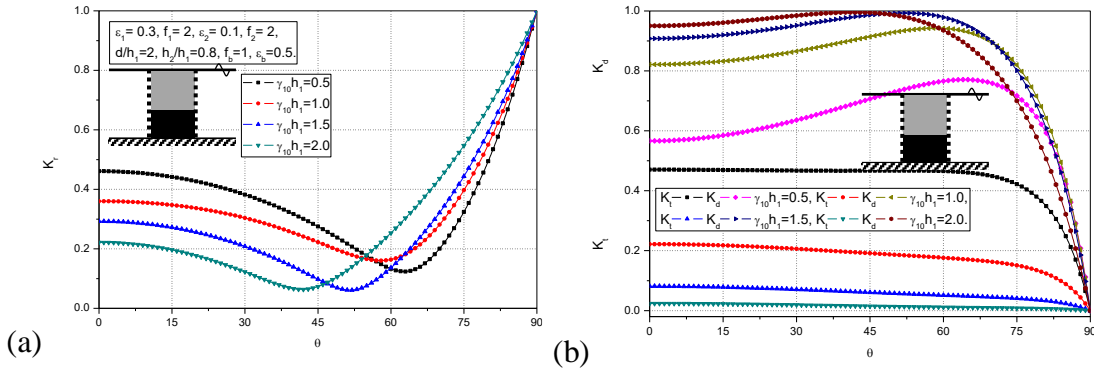


Figure 3.5. Variation of (a)  $K_r$  (b)  $K_t$  and  $K_d$  versus  $\theta$  for various values of  $\gamma_{10}h_1$  considering  $h_2/h_1 = 0.8$  and  $d/h_1 = 2$ .

### 3.4.1.4 Role of step bottom

Figure 3.6(a-b) illustrates  $K_r$ ,  $K_t$  and  $K_d$  for variable structural height/bottom rigid step-height  $h_2/h_1$  considering seaward barrier porosity  $\varepsilon_1 = 0.3$  and  $\varepsilon_1 = 0.6$  in the presence of barrier-rock porous structure. The increase in  $h_2/h_1$  maximizes  $K_r$  and deviation in  $K_r$  is evident within  $0.7 \leq h_2/h_1 \leq 0.9$ . Almost uniform values in wave transmission  $K_t$  is obtained for all the combinations of step height. The higher step height minimizes the  $K_d$  as compared with the uniform bottom.

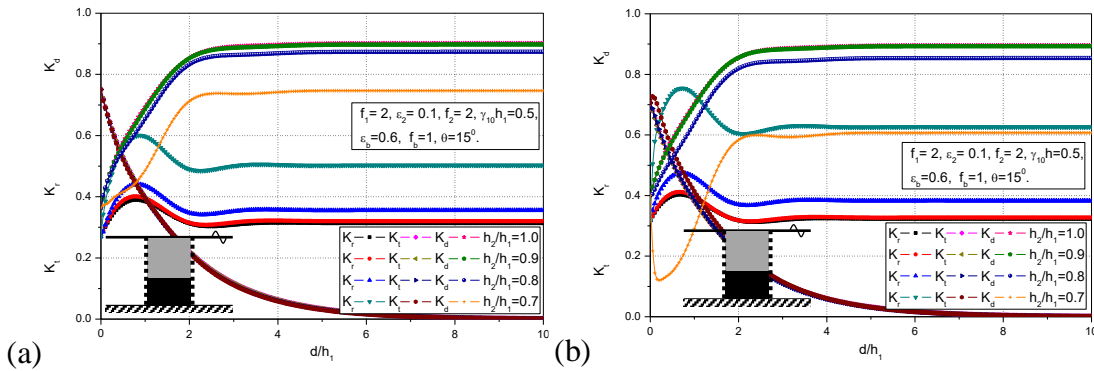


Figure 3.6. Variation of  $K_r$ ,  $K_t$  and  $K_d$  versus  $d/h_1$  for seaward barrier porosity (a)  $\varepsilon_1 = 0.3$  and (b)  $\varepsilon_1 = 0.6$  considering  $\gamma_{10}h_1 = 0.5$  and  $\theta = 15^\circ$ .

The higher seaward barrier porosity  $\varepsilon_1 = 0.6$  (Figure 3.6b) shows considerable variation in  $K_r$  as compared with minimal seaward barrier porosity  $\varepsilon_1 = 0.3$  (Figure 3.6a). The step height  $h_2/h_1 = 0.7$  shows a significant role in increasing the  $K_r$  for  $\varepsilon_1 = 0.6$ . However, moderate rigid step height with the porous structure  $h_2/h_1$  within

$0.8 \leq h_2 / h_1 \leq 0.9$  can perform significant wave decay due to larger porous structure depth and minimal rigid step height.

### 3.4.2 Barrier-rock porous structure placed away from a rigid wall

In the present section, the wave reflection  $K_r$ , wave force on rigid wall  $K_{fw}$ , wave force on the seaward barrier  $K_{fs}$  and the leeward barrier  $K_{fb}$  are presented for a barrier-rock porous structure placed far away from the rigid wall. The spacing between the rigid wall and barrier-rock structure is termed as trapping chamber and denoted as  $L / h_1$ .

#### 3.4.2.1 Role of structural width

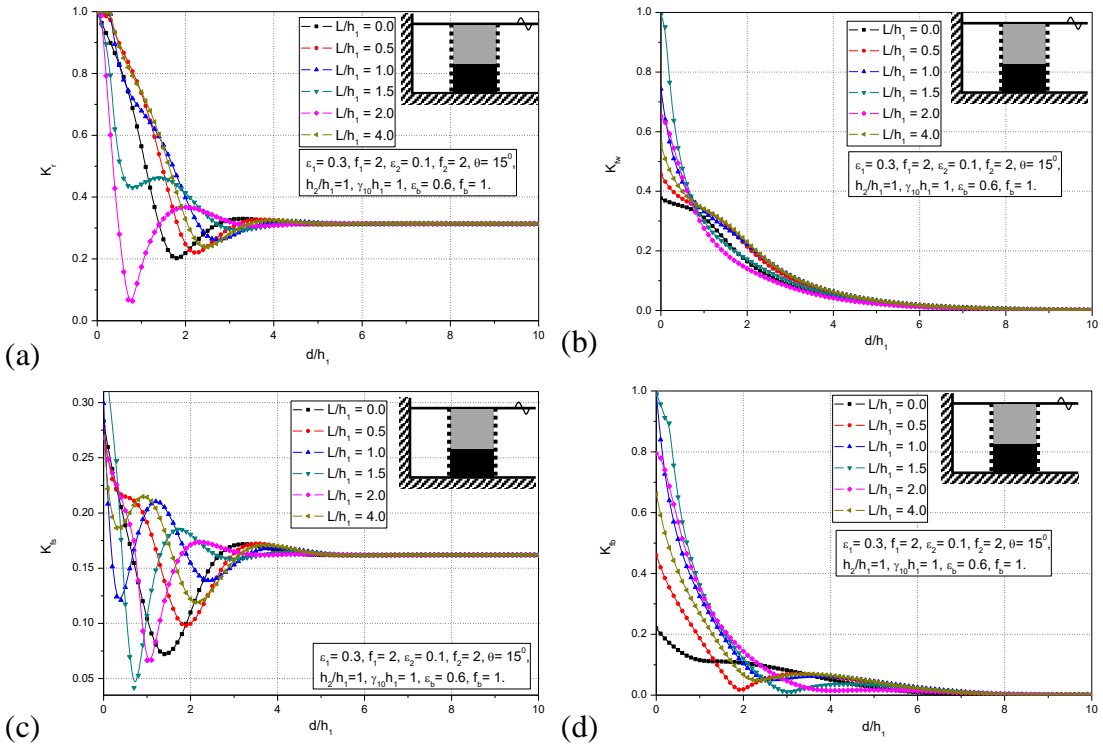


Figure 3.7. Variation of (a)  $K_r$  (b)  $K_{fw}$  (c)  $K_{fs}$  and (d)  $K_{fb}$  versus  $d / h_1$  for various values of trapping chamber length  $L / h_1$  considering  $\gamma_{10}h_1 = 1$  and  $\theta = 15^\circ$ .

The effect of structural width  $d / h_1$  on wave trapping is presented for variable trapping chamber spacing  $L / h_1$  in Figure 3.7(a-d). The resonating effect in  $K_r$  (Figure 3.7a),  $K_{fw}$  (Figure 3.7b),  $K_{fs}$  (Figure 3.7c) and  $K_{fb}$  (Figure 3.7d) is observed with increase in  $d / h_1$  within  $0.01 \leq d / h_1 \leq 5$  for all the combinations of  $L / h_1$ . Thereafter, a uniform value of  $K_r$ ,  $K_{fw}$ ,  $K_{fs}$  and  $K_{fb}$  is observed with enhance in the  $d / h_1$  within

$5 \leq d/h_1 \leq 10$  for all the combinations of  $L/h_1$ . Thus, the present study suggests that the resonating pattern in wave trapping is evident for a specific interval of  $L/h_1$  for  $\gamma_{10}h_1 = 1$ . The zero wave reflection and minimal wave force impact on the structure and the rigid wall is obtained for particular values, which is effective in the design and construction of barrier-rock porous structures in the presence of the seawall. It is also noted that the increase in  $d/h_1$  shows almost uniform values of  $K_r$  within  $4 \leq d/h_1 \leq 10$ , which shows that the role of the trapping chamber is very minimal in the case of higher values of structural width. The corresponding  $K_{fw}$ ,  $K_{fs}$  and  $K_{fb}$  also approaches to very minimal values due to the effective damping within  $4 \leq d/h_1 \leq 10$ . In the case of dimensionless structural width  $d/h_1$  within  $0.01 \leq d/h_1 \leq 1$ , the high wave force impact on the seawall  $K_{fw}$  (Figure 3.7b), high wave impact on the leeward barrier  $K_{fb}$  (Figure 3.7d) is obtained as compared with the wave force impact on seaward barrier  $K_{fs}$  due to the minimal structural width and wave trapping in the finite spacing  $L/h_1$ . On increasing the structural width, the  $K_{fw}$  and  $K_{fb}$  is observed to be reduced due to an effective wave damping.

#### **3.4.2.2 Role of trapping chamber spacing**

The effect of trapping chamber spacing  $L/h_1$  on  $K_r$  (Figure 3.8a),  $K_{fw}$  (Figure 3.8b),  $K_{fs}$  (Figure 3.8c) and  $K_{fb}$  (Figure 3.8d) is reported for various combinations of structural porosity varied within  $0.2 \leq \varepsilon_b \leq 0.8$ . The lower values of  $\varepsilon_b$  shows the higher values of  $K_r$  in a resonating manner. The increase in  $\varepsilon_b$  shows a considerable decrease in  $K_r$  and variation at each of the resonating crest and trough is evident for the effective design of the barrier-rock porous structure. In addition,  $K_{fw}$ ,  $K_{fs}$  and  $K_{fb}$  shows the multiple oscillations with enhance in  $L/h_1$ . The resonating troughs in  $K_{fw}$ , resonating crests in  $K_{fs}$  and  $K_{fb}$  is observed for the same values of  $L/h_1$ , which suggests that the increase in  $L/h_1$  shows either high wave impact on rigid wall or maximum wave force on the seaward porous barrier. The resonating troughs and higher structural width can perform minimum values in hydrodynamic characteristics. It is also

noted that the structural porosity shows minimal role in the wave impact on the leeward porous barrier due to wave reflection by a rigid wall.

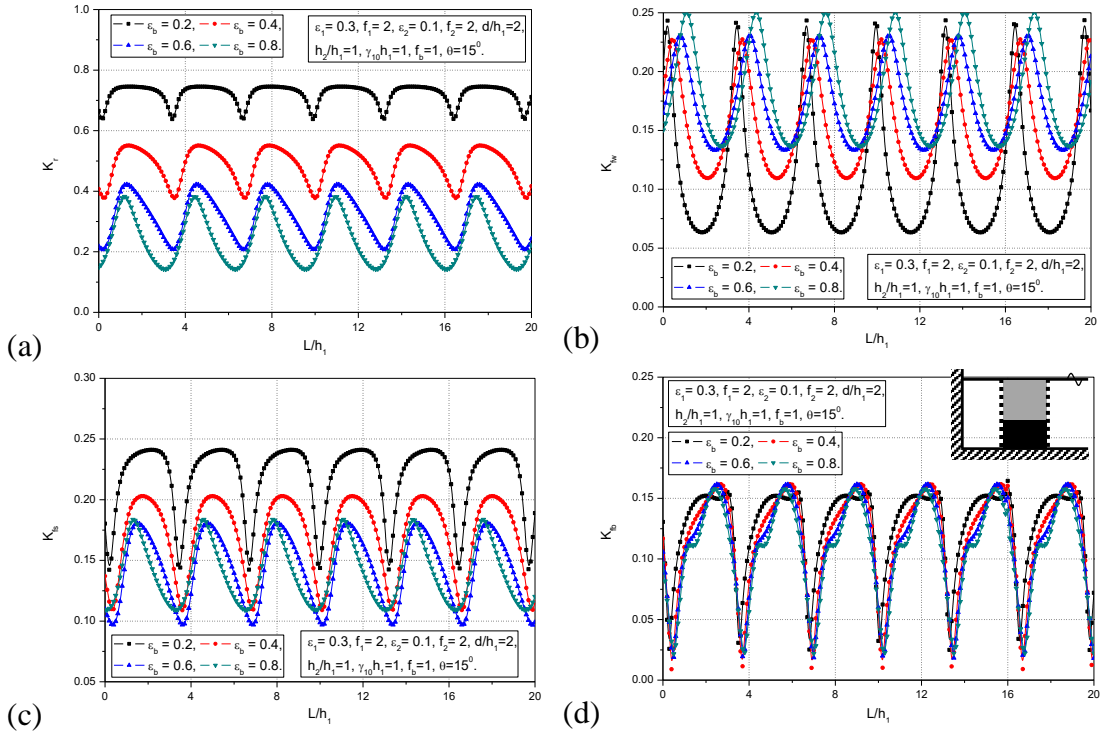


Figure 3.8. Variation of (a)  $K_r$  (b)  $K_{fw}$  (c)  $K_{fs}$  and (d)  $K_{fb}$  versus  $L/h_1$  for various values of porosity  $\epsilon_b$  considering  $\gamma_{10}h_1=1$  and  $\theta=15^\circ$ .

### 3.4.3 Barrier-rock porous structure backed by a rigid wall

The barrier-rock porous structure backed by a rigid wall consists of a porous rock fill within the seaward permeable barrier and the leeward rigid wall (porous structure at New Kelsey bay Canada). The wave reflection is reported for various values of structural porosity, friction factor, angle of wave attack and dimensionless wave number.

#### 3.4.3.1 Role of structural width

The Figure 3.9(a-d) shows  $K_r$  due to barrier-rock porous structure backed by the rigid wall for various values of structural porosity  $\epsilon_b$  (Figure 3.9a), friction factor  $f_b$  (Figure 3.9b), angle of incidence  $\theta$  (Figure 3.9c) and dimensionless wave number  $\gamma_{10}h_1$  (Figure 3.9d) versus dimensionless structural width  $d/h_1$ . Higher values of  $\epsilon_b$  reduces the  $K_r$  due to wave decay and the oscillations in  $K_r$  vanishes for higher values of  $f_b$ . In

addition, the minimum variation of  $K_r$  is achieved with an increase in friction factor. However,  $f_b = 0.25$  shows the high oscillations and zero values in  $K_r$  for specific values of  $d/h_1$  which may be due to the formation of standing waves. The variation in  $\theta$  shows a significant role in reducing the  $K_r$  and the variation between the  $\theta = 0^\circ$  and  $\theta = 15^\circ$  is very minimal, thereafter the significant reduction in  $K_r$  is noted for higher values of  $\theta$ . Moreover, almost zero values of  $K_r$  is achieved for  $\theta = 60^\circ$  due to the effect of standing waves. The increase in  $\gamma_{10}h_1$  shows little reduction in  $K_r$  for variable  $d/h_1$  within  $4 \leq d/h_1 \leq 10$ . However, a sharp decreasing pattern in  $K_r$  is noted for variable dimensionless structural width within  $0.01 \leq d/h_1 \leq 3$ .

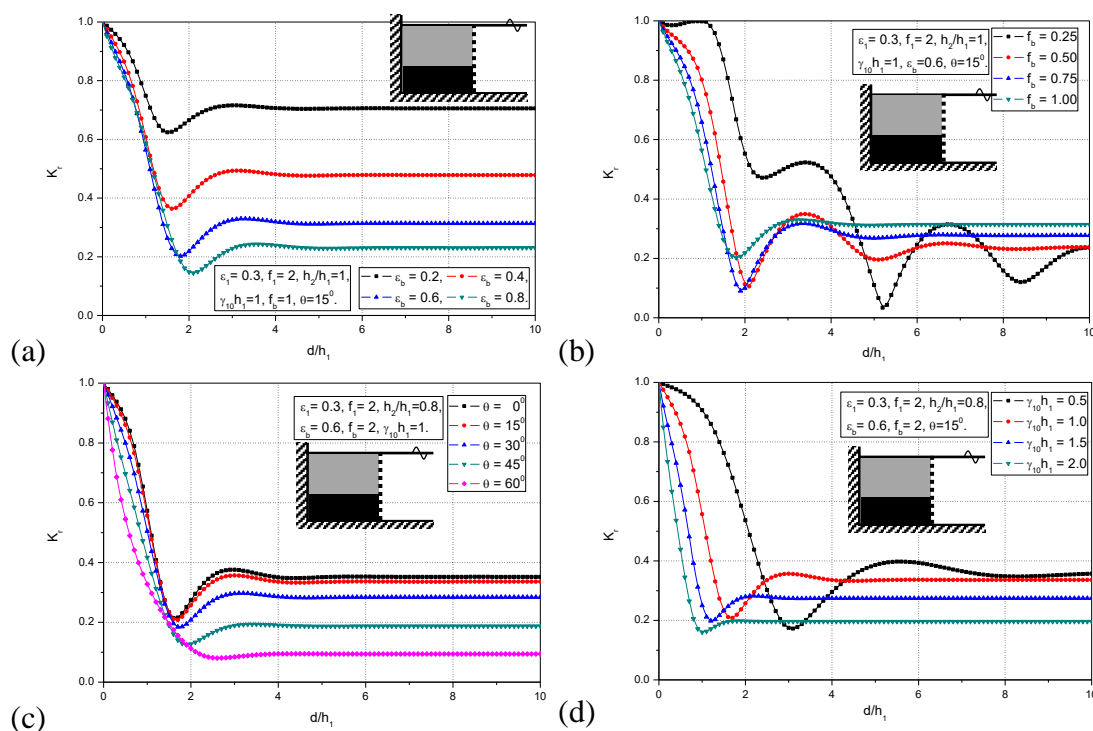


Figure 3.9. Variation of  $K_r$  versus  $d/h_1$  for various values of (a) porosity  $\varepsilon_b$  (b) friction factor  $f_b$  (c) angle of incidence  $\theta$  and (d) dimensionless wave number  $\gamma_{10}h_1$  considering  $\varepsilon_1 = 0.3$  and  $f_1 = 2$ .

Almost unity in  $K_r$  is obtained for all the combinations of porosity, friction factor, angle of incidence and dimensionless wavenumber at  $d/h_1 = 0.1$  due to the no-flow condition applied at the rigid seawall. In general, the rigid seawalls usually reflect the total waves towards the incident wave region (Madsen, 1983; Mallayachari and Sundar



1994). In all the cases (Figure 3.9a-3.9d), the minimum values in  $K_r$  is observed for  $d/h_1 \geq 2$  and  $\varepsilon_b = 0.6$ , which is effective for the design of barrier-rock porous structure backed by a rigid wall for optimal wave decay.

#### **3.4.4 Barrier-rock porous structure of semi-infinite thickness**

In the case of the barrier-rock porous structure of semi-infinite thickness, the porous structure is assumed to occupy the whole leeward region from the seaward point of construction. The wave reflection  $K_r$  due to semi-infinite barrier-rock porous structure is examined for the variable angle of incidence, structure/rigid step-height and skin depth.

##### **3.4.4.1 Role of angle of incidence**

Figure 3.10(a-b) shows  $K_r$  versus  $\theta$  for variable porosity  $\varepsilon_b$  (Figure 3.10a) and friction factor  $f_b$  (Figure 3.10b). The increase in  $\varepsilon_b$  minimizes the  $K_r$  and almost zeros in  $K_r$  is obtained due to the formation of standing waves and the point of zero reflection is referred to as the critical angle of impinging. In addition, the critical angle is observed to be moving towards the left side with an increase in  $\varepsilon_b$ . The enhance in friction factor  $f_b$  (Figure 3.10b) minimizes the  $K_r$  and critical angle is observed at  $\theta = 65^\circ$  for  $\varepsilon_b = 0.6$  and  $\theta = 82^\circ$  for  $\varepsilon_b = 0.2$ . The lower structural porosity  $\varepsilon_b = 0.2$  shows higher values in  $K_r$  and moderate structural porosity  $\varepsilon_b = 0.6$  shows minimal values in  $K_r$  due to constructive and destructive interferences. Finally, the study suggests that structural porosity  $\varepsilon_b = 0.6$  is suitable to construct the barrier-rock semi-infinite structure for effective wave decay.

##### **3.4.4.2 Role of step bottom**

Figures 3.11(a-b) shows  $K_r$  versus  $\theta$  for variable bottom rigid step height  $h_2/h_1$  for the full solution (Figure 3.11a) and long-wave approximation (Figure 3.11b). The increase in rigid step height shows a minimal variation in the  $K_r$  at the point of critical angle in the case of the full solution. In addition, the variation in  $h_2/h_1$  shows considerable change in  $K_r$  for long-wave approximation as compared with the full

solution. In both cases, the critical angle for each of the structural porosity is observed to be  $\theta = 74^\circ$  for  $\varepsilon_b = 0.2$ ,  $\theta = 70^\circ$  for  $\varepsilon_b = 0.6$  and  $\theta = 60^\circ$  for  $\varepsilon_b = 0.6$ , which is due to the formation of standing waves.

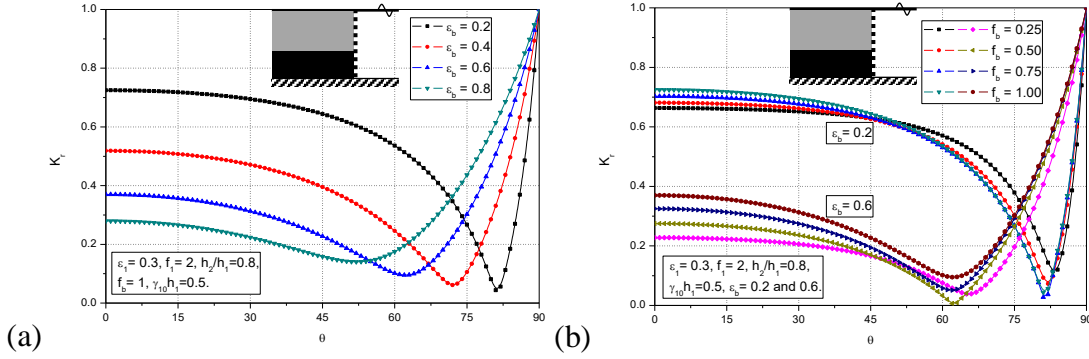


Figure 3.10. Variation of  $K_r$  versus angle of incidence  $\theta$  for various values of (a) porosity  $\varepsilon_b$  (b) friction factor  $f_b$  considering  $h_2/h_1 = 0.8$  and  $\gamma_{10}h_1 = 0.5$ .

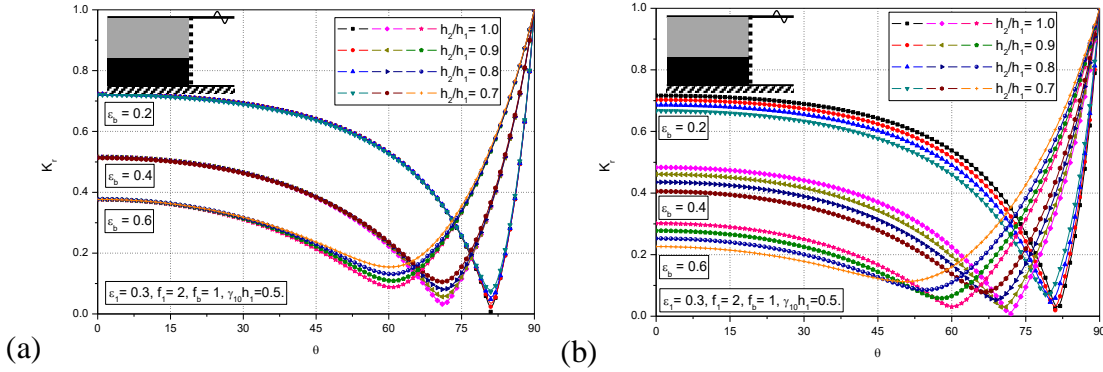


Figure 3.11. Variation of  $K_r$  versus angle of incidence  $\theta$  for various values of structural porosity  $\varepsilon_b$  considering  $f_b = 1$  and  $\gamma_{10}h_1 = 0.5$  for (a) full solution and (b) long-wave approximation.

### 3.4.4.3 Role of skin depth

The oblique wave decay by a barrier-rock porous structure of semi-infinite thickness is measured using the skin depth  $K_{sd}$  (Dalrymple et al., 1991). In the present study, the oblique wave decay is reported in terms of  $K_{sd}$  as a function of angle of impinging  $\theta$  for variable dimensionless wave number  $\gamma_{10}h_1$  as in Figure 3.12(a). In most of the cases, the  $K_{sd}$  is observed to be minimum as compared with the dimensionless wavenumber  $\gamma_{10}h_1$ , which suggests that the barrier-rock structure having high structural width

(structural width is more than the wavelength) can perform as a semi-infinite porous breakwater (Dalrymple et al., 1991).

### 3.4.5 Comparative study of various barrier-rock porous structures

The comparative study is conducted between the four-types of porous structures and presented in Figure 3.12(b). An almost uniform value in  $K_r$  is noted with an increase in  $\gamma_{10}h_1$  for semi-infinite structure. The minimal/zero  $K_r$  is obtained for  $\gamma_{10}h_1 = 0.01$  in the presence of finite structure. In the case of barrier-rock porous structure very near/far away from the rigid wall, the unity in  $K_r$  is obtained due to the zero-velocity condition at the wall. However,  $K_r$  for all four types of barrier-rock porous structures are observed to be the same at  $\gamma_{10}h_1 = 1.35$ , which is termed as the first converging point. Then, a little deviation of  $K_r$  is noted within  $1.35 \leq \gamma_{10}h_1 \leq 1.75$ . Thereafter, four types of structures show a uniform  $K_r$  at  $\gamma_{10}h_1 = 1.75$  which is called as second converging point and then a very minimal deviation in  $K_r$  is observed.

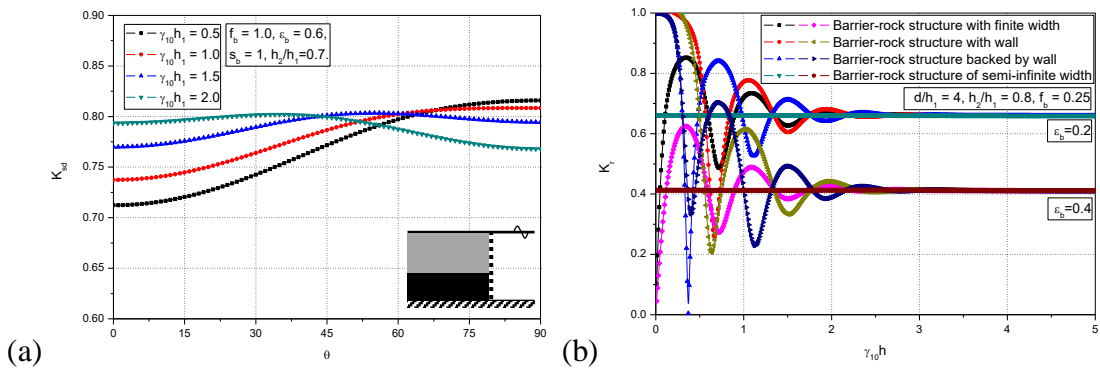


Figure 3.12. (a) Variation of skin depth versus angle of incidence, (b) comparative study of four types of barrier-rock porous structures.

In addition, four types of structures show exactly similar values in  $K_r$  for variable  $\gamma_{10}h_1$  within  $3 \leq \gamma_{10}h_1 \leq 5$  for structural porosity  $\varepsilon_b = 0.2$  and  $\varepsilon_b = 0.4$ . The width of all the three finite porous structures is kept fixed  $d/h_1 = 4$ . The ratio of barrier-rock structure width and wavelength is obtained as  $d/\lambda = 0.86$  for  $\gamma_{10}h_1 = 1.35$ ,  $d/\lambda = 1.1$  for  $\gamma_{10}h_1 = 1.75$  and  $d/\lambda = 1.91$  for  $\gamma_{10}h_1 = 3$ . Finally, the study shows that, if the ratio of width and wavelength  $d/\lambda$  approaches to unity/higher, then the finite structure with/without rigid wall will behave as semi-infinite structure. In general, the

construction cost is identical for four different types of porous structures for fixed structural width. But, in the case of a porous structure with a rigid wall (Figure 3.1b,c), the construction cost is higher due to the addition of the seawall. However, the major advantage of the seawall is the full-wave reflection in the case of a higher wavelength. But in the case of the porous structure without a seawall, there will be a considerable wave transmission for higher wavelengths. Finally, if  $d/\lambda \geq 1$ , then the finite structure with/without wall can be treated as a semi-infinite structure, but the major disadvantage of the semi-infinite structure is high capital cost due to the larger structural width. In those situations, the resonating troughs and critical angle plays a vital role in wave scattering/trapping in the design of offshore/near-shore barrier-rock porous structures. Hence, the structural configuration with/without a rigid wall solely depends upon the site condition.

### **3.5 CLOSURE**

The oblique wave transformation due to the presence of four types of barrier-rock porous structures are examined using the eigenfunction expansion method and the study outcomes are summarised below:

- The results for  $K_r$  and  $K_t$  agrees well with available numerical/analytical results.
- The analytical relations for  $K_r$  and  $K_t$  is derived for four-types of barrier-rock porous structures placed on uniform/step-bottom.
- The 90% of wave energy damping is achieved for dimensionless wave number  $\gamma_{10}h_1 = 1.5$  and  $\gamma_{10}h_1 = 2$  within  $0^\circ \leq \theta \leq 60^\circ$  due to barrier-rock porous structure.
- The barrier-rock porous structure placed on a rigid step within  $0.8 \leq h_2/h_1 \leq 0.9$  is suitable for effective wave damping.
- The resonating troughs are evident in the design of barrier-rock porous structure placed far away from the rigid wall within  $0.1 \leq d/h_1 \leq 5$ . Thereafter, almost uniform values in  $K_r$ ,  $K_{fw}$ ,  $K_{fs}$  and  $K_{fb}$  are observed within  $5 \leq d/h_1 \leq 10$  for all the combinations of trapping chamber length  $L/h_1$ .

- Almost zero values of  $K_r$  is achieved for  $d/h_1 = 2$  and  $\varepsilon_b = 0.6$ , which is suitable for the design of barrier-rock porous structure backed by the wall for better wave decay.
- The moderate values of  $\varepsilon_b = 0.6$  is suitable to construct the barrier-rock semi-infinite structure for effective wave decay.
- The finite structure with/without seawall behaves as a semi-infinite barrier-rock porous structure as the ratio of barrier-rock porous structure width and incident wavelength reaches to unity/higher (i.e  $d/\lambda \geq 1$ ).



## CHAPTER 4

# WAVE DAMPING BY MULTIPLE HORIZONTALLY STRATIFIED POROUS STRUCTURES

### 4.1 GENERAL INTRODUCTION

In order to create the tranquil wave climate in the harbors and ports, the rigid breakwaters having different structural configurations are preferred due to the significant increase in the developmental activities along the coastline. The rigid breakwaters usually collapse due to the extreme wave impact and cause huge damage (Behera and Sahoo, 2014) in the coastal regions. So, based on the studies conducted in the recent decades, the researchers suggested various concepts in constructing the breakwaters, which are permeable in nature and allows the wave motion through the structure (Sollitt and Cross, 1972; Madsen, 1983) which enhances the energy damping and reduces the wave impact on seaward and leeward interfaces of breakwaters. Hence, the porous structures are developed and treated as unique solutions to decay the unwanted wave oscillations. Usually, the breakwaters consist of pore spaces for fluid flow and are being implemented in different physical configurations, such as, vertical (Gudong sea dike, China), trapezoidal, semi-trapezoidal (Bengre, Mangalore, India), rectangular (Zhuangxi sea dike, China), quarter circular and semi-circular structures (Weihai city, China), which are having the finite thickness in nature.

In recent years, the studies on the multi-layered concept in a single porous structure are a subject of great interest due to its wave absorbing performance in the nearshore regions. Numerous studies have investigated the significance of stratified/ multi-layered concepts in a single porous structure considering vertical stratification (Twu and Chieu, 2000; Twu et al, 2002) and horizontal stratification (Yu and Chwang, 1994; Liu et al., 2007) to enhance the energy dissipation. Very recently, the multi-layer horizontal plate breakwater (Wang et al., 2006; Fang et al., 2018) is also suggested for optimal wave damping. Therefore, the detailed research on the horizontal stratified

porous structures in series is required for the optimal design and construction of the novel breakwater configuration for practical engineering applications.

In the present study, the wave reflection, transmission and energy damping due to single and multiple porous structures are examined considering different horizontal porosities. Initially, the wave damping by multiple porous structures having two horizontal porous layers is examined in the presence of free spacing. Further, the study is extended for three-layered horizontal porous structures. In the case of the three-layered horizontal porous structures, the bottom layer is considered to be impermeable throughout the study. Hence, the bottom layer can replace the natural seabed variation and also it can be regarded as an artificial impermeable layer. After that, the submerged two-layered porous structure is investigated considering free surface wave motion. The dispersion relation is solved for the two-layer fully-extended and submerged porous structure. The effect of multiple porosities, porous layer depth, angle of contact, bottom layer height, the free spacing between the multiple structures, structural width, number of structures and dimensionless wave number on scattering coefficients, such as wave reflection, transmission and wave damping are presented. The number of porous structures is limited for five and a comparative study is made between the single and multiple porous structures. Finally, the wave transformation is reported for single and two submerged two-layered porous structures for fixed and variable structural width.

## **4.2 THEORETICAL FORMULATION**

The oblique wave damping by multiple fully-extended and submerged porous structures placed in the water of finite depth is investigated using linearized wave theory. The porous structure is composed of multiple horizontal porous layers. A number of two-layers, three-layers and submerged two-layer porous structure in series is examined using the eigenfunction expansion method. The 3D coordinate system is considered for the theoretical analysis of multiple porous structures of variable horizontal porosity with positive  $y$  – axis in the vertical direction,  $x$  and  $z$  – axis in the horizontal direction. The multiple porous structures of a finite number  $2N$  are located at  $x = -b_j$  for  $j = 1, 2, 3, \dots, 2N$ . The free spacing  $w/h_1$  is provided between consecutive porous structures for the fluid resonance and wave blocking. The fluid field is separated



into multiple free surface regions and multiple porous structure regions of finite width and depth  $0 \leq y \leq h_j$  for  $j=1,2,\dots,2N+1$ . The whole fluid domain is considered to occupy the regions  $\bigcup_{j=1}^{2N+1} I_j$  considering seaward open water region  $I_1 \equiv (-b_1 \leq x \leq \infty, 0 \leq y \leq h_1)$ , multiple free spacing regions and porous structure regions of finite width and depth  $I_j \equiv (-b_j \leq x \leq -b_{j-1}, 0 \leq y \leq h_j)$  for  $j=2,3,\dots,2N$  along with the leeward open water region  $I_{2N+1} \equiv (-\infty \leq x \leq -b_{2N}, 0 \leq y \leq h_{2N+1})$  as in Figure 4.1.

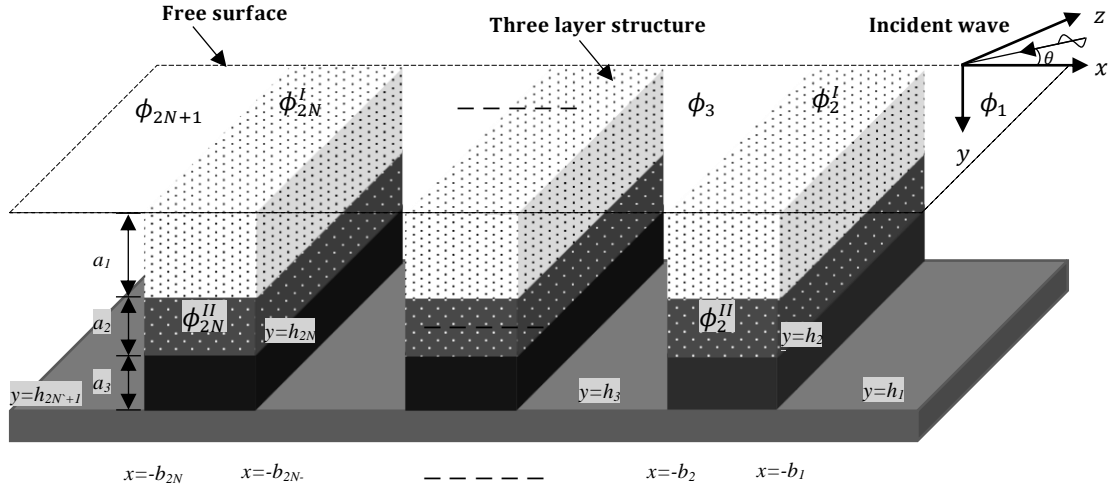


Figure 4.1: Schematic diagram for multiple fully-extended porous structures.

In the present investigation, the fluid is assumed as ideal fluid, which is treated as inviscid, motion is irrotational, incompressible and simple harmonic in nature of angular frequency  $\omega$ . The velocity potentials  $\Phi(x, y, z, t)$  and surface deflection  $\zeta_j(x, z, t)$  presents the wave motion in multiple free surface and porous structures regions and, the velocity potential along with the surface deflection is given in the form of  $\Phi(x, y, z, t) = \text{Re}\{\phi_j(x, y)e^{i(lz-\omega t)}\}$  and  $\zeta_j(x, z, t) = \text{Re}\{\eta_j(x)e^{i(lz-\omega t)}\}$  in which  $\text{Re}$  is the real part,  $l = \gamma_{10} \sin \theta$  is wave number in  $z$ -direction. The  $\gamma_{10}$  ( $\gamma_{10} = 2\pi / \lambda$ ) is wave number in  $y$ -direction and  $\theta$  is the angle of contact on the seaward porous structure at  $x = -b_1$ . The velocity potentials  $\phi_j$  for  $j=1,2,\dots,2N+1$  satisfies the governing Helmholtz equation given by

$$\frac{\partial^2 \phi_j(x, y)}{\partial x^2} + \frac{\partial^2 \phi_j(x, y)}{\partial y^2} - l^2 \phi_j(x, y) = 0, \quad 0 \leq y \leq h_j \quad (4.1)$$

The velocity potential in the free water and porous structure regions satisfies the mean free-surface condition given by

$$\frac{\partial \phi_j(x, y)}{\partial y} + \Gamma_j \phi_j(x, y) = 0 \quad \text{on} \quad y = 0, \quad (4.2a)$$

where  $\Gamma_j = \frac{\omega^2(S_1 + if_1)}{g}$  for  $j = 2, 4, \dots, 2N$ , in the case of two-layered and three-layered

porous structures,  $\Gamma_j = \frac{\omega^2}{g}$  for  $j = 1, 3, \dots, 2N + 1$ , in the case of free water regions and

$\Gamma_j = \frac{\omega^2}{g}$  for  $j = 1, 2, \dots, 2N + 1$ , in each of the region in the case of submerged two-layered porous structures.

The seabed is assumed to be impermeable, the zero-flow near sea bottom in each of the open water and porous structure regions  $j = 1, 2, \dots, 2N + 1$  is given by

$$\frac{\partial \phi_j(x, y)}{\partial y} = 0 \quad \text{on} \quad y = h_j. \quad (4.2b)$$

The porous structure is composed of two porous layers and three porous layers. However, in the case of a three-layered porous structure, the third layer, which is near to the seabed is assumed to be impermeable ( $\varepsilon_3 = 0$ ,  $f_3 = 0$ ) and kept fixed throughout the study. Hence there exists a flow within the multiple porous layers ( $j = 2, 4, \dots, 2N$ ) in the vertical direction (Losada et al., 1996; Liu et al., 2007), which is defined as

$$(S_1 + if_1) \phi_j^I(x, y) = (S_2 + if_2) \phi_j^{II}(x, y) \quad \text{on} \quad y = a_1, \quad (4.3a)$$

$$\varepsilon_1 \frac{\partial \phi_j^I(x, y)}{\partial y} = \varepsilon_2 \frac{\partial \phi_j^{II}(x, y)}{\partial y} \quad \text{on} \quad y = a_1. \quad (4.3b)$$

The two-layered, three-layered and submerged two-layered porous structures are assumed to be of finite width placed at finite water depth, which obstructs the free wave motion (continuity of pressure and velocity). To model the continuity of pressure and velocity due to the existence of two/three-layered porous structures, the relation is given in the form

$$\phi_j(x, y) = \begin{cases} (S_1 + if_1)\phi'_{j+1}(x, y) \\ (S_2 + if_2)\phi''_{j+1}(x, y) \end{cases} \quad \text{on } x = -b_j, \quad j = 1, 3, \dots, 2N+1, \quad (4.4a)$$

$$\frac{\partial \phi_j(x, y)}{\partial x} = \begin{cases} \varepsilon_1 \frac{\partial \phi'_{j+1}(x, y)}{\partial x} \\ \varepsilon_2 \frac{\partial \phi''_{j+1}(x, y)}{\partial x} \end{cases} \quad \text{on } x = -b_j, \quad j = 1, 3, \dots, 2N+1, \quad (4.4b)$$

$$\phi_{j+1}(x, y) = \begin{cases} (S_1 + if_1)\phi'_j(x, y) \\ (S_2 + if_2)\phi''_j(x, y) \end{cases} \quad \text{on } x = -b_j, \quad j = 2, 4, \dots, 2N, \quad (4.5a)$$

$$\frac{\partial \phi_{j+1}(x, y)}{\partial x} = \begin{cases} \varepsilon_1 \frac{\partial \phi'_j(x, y)}{\partial x} \\ \varepsilon_2 \frac{\partial \phi''_j(x, y)}{\partial x} \end{cases} \quad \text{on } x = -b_j, \quad j = 2, 4, \dots, 2N, \quad (4.5b)$$

where  $b_j$  for  $j = 1, 2, \dots, 2N+1$  are interface points between each of the free surface and porous structures,  $\varepsilon_1$  and  $\varepsilon_2$  are surface and bottom layer porosity,  $f_1$  and  $f_2$  are surface and bottom layer friction factors,  $S_1$  and  $S_2$  are surface and bottom layer inertia coefficients. In the case of a submerged two-layered porous structure, the  $\varepsilon_1 = 1$  and  $f_1 = 0$  due to the absence of a surface porous layer, which is treated as a free surface region. The inertia offered by each of the surface and bottom porous layer is computed using the relations (Sollitt and Cross, 1972) given by

$$S_j = 1 + \left( \frac{1 - \varepsilon_j}{\varepsilon_j} \right) A_m, \quad \text{on } j = 1, 2, \quad (4.6)$$

where  $A_m$  is added mass coefficient in surface and bottom porous layers. The far-field radiation conditions are given by

$$\phi_j(x) = \begin{cases} (I_{10}e^{-ik_{10}x} + R_{10}e^{ik_{10}x})f_{10}(y) & \text{as } x \rightarrow \infty, \\ (T_{(2N+1)0}e^{-ik_{(2N+1)0}x})f_{(2N+1)0}(y) & \text{as } x \rightarrow -\infty, \end{cases} \quad (4.7)$$

where  $I_{10}$ ,  $R_{10}$ , and  $T_{(2N+1)0}$  are the complex amplitudes of the incident, reflected and transmitted gravity waves. The wavenumber  $\gamma_{j0}$  for  $j = 1, 3, \dots, (2N+1)$  in the free surface region and the wavenumber  $\gamma_{j0}$  for  $j = 2, 4, \dots, 2N$  in the two/three-layered

(impermeable third layer) porous structure region satisfies the dispersion relations given by

$$\omega^2 = g\gamma_{j0} \tanh \gamma_{j0} h_j, \quad (4.8a)$$

$$(S_1 + if_1)\omega^2 - g\gamma_{j0} \tanh \gamma_{j0} h_j = P_n \left[ (S_1 + if_1)\omega^2 \tanh \gamma_{j0} h_j - g\gamma_{j0} \right], \quad (4.8b)$$

where  $P_n = \left[ \left( 1 - \frac{\varepsilon_2 (S_1 + if_1)}{\varepsilon_1 (S_2 + if_2)} \right) \tanh \gamma_{20} a_2 \right] / \left[ 1 - \frac{\varepsilon_2 (S_1 + if_1)}{\varepsilon_1 (S_2 + if_2)} \tanh^2 \gamma_{20} a_2 \right]$ . In the case

of two-layered submerged porous structure (bottom rigid layer and submerged porous layer), the surface layer behaves as open water region by considering the surface porosity  $\varepsilon_1 = 1$  and friction factor  $f_1 = 0$ . The dispersion relation for the submerged two-layer porous structure region (submerged porous layer placed on the elevated rigid layer) is given by

$$\omega^2 - g\gamma_{j0} \tanh \gamma_{j0} h_j = P_n \left[ \omega^2 \tanh \gamma_{j0} h_j - g\gamma_{j0} \right], \quad (4.8c)$$

where  $P_n = \left[ \left( 1 - \frac{\varepsilon_2}{(S_2 + if_2)} \right) \tanh \gamma_{20} a_2 \right] / \left[ 1 - \frac{\varepsilon_2}{(S_2 + if_2)} \tanh^2 \gamma_{20} a_2 \right]$ , which is similar

as in Losada et al. (1996) and Koley et al. (2015). In the case of the three-layered porous structure, the bottom layer is assumed as impermeable and the zero-flow near the rigid layer ( $h_{j+1} \leq y \leq h_j$ ) for  $j = 1, 3, \dots, (2N+1)$  and ( $h_j \leq y \leq h_{j+1}$ ) for  $j = 2, 4, \dots, 2N$  satisfies the condition given by

$$\frac{\partial \phi_j(x, y)}{\partial x} = 0 \quad \text{on} \quad x = -b_j. \quad (4.9)$$

### 4.3 METHOD OF SOLUTION

In the present section, the solution approach for two-layered, three-layered and submerged two-layered multiple porous structures is presented using the matched eigenfunction expansion method. It is cumbersome to present the full solution for each of the cases when the number of structures is increased. But, in the present section, the solution approach is presented using a closed-form solution. In addition, the system of equations is reported for a single two-layered porous structure, single three-layer porous structure and submerged two-layer porous structures using the closed-form solution based on the edge conditions.

### 4.3.1 Multiple porous structures

The multiple porous structures considering horizontal variable porosity are investigated using the eigenfunction expansion method under the assumption of linearized water wave theory. The porous structures are assumed to be occupied finite width and placed in depth. Thus, there exist the velocity potentials in each of the regions, and the velocity potentials in seaward and leeward open water regions are given by

$$\phi_1(x, y) = \left\{ I_{10} e^{-ik_{10}(x+b_1)} + R_{10} e^{ik_{10}(x+b_1)} \right\} f_{10}(y) + \sum_{n=1}^{\infty} \left\{ R_{1n} e^{-\kappa_{1n}(x+b_1)} \right\} f_{1n}(y), \quad (4.10a)$$

for  $-b_1 \leq x \leq \infty, 0 \leq y \leq h_1,$

$$\phi_{2N+1}(x, y) = \left\{ T_{(2N+1)0} e^{-ik_{(2N+1)0}(x+b_{2N})} \right\} f_{(2N+1)0}(y) + \sum_{n=1}^{\infty} \left\{ T_{(2N+1)n} e^{\kappa_{(2N+1)n}(x+b_{2N})} \right\} f_{(2N+1)n}(y),$$

for  $-\infty \leq x \leq -b_{2N}, 0 \leq y \leq h_{(2N+1)}.$

(4.10b)

The velocity potentials in each of the free surface region available between two porous structures regions are given by

$$\phi_j(x, y) = \sum_{n=0}^{\infty} \left\{ A_{jn} e^{-ik_{jn}(x+b_{j-1})} + B_{jn} e^{ik_{jn}(x+b_j)} \right\} f_{jn}(y) \quad (4.10c)$$

for  $-b_j \leq x \leq -b_{j-1}, 0 \leq y \leq h_j, \quad j = 3, 5, \dots, 2N-1.$

The velocity potentials in each of the porous structures considering surface and bottom porous layers are given by

$$\phi_j^I(x, y) = \sum_{n=0}^{\infty} \left\{ A_{jn} e^{-ik_{jn}(x+b_{j-1})} + B_{jn} e^{ik_{jn}(x+b_j)} \right\} f_{jn}^I(y) \quad (4.10d)$$

for  $-b_j \leq x \leq -b_{j-1}, 0 \leq y \leq a_1, \quad j = 2, 4, \dots, 2N,$

$$\phi_j^{II}(x, y) = \sum_{n=0}^{\infty} \left\{ A_{jn} e^{-ik_{jn}(x+b_{j-1})} + B_{jn} e^{ik_{jn}(x+b_j)} \right\} f_{jn}^{II}(y) \quad (4.10e)$$

for  $-b_j \leq x \leq -b_{j-1}, a_1 \leq y \leq h_2, \quad j = 2, 4, \dots, 2N,$

where  $R_{1n}$  and  $T_{(2N+1)n}$  are the amplitude of reflection and transmission coefficient,  $A_{jn}$  and  $B_{jn}$  for  $j = 3, 5, \dots, (2N-1)$  are unknowns in each of the open water regions,  $A_{jn}$

and  $B_{jn}$  for  $j = 2, 4, \dots, 2N$  are unknown constants in surface porous layer and bottom porous layer regions,  $d = -(b_{j+1} - b_j)$  for  $j = 1, 3, \dots, (2N + 1)$  is the width of the porous structure  $j = 2, 4, \dots, 2N$  is the free spacing between two consecutive porous structures. The vertical eigenfunction for each of the free water region is given by

$$f_{jn}(y) = \begin{cases} \left( \cosh \gamma_{j0} (h_j - y) \right) / \left( \cosh \gamma_{j0} h_j \right) & \text{for } n = 0 \\ \left( \cos \gamma_{jn} (h_j - y) \right) / \left( \cos \gamma_{jn} h_j \right) & \text{for } n = 1, 2, \dots, \end{cases} \quad \gamma_{jn} = i\gamma_{jn} \text{ for } n = 1, 2, \dots \text{ and}$$

$j = 1, 3, \dots, 2N + 1$ . The vertical eigenfunction in each of the surface porous layer

$$j = 2, 4, \dots, 2N \text{ is } f_{jn}^I(y) = \frac{\cosh \gamma_{jn} (h_j - y) - P_n \sinh \gamma_{jn} (h_j - y)}{\cosh \gamma_{jn} h_j - P_n \sinh \gamma_{jn} h_j} \text{ and the bottom porous}$$

$$\text{layer is } f_{jn}^{II}(y) = \frac{(S_1 + if_1)(1 - P_n \tanh \gamma_{jn} a_2) \cosh \gamma_{jn} (h_j - y)}{(S_2 + if_2)(\cosh \gamma_{jn} h_j - P_n \sinh \gamma_{jn} h_j)}.$$

The depth-dependent function for two-layered porous structure (Liu et al., 2007; Koley et al., 2015; Das and Bora, 2014b) is given by

$$\langle f_{jn}, f_{jm} \rangle_{j=1,3,\dots,(2N+1)} = \begin{cases} 0 & \text{for } m \neq n, \\ \Lambda_n & \text{for } m = n. \end{cases} \text{ and } \Lambda_n = \left\{ \begin{array}{l} 2\gamma_{jn} h_j + \sinh 2\gamma_{jn} h_j \\ 4\gamma_{jn} \cosh^2 \gamma_{jn} h_j \end{array} \right\} \quad (4.11a)$$

$$\langle f_{jn}, f_{jm} \rangle_{j=2,4,\dots,2N} = \int_0^{h_j} f_{jn}(y) f_{jm}(y) dy = \int_0^{a_1} f_{jn}^I(y) f_{jm}^I(y) dy + \int_{a_1}^{a_2} f_{jn}^{II}(y) f_{jm}^{II}(y) dy. \quad (4.11b)$$

The orthogonal mode-coupling relation for the three-layered porous structure is similar as in Equation (4.11b) along with zero velocity condition to model the bottom rigid layer  $(h_{j+1} \leq y \leq h_j)$  for  $j = 1, 3, \dots, (2N + 1)$  and  $(h_j \leq y \leq h_{j+1})$  for  $j = 2, 4, \dots, 2N$  given by

$$\frac{\partial \phi_j(x, y)}{\partial x} = 0 \quad \text{on } x = -b_j. \quad (4.11c)$$

The velocity potentials as in Equation (4.10a-e) are substituted in the continuity of pressure as in Equation (4.4a) and continuity of velocity as in Equation (4.4b) along with orthogonal relation as in Equation (4.11a) given by

$$\begin{aligned} \langle \phi_j(x, y), f_{jm}(y) \rangle &= \int_0^{h_j} \phi_j(x, y) f_{jm}(y) dy = \left\{ \int_0^{a_1} + \int_{a_1}^{a_2} \right\} \phi_j(x, y) f_{jm}(y) dy \\ &= \left\{ (S_1 + if_1) \int_0^{a_1} \phi_{(j+1)}^I(x, y) f_{jm}(y) dy \right\} + \left\{ (S_2 + if_2) \int_{a_1}^{a_2} \phi_{(j+1)}^{II}(x, y) f_{jm}(y) dy \right\} \quad (4.12) \\ &\quad \text{for } m = 0, 1, 2, \dots \text{ and } j = 1, 3, \dots, (2N - 1), \end{aligned}$$

$$\begin{aligned} \langle \phi_{jx}(x, y), f_{jm}(y) \rangle &= \int_0^{h_j} \phi_{jx}(x, y) f_{jm}(y) dy = \left\{ \int_0^{a_1} + \int_{a_1}^{a_2} \right\} \phi_{jx}(x, y) f_{jm}(y) dy \\ &= \varepsilon_1 \int_0^{a_1} \phi_{(j+1)x}^I(x, y) f_{jm}(y) dy + \varepsilon_2 \int_{a_1}^{a_2} \phi_{(j+1)x}^{II}(x, y) f_{jm}(y) dy \quad (4.13) \\ &\quad \text{for } m = 0, 1, 2, \dots \text{ and } j = 1, 3, \dots, (2N - 1), \end{aligned}$$

The velocity potentials as in Equation (4.10a-e) are substituted in the continuity of pressure as in Equation (4.5a) and continuity of velocity as in Equation (4.5b) along with orthogonal relation as in Equation (4.11a) given by

$$\begin{aligned} \langle \phi_{j+1}(x, y), f_{(j+1)m}(y) \rangle &= \int_0^{h_j} \phi_{j+1}(x, y) f_{(j+1)m}(y) dy = \left\{ \int_0^{a_1} + \int_{a_1}^{a_2} \right\} \phi_{j+1}(x, y) f_{(j+1)m}(y) dy \\ &= (S_1 + if_1) \int_0^{a_1} \phi_j^I(x, y) f_{(j+1)m}(y) dy + (S_2 + if_2) \int_{a_1}^{a_2} \phi_j^{II}(x, y) f_{(j+1)m}(y) dy \\ &\quad \text{for } m = 0, 1, 2, \dots \text{ and } j = 2, 4, \dots, 2N, \end{aligned} \quad (4.14)$$

$$\begin{aligned} \langle \phi_{(j+1)x}(x, y), f_{(j+1)m}(y) \rangle &= \int_0^{h_j} \phi_{(j+1)x}(x, y) f_{(j+1)m}(y) dy = \left\{ \int_0^{a_1} + \int_{a_1}^{a_2} \right\} \phi_{(j+1)x}(x, y) f_{(j+1)m}(y) dy \\ &= \varepsilon_1 \int_0^{a_1} \phi_{jx}^I(x, y) f_{(j+1)m}(y) dy + \varepsilon_2 \int_{a_1}^{a_2} \phi_{jx}^{II}(x, y) f_{(j+1)m}(y) dy \\ &\quad \text{for } m = 0, 1, 2, \dots \text{ and } j = 2, 4, \dots, 2N. \end{aligned} \quad (4.15)$$

In the case of two-layered porous structure  $h_1 = h_2 = a_1 + a_2$ , similarly, in the case of three-layered porous structure  $h_1 = h_2 + a_3$ . The system of linear equations as in Equation (4.12) – (4.15) for two-layered porous structure, similarly, Equation (4.12) – (4.15) along with no-flow condition as in Equation (4.11c) for the three-layer porous structure is truncated for a finite number of  $M$  terms to obtain  $4j(M + 1)$  equations to

obtain the  $4j(M+1)$  unknown coefficients (where  $j=1,2,\dots$  is the number of porous structures). The reflection, transmission and damping coefficients (Yu and Chwang, 1994) are determined using the relations given by

$$K_r = \left| \frac{R_{10}}{I_{10}} \right| \quad \text{and} \quad K_t = \left| \frac{T_{(2N+1)0}}{I_{10}} \right|, \quad (4.16)$$

$$K_d = 1 - (K_r^2 + K_t^2). \quad (4.17)$$

### 4.3.2 Fully extended two-layered porous structure

The closed-form solution as in Section 4.3.1 is used to perform wave motion through a single porous structure considering horizontal variable porosity. The porous structure consisting of two porosities and friction factors in the surface and bottom layers. The two-layered porous structure of finite width placed in the water of finite depth is examined. The velocity potentials in each of the regions are given by

$$\phi_1(x, y) = \left\{ I_{10} e^{-ik_{10}(x+b_1)} + R_{10} e^{ik_{10}(x+b_1)} \right\} f_{10}(y) + \sum_{n=1}^{\infty} \left\{ R_{1n} e^{-\kappa_{1n}(x+b_1)} \right\} f_{1n}(y), \quad (4.18a)$$

for  $-b_1 \leq x \leq \infty, 0 \leq y \leq h_1,$

$$\phi_2^I(x, y) = \sum_{n=0}^{\infty} \left\{ A_{2n} e^{-ik_{2n}(x+b_1)} + B_{2n} e^{ik_{2n}(x+b_2)} \right\} f_{2n}^I(y) \quad \text{for } -b_2 \leq x \leq -b_1, 0 \leq y \leq a_1, \quad (4.18b)$$

$$\phi_2^{II}(x, y) = \sum_{n=0}^{\infty} \left\{ A_{2n} e^{-ik_{2n}(x+b_1)} + B_{2n} e^{ik_{2n}(x+b_2)} \right\} f_{2n}^{II}(y) \quad (4.18c)$$

for  $-b_2 \leq x \leq -b_1, a_1 \leq y \leq a_2,$

$$\phi_3(x, y) = \left\{ T_{30} e^{-ik_{30}(x+b_2)} \right\} f_{30}(y) + \sum_{n=1}^{\infty} \left\{ T_{3n} e^{\kappa_{3n}(x+b_2)} \right\} f_{3n}(y), \quad (4.18d)$$

for  $-\infty < x < -b_2, 0 < y < h_3,$

where the vertical eigenfunctions in the seaward and leeward free water region are

$$\text{given in the form of } f_{jn}(y) = \begin{cases} \cosh \gamma_{jn}(h_j - y) / \cosh \gamma_{jn} h & \text{for } n = 0, \\ \cos \gamma_{jn}(h_j - y) / \cos \gamma_{jn} h & \text{for } n = 1, 2, \dots, \end{cases} \quad \text{for } j = 1, 3, \text{ the}$$

$$\text{surface porous layer } f_{2n}^I(y) = \frac{\cosh \gamma_{2n}(h_2 - y) - P_n \sinh \gamma_{2n}(h_2 - y)}{\cosh \gamma_{2n} h_2 - P_n \sinh \gamma_{2n} h_2}, \text{ the bottom porous}$$

$$\text{layer } f_{2n}^{II}(y) = \frac{(S_1 + if_1)(1 - P_n \tanh \gamma_{2n} a_2) \cosh \gamma_{2n}(h_2 - y)}{(S_2 + if_2)(\cosh \gamma_{2n} h_2 - P_n \sinh \gamma_{2n} h_2)} \quad \text{and } a_1 + a_2 = h_2.$$



The velocity potentials as in Equation (4.18a) – (4.18d) are substituted in the dynamic pressure and velocity continuum as in Equation (4.4) – (4.5), and the orthogonal relation is applied to form the system of equations given by

$$\{I_{10}\delta_{nm} + R_{1n}\} \langle f_{1n}(y), f_{1m}(y) \rangle = \sum_{n=0}^{\infty} (A_{2n} + B_{2n}e^{-ik_{2n}d}) \left[ (S_1 + if_1) \int_0^{a_1} f_{2n}^I(y) f_{1m}(y) dy + (S_2 + if_2) \int_{a_1}^{a_2} f_{2n}^{II}(y) f_{1m}(y) dy \right] \quad (4.19a)$$

$$-ik_{1n} \{I_{10}\delta_{nm} - R_{1n}\} \langle f_{1n}(y), f_{1m}(y) \rangle = \sum_{n=0}^{\infty} -ik_{2n} (A_{2n} - B_{2n}e^{-ik_{2n}d}) \left[ \varepsilon_1 \int_0^{a_1} f_{2n}^I(y) f_{1m}(y) dy + \varepsilon_2 \int_{a_1}^{a_2} f_{2n}^{II}(y) f_{1m}(y) dy \right] \quad (4.19b)$$

$$\sum_{n=0}^{\infty} (A_{2n}e^{-ik_{2n}d} + B_{2n}) \left[ (S_1 + if_1) \int_0^{a_1} f_{2n}^I(y) f_{3m}(y) + (S_2 + if_2) \int_{a_1}^{a_2} f_{2n}^{II}(y) f_{3m}(y) \right] = T_{3n} \langle f_{3n}(y), f_{3m}(y) \rangle, \quad (4.19c)$$

$$\sum_{n=0}^{\infty} -ik_{2n} (A_{2n}e^{-ik_{2n}d} - B_{2n}) \left[ \varepsilon_1 \int_0^{a_1} f_{2n}^I(y) f_{3m}(y) + \varepsilon_2 \int_{a_1}^{a_2} f_{2n}^{II}(y) f_{3m}(y) \right] = -ik_{3n} T_{3n} \langle f_{3n}(y), f_{3m}(y) \rangle, \quad (4.19d)$$

where  $\delta_{nm} = \begin{cases} 1 & \text{for } m = n = 0 \\ 0 & \text{for } m = n = 1, 2, \dots \end{cases}$ ,  $d = -(b_2 - b_1)$ ,  $n = 0, 1, 2, \dots$  and  $m = 0, 1, 2, \dots$

The system of linear equations as in Equation (4.19a) – (4.19d) are truncated upto a finite term  $M$ , and the reflection and transmission coefficients due to single porous structure considering horizontal two porous layers are determined using the relations given by

$$K_r = \left| \frac{R_{10}}{I_{10}} \right| \quad \text{and} \quad K_t = \left| \frac{T_{30}}{I_{10}} \right| \quad (4.20)$$

### 4.3.3 Fully extended three-layered porous structure

In the case of a single three-layered porous structure, the third bottom layer is assumed to be impermeable and the velocity potentials are similar as in Equation (4.18a) - (4.18d). Hence, the bottom rigid layer does not have the porosity and friction factor. The additional wave reflection by each of the rigid bottom layer is modelled using Equation (4.11c), and the system of equations is given by

$$\begin{aligned} & \{\delta_{nm} + R_{10}\} \int_0^{h_2} f_{1n}(y) f_{1m}(y) dy + \sum_{n=1}^{\infty} R_{1n} \int_0^{h_2} f_{1n}(y) f_{1m}(y) dy = \\ & \sum_{n=0}^{\infty} (A_{2n} + B_{2n} e^{-ik_{2n}d}) \left[ (S_1 + if_1) \int_0^{a_1} f_{2n}^I(y) f_{1m}(y) dy + (S_2 + if_2) \int_{a_1}^{a_2} f_{2n}^{II}(y) f_{1m}(y) dy \right] \end{aligned} \quad (4.21a)$$

$$\begin{aligned} & -ik_{1n} \{I_{10} \delta_{nm} - R_{1n}\} \int_0^{h_1} f_{1n}(y) f_{1m}(y) dy = \\ & \sum_{n=0}^{\infty} -ik_{2n} (A_{2n} - B_{2n} e^{-ik_{2n}d}) \left[ \varepsilon_1 \int_0^{a_1} f_{2n}^I(y) f_{1m}(y) dy + \varepsilon_2 \int_{a_1}^{a_2} f_{2n}^{II}(y) f_{1m}(y) dy \right] \end{aligned} \quad (4.21b)$$

$$\begin{aligned} & \sum_{n=0}^{\infty} (A_{2n} e^{-ik_{2n}d} + B_{2n}) \left[ (S_1 + if_1) \int_0^{a_1} f_{2n}^I(y) f_{3m}(y) dy + (S_2 + if_2) \int_{a_1}^{a_2} f_{2n}^{II}(y) f_{3m}(y) dy \right] \\ & = T_{30} \int_0^{h_2} f_{30}(y) f_{30}(y) dy + \sum_{n=1}^{\infty} T_{3n} \int_0^{h_2} f_{3n}(y) f_{3m}(y) dy, \end{aligned} \quad (4.21c)$$

$$\begin{aligned} & \sum_{n=0}^{\infty} -ik_{2n} (A_{2n} e^{-ik_{2n}d} - B_{2n}) \left[ \varepsilon_1 \int_0^{a_1} f_{2n}^I(y) f_{3m}(y) dy + \varepsilon_2 \int_{a_1}^{a_2} f_{2n}^{II}(y) f_{3m}(y) dy \right] \\ & = -ik_{3n} T_{3n} \int_0^{h_3} f_{3n}(y) f_{3m}(y) dy, \end{aligned} \quad (4.21d)$$

where  $\delta_{nm} = \begin{cases} 1 & \text{for } m = n = 0 \\ 0 & \text{for } m = n = 1, 2, \dots \end{cases}$ ,  $d = -(b_2 - b_1)$ ,  $n = 0, 1, 2, \dots$  and  $m = 0, 1, 2, \dots$

The system of linear equations as in Equation (4.21a) – (4.21d) is truncated upto a finite term  $M$ , and the  $K_r$  and  $K_t$  due to a single porous structure consisting of three layers (two porous layers along with rigid bottom layer) are determined using the relations as in Equation (4.20).

#### 4.3.4 Two-layered submerged porous structure

In the case of the submerged two-layered porous structure, the structure is composed of two porous layers considering the rigid bottom layer and the middle porous layer. The surface porous layer becomes transparent to the incident waves for unity value of porosity  $\varepsilon_1 = 1$  and zero value of friction factor  $f_1 = 0$ . Hence, the surface layer becomes the open water region, and the velocity potentials in each of the regions are given by

$$\phi_1(x, y) = \left\{ I_{10} e^{-ik_{10}(x+b_1)} + R_{10} e^{ik_{10}(x+b_1)} \right\} f_{10}(y) + \sum_{n=1}^{\infty} \left\{ R_{1n} e^{-\kappa_{1n}(x+b_1)} \right\} f_{1n}(y), \quad (4.22a)$$

for  $-b_1 \leq x \leq \infty$ ,  $0 \leq y \leq h_1$ ,

$$\phi_2^I(x, y) = \sum_{n=0}^{\infty} \left\{ A_{2n} e^{-ik_{2n}(x+b_1)} + B_{2n} e^{ik_{2n}(x+b_2)} \right\} f_{2n}^I(y) \quad (4.22b)$$

for  $-b_2 \leq x \leq -b_1$ ,  $0 \leq y \leq a_1$ ,

$$\phi_2^{II}(x, y) = \sum_{n=0}^{\infty} \left\{ A_{2n} e^{-ik_{2n}(x+b_1)} + B_{2n} e^{ik_{2n}(x+b_2)} \right\} f_{2n}^{II}(y) \quad (4.22c)$$

for  $-b_2 \leq x \leq -b_1$ ,  $a_1 \leq y \leq a_2$ ,

$$\phi_3(x, y) = \left\{ T_{30} e^{-ik_{30}(x+b_2)} \right\} f_{30}(y) + \sum_{n=1}^{\infty} \left\{ T_{3n} e^{\kappa_{3n}(x+b_2)} \right\} f_{3n}(y), \quad (4.22d)$$

for  $-\infty \leq x \leq -b_2$ ,  $0 \leq y \leq h_3$ ,

where the vertical eigenfunctions in the seaward and leeward open water regions are similar as in the Section 4.1.2, the eigenfunction in each of the surface layer region is

given in the form of  $f_{2n}^I(y) = \frac{\cosh \gamma_{2n}(h_2 - y) - P_n \sinh \gamma_{2n}(h_2 - y)}{\cosh \gamma_{2n} h_2 - P_n \sinh \gamma_{2n} h_2}$ , the eigenfunction

in the bottom porous layer is of the form  $f_{2n}^{II}(y) = \frac{(1 - P_n \tanh \gamma_{2n} a_2) \cosh \gamma_{2n}(h_2 - y)}{(S_2 + if_2)(\cosh \gamma_{2n} h_2 - P_n \sinh \gamma_{2n} h_2)}$

$$\text{and } P_n = \left[ \left( 1 - \frac{\varepsilon_2}{(S_2 + if_2)} \right) \tanh \gamma_{20} a_2 \right] / \left[ 1 - \frac{\varepsilon_2}{(S_2 + if_2)} \tanh^2 \gamma_{20} a_2 \right].$$

On applying the mode-coupling relation and the edge conditions, the system of equations is given by

$$\left\{ \delta_{nm} + R_{10} \right\} \int_0^{h_2} f_{10}(y) f_{1m}(y) dy + \sum_{n=1}^{\infty} R_{1n} \int_0^{h_2} f_{1n}(y) f_{1m}(y) dy = \sum_{n=0}^{\infty} (A_{2n} + B_{2n} e^{-ik_{2n}d}) \left[ \int_0^{a_1} f_{2n}^I(y) f_{1m}(y) dy + (S_2 + if_2) \int_{a_1}^{a_2} f_{2n}^{II}(y) f_{10}(y) dy \right] \quad (4.23a)$$

$$-ik_{1n} \left\{ I_{10} \delta_{nm} - R_{1n} \right\} \int_0^{h_1} f_{1n}(y) f_{1m}(y) dy = \sum_{n=0}^{\infty} -ik_{2n} (A_{2n} - B_{2n} e^{-ik_{2n}d}) \left[ \int_0^{a_1} f_{2n}^I(y) f_{1m}(y) dy + \varepsilon_2 \int_{a_1}^{a_2} f_{2n}^{II}(y) f_{1m}(y) dy \right] \quad (4.23b)$$

$$\sum_{n=0}^{\infty} (A_{2n} e^{-ik_{2n}d} + B_{2n}) \left[ \int_0^{a_1} f_{2n}^I(y) f_{3m}(y) + (S_2 + if_2) \int_{a_1}^{a_2} f_{2n}^{II}(y) f_{3m}(y) \right] \quad (4.23c)$$

$$= T_{30} \int_0^{a_2} f_{30}(y) f_{30}(y) dy + \sum_{n=1}^{\infty} T_{3n} \int_0^{a_2} f_{3n}(y) f_{3m}(y) dy,$$

$$\sum_{n=0}^{\infty} -ik_{2n} (A_{2n} e^{-ik_{2n}d} - B_{2n}) \left[ \int_0^{a_1} f_{2n}^I(y) f_{3m}(y) + \varepsilon_2 \int_{a_1}^{a_2} f_{2n}^{II}(y) f_{3m}(y) \right] \quad (4.23d)$$

$$= -ik_{3n} T_{3n} \int_0^{h_3} f_{3n}(y) f_{3m}(y) dy,$$

The system of linear equations as in Equation (4.23a) – (4.23d) is truncated upto a finite term  $M$ , and the  $K_r$  and  $K_t$  due to single submerged structure placed on the rigid bottom layer are determined using the relations as in Equation (4.20).

### 4.3.5 Solution approach for finding the roots of dispersion relation

In general, the root-finding process for a two-layered porous structure is complicated due to the presence of imaginary values. The dispersion relation for each of the fully-extended two-layered porous structure  $j = 0, 1, 2, \dots$  is given by

$$(S_1 + if_1) \omega^2 - g \gamma_{jn} \tanh \gamma_{jn} h_j = P_n \left[ (S_1 + if_1) \omega^2 \tanh \gamma_{jn} h_j - g \gamma_{jn} \right], \text{ for } n = 0, 1, 2, \dots \quad (4.24a)$$

where  $P_n = \left[ \left( 1 - \frac{\varepsilon_2 (S_1 + if_1)}{\varepsilon_1 (S_2 + if_2)} \right) \tanh \gamma_{jn} a_2 \right] / \left[ 1 - \frac{\varepsilon_2 (S_1 + if_1)}{\varepsilon_1 (S_2 + if_2)} \tanh^2 \gamma_{jn} a_2 \right]$ .

In addition, the dispersion relation for the fully-extended two-layered porous structure is simplified in the following form given by

$$(S_1 + if_1) \Delta - \Upsilon \tanh \beta \Upsilon = \varphi \left[ \Upsilon - (S_1 + if_1) \Delta \tanh \beta \Upsilon \right] \tanh \alpha \Upsilon, \quad (4.24b)$$

where  $\Delta = \frac{\omega^2 h_j}{g}$ ,  $\beta = \frac{a_2}{h_j}$ ,  $\alpha = \frac{a_1}{h_j}$ ,  $\Upsilon = \gamma_{jn} h_j$ ,  $\varphi = \frac{\varepsilon_2 (S_1 + if_1)}{\varepsilon_1 (S_2 + if_2)}$ . In the case of the

single-layered porous structure, the  $\varepsilon_1 = \varepsilon_2 = \varepsilon$ ,  $S_1 = S_2 = S$  and  $f_1 = f_2 = f$ . Hence, the two-layered porous structure dispersion relation reduces to the complex single-layered porous structure dispersion relation given by

$$\omega^2 (S + if) = g \gamma_{jn} \tanh \gamma_{jn} h_j \quad (4.24c)$$

On considering the surface layer porosity  $\varepsilon_1 = 1$  and friction factor  $f_1 = 0$  in Equation (4.24a), the two-layered fully-extended porous structure dispersion relation reduces to submerged two-layered porous structure dispersion relation as in Equation (4.8c). In the previous studies, numerous scientists and engineers reported various methods such as Newton-Raphson method, step approach and contour plots (Sollitt and Cross, 1972; Dalrymple et al., 1991; Yu and Chwang, 1994; Mendez and Losada, 2004; Liu et al., 2007; Behera and Sahoo, 2014; Zhao et al., 2017) for finding multiple roots of the complex dispersion relation.

Table. 4.1: Roots of the two-layered ( $\varepsilon_1 = 0.8$ ,  $f_1 = 0.4$ ) and submerged two-layered ( $\varepsilon_1 = 1$ ,  $f_1 = 0$ ) dispersion relation considering  $a_1/h_2 = 0.5$ ,  $a_2/h_2 = 0.5$ ,  $a_3/h_1 = 0.2$ ,  $\varepsilon_2 = 0.5$ ,  $f_2 = 1$ ,  $S_1 = S_2 = 1$ ,  $\theta = 20^\circ$  and  $h_1/\lambda = 0.1$ .

Evanescent waves	Two/three-layered porous structure		The submerged two-layered porous structure	
	Root	Error	Root	Error
$M = 0$	$0.0810 + 0.0221i$	$3.4792 \times 10^{-17}$	$0.0854 + 0.0078i$	$1.8440 \times 10^{-17}$
$M = 1$	$0.0041 + 0.7781i$	$8.0531 \times 10^{-16}$	$0.0018 + 0.7767i$	$1.7743 \times 10^{-16}$
$M = 2$	$0.0020 + 1.5672i$	$5.5612 \times 10^{-15}$	$0.0009 + 1.5665i$	$4.9881 \times 10^{-15}$
$M = 3$	$0.0014 + 2.3538i$	$1.1422 \times 10^{-14}$	$0.0006 + 2.3533i$	$3.2745 \times 10^{-16}$
$M = 4$	$0.0010 + 3.1398i$	$5.7771 \times 10^{-15}$	$0.0004 + 3.1394i$	$2.0345 \times 10^{-14}$
$M = 5$	$0.0008 + 3.9255i$	$2.1287 \times 10^{-14}$	$0.0003 + 3.9253i$	$2.5881 \times 10^{-14}$
$M = 6$	$0.0007 + 4.7112i$	$9.2078 \times 10^{-14}$	$0.0003 + 4.7110i$	$5.1238 \times 10^{-14}$
$M = 7$	$0.0006 + 5.4968i$	$3.4792 \times 10^{-17}$	$0.0002 + 5.4966i$	$1.7347 \times 10^{-17}$

In the present study, the Newton-Raphson method is used for finding the roots of the two-layered porous structure dispersion relation and the step approach technique as in Mendez and Losada (2004) is used for finding the initial values for fast convergence. The multiple roots of the dispersion relation for a two-layered fully-extended and the submerged porous structure are given in Table 4.1.

#### 4.4 RESULTS AND DISCUSSION

The reflection coefficient  $K_r$ , transmission coefficient  $K_t$  and energy dissipation coefficient  $K_d$  versus evanescent wave modes  $M$  are presented in Figure 4.2(a) for

single and multiple porous structures considering variable porosity. The increase in the evanescent wave modes  $M$  shows the almost uniform estimation in  $K_r$ ,  $K_t$  and  $K_d$  for one, two, three, four and five number of porous structures considering horizontal variable porosity. The convergence in  $K_r$ ,  $K_t$  and  $K_d$  is observed for  $M \geq 7$  for single and multiple porous structures upto 4 decimal places. In the present case, the  $M = 0$  shows the wave motion through the multiple structures in the absence of evanescent waves or plane-wave assumption. However, the variation between the plane-wave assumption and full solution (considering evanescent waves) is minimum for a single porous structure considering variable porosity. An increasing trend in the  $K_r$  is observed between the plane-wave assumption and full solution in the presence of multiple porous structures as compared with the single porous structure. However, the evanescent wave modes are truncated for a finite number  $M = 7$  and kept fixed throughout the study, due to the convergence of scattering coefficients.

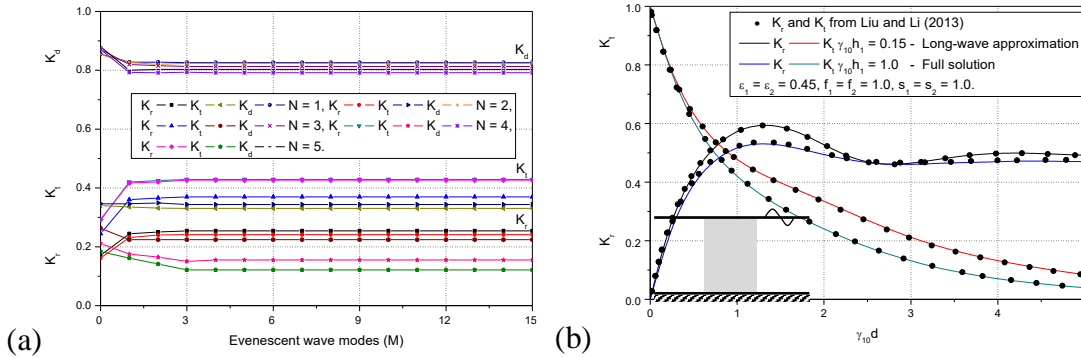


Figure 4.2: (a) Convergence study of wave transformation for different evanescent wave modes and (b) validation of present study results with Liu and Li (2013) for long-wave approximation and full solution.

In order to confirm the present study analytical results, the computation results are validated with the previous analytical results presented by Liu and Li (2013) in Figure 4.2(b) on considering uniform porosity  $\epsilon_1 = \epsilon_2$  and friction factor  $f_1 = f_2$  in each of the porous layer, which converts the multi-layered porous structure into conventional porous breakwater of uniform porosity. The wave reflection and transmission (Figure 4.2b) due to the single porous structure is investigated for long-wave assumption and full solution and also compared with Liu and Li (2013). The comparative study shows a considerable agreement between the present study and previous study results. Hence, the present study is extended for single and multiple porous structures considering

variable horizontal porosity and friction factor. The structural width is denoted as  $d_j$  for  $j=1,2,\dots,N$  and the cumulative structural width  $d$  is denoted as  $d = \sum_{j=1}^N d_j$  throughout the study.

#### 4.4.1 Two-layered fully extended multiple porous structures

The reflection coefficient  $K_r$ , transmission coefficient  $K_t$  and energy dissipation coefficient  $K_d$  are studied for various influencing parameters. The water depth is denoted as  $h_1$ , the depth of fully extended porous structure is denoted as  $h_2$ , surface porous layer depth is denoted as  $a_1$ , bottom porous layer depth is denoted as  $a_2$  and in the case of two-layered fully-extended multiple structures  $h_1 = h_2 = a_1 + a_2$ . The depth of the fully extended structure is kept fixed ( $h_2 = a_1 + a_2$ ) and as the surface porous layer depth increases, the bottom porous depth decreases.

##### 4.4.1.1 Single porous structure

The  $K_r$  (Figure 4.3a),  $K_t$  and  $K_d$  (Figure 4.3b) versus dimensionless cumulative structural width  $d/h_1$  are presented for variable surface porous layer depth  $a_1/h_2$  and bottom porous layer depth  $a_2/h_2$  considering a single porous structure. The increase in  $d/h_1$  shows a rapid increase in  $K_r$  and attains a peak value, which is termed as the resonating crest and rapidly decreases and again attains a uniform value of  $K_r$  for all the combinations of surface layer depth within  $0.2 \leq a_1/h_2 \leq 0.8$ . The increase in the surface porous layer depth shows a considerable decrease in  $K_r$  and a slight increase in  $K_t$  is obtained within  $2 \leq d/h_1 \leq 10$  which causes significant changes in the  $K_d$  within  $1 \leq d/h_1 \leq 5$ . The main reason behind the change in energy damping with an increase in the surface layer depth is due to the presence of high porosity in the surface layer. The increase in surface layer depth shows an increase in surface layer porosity, which allows more wave energy to penetrate easily through the structure and encourages the oblique wave interaction with a two-layered structure, which causes high energy dissipation. However, the  $a_1/h_2=0.8$  shows the minimal estimation in

$K_r$ , moderate values in  $K_t$  and significant change in  $K_d$  within  $2 \leq d/h_1 \leq 6$  as compared with other combinations in the presence of a single porous structure.

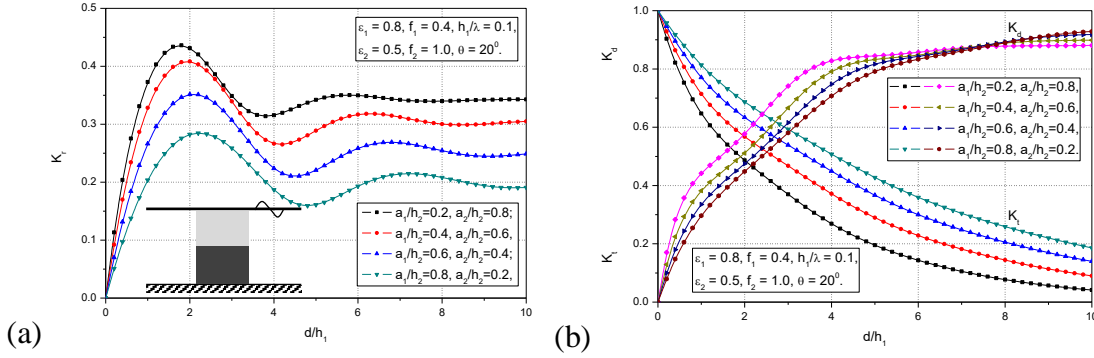


Figure 4.3: Variation of (a)  $K_r$ , (b)  $K_t$  and  $K_d$  versus  $d/h_1$  due to a single structure for variable  $a_1/h_2$  and  $a_2/h_2$  composed of double porous layers considering  $h_1/\lambda = 0.1$  and  $\theta = 20^\circ$ .

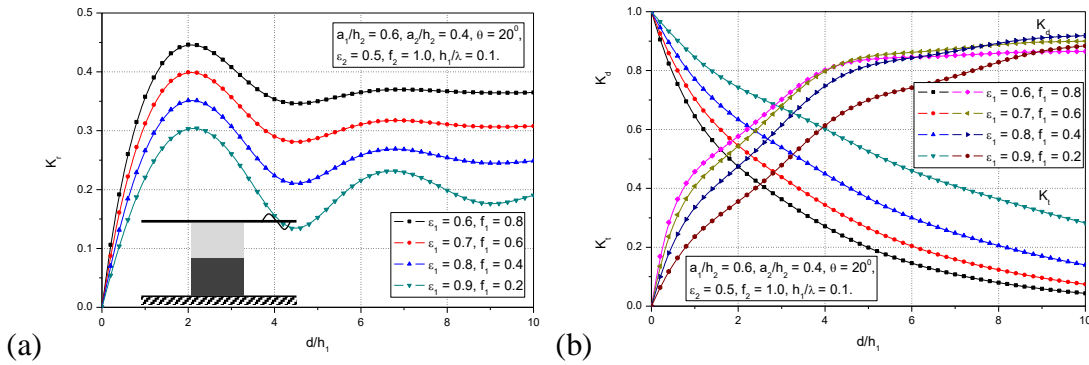


Figure 4.4: Variation of (a)  $K_r$ , (b)  $K_t$  and  $K_d$  versus  $d/h_1$  due to a single structure for variable  $\varepsilon_1$  and  $f_1$  composed of double porous layers considering  $h_1/\lambda = 0.1$  and  $\theta = 20^\circ$ .

The  $K_r$  (Figure 4.4a),  $K_t$  and  $K_d$  (Figure 4.4b) versus dimensionless cumulative structural width  $d/h_1$  are presented for variable surface layer porosity  $\varepsilon_1$  and friction factor  $f_1$  considering constant values of  $a_1/h_2$  and  $a_2/h_2$  in the presence of a single porous structure. The hydrodynamic characteristics trend remains the same as in Figure 4.3(a,b), but there exist a resonating peak and trough in the  $K_r$  at  $d/h_1 = 2$  for all the combinations of variable porosity and friction factor. The resonating peak is observed to be high for  $\varepsilon_1 = 0.6$ ,  $f_1 = 0.8$  whereas 10.5% for  $\varepsilon_1 = 0.7$ ,  $f_1 = 0.6$ ; 21.2% for  $\varepsilon_1 = 0.8$ ,  $f_1 = 0.4$  and 31.9% for  $\varepsilon_1 = 0.9$ ,  $f_1 = 0.2$  the reduction in  $K_r$  is observed as compared with the high resonating peak observed for  $\varepsilon_1 = 0.6$  and  $f_1 = 0.8$  at



$d/h_1 = 2$  due to the change in the surface layer porosity and friction factor. Similarly, the increase in  $\varepsilon_1$  shows a considerable increase in  $K_t$  and considerable reduction in  $K_d$ . Particularly, it is observed that the surface layer porosity  $\varepsilon_1 = 0.9$  shows minimal values of  $K_r$ , higher values of  $K_t$  and minimum wave damping as compared with the other combinations due to the minimum friction factor  $f_1 = 0.2$ . The performance of the structural configuration  $\varepsilon_1 = 0.9$  and  $f_1 = 0.2$  can be improved by increasing the friction factor, which can enhance the energy damping. However, it is proved that the minimum friction factor shows the minimal values of energy damping in an oscillatory manner and higher friction factor shows the higher estimation in wave reflection, but the main aim for the use of the porous structure is to have optimal wave damping for gentle wave action on leeward regions (Twu and Chieu, 2000; Zhu and Chwang, 2001).

#### 4.4.1.2 Two porous structures

The  $K_r$  and  $K_t$  versus angle of contact  $\theta$  are presented for variable surface layer porosity  $\varepsilon_1$  and friction factor  $f_1$  considering the dimensionless cumulative structural width  $d/h_1 = 1$  (Figure 4.5a) and  $d/h_1 = 2$  (Figure 4.5b) in the presence of two porous structures. The increase in surface layer porosity shows a significant decrease in  $K_r$  and a considerable increase in the  $K_t$  within  $0^\circ \leq \theta \leq 66^\circ$  as in Figure 4.5(a). However, minimal  $K_r$  is noted for all the combinations of porosity and friction factor at  $\theta = 64^\circ$  due to interaction between the reflected waves by porous structure and oblique incoming waves at the seaward interface of the primary structure. The  $\theta = 64^\circ$  is termed as the critical angle of contact, which is mandatory to identify in the design of offshore porous breakwaters. Thereafter, a sharp surge in  $K_r$  is observed and  $K_r$  reaches to the unity for  $\theta = 90^\circ$ . Similarly, a sudden fall in the  $K_t$  is obtained and approaches to zero at  $\theta = 90^\circ$ . But,  $\theta = 90^\circ$  is not suitable for the construction of two porous structures due to the minimum values in energy damping. It is reported that the porous structure must perform minimal estimation in  $K_r$  and  $K_t$  along with high values in  $K_d$  for a better life span (Twu and Chieu 2000). On the other hand, in Figure 4.5(b), the width of the structure is considered to be two times as compared with the previous case

(Figure 4.5a) to study the variation of hydrodynamic characteristics considering variable porosity. The  $K_r$  and  $K_t$  pattern remains the same as in Figure 4.5(a) and the critical angle is observed at  $\theta = 64^\circ$ . However, a little increase in the  $K_r$  and decrease in the  $K_t$  is noted for  $d/h_1 = 2$  (Figure 4.5b) as compared with  $d/h_1 = 1$  (Figure 4.5a) which may be due to the resonating crest as explained in Figure 4.3(a). Further, the increase in  $d/h_1$  is observed to enhance the energy damping due to the larger structural width.

The wave reflection  $K_r$  and wave transmission coefficient  $K_t$  versus free spacing between two wave energy damping structures  $w/h_1$  are presented for variable surface layer depth  $a_1/h_2$  and bottom layer depth  $a_2/h_2$  considering the different angle of contact  $\theta = 0^\circ$  (Figure 4.6a) and  $\theta = 30^\circ$  (Figure 4.6b) in the presence of two horizontal porous layers. The increase in free spacing  $w/h_1$  shows the local minima and local maxima at particular intervals as in Figure 4.6(a) due to the fluid resonance. The local maxima and local minima in  $K_r$  and  $K_t$  vanishes with the increase in the surface porous layer depth due to free passages of incident waves as a result of higher porosity in surface layer  $\varepsilon_1 = 0.8$ . As a comparison with local maxima in the  $K_r$  for  $a_1/h_2 = 0.2$ , the 11.6% for  $a_1/h_2 = 0.4$ , 27.7% for  $a_1/h_2 = 0.6$  and 44% for  $a_1/h_2 = 0.8$  the reduction in  $K_r$  is obtained at each of the resonating peak/local maxima for two porous structures considering variable porosity.

On the other hand, the  $K_r$  and  $K_t$  versus free spacing  $w/h_1$  are analysed for the oblique wave contact  $\theta = 30^\circ$  (Figure 4.6b) considering two porous structures and a similar trend is obtained in  $K_r$  and  $K_t$  as observed in the earlier case (Figure 4.6a). The only difference between the normal wave contact  $\theta = 0^\circ$  (Figure 4.6a) and oblique wave contact  $\theta = 30^\circ$  (Figure 4.6b) on the hydrodynamic characteristics is the occurrences of the local minima and local maxima for the variable  $w/h_1$ , which is due to the enhancement in the wave damping. As a comparison, a number of four resonating peaks for normal wave contact  $\theta = 0^\circ$  (Figure 4.6a) and three resonating peaks for oblique wave contact  $\theta = 30^\circ$  (Figure 4.6b) is observed in the  $K_r$ , and also 16.3% reduction in

the  $K_r$  is noted for oblique wave contact (Figure 4.6b) at each of the resonating peak as compared with the normal wave contact (Figure 4.6a). The increase in  $a_1/h_2$  shows the considerable rise in  $K_r$  for normal wave contact (Figure 4.6a) and oblique wave contact (Figure 4.6b) due to the increase in the structural porosity, which is helpful for the enhancement of the wave damping and also reduces the wave oscillations.

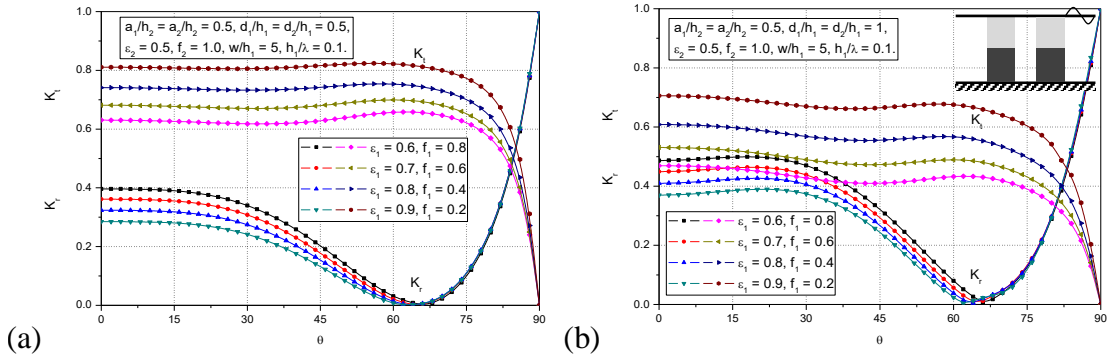


Figure 4.5: Variation of  $K_r$  and  $K_i$  versus  $\theta$  due to two structures for variable  $\epsilon_1$  and  $f_1$  composed of double porous layers for  $h_1/\lambda = 0.1$ ,  $w/h_1 = 5$ , considering (a)  $d/h_1 = 1$  and (b)  $d/h_1 = 2$ .

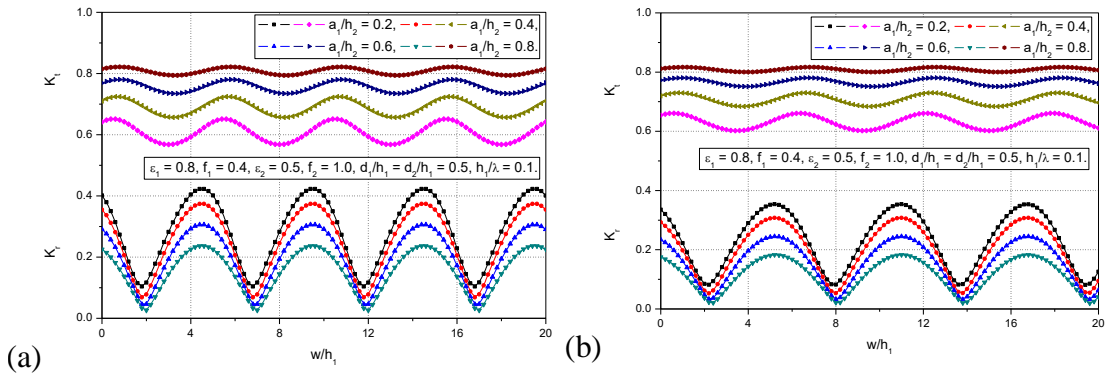


Figure 4.6: Variation of  $K_r$  and  $K_i$  versus  $w/h_1$  due to two structures for variable  $a_1/h_2$  composed of double porous layers considering  $h_1/\lambda = 0.1$  (a)  $\theta = 0^\circ$  and (b)  $\theta = 30^\circ$ .

The  $K_r$  (Figure 4.7a),  $K_i$  and  $K_d$  (Figure 4.7b) versus  $w/h_1$  are presented for the variable angle of contact  $\theta$  in the presence of two porous structures. The reduction in the  $h_1/\lambda = 0.2$  shows more resonating crests and resonating troughs in the  $K_r$  due to the combined effect of wave blocking in the free spacing  $w/h_1$  for particular intervals (occurrence of local maxima), and high wave penetration of incident waves for specific

intervals (occurrence of local minima) of  $w/h_1$  is achieved. The increase in the  $w/h_1$  shows the moderate estimation in  $K_r$  for  $\theta = 0^\circ$  and the increase in  $\theta$  shows the reduction in  $K_r$  in oscillating pattern within  $0^\circ \leq \theta \leq 30^\circ$ . Thenceforth, for  $\theta = 45^\circ$  shows a significant reduction in the  $K_r$  as compared with  $\theta = 30^\circ$ , whereas the  $\theta = 60^\circ$  presents the very minimal theoretical estimation in  $K_r$  as compared with all other combinations. But the  $K_t$  is observed to be decreasing and  $K_d$  is observed varying in the particular range for all the values of angle of contact within  $0^\circ \leq \theta \leq 60^\circ$  in oscillatory pattern. The angle of contact  $\theta = 60^\circ$  illustrates very minimal values in  $K_r$  and  $K_t$  along with reasonable values in  $K_d$  as compared with the other combinations due to the formation of standing oblique waves at that particular point of wave impinging. The study suggests that the angle of contact  $\theta = 60^\circ$  can perform required scattering coefficients in the presence of a pair of two-layered porous structures considering the minimal structural thickness. However, the finite free spacing  $w/h_1$  and structural width  $d/h_1$  are useful in enhancing the energy damping and the zero transmission coefficient can be achieved with either increase in the  $d/h_1$  or increase in the number of porous structures.

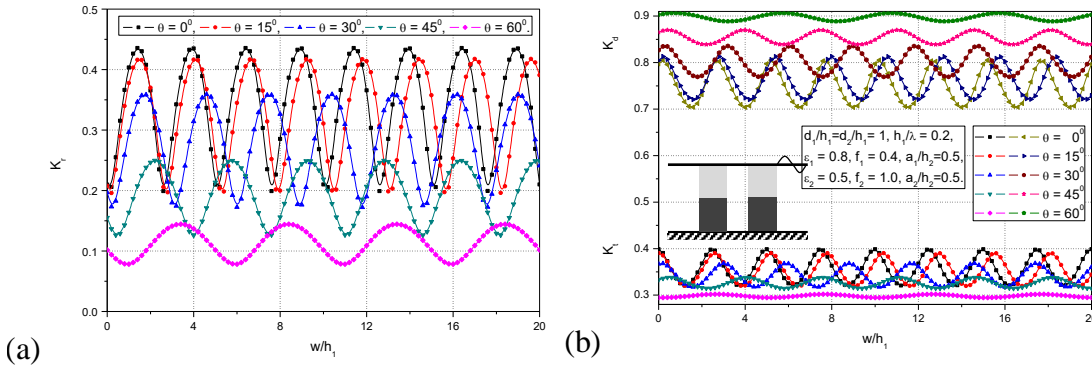


Figure 4.7: Variation of (a)  $K_r$  (b)  $K_t$  and  $K_d$  versus  $w/h_1$  due to two structures for variable  $a_1/h_1$  composed of two porous layers considering  $h_1/\lambda = 0.2$  and  $d/h_1 = 2$ .

#### 4.4.1.3 Three porous structures

The  $K_r$  (Figure 4.8a),  $K_t$  and  $K_d$  (Figure 4.8b) versus dimensionless free spacing  $w/h_1$  are presented for variable surface layer porosity  $\varepsilon_1$  and friction factor  $f_1$  for three porous structures. The dimensionless cumulative structural width  $d/h_1$  is

correlated with the finite free spacing  $w/h_1$ , where the change in  $w/h_1$  shows change in  $d/h_1$  and  $d = 0.5w$ . The oscillating phenomenon is observed in  $K_r$ ,  $K_t$  and  $K_d$  for all the combinations of structural porosity within  $0.6 \leq \varepsilon_1 \leq 0.9$  and friction factor  $0.2 \leq f_1 \leq 0.8$ . The  $K_r$  reaches to highest value and then shows uniform estimation for all combinations of porosity. As discussed in the above section (Figure 4.7), the change in the free spacing shows the resonating crests and troughs, but eventually, the resonating phenomenon is limited within  $0.1 \leq w/h_1 \leq 12$ , thereafter almost uniform values in the  $K_r$  (Figure 4.8a), almost zero transmission  $K_t$  and full energy damping  $K_d$  (Figure 4.8b) are obtained within  $12 \leq w/h_1 \leq 30$  for all the combinations of porosity and friction factor due to increase in structural width, which is correlated with free spacing. However, change in surface layer porosity and friction factor shows a significant decrease in  $K_r$  and  $K_t$ , and a considerable surge in  $K_d$ . But, the performance of three porous structures for  $\varepsilon_1 = 0.8$  and  $f_1 = 0.4$  shows considerable values in  $K_r$ ,  $K_t$  and  $K_d$  as compared with other combinations.

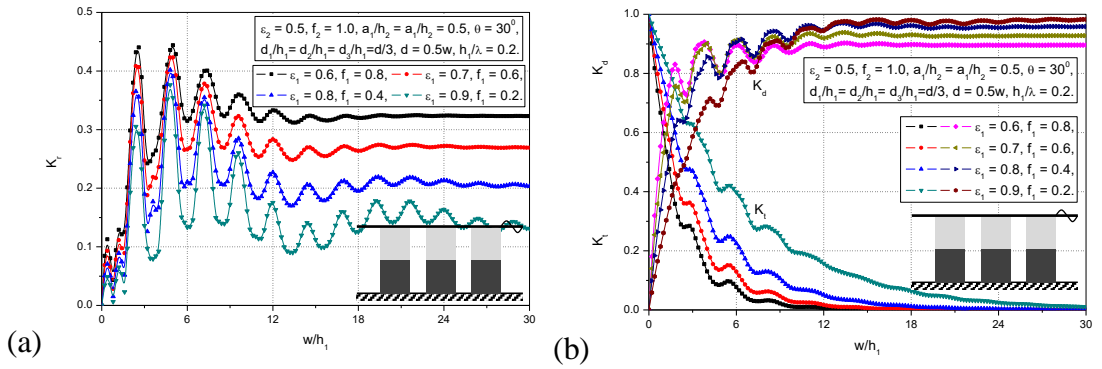


Figure 4.8: Variation of (a)  $K_r$  (b)  $K_t$  and  $K_d$  versus  $w/h_1$  due to three structures for variable  $\varepsilon_1$  and  $f_1$  composed of two porous layers considering  $h_1/\lambda = 0.2$  and  $\theta = 30^\circ$ .

The minimal  $K_r$ , zero  $K_t$  and 98% of  $K_d$  are achieved in the case of  $\varepsilon_1 = 0.8$  and  $f_1 = 0.4$  within  $12 \leq w/h_1 \leq 30$ . However, the impedance of the bottom porous layer is evident in the trapping of waves within the free spacing available between the multiple structures, but in the present case the  $\varepsilon_2 = 0.5$  and  $f_2 = 1$  is kept fixed for simplicity. The structural configuration  $\varepsilon_1 = 0.9$  and  $f_1 = 0.2$  shows high oscillation as compared with the other combinations due to the minimal friction factor, which shows minimal

wave damping. Hence, the three porous structures having  $\varepsilon_1 = 0.8$  and  $f_1 = 0.4$  are suitable for better hydraulic performance.

#### 4.4.1.4 Four porous structures

The wave reflection  $K_r$  (Figure 4.9a) and transmission  $K_t$  (Figure 4.9b) versus dimensionless free spacing  $w/h_1$  are presented for variable surface layer depth  $a_1/h_2$  for four porous structures. The primary resonating peaks are obtained in the  $K_r$  in periodic intervals and also the secondary resonating peaks are noticed within the primary resonating peaks due to the fluid oscillations in the free spacing  $w/h_1$ . The increase in  $a_1/h_2$  reduces the impact of resonating crests and resonating troughs in the  $K_r$  and  $K_t$ . The high resonating peak is observed for  $a_1/h_2 = 0.2$  whereas 8% for  $a_1/h_2 = 0.4$ , 21% for  $a_1/h_2 = 0.6$ , 37% for  $a_1/h_2 = 0.8$  the decrease in  $K_r$  is obtained as compared with the  $a_1/h_2 = 0.2$ . The  $K_t$  is observed to be varying near to unity for all the combinations of  $a_1/h_2$  due to the minimal structural width  $d_j/h_1 = 0.5$  for  $j=1,2,3,4$  and higher  $h_1/\lambda = 0.1$ . Present study considered the minimal structural width  $d_j/h_1 = 0.5$  to examine the effect of the multiple free spacing on the hydraulic characteristics. The higher structural width  $d/h_1$  can perform minor values in the  $K_t$  and it can enhance the wave damping  $K_d$  which can be suitable for the practical application.

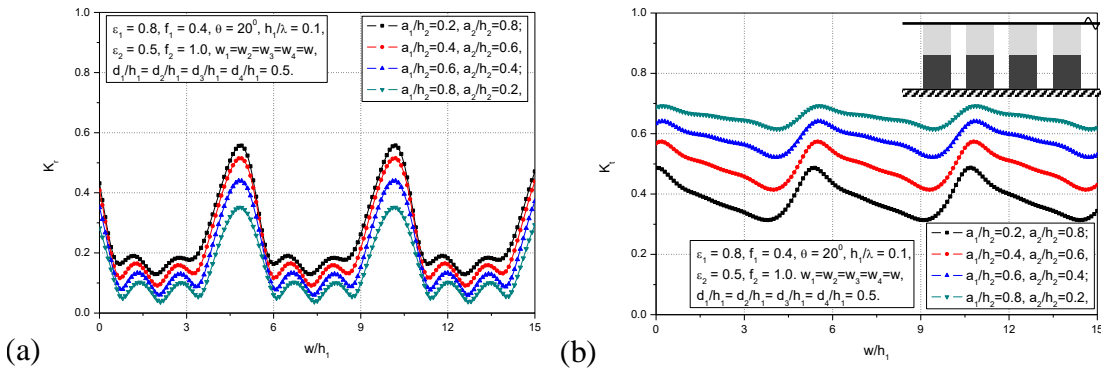


Figure 4.9: Variation of (a)  $K_r$  and (b)  $K_t$  versus  $w/h_1$  due to four porous structures for variable  $a_1/h_2$  composed of double porous layers considering  $h_1/\lambda = 0.1$  and  $\theta = 20^\circ$ .

#### 4.4.1.5 Comparative study between the multiple porous structures

In order to show the effect of free spacing on hydrodynamic characteristics, such as  $K_r$  (Figure 4.10a),  $K_t$  and  $K_d$  (Figure 4.10b) versus  $\gamma_{10}d$  are presented for single and multiple porous structures. The width of the single porous structure is equally divided into two, three, four and five structures considering variable horizontal porosity. The hydrodynamic characteristics due to the presence of two, three, four and five structures are compared with a single porous structure for fixed structural width. Hence the cumulative structural width is identical in each case, and multiple free spacing impact on wave transformation can be revealed. The mono resonating peak and trough in  $K_r$  is observed for  $N=1$  but a forward shift in  $K_r$  in the form of resonating peaks and troughs is noticed for multiple structures. However, each of the resonating peaks due to multiple structures shows high values as compared with a single structure. Similarly, the resonating troughs are observed to be minimum for multiple porous structures as compared with the single porous structure due to the wave blocking in the free spacing. The variation in the  $K_t$  and  $K_d$  (Figure 4.10b) is minimal within the  $1 \leq \gamma_{10}d \leq 10$  and thereafter a uniform estimation in  $K_t$  and  $K_d$  is achieved for single and multiple porous structures. However, the multiple porous structures are evident at each of the resonating troughs in reducing the wave impact on structure and performance characteristics of the porous structures can be improved by finding the optimum free spacing provided between the multiple porous structures, which is discussed in detail in Figure 4.6 and Figure 4.7.

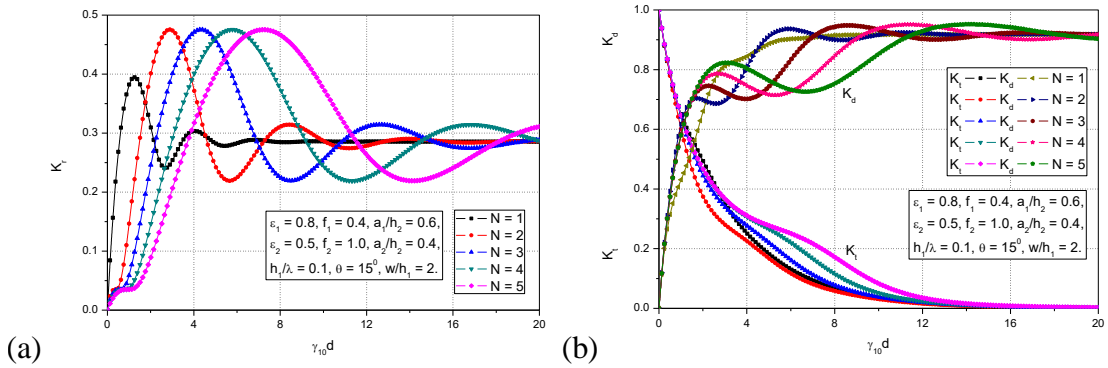


Figure 4.10: Variation of (a)  $K_r$  (b)  $K_t$  and  $K_d$  due to single and multiple structures composed of double porous layers considering  $h_1 / \lambda = 0.1$  and  $\theta = 15^\circ$ .

## **4.4.2 Three-layered fully extended multiple porous structures**

In the present section, a three-layered porous structure is analysed under the assumption of linearized wave theory. The three-layered structure is assumed to be composed of surface porous layer, middle porous layer and bottom rigid layer. In Section 4.4.1, the porous structure depth is divided into two porous layers  $h_2 = a_1 + a_2$ , and in the present case, the three-layer structure is examined. But the total structural depth (two porous layers and one rigid bottom layer) is kept fixed given as  $h_1 = h_2 + a_3$  or  $h_1 = a_1 + a_2 + a_3$ . However, the  $h_2 / h_1$  or  $a_3 / h_1$  show the rigid layer depth and  $a_3 / h_1$  is used throughout the study.

### **4.4.2.1 Single porous structure**

The  $K_r$  (Figure 4.11a),  $K_t$  and  $K_d$  (Figure 4.11b) versus dimensionless structural width  $d / h_1$  are presented for variable bottom rigid layer height  $a_3 / h_1$  for a single porous structure. The  $K_r$  is observed to reach a peak value and attains a uniform estimation which is observed to be similar to the previous cases as in Section 4.4.1. The increase in  $a_3 / h_1$  means reduction in surface porous layer  $a_1 / h_2$  and middle porous layer  $a_2 / h_2$  due to fixed structural depth  $h_1 = a_1 + a_2 + a_3$ . The variation in  $K_r$  is evident within  $0 \leq a_3 / h_1 \leq 2$  thereafter, a minimal gain in  $K_r$  is observed for higher values of  $a_3 / h_1$ . Almost uniform values in  $K_r$  is observed for all the combinations of  $a_3 / h_1$  within  $6 \leq d / h_1 \leq 10$  may be due to the increase in the  $d / h_1$  as compared to incident wavelength (Dalrymple et al., 1991). The increase in  $d / h_1$  illustrates the effective decrease in  $K_t$  monotonously. But, the increase in  $a_3 / h_1$  shows the minor impact on  $K_t$  due to wave blocking at the seaward interface. Further,  $K_d$  is observed to be decreasing for the surge in the third layer  $a_3 / h_1$  and minor variation in  $K_d$  is noted within  $0.1 \leq d / h_1 \leq 4$  and the deviation becomes larger in  $K_d$  within  $4 \leq d / h_1 \leq 10$ . The major reason is, increase in  $a_3 / h_1$  shows the reduction in  $a_1 / h_2$  and  $a_2 / h_2$  due to fixed structural depth, which means that the increase in  $a_3 / h_1$  causes a significant reduction in porous structure depth which causes the minimal wave transport through



the structures and some quantity of wave amplitude is observed to be attenuated by the rigid layer due to the constructive seaward interferences. However, the present study suggests that the minimal bottom rigid layer height is suitable to achieve the required energy damping, as the significance of porous structure is to dissipate the incoming oblique waves.

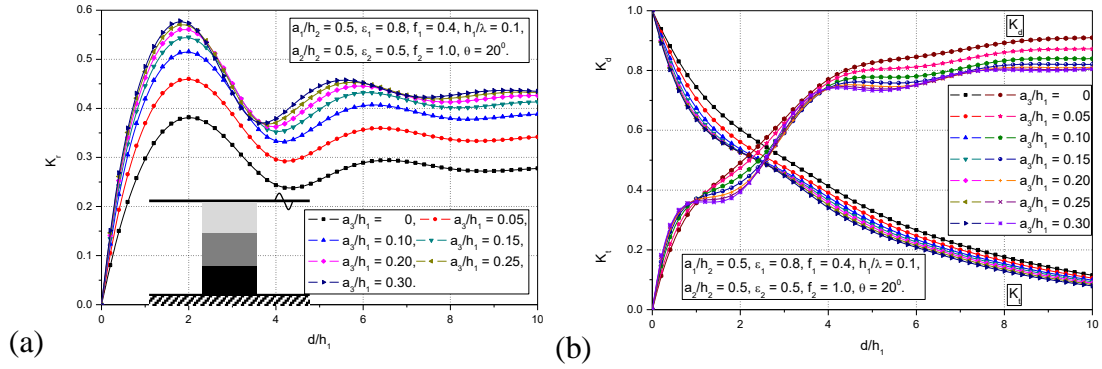


Figure 4.11: Variation of (a)  $K_r$  (b)  $K_t$  and  $K_d$  versus  $d/h_1$  due to a single structure for variable  $a_3/h_1$  composed of triple layers considering  $h_1/\lambda = 0.1$  and  $\theta = 20^\circ$ .

On the other hand, the significance of the angle contact  $\theta$  on the wave transformation is analysed for variable bottom layer height in Figure 4.12(a,b). The increase in the bottom rigid layer shows a considerable variation in wave transformation. The pattern of  $K_r$  (Figure 4.12a) is observed to be similar for all the combinations of  $a_3/h_1$  but a gradual increase in  $K_r$  is observed, and also the critical angle is noted within  $64^\circ \leq \theta \leq 75^\circ$ , which is evident in the design of the angle of contact with a single porous structure composed of three layers. The  $K_t$  (Figure 4.12b) is observed to be decreasing with increase in the bottom rigid layer height  $a_3/h_1$  within  $0^\circ \leq \theta \leq 60^\circ$ . Thenceforth, almost uniform estimation in  $K_t$  is obtained within  $60^\circ \leq \theta \leq 90^\circ$  for all the combinations of  $a_3/h_1$ . The present case suggests that the rigid bottom layer plays a vital role in the case of normal wave contact  $\theta = 0^\circ$  but, the occurrence of standing waves (where minimal  $K_r$  occurs) can dominate the entire wave transformation, and this results in considerable outcomes from the structure. The  $K_r$  reaches to unity and  $K_t$  reaches to zero for  $\theta = 90^\circ$ , which is not suitable for practical application due to the zero-energy damping by the structure.

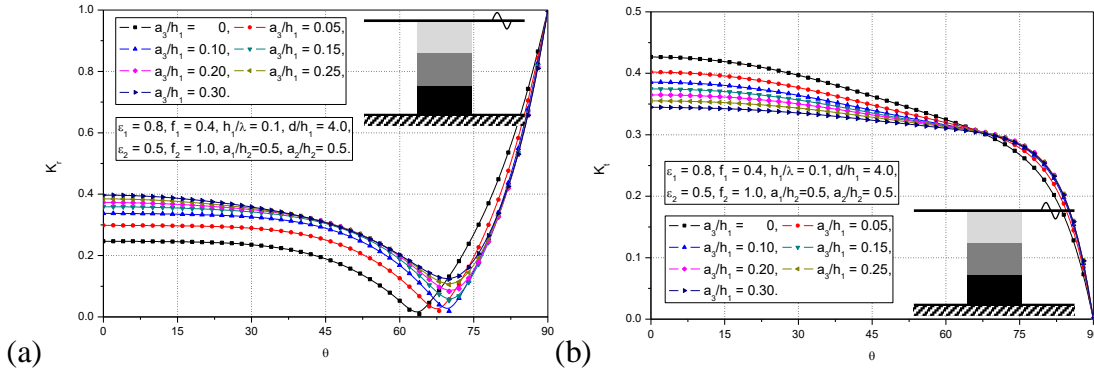


Figure 4.12: Variation of (a)  $K_r$  and (b)  $K_t$  versus  $\theta$  due to single structure for variable  $a_1/h_2$  and  $a_2/h_2$  composed of triple layers considering  $h_1/\lambda = 0.1$  and  $d/h_1 = 4$ .

#### 4.4.2.2 Two porous structures

The wave reflection  $K_r$  (Figure 4.13a), wave transmission  $K_t$  and wave damping coefficients  $K_d$  (Figure 4.13b) versus dimensionless structural width  $\gamma_{10}d$  are presented for variable bottom rigid layer height  $a_3/h_1$  for two porous structures. The  $K_r$  pattern is observed to be different as compared with the regular patterns. A minor resonating peak followed by a primary resonating peak is observed for irrespective values of  $a_3/h_1$ . Then, the mono resonating trough is noticed followed by a uniform value for all the combination of  $a_3/h_1$  with change in  $\gamma_{10}d$ . The resonating peaks and troughs in  $K_r$  is observed to reduce for higher  $\gamma_{10}d$  due to the wave trapping in the confined region available in the free spacing between the two bottom rigid layers. The  $K_t$  and  $K_d$  pattern remains the same as in Section 4.4.1, but, the resonating phenomena of  $K_t$  and  $K_d$  is evident within  $0.5 \leq \gamma_{10}d \leq 5$  due to the obstruction caused by the second porous structure, which is predominant in reflecting the transmitted waves from the first porous structure. As compared with the single porous structure, the rigid layer height  $a_3/h_1$  shows the minor variation in the wave transformation due to the destructive interference. The two porous structures show higher values in the wave reflection  $K_r$ , reduction in the wave transmission  $K_t$  and energy damping  $K_d$  as compared with the single porous structure, which may be due to the angle of contact and wave blocking in the free spacing.

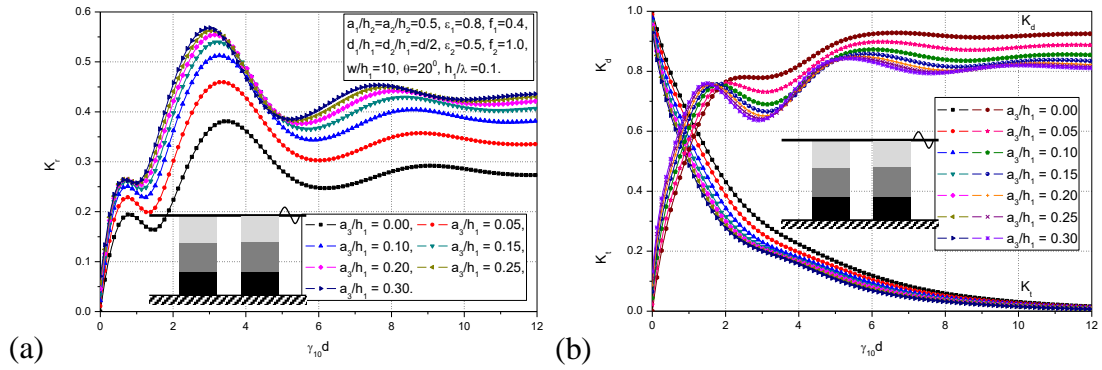


Figure 4.13: Variation of (a)  $K_r$  (b)  $K_t$  and  $K_d$  versus  $\gamma_{10}d$  due to two structures for variable  $a_3/h_1$  composed of triple layers considering  $h_1/\lambda = 0.1$  and  $\theta = 20^\circ$ .

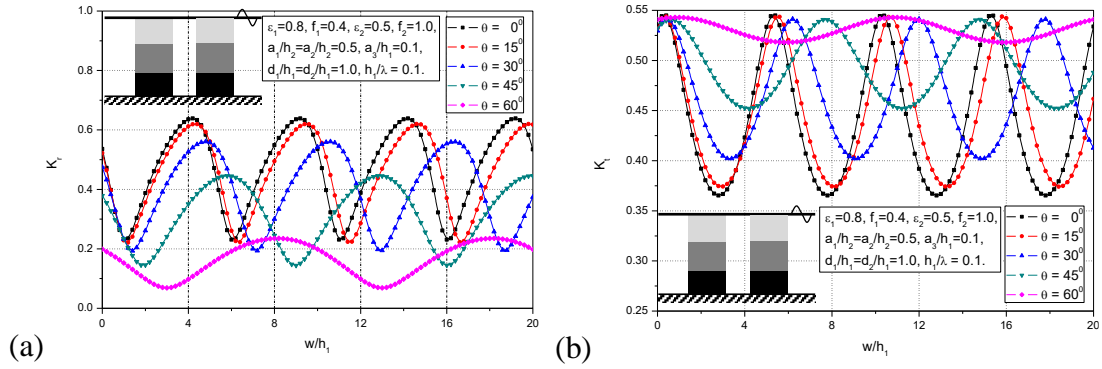


Figure 4.14: Variation of (a)  $K_r$  and (b)  $K_t$  versus  $w/h_1$  due to two structures for variable  $a_3/h_1$  composed of triple layers considering  $h_1/\lambda = 0.1$  and  $d/h_1 = 2$ .

As stated in Section 4.4.1, the free spacing shows a critical impact in the design of multiple porous structures due to a surge in resonating crests and troughs. The generation of oscillations in  $K_r$  (Figure 4.14a) and  $K_t$  (Figure 4.14b) is observed for the variable  $w/h_1$ , which is due to the presence of two porous structures considering the variable angle of contact  $\theta$ . The increase in  $\theta$  influences the resonating peaks in  $K_r$  and observed to reach higher estimation for normal wave contact  $\theta = 0^\circ$ . The increase in the angle of contact vanishes the oscillations and almost uniform values in  $K_r$  is observed for  $\theta = 60^\circ$ . Similarly, the resonating troughs in  $K_t$  is observed to approach the minimal values for normal wave contact  $\theta = 0^\circ$ . The minimal oscillations in  $K_r$  and  $K_t$  for  $\theta = 60^\circ$  is evident in the design of coastal structures and this case is possible only if the wave transport is subjected to formation of standing waves. In Section 4.4.1, the resonating peaks and troughs are observed in  $K_r$  and  $K_t$ , but the

range of variation (the difference between the resonating crest and trough in the  $K_r$  and  $K_t$ ) is almost uniform. However, in the presence of a rigid layer with two-porous layers, the resonating peak becomes higher, but a gradual variation in  $K_r$  with forward shift is observed due to the presence of rigid step height, which causes the additional wave reflection and also encourages the high energy trapping in the confined region.

#### 4.4.2.3 Three porous structures

The  $K_r$  (Figure 4.15a),  $K_t$  and  $K_d$  (Figure 4.15b) versus free spacing  $w/h_1$  are presented for variable bottom rigid layer height  $a_3/h_1$  for three porous structures. In the case of  $a_3/h_1 = 0$ , the depth of the rigid bottom layer reaches to zero, hence the three-layered structure becomes a two-layered porous structure. The oscillating peaks and troughs are observed to be high within  $0.1 \leq w/h_1 \leq 10$  in the  $K_r$ ,  $K_t$  and  $K_d$  due to minimum  $w/h_1$ , which causes the high interaction between transmitted waves and reflected waves in the free spacing. The increase in  $w/h_1$  shows almost uniform values of  $K_r$ ,  $K_t$  and  $K_d$  within  $10 \leq w/h_1 \leq 30$  for all the combinations of  $a_3/h_1$  with minor oscillations due to the wave trapping in the free spacing and enhancement in the energy damping by three structures.

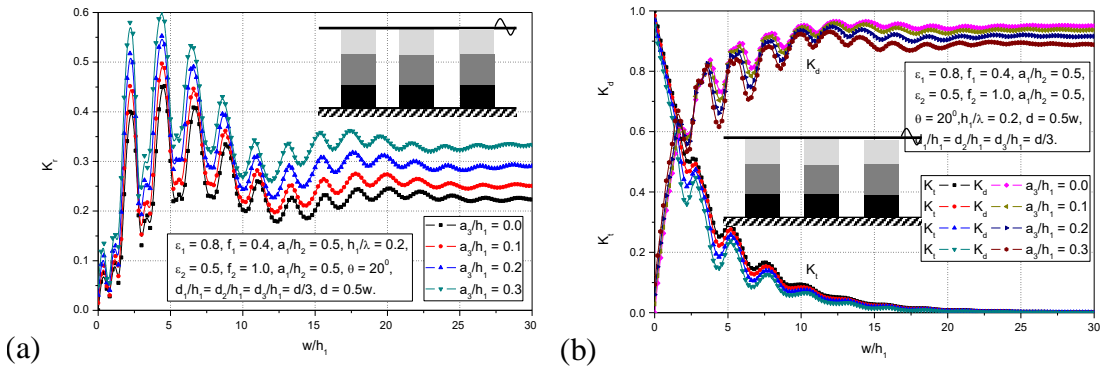


Figure 4.15: Variation of (a)  $K_r$  (b)  $K_t$  and  $K_d$  versus  $w/h_1$  due to three structures for variable  $a_3/h_1$  composed of triple layers considering  $h_1/\lambda = 0.2$  and  $\theta = 20^\circ$ .

The higher values in  $K_r$  are observed for  $a_3/h_1 = 0.3$  rigid step height whereas the 10.6% for  $a_3/h_1 = 0.2$ , 21.5% for  $a_3/h_1 = 0.1$  and 30% for  $a_3/h_1 = 0$  the reduction in  $K_r$  is achieved as compared with  $a_3/h_1 = 0.3$  at  $w/h_1 = 18$ . The variation in  $K_r$  is

high at  $w/h_1 = 4$  which may due to the constructive seaside interference. However, rigid step height  $a_3/h_1$  shows a significant role in reducing  $K_t$  at each of the resonating troughs and also a minor reduction in  $K_d$  is achieved due to the decrease in pore spaces. Further, a higher rigid step causes the higher values in  $K_r$ , lower values in  $K_t$  and  $K_d$ . So, proper estimation of hydrodynamic characteristics is useful for reducing the wave impact on the structure at seaward interface, which can provide a better life span of the structure.

#### 4.4.2.4 Four porous structures

The  $K_r$ ,  $K_t$  (Figure 4.16a) and  $K_d$  (Figure 4.16b) versus  $w/h_1$  are plotted for various values of dimensionless cumulative structural width  $d/h_1$  considering four porous structures. Bragg's resonance phenomenon in  $K_r$  is observed, which is exactly similar to the previous case for four porous structures composed of two porous layers for variable layer depth as in Figure 4.9(a,b).

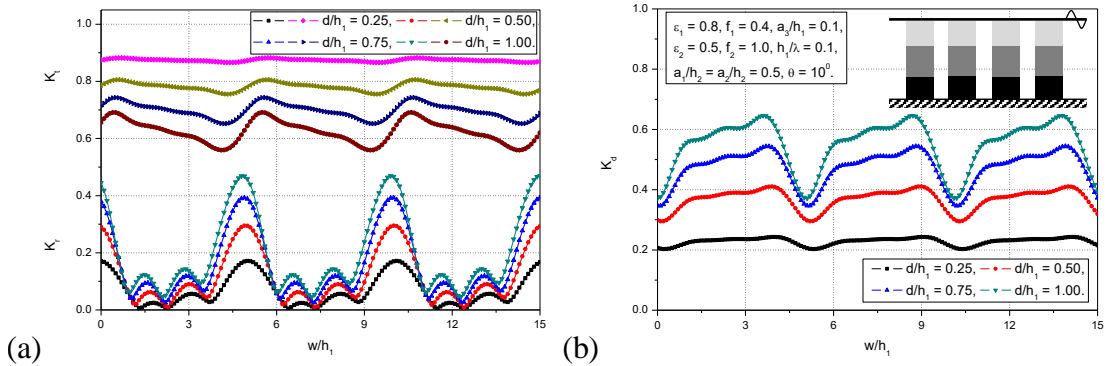


Figure 4.16: Variation of (a)  $K_r$  (b)  $K_t$  and  $K_d$  versus  $\theta$  due to four structures for variable  $\varepsilon_1$  and  $f_1$  composed of triple layers considering  $h_1/\lambda = 0.1$  and  $a_3/h_1 = 0.1$ .

In the present case, the structural width is considered as a dominating parameter and there exist primary and secondary resonating crests. In the previous studies, the similar Bragg's resonating phenomenon in  $K_r$  is observed for variable friction factor (Losada et al., 1993), intrinsic permeability (Twu and Liu, 2004) and variable structural porosity due to multiple porous structures. In the present study, the primary resonating peaks reach to higher amplitude with the increase in the cumulative structural width. Further,  $K_t$  leads to minimal estimation and  $K_d$  shows a drastic rise in periodic intervals. The

variation in the number of resonating primary and secondary peaks and troughs in the wave transformation plays a vital role in the design of the multiple coastal structures for better wave decay.

#### 4.4.2.5 Comparative study between the multiple porous structures

A comparative study is performed between single and multiple three-layered structures considering variable porosity for variable cumulative structural width  $d/h_1$  in Figure 4.17(a,b) to find the number of structures required for controlling the incoming wave for  $h_1/\lambda = 0.2$ .

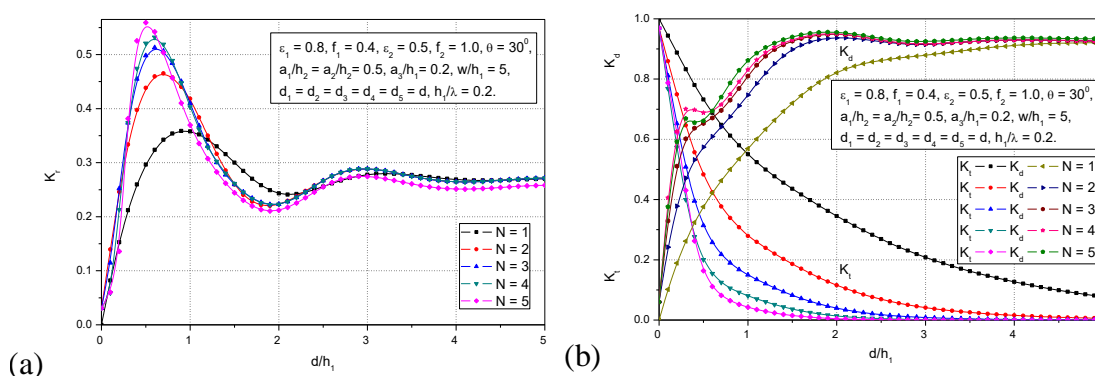


Figure 4.17: Variation of (a)  $K_r$  (b)  $K_t$  and  $K_d$  due to single and multiple structures composed of triple porous layers considering  $h_1/\lambda = 0.2$  and  $a_3/h_1 = 0.2$ .

In the previous case (Figure 4.10a,b), the structural width is uniformly divided into multiple structures for finding the significance of the free spacing on wave transformation. But in the present case, the comparative study is performed between the single and multiple structures, wherein the second structure is added to the first structure and the third structure is added to the second structure of identical width. The resonating crest in  $K_r$  (Figure 4.17a) is observed to be higher for two, three, four and five structures as compared with the single structure due to the addition of wave reflection by each bottom rigid layer. Thereafter, the uniform values in  $K_r$  is observed within  $2.5 \leq d/h_1 \leq 5$ . But, in the case of  $K_t$  and  $K_d$  (Figure 4.17b), the sharp reduction in  $K_t$  and a drastic rise in  $K_d$  is obtained, when the second structure is added to the first structure within  $0.5 \leq d/h_1 \leq 3$ . Thereafter, there exists a considerable decrease in  $K_t$  within  $0.5 \leq d/h_1 \leq 2$  by adding the third structure whereas the fourth and fifth

structure shows the decrease in  $K_t$  within  $1.0 \leq d/h_1 \leq 1.5$ . But, the three, four and five structures shows minimal variation in the  $K_d$  as compared with two porous structures. The  $K_r$  and  $K_d$  remains uniform for multiple structures within  $3 \leq d/h_1 \leq 5$ , but the  $K_t$  is observed to be reduced, which may be due to the formation of resonating troughs at that particular interval for multiple structures, and diminishes the  $K_t$  due to wave blocking in the multiple confined regions. Thus, the incident wavelength of  $h_1/\lambda = 0.2$  can attenuate with either two or three porous structures of width  $d/h_1 = 1.5$  in the presence of the three-layers.

#### 4.4.3 Submerged two-layered multiple porous structures

In the present section, the submerged two-layered structure considering one porous layer upon a rigid layer is studied varying rigid layer height, structural width, porosity, friction factor and angle of contact. The structures are assumed to be deeply submerged and the study is extended for multiple submerged porous structures with finite free spacing. The variation between the present case and previous case (Section 4.4.2) is the surface layer porosity and friction factor. If the surface layer porosity reaches unity  $\varepsilon_1 = 1$  and friction approaches to zero  $f_1 = 0$ , then the porous layer becomes the open water region and it is kept fixed throughout the investigation.

##### 4.4.3.1 Single submerged porous structure

In Figure 4.18(a,b), the  $K_r$  and  $K_t$  versus  $d/h_1$  are presented for variable porosity and friction factor  $\varepsilon_2 = 0.8$ ,  $f_2 = 0.4$  (Figure 4.18a) and  $\varepsilon_2 = 0.5$ ,  $f_2 = 1$  (Figure 4.18b) considering different rigid step height  $a_3/h_1$ . The oscillation pattern in  $K_r$  and  $K_t$  (Figure 4.18a) is observed for all the combinations of  $a_3/h_1$ , but a backward shift in resonating peaks and troughs in  $K_r$  is observed with the surge in  $a_3/h_1$ . However, the peak value in  $K_r$  is observed almost similar for all the combinations of  $a_3/h_1$  due to the fixed surface layer depth  $a_1/h_2$ . The resonating troughs in  $K_r$  is observed very near to zero due to the high structural porosity, which allows more waves to pass through the structure. In Figure 4.18(b) there exists a significant surge in  $K_r$  with the increase

in  $a_3/h_1$  and the resonating peaks are observed to be high in wave reflection  $K_r$  as compared with the previous case (Figure 4.18a) due to the reduction in the porosity, which allows the minimal wave penetration. However, in the case of submerged two-layered structure, the rigid bottom layer  $a_3/h_1$  shows a significant impact on the wave transformation in the presence of lower porosity and moderate friction factors  $\varepsilon_2 = 0.5$ ,  $f_2 = 1$  as compared with the higher porosity and lower friction factor  $\varepsilon_2 = 0.8$ ,  $f_2 = 0.4$ .

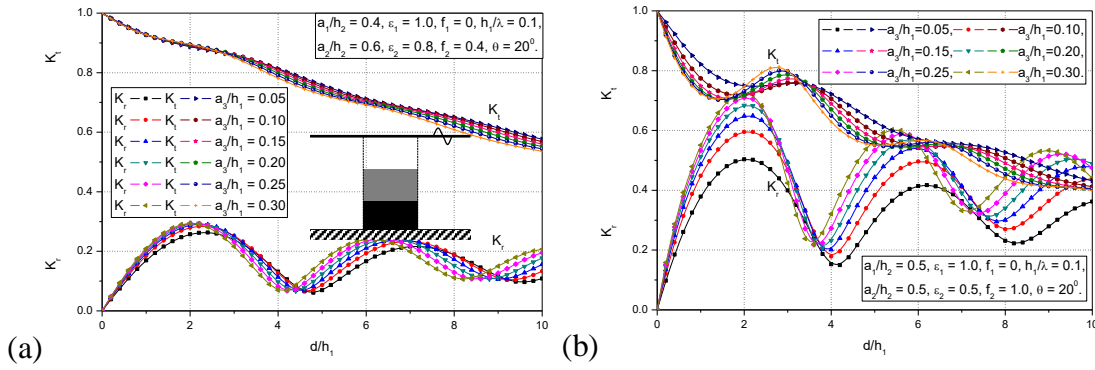


Figure 4.18: Variation of  $K_r$  and  $K_t$  versus  $d/h_1$  due to single submerged structure for variable  $h_2/h_1$  composed of two layers for  $h_1/\lambda = 0.1$ ,  $\theta = 20^\circ$  considering (a)  $\varepsilon_2 = 0.8$ ,  $f_2 = 0.4$  and (b)  $\varepsilon_2 = 0.5$ ,  $f_2 = 1.0$ .

#### 4.4.3.2 Two submerged porous structures

In Figure 4.19(a), the  $K_r$  and  $K_t$  versus  $\theta$  are presented considering various values of  $d/h_1$  for a pair of submerged porous structures. The  $K_r$  is observed to be increasing and  $K_t$  is observed to be reduced with an increase in the  $d/h_1$  due to an increase in energy damping by the structure. The critical angle is observed to be moving towards the higher values of  $\theta$  within  $20^\circ \leq \theta \leq 65^\circ$  due to the formation of standing waves. It is noted that the  $\theta = 90^\circ$  shows the unity in  $K_r = 1$  and zero in  $K_t$  which is observed in Section 4.4.1. On the other hand, the significance of the bottom rigid layer on wave transformation is presented for a pair of submerged porous structures for variable free spacing  $w/h_1$  in Figure 4.19(b). The resonating peaks are observed to be high in  $K_r$  and moderate in  $K_t$ . The increase in the rigid layer height shows a minimal increase in  $K_r$  and minimal reduction in the  $K_t$  due to the zero velocity near the rigid steps.



However,  $K_t$  decreases with the increase in the structural height/structural width. In the previous sections (in the case of fully extended two-layered and three-layered structures) the minimal  $K_t$  is achieved for most of the structural configurations. In the case of submerged porous structures, the  $K_t$  is observed to be very near to the unity due to the wave propagation at the free surface.

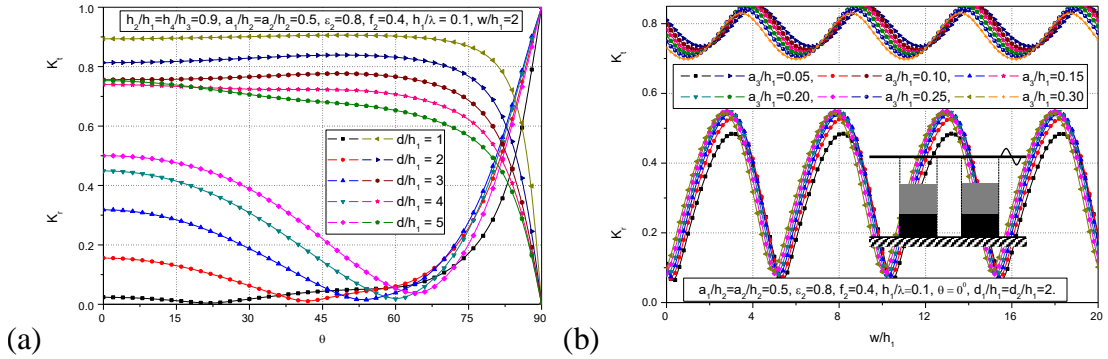


Figure 4.19: Variation of  $K_r$  and  $K_t$  versus (a)  $\theta$  for variable  $d/h_1$  and (b)  $w/h_1$  for variable  $a_3/h_1$  due to two submerged structures composed of two layers considering  $h_1/\lambda = 0.1$ .

#### 4.4.3.3 Three submerged porous structures

In Figure 4.20(a,b), the wave reflection  $K_r$  (Figure 4.20a), wave transmission  $K_t$  and energy damping  $K_d$  (Figure 4.20b) versus  $\gamma_{10}d$  are plotted for variable  $\varepsilon_2$  and  $f_2$  due to the three submerged porous structures composed of two-layers. The bottom rigid layer height is kept fixed  $a_3/h_1 = 0.2$  and free spacing available between any two porous structures is  $w/h_1 = 1$ . The increase in the  $\gamma_{10}d$  shows the higher oscillations in  $K_r$ , but  $K_r$  approaches to minimal oscillation for each of the individual porosity and friction factor. Similarly, the resonating peak is observed in  $K_t$  (Figure 4.20b) where a high resonating peak is observed in  $K_r$  at  $\gamma_{10}d = 1.8$  which may be due to Bragg's resonance. Afterward, the increase in  $\gamma_{10}d$  shows the drastic reduction in  $K_t$  due to enhancement in structural width, which helps in the high energy damping. The resonating peaks and troughs are observed to be high in the present case due to the confined region. The high values of  $K_r$  and low values of  $K_t$  is observed for minimum porosity  $\varepsilon_2 = 0.6$  and moderate friction factor  $f_2 = 0.8$ . The increase in  $\varepsilon_2$  shows the

significant reduction in  $K_r$  and the considerable increase in  $K_t$  is due to the change in energy dissipation.

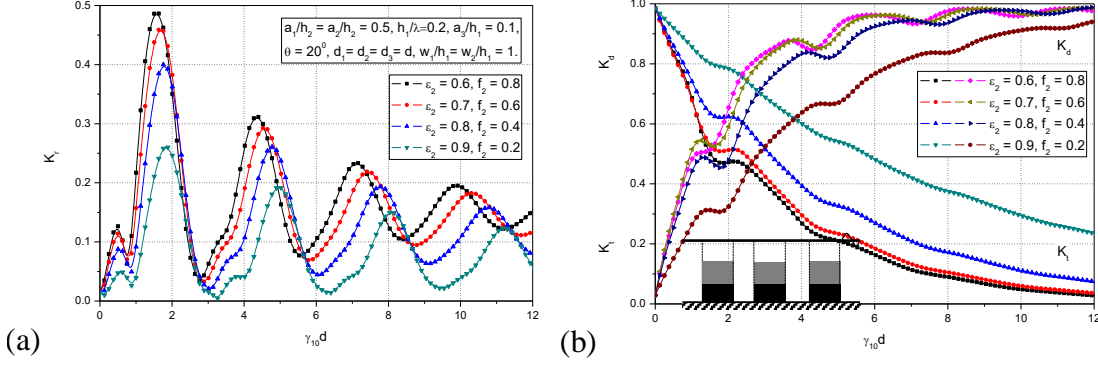


Figure 4.20: Variation of (a)  $K_r$  and (b)  $K_t$  versus  $\gamma_{10}d$  for variable  $\varepsilon_2$  and  $f_2$  due to three structures composed of two layers considering  $h_1 / \lambda = 0.2$  and  $\theta = 20^\circ$ .

As a comparison, the 10% reduction for  $\varepsilon_2 = 0.7$ , 28% reduction for  $\varepsilon_2 = 0.8$  and 57% reduction for  $\varepsilon_2 = 0.9$  in  $K_r$  is observed as compared with  $\varepsilon_2 = 0.6$  at the highest resonating peak for  $\gamma_{10}d = 1.5$ . In the previous conditions, the uniform estimation in  $K_r$  is obtained for higher structural width, but in the present case, the uniform estimation in the  $K_r$  is observed within  $6 \leq \gamma_{10}d \leq 12$  in the oscillatory manner which may be due to the confined region causing the gain in the wave transformation and encouraging the vortex formation at the tip of each porous structures (Yip et al., 2002). However, the vortex formation is higher for the case of minimal porosity due to the minimal energy damping, that might be the major reason behind the oscillations and the oscillations can diminish with the increase in the structural height as noted in the Section 4.4.1 and Section 4.4.2.

#### 4.4.3.4 Four submerged porous structures

The wave reflection  $K_r$  (Figure 4.21a) and wave transmission  $K_t$  (Figure 4.21b) versus relative free spacing between the structures  $w/h_1$  for the variable angle of contact  $\theta$  are reported for four submerged two-layered porous structures in series to determine the impact of the angle of contact on wave scattering. The increase in  $w/h_1$  broadens the resonating crests and troughs in  $K_r$  and  $K_t$  due to the constructive and destructive interferences and also the effect of rigid layer height. The high value in  $K_r$  is obtained

for  $\theta = 0^\circ$  and a gradual reduction in  $K_r$  and gradual enhance in  $K_t$  is achieved with an increase in the angle of contact.

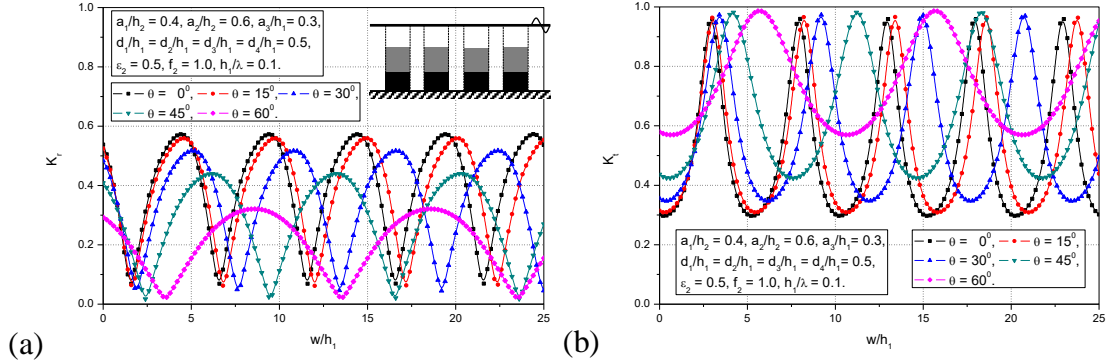


Figure 4.21: Variation of (a)  $K_r$  and (b)  $K_t$  versus  $w/h_1$  for variable  $\theta$  due to four submerged structures composed of two layers considering  $h_1/\lambda = 0.1$  and  $a_3/h_1 = 0.3$ .

The oscillations are observed to be high in  $K_r$  and resonating crests observed very near to the unity due to minimum thickness and moderate depth of the porous structure. The previous studies performed by Twu and Liu (2004) examined the submerged multiple bars and the study reported that the increase in the number of bars (study examined 6 bars) and porosity shows the minimal values in  $K_r$  and  $K_t$  due to an increase in energy dissipation. Similarly, in the case of fully extended two-layered porous structures as in Section 4.4.1 and three-layered porous structures as in Section 4.4.2 shows the almost zero transmission due to the structural height. In the present case, the zero transmission coefficient is possible with higher structural width, and the increase in the number of submerged two-layered structures are also useful for achieving minimal wave transmission. In addition, the resonating peaks in  $K_r$  and troughs in  $K_t$  are useful to determine the optimal free spacing  $w/h_1$ , which helps in the design of the novel coastal structure along with the reduction in the wave impact on porous structures.

#### 4.4.3.5 Comparative study between the submerged porous structures

The comparative study is performed between the single and two submerged porous structures considering uniform width (Figure 4.22a) and variable width (Figure 4.22b). In case of uniform width (Figure 4.22a) the single structural width is separated into two equal structures and the  $K_r$ ,  $K_t$  and  $K_d$  are presented versus  $d/h_1$ . As study sated earlier in the Sections 4.4.1 and 4.4.2, the resonating pattern in the wave transformation

is observed to be high for the two porous structures as compared with the single porous structure. In the present case, a minimal reduction in  $K_t$  and a minimal increase in  $K_d$  at each of the resonating peaks is achieved due to the presence of free spacing available between two consecutive structures.

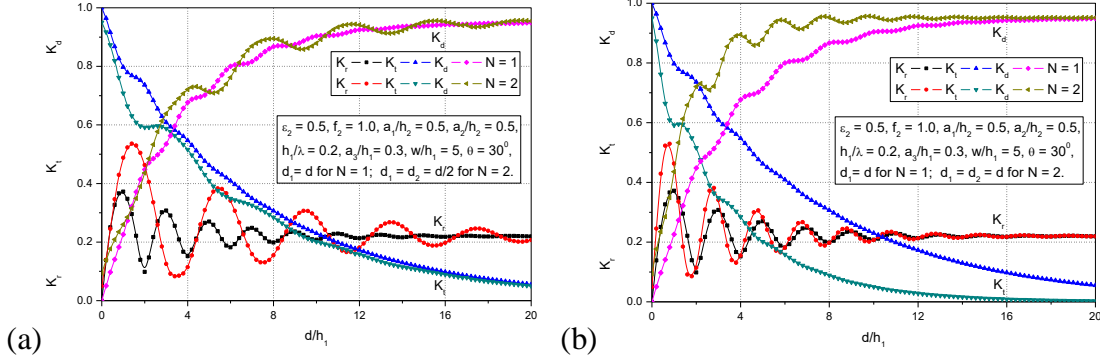


Figure 4.22: Variation of  $K_r$ ,  $K_t$  and  $K_d$  due to single and two submerged porous structures for (a) uniform width, (b) variable width considering  $h_1 / \lambda = 0.2$  and  $\theta = 30^\circ$ .

On the other hand, in the case of variable width (Figure 4.22b), two porous structures width is almost double as compared with the single porous structure. Hence there is a significant increase in wave reflection  $K_r$  at each of the resonating peaks. The significant reduction in wave transmission  $K_t$  and the massive surge in damping coefficient  $K_d$  is achieved for two-structures as compared with the single structure within  $0.1 \leq d/h_1 \leq 10$ . Thereafter, the uniform estimation in  $K_r$  and  $K_d$  is achieved within  $10 \leq d/h_1 \leq 20$ , but  $K_t$  is observed to be decreasing and reaches zero. Hence, the second porous structure is evident in reducing  $K_t$  due to wave trapping/blocking in the free spacing available between two consecutive structures. As a comparison in the  $K_t$  (Figure 4.22b), the 48% reduction at  $d/h_1 = 4$ , 71% reduction at  $d/h_1 = 8$ , 84% reduction at  $d/h_1 = 12$  and 91% reduction at  $d/h_1 = 12$  is obtained due to the presence of secondary structure. The comparison between the single and two porous structures shows the considerable variation in  $K_t$  within  $12 \leq d/h_1 \leq 20$  and a negligible increase in the  $K_d$  but the construction cost may increase due to the large structural width. Finally, the addition of the second porous structure is effective within  $4 \leq d/h_1 \leq 12$  for minimal wave transmission and high energy damping.

## 4.5 CLOSURE

The oblique wave transformation due to fully extended two-layered, three-layered porous structures and submerged two-layered porous structures is analysed considering various design parameters. The eigenfunction expansion approach is used to analyse the wave scattering performance of multiple structures and the conclusions made from the present study are as follows:

- The increase in surface layer depth shows the surge in energy damping due to high surface layer porosity. The 31.9% reduction in wave reflection is obtained with the increase in the surface layer porosity at the resonating crest.
- The minimum values of friction factor illustrate the minimal impact on  $K_d$  and high values of the friction factor enhance  $K_r$ . Thus, the moderate friction factor and high porosity in the surface layer are suggested for high energy damping.
- The decrease in the wavelength widens the resonating crests and troughs for two porous structures and zero  $K_r$  is noted for the angle of incidence  $\theta = 64^\circ$ .
- The angle of contact  $\theta = 30^\circ$  shows the 16.3% reduction in  $K_r$  as compared with the normal angle of contact  $\theta = 0^\circ$  due to the increase in energy damping. Hence, it is better to construct the porous structure on determining the critical angle of contact for minimal wave reflection and high energy damping.
- The 98% of  $K_d$  is achieved for high surface layer porosity  $\varepsilon_1 = 0.8$  and moderate friction factor  $f_1 = 0.4$  for variable free spacing within  $12 \leq w/h_1 \leq 30$  in the presence of the three porous structures.
- The surface porous layer depth  $a_1/h_2$  shows a significant impact in reducing the resonating peaks and troughs. The high resonating peak is observed for  $a_1/h_2 = 0.2$  and 8% for  $a_1/h_2 = 0.4$ , 21% for  $a_1/h_2 = 0.6$ , 37% for  $a_1/h_2 = 0.8$  the decrease in  $K_r$  is obtained as compared with  $a_1/h_2 = 0.2$  for four porous structures.
- The increase in the bottom rigid layer height  $a_3/h_1$  enhances the  $K_r$  and reduces the energy damping. Hence the minimal bottom rigid layer height is suggested for the construction of three-layer porous structures for better performance.

- The multiple porous structures are useful if the structural width is higher. But, for fixed structural width (if one structure width is separated into two structures), the resonating crests and troughs have a major role in reducing the  $K_r$  and  $K_t$ , thus, the high values of  $K_d$  can be achieved.
- The minimal values in  $K_r$ ,  $K_t$  and high values in  $K_d$  can be achieved with two/three triple-layered structures for structural width  $d/h_1 = 1.5$ .
- The double submerged two-layered structures show a significant reduction in  $K_r$  and  $K_t$  at each of the resonating trough as compared with a single structure for fixed width. The reduction in  $K_r$  and  $K_t$  is evident with the addition of the second structure as compared with the single structure. The addition of the second structure is effective within  $4 \leq d/h_1 \leq 12$  for minimal wave transmission and high energy damping in the design and construction of offshore structures.
- The present investigation provides an extensive data set for multiple two-layered, three-layered and submerged two-layered porous structures (limited upto five structures), which can be implemented in the actual field as an effective wave damping system based on the field conditions.

## CHAPTER 5

# WAVE TRAPPING BY HORIZONTALLY STRATIFIED POROUS STRUCTURES WITH END WALL

### 5.1 GENERAL INTRODUCTION

The seawalls are the most common coastal structures constructed in various locations for reflecting the incident waves towards offshore regions. Various types of porous and non-porous seawalls of different physical configurations such as vertical seawalls, sloping seawall, stepped seawalls, semi-infinite permeable seawalls and curved seawalls are designed, fabricated and positioned in the coast. However, few of the seawalls are subjected to tremendous wave contact and gets collapsed. To reduce the wave impact on seawalls, the finite submerged/surface porous objects are introduced, having various configurations that depend upon the ocean floor condition and water depth. The submerged and surface thick/thin porous structures have received more attention as compared with other types of conventional structures due to its high wave damping performance. Hence, the porous breakwaters have been constructed in various physical configurations at various locations to shelter the islands, harbours, marinas, wharfs and mainlands. The functional efficiency of submerged/surface piercing porous structures usually estimates based on hydrodynamic characteristics such as wave reflection, transmission and energy damping characteristics. However, the functional efficiency of breakwater generally depends upon structural porosity, friction factor, angle of contact, structural width and incident wavelength. Recent studies reported that effective breakwater must perform minimum values of wave reflection, transmission and maximum values of wave damping for a better structural life span. However, the high wave damping can be possible for higher structural width, higher structural porosity and multiple structures. In addition, the increase in structural width can maximize the capital cost of the breakwater. Thus, the only alternative is to have high structural porosity to achieve significant wave dissipation. But the high structural porosity affects the lift of breakwater due to the minimal dead weight of the structure.

Specifically, in the case of a porous structure with a vertical wall, the higher structural porosity shows a higher wave force on the vertical wall due to more wave penetration. Hence, a new structural configuration is introduced by Yu and Chwang (1994), having two porosities in a single structure in the horizontal direction.

In the present study, a series of porous structures are examined on considering horizontal variable porosity, which is termed as horizontally stratified porous structures. The series of horizontally stratified porous structures are placed far away from the (a) vertical wall (b) semi-infinite permeable wall and (c) stepped seawall. The wave reflection, transmission and wave damping by various types of porous structures are analysed and validated with the available experimental and theoretical results. Thereafter, the study is extended to examine the series of porous structures away from the vertical wall, stepped wall and permeable wall. The porous structure is divided into two and three-layers considering the high porosity in the surface porous layer, moderate porosity in the middle porous layer and the bottom layer is treated as impermeable, which is useful for the consideration of seabed variation. The effect of multiple horizontal porosities, friction factors, angle of incidence, confined region (free spacing between the two consecutive porous structures), trapping chamber, layer height and structural thickness is reported for trapping of incident waves. The oblique wave reflection by two-layered, three-layered and submerged two-layered structures are examined and bottom layer porosity is considered zero to resemble the natural elevated rigid seabed using zero-velocity condition. The harmonic peaks and troughs due to the presence of series of porous structures and wave trapping in free spacing are reported in detail and the effect of generation of clapotis due to fluid resonance is also discussed. The effective wave trapping points, cushion effect, critical angle and critical width is discussed for the design and development of stratified porous structures.

## **5.2 MATHEMATICAL FORMULATION**

The gravity wave trapping by a series of stratified porous structures placed far away from various walls (vertical, permeable and stepped walls) are examined using the eigenfunction expansion method based on linearized water wave theory. The wave trapping by stratified porous structures consisting of two horizontal porous layers and one rigid bottom layer, having higher porosity in the surface layer, moderate porosity



in the middle layer and zero porosity in the bottom layer is considered. The 3-D Cartesian coordinate system is adopted for the theoretical analysis of stratified porous structures in series considering downward positive  $y$ -axis,  $x$  and  $z$ -axis in the horizontal direction. A series of  $2N$  multiple stratified porous structures are placed at  $x = b_j$  considering the finite spacing  $w/h_1$  between any two adjacent stratified porous structures. In each of the cases, the spacing between the vertical wall and series of stratified porous structures is considered  $L/h_1$  and varied for finding the effective wave trapping points. The fluid realm is divided into multiple open sea regions and structure occupied regions. The fluid field is considered to occupy  $\bigcup_{j=1}^{2N+1} I_j$  with the upstream open sea region  $I_1 \equiv (-b_1 \leq x \leq \infty, 0 \leq y \leq h_1)$ , multiple finite open sea regions and stratified porous structure occupied regions of finite width placed in the finite depth  $I_j \equiv (-b_j \leq x \leq -b_{j-1}, 0 \leq y \leq h_j)$  for  $j = 2, 3, \dots, 2N$  along with the leeward/downward open sea regions  $I_{2N+1} \equiv (-b_{2N} - L \leq x \leq -b_{2N}, 0 \leq y \leq h_{2N+1})$  as in Figure 5.1(a) in the presence of the vertical wall. Further, the analytical study is extended on considering leeward permeable wall and stepped wall as in Figure 5.1(b,c).

The fluid is considered as inviscid, irrotational motion, incompressible and simple harmonic in nature of angular frequency  $\omega$ . So, the velocity potentials  $\Phi(x, y, z, t)$  and surface deflection  $\zeta_j(x, z, t)$  are given in the form of  $\Phi(x, y, z, t) = \text{Re}\{\phi_j(x, y)e^{i(lz - \omega t)}\}$  and  $\zeta_j(x, z, t) = \text{Re}\{\eta_j(x)e^{i(lz - \omega t)}\}$  wherein, the  $\text{Re}$  explains the real part,  $l = \gamma_{10} \sin \theta$  is wavenumber in  $z$ -direction. The  $\gamma_{10} = 2\pi/\lambda$  is the wavenumber in  $y$ -direction and  $\theta$  is the angle of incidence. The velocity potentials  $\phi_j$  for  $j = 1, 2, 3, \dots, 2N + 1$  satisfies the Helmholtz equation given by

$$\frac{\partial^2 \phi_j(x, y)}{\partial x^2} + \frac{\partial^2 \phi_j(x, y)}{\partial y^2} - l^2 \phi_j(x, y) = 0, \quad 0 \leq y \leq h_j \quad (5.1)$$

The velocity potential for the open sea region and structure occupied region satisfies the mean free-surface boundary condition given by

$$\frac{\partial \phi_j(x, y)}{\partial y} + \Gamma_j \phi_j(x, y) = 0 \quad \text{on} \quad y = 0, \quad (5.2a)$$

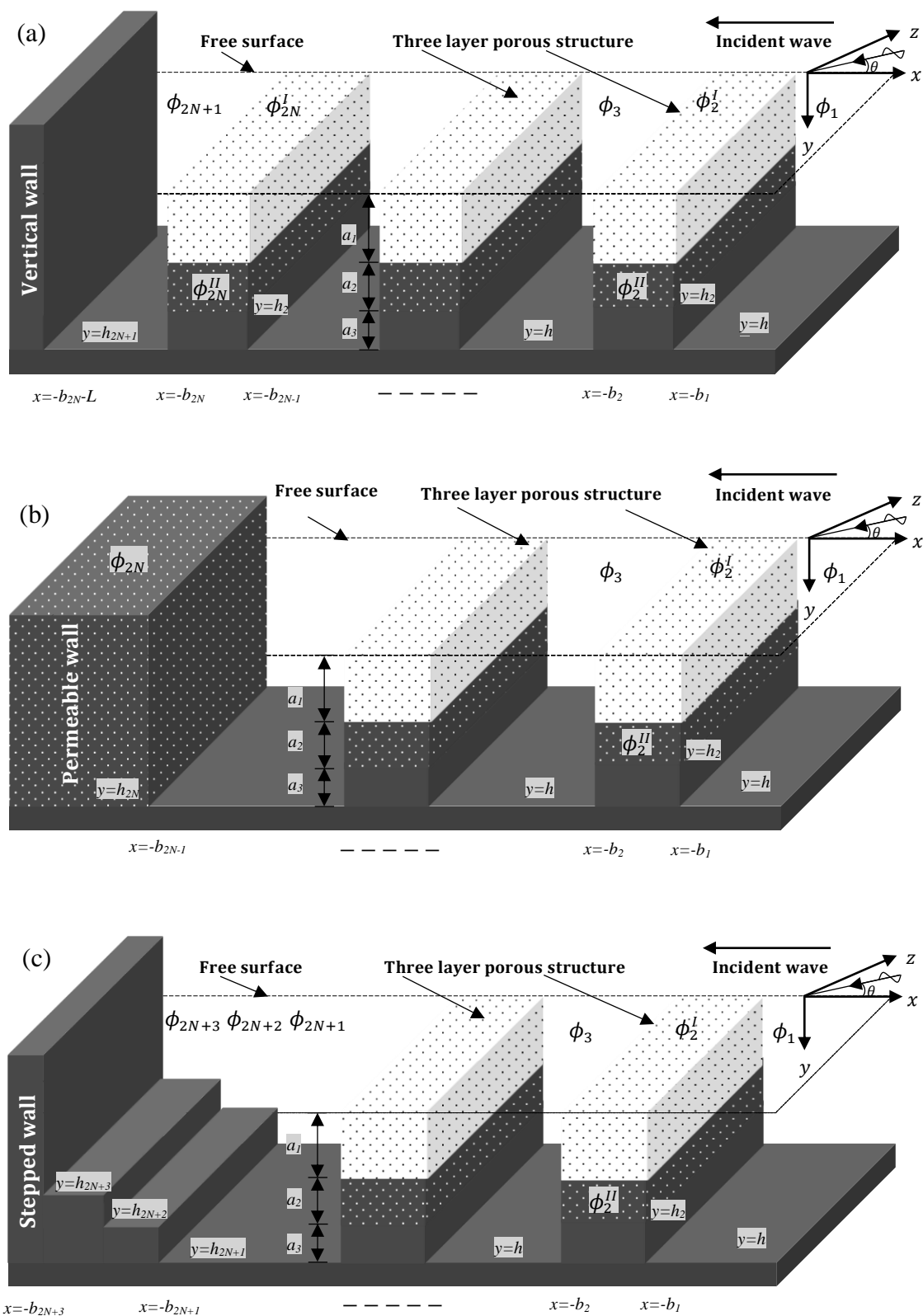


Figure 5.1: Oblique wave transport through a series of stratified porous structures away from the (a) vertical impermeable wall (b) permeable wall and (c) stepped wall.

where  $\Gamma_j = \frac{\omega^2(S_1 + if_1)}{g}$  for  $j = 2, 4, \dots, 2N$  in the case of porous structure occupied regions,  $\Gamma_j = \frac{\omega^2}{g}$  for  $j = 1, 3, \dots, 2N + 1$  in the case of multiple open sea regions.

The bottom zero-flow condition in each of the region  $j = 1, 2, \dots, 2N + 1$  is given by

$$\frac{\partial \phi_j(x, y)}{\partial y} = 0 \quad \text{on} \quad y = h_j. \quad (5.2b)$$

In the case of a three-layered stratified porous structure, the bottom layer, which is near to the seabed is assumed to be impermeable ( $\varepsilon_3 = 0$ ,  $f_3 = 0$ ) and kept fixed throughout the study. Hence there exists a flow within the surface and middle porous layers (Liu et al., 2007) in the vertical direction ( $j = 2, 4, \dots, 2N$ ) given by

$$(S_1 + if_1)\phi_j'(x, y) = (S_2 + if_2)\phi_j''(x, y) \quad \text{on} \quad y = a_1, \quad (5.3a)$$

$$\varepsilon_1 \frac{\partial \phi_j'(x, y)}{\partial y} = \varepsilon_2 \frac{\partial \phi_j''(x, y)}{\partial y} \quad \text{on} \quad y = a_1. \quad (5.3b)$$

The stratified porous structures are assumed of finite width placed at finite depth, which obstructs the free wave motion (continuity of pressure and velocity). To model the continuity of pressure and velocity due to the existence of stratified porous structure, the matching equations are given by

$$\phi_j(x, y) = \begin{cases} (S_1 + if_1)\phi_{j+1}'(x, y) \\ (S_2 + if_2)\phi_{j+1}''(x, y) \end{cases} \quad \text{on} \quad x = -b_j, \quad j = 1, 3, \dots, 2N + 1, \quad (5.4a)$$

$$\frac{\partial \phi_j(x, y)}{\partial x} = \begin{cases} \varepsilon_1 \frac{\partial \phi_{j+1}'(x, y)}{\partial x} \\ \varepsilon_2 \frac{\partial \phi_{j+1}''(x, y)}{\partial x} \end{cases} \quad \text{on} \quad x = -b_j, \quad j = 1, 3, \dots, 2N + 1, \quad (5.4b)$$

$$\phi_{j+1}(x, y) = \begin{cases} (S_1 + if_1)\phi_j'(x, y) \\ (S_2 + if_2)\phi_j''(x, y) \end{cases} \quad \text{on} \quad x = -b_j, \quad j = 2, 4, \dots, 2N, \quad (5.5a)$$

$$\frac{\partial \phi_{j+1}(x, y)}{\partial x} = \begin{cases} \varepsilon_1 \frac{\partial \phi_j'(x, y)}{\partial x} \\ \varepsilon_2 \frac{\partial \phi_j''(x, y)}{\partial x} \end{cases} \quad \text{on} \quad x = -b_j, \quad j = 2, 4, \dots, 2N, \quad (5.5b)$$

where  $b_j$  for  $j=1,2,\dots,2N+1$  are interface points between each of the free water and porous structures,  $\varepsilon_1$  and  $\varepsilon_2$  are porosities,  $f_1$  and  $f_2$  are friction factors,  $S_1$  and  $S_2$  are inertia coefficients in each of the surface and bottom porous layers. The  $\varepsilon_1 = 1$  and  $f_1 = 0$  shows the wave motion over the submerged porous structures due to the absence of a surface porous bar. The inertia and friction factor due to the surface and bottom porous layers are computed using the relation given by

$$S_j = 1 + \left( \frac{1 - \varepsilon_j}{\varepsilon_j} \right) A_m, \quad \text{on } j = 1, 2, \quad (5.6a)$$

$$f_j = \frac{1}{\omega} \frac{\int_V dV \int_t^{t+T} \varepsilon_j^2 \left( \frac{\nu q_i^2}{K_{ip}} + \frac{C_f \varepsilon_j}{\sqrt{K_{ip}}} |q_i|^3 \right) dt}{\int_V dV \int_t^{t+T} \varepsilon_j q_i^2 dt}, \quad \text{on } j = 1, 2, \quad (5.6b)$$

where  $A_m$  is added mass coefficient,  $\omega$  is wave frequency,  $K_{ip}$  is intrinsic permeability  $K_{ip} / h_1^2 = 0.95 * 10^{-6}$ ,  $0.22 * 10^{-5}$  and  $0.345 * 10^{-5}$  (Twu and Liu, 2004)  $q_i$  is the instantaneous Eulerian velocity vector,  $C_f = 0.228$  is a turbulent resistant coefficient (Twu and Liu, 2004),  $\nu$  is kinematic viscosity,  $V$  is volume and  $T$  is wave period. The inertia effect is kept fixed  $S_1 = S_2 = 1$  throughout the analytical study (Sollit and Cross, 1972). In the case of a vertical wall, far-field radiation conditions are given by

$$\phi_j(x) = \begin{cases} (I_{10} e^{-i\gamma_{10}x} + R_{10} e^{i\gamma_{10}x}) f_{10}(y) & \text{as } x \rightarrow \infty, \\ (T_{(2N+1)0} e^{-i\gamma_{(2N+1)0}x}) f_{(2N+1)0}(y) & \text{as } x \rightarrow -(b_{2N} + L), \end{cases} \quad (5.7)$$

where  $I_{10}$ ,  $R_{10}$ , and  $T_{(2N+1)0}$  are complex amplitudes of the incident, reflected and transmitted gravity waves. The wavenumber  $\gamma_{j0}$  for  $j=1,3,\dots,(2N+1)$  in the open sea region and the wavenumber  $\gamma_{j0}$  for  $j=2,4,\dots,2N$  in the stratified porous structure region satisfies the water-wave dispersion relations given by

$$\omega^2 = g\gamma_{j0} \tanh \gamma_{j0} h_j, \quad (5.8a)$$

$$(S_1 + if_1) \omega^2 - g\gamma_{j0} \tanh \gamma_{j0} h_j = P_n \left[ (S_1 + if_1) \omega^2 \tanh \gamma_{j0} h_j - g\gamma_{j0} \right], \quad (5.8b)$$

where  $P_n = \left[ \left( 1 - \frac{\varepsilon_2 (S_1 + if_1)}{\varepsilon_1 (S_2 + if_2)} \right) \tanh \gamma_{2n} a_1 \right] / \left[ 1 - \frac{\varepsilon_2 (S_1 + if_1)}{\varepsilon_1 (S_2 + if_2)} \tanh^2 \gamma_{2n} a_1 \right]$ . In the case

of the submerged porous structure, the surface layer transform as free water region by considering the surface porosity  $\varepsilon_1 = 1$  and friction factor  $f_1 = 0$ . The dispersion relation for the submerged porous structure is given by

$$\omega^2 - g \gamma_{j0} \tanh \gamma_{j0} h_j = P_n \left[ \omega^2 \tanh \gamma_{j0} h_j - g \gamma_{j0} \right], \quad (5.8c)$$

where  $P_n = \left[ \left( 1 - \frac{\varepsilon_2}{(S_2 + if_2)} \right) \tanh \gamma_{2n} a_1 \right] / \left[ 1 - \frac{\varepsilon_2}{(S_2 + if_2)} \tanh^2 \gamma_{2n} a_1 \right]$ , which is similar

as in Losada et al. (1996) and Li et al. (2019). In the case of bottom rigid layers, the fluid flow near each rigid layer  $(h_{j+1} \leq y \leq h_j)$  for  $j = 1, 3, \dots, (2N + 1)$  and  $(h_j \leq y \leq h_{j+1})$  for  $j = 2, 4, \dots, 2N$  satisfies the zero-flow condition given by

$$\frac{\partial \phi_j(x, y)}{\partial x} = 0 \quad \text{on} \quad x = -b_j. \quad (5.9a)$$

The series of stratified porous structures are placed far away from the vertical wall. Hence, the no-flow condition due to the presence of vertical wall is given by

$$\frac{\partial \phi_j(x, y)}{\partial x} = 0 \quad \text{on} \quad x = -(b_{2N} + L). \quad (5.9b)$$

### 5.3 METHOD OF SOLUTION

The present study proposed the series of stratified porous structures placed far away from vertical, permeable and stepped walls as an effective energy trapping system. To reduce the complexity of the present solution approach, the closed-form solution using the eigenfunction method is preferred, which is applicable for solving the wave trapping due to series of porous structures. The set of equations for finding the wave reflection by the single three-layered structure is reported.

#### 5.3.1 Multiple porous structures away from the vertical wall

The velocity potentials in each of the open sea regions and structure occupied regions satisfying the governing equation and boundary conditions as in Section 5.2 are presented using the method of separation of variables. The velocity potentials in each of the open water region are given by

$$\phi_1(x, y) = \left\{ I_{10} e^{-ik_{10}(x+b_1)} + R_{10} e^{ik_{10}(x+b_1)} \right\} f_{10}(y) + \sum_{n=1}^{\infty} \left\{ R_{1n} e^{-\kappa_{1n}(x+b_1)} \right\} f_{1n}(y), \quad (5.10a)$$

for  $-b_1 \leq x \leq \infty, 0 \leq y \leq h_1$ ,

$$\phi_j(x, y) = \sum_{n=0}^{\infty} \left\{ A_{jn} e^{-ik_{jn}(x+b_{j-1})} + B_{jn} e^{ik_{jn}(x+b_j)} \right\} f_{jn}(y) \quad (5.10b)$$

for  $-b_j \leq x \leq -b_{j-1}, 0 \leq y \leq h_j, \quad j = 3, 5, \dots, 2N-1$ .

$$\begin{aligned} \phi_{2N+1}(x, y) = C_{(2N+1)0} & \left\{ e^{-ik_{(2N+1)0}(x+b_{2N})} + e^{ik_{(2N+1)0}(x+b_{2N}+2L)} \right\} f_{(2N+1)0}(y) \\ & + \sum_{n=1}^{\infty} C_{(2N+1)n} \left\{ e^{\kappa_{(2N+1)n}(x+b_{2N})} + e^{-\kappa_{(2N+1)n}(x+b_{2N}+2L)} \right\} f_{(2N+1)n}(y), \quad (5.10c) \end{aligned}$$

for  $-(b_{2N} + L) \leq x \leq -b_{2N}, 0 \leq y \leq h_{(2N+1)}$ .

The velocity potential for multiple stratified porous structure regions considering surface and bottom porous layers are given by

$$\phi_j^I(x, y) = \sum_{n=0}^{\infty} \left\{ A_{jn} e^{-ik_{jn}(x+b_{j-1})} + B_{jn} e^{ik_{jn}(x+b_j)} \right\} f_{jn}^I(y) \quad (5.10d)$$

for  $-b_j \leq x \leq -b_{j-1}, 0 \leq y \leq a_1, \quad j = 2, 4, \dots, 2N$ ,

$$\phi_j^{II}(x, y) = \sum_{n=0}^{\infty} \left\{ A_{jn} e^{-ik_{jn}(x+b_{j-1})} + B_{jn} e^{ik_{jn}(x+b_j)} \right\} f_{jn}^{II}(y) \quad (5.10e)$$

for  $-b_j \leq x \leq -b_{j-1}, a_1 \leq y \leq h_2, \quad j = 2, 4, \dots, 2N$ ,

where  $R_{1n}$ ,  $A_{jn}$ ,  $B_{jn}$  and  $C_{(2N+1)0}$  are unknowns to be determined. The eigenfunctions

$$\text{in the open water region are } f_{jn}(y) = \begin{cases} \cosh \gamma_{j0}(h_j - y) / \cosh \gamma_{j0} h_j & \text{for } n = 0, \\ \cos \gamma_{jn}(h_j - y) / \cos \gamma_{jn} h_j & \text{for } n = 1, 2, \dots, \end{cases} \quad \text{for}$$

$j = 1, 3, \dots, 2N+1$  and  $\gamma_{jn} = i\gamma_{jn}$  for  $n = 1, 2, \dots$ . The eigenfunctions for surface porous

$$\text{layer region are } f_{jn}^I(y) = \frac{\cosh \gamma_{jn}(h_j - y) - P_n \sinh \gamma_{jn}(h_j - y)}{\cosh \gamma_{jn} h_j - P_n \sinh \gamma_{jn} h_j}, \quad \text{for the bottom porous}$$

$$\text{layer region are } f_{jn}^{II}(y) = \frac{(S_1 + if_1)(1 - P_n \tanh \gamma_{jn} a_1) \cosh \gamma_{jn}(h_j - y)}{(S_2 + if_2)(\cosh \gamma_{jn} h_j - P_n \sinh \gamma_{jn} h_j)} \quad \text{for } j = 2, 4, \dots, 2N.$$

The eigenfunction  $f_{jn}(y)$  for  $j = 1, 3, \dots, 2N+1$  satisfy the orthogonal mode-coupling relation given by

$$\langle f_{jn}, f_{jm} \rangle_{j=1,3,\dots,(2N+1)} = \begin{cases} 0 & \text{for } m \neq n, \\ \Lambda_n & \text{for } m = n. \end{cases} \quad \text{and } \Lambda_n = \left\{ \frac{2\gamma_{jn} h_j + \sinh 2\gamma_{jn} h_j}{4\gamma_{jn} \cosh^2 \gamma_{jn} h_j} \right\} \quad (5.11a)$$

The orthogonal relation in the presence of the two-layered structure ( $h_j = a_1 + a_2$ ) is given by

$$\langle f_{jn}, f_{jm} \rangle_{j=1,3,\dots,(2N+1)} = \int_0^{h_j} f_{jn}(y) f_{jm}(y) dy = \int_0^{a_1} f_{jn}(y) f_{jm}(y) dy + \int_{a_1}^{h_j} f_{jn}(y) f_{jm}(y) dy. \quad (5.11b)$$

The orthogonal relation for the three-layered structure is similar as in Equation (5.11b) along with zero-flow condition for a rigid bottom layer ( $h_{j+1} \leq y \leq h_j$ ) for  $j = 1, 3, \dots, (2N + 1)$  and ( $h_j \leq y \leq h_{j+1}$ ) for  $j = 2, 4, \dots, 2N$  given by

$$\frac{\partial \phi_j(x, y)}{\partial x} = 0 \quad \text{on } x = b_j. \quad (5.11c)$$

The velocity potentials as in Equation (5.10a) – (5.10e) are substituted in the continuity of pressure and velocity as in Equation (5.4a,b) along with orthogonal relation as in Equation (5.11a) given by

$$\begin{aligned} \langle \phi_j(x, y), f_{jm}(y) \rangle &= \int_0^{h_j} \phi_j(x, y) f_{jm}(y) dy = \left\{ \int_0^{a_1} + \int_{a_1}^{h_j} \right\} \phi_j(x, y) f_{jm}(y) dy \\ &= (S_1 + if_1) \int_0^{a_1} \phi_{(j+1)}^I(x, y) f_{jm}(y) dy + (S_2 + if_2) \int_{a_1}^{h_j} \phi_{(j+1)}^{II}(x, y) f_{jm}(y) dy \end{aligned} \quad (5.12)$$

for  $m = 0, 1, 2, \dots$  and  $j = 1, 3, \dots, (2N - 1)$ ,

$$\begin{aligned} \langle \phi_{jx}(x, y), f_{jm}(y) \rangle &= \int_0^{h_j} \phi_{jx}(x, y) f_{jm}(y) dy = \left\{ \int_0^{a_1} + \int_{a_1}^{h_j} \right\} \phi_{jx}(x, y) f_{jm}(y) dy \\ &= \varepsilon_1 \int_0^{a_1} \phi_{(j+1)x}^I(x, y) f_{jm}(y) dy + \varepsilon_2 \int_{a_1}^{h_j} \phi_{(j+1)x}^{II}(x, y) f_{jm}(y) dy \end{aligned} \quad (5.13)$$

for  $m = 0, 1, 2, \dots$  and  $j = 1, 3, \dots, (2N - 1)$ ,

The velocity potentials as in Equation (5.10a) – (5.10e) are substituted in the continuity of pressure and velocity as in Equation (5.5a,b) along with orthogonal relation as in Equation (5.11a) given by

$$\begin{aligned}
 \langle \phi_{j+1}(x, y), f_{(j+1)m}(y) \rangle &= \int_0^{h_j} \phi_{j+1}(x, y) f_{(j+1)m}(y) dy = \left\{ \int_0^{a_1} + \int_{a_1}^{h_j} \right\} \phi_{j+1}(x, y) f_{(j+1)m}(y) dy \\
 &= (S_1 + if_1) \int_0^{a_1} \phi_j^I(x, y) f_{(j+1)m}(y) dy + (S_2 + if_2) \int_{a_1}^{h_j} \phi_j^{II}(x, y) f_{(j+1)m}(y) dy \\
 &\quad \text{for } m = 0, 1, 2, \dots \quad \text{and} \quad j = 2, 4, \dots, 2N,
 \end{aligned} \tag{5.14}$$

$$\begin{aligned}
 \langle \phi_{(j+1)x}(x, y), f_{(j+1)m}(y) \rangle &= \int_0^{h_j} \phi_{(j+1)x}(x, y) f_{(j+1)m}(y) dy = \left\{ \int_0^{a_1} + \int_{a_1}^{h_j} \right\} \phi_{(j+1)x}(x, y) f_{(j+1)m}(y) dy \\
 &= \varepsilon_1 \int_0^{a_1} \phi_{jx}^I(x, y) f_{(j+1)m}(y) dy + \varepsilon_2 \int_{a_1}^{h_j} \phi_{jx}^{II}(x, y) f_{(j+1)m}(y) dy \\
 &\quad \text{for } m = 0, 1, 2, \dots \quad \text{and} \quad j = 2, 4, \dots, 2N.
 \end{aligned} \tag{5.15}$$

In the case of the two-layer porous structure, structure depth is  $h_1 = h_2 = a_1 + a_2$ , for three-layer stratified porous structure  $h_1 = a_1 + a_2 + a_3$ . The system of series solutions as in Equation (5.12) - (5.15) for two-layered stratified porous structure, similarly, Equation (5.12) - (5.15) along with no-flow condition as in Equation (5.11c) for three-layered stratified porous structure are coined and truncated for a finite number  $M$  to obtain  $4j(M+1)$  linear equation system to obtain the  $4j(M+1)$  unknown coefficients (where  $j=1, 2, \dots$  is the number of stratified porous structures). The wave reflection due to multiple stratified porous structures are obtained as

$$K_r = \left| \frac{R_{10}}{I_{10}} \right| \tag{5.16}$$

### 5.3.2 Three-layered stratified porous structure away from the vertical wall

The three-layered stratified porous structure is considered to be having two porous layers and a rigid bottom layer. Thus, the rigid bottom layer replaces the natural and artificial seabed variations. The analytical solution as in Section 5.3.1 is adopted to examine the wave trapping phenomena by a single three-layered stratified porous structure. The velocity potentials in each of the regions are solved using the boundary conditions and method of separation of variables given in the form of



$$\phi_1(x, y) = \left\{ I_{10} e^{-ik_{10}(x+b_1)} + R_{10} e^{ik_{10}(x+b_1)} \right\} f_{10}(y) + \sum_{n=1}^{\infty} \left\{ R_{1n} e^{-\kappa_{1n}(x+b_1)} \right\} f_{1n}(y), \quad (5.17a)$$

for  $-b_1 \leq x \leq \infty, 0 \leq y \leq h_1,$

$$\phi_2^I(x, y) = \sum_{n=0}^{\infty} \left\{ A_{2n} e^{-ik_{2n}(x+b_1)} + B_{2n} e^{ik_{2n}(x+b_2)} \right\} f_{2n}^I(y) \quad (5.17b)$$

for  $-b_2 \leq x \leq -b_1, 0 \leq y \leq a_1,$

$$\phi_2^{II}(x, y) = \sum_{n=0}^{\infty} \left\{ A_{2n} e^{-ik_{2n}(x+b_1)} + B_{2n} e^{ik_{2n}(x+b_2)} \right\} f_{2n}^{II}(y) \quad (5.17c)$$

for  $-b_2 \leq x \leq -b_1, a_1 \leq y \leq a_2,$

$$\phi_3(x, y) = C_{30} \left\{ e^{-ik_{30}(x+b_2)} + e^{ik_{30}(x+b_2+2L)} \right\} f_{30}(y) + \sum_{n=1}^{\infty} C_{3n} \left\{ e^{\kappa_{3n}(x+b_2)} + e^{-\kappa_{3n}(x+b_2+2L)} \right\} f_{3n}(y), \quad (5.17d)$$

for  $-(b_2 + L) \leq x \leq -b_2, 0 \leq y \leq h_3.$

where  $f_{jn}(y)$  are the eigenfunctions in open sea and breakwater occupied regions is

$$\text{given in the form of } f_{jn}(y) = \begin{cases} \cosh \gamma_{jn}(h_j - y) / \cosh \gamma_{jn} h & \text{for } n = 0, \\ \cos \gamma_{jn}(h_j - y) / \cos \gamma_{jn} h & \text{for } n = 1, 2, \dots, \end{cases} \quad \text{for } j = 1, 3, \text{ in}$$

$$\text{the case of surface porous layer } f_{2n}^I(y) = \frac{\cosh \gamma_{2n}(h_2 - y) - P_n \sinh \gamma_{2n}(h_2 - y)}{\cosh \gamma_{2n} h_2 - P_n \sinh \gamma_{2n} h_2}, \text{ for}$$

$$\text{bottom porous layer } f_{2n}^{II}(y) = \frac{(S_1 + if_1)(1 - P_n \tanh \gamma_{2n} a_1) \cosh \gamma_{2n}(h_2 - y)}{(S_2 + if_2)(\cosh \gamma_{2n} h_2 - P_n \sinh \gamma_{2n} h_2)} \text{ and}$$

$$a_1 + a_2 = h_2.$$

The matching equations as in Equation (5.4) – (5.5), the no-flow condition due to bottom rigid layer as in Equation (5.9a) and orthogonal mode-coupling relation as Equation (5.11a) – (5.11c) are applied on the velocity potentials representing the seaward, leeward open sea regions and porous structure occupied region as in Equation (5.17a) – (5.17d) to coin the equation system given by

$$\left\{ I_{10} \delta_{nm} + R_{10} \right\} \int_0^{h_2} f_{10}(y) f_{1m}(y) dy + \sum_{n=1}^{\infty} R_{1n} \int_0^{h_2} f_{1n}(y) f_{1m}(y) dy =$$

$$\sum_{n=0}^{\infty} \left( A_{2n} + B_{2n} e^{-ik_{2n}d} \right) \left[ (S_1 + if_1) \int_0^{a_1} f_{2n}^I(y) f_{1m}(y) dy + (S_2 + if_2) \int_{a_1}^{a_2} f_{2n}^{II}(y) f_{1m}(y) dy \right], \quad (5.18a)$$

for  $m = 0, 1, 2, \dots$

$$-ik_{1n} \{I_{10}\delta_{nm} - R_{1n}\} \langle f_{1n}(y), f_{1m}(y) \rangle = \sum_{n=0}^{\infty} -ik_{2n} (A_{2n} - B_{2n}e^{-ik_{2n}d}) \left[ \varepsilon_1 \int_0^{a_1} f_{2n}^I(y) f_{1m}(y) dy + \varepsilon_2 \int_{a_1}^{a_2} f_{2n}^{II}(y) f_{1m}(y) dy \right], \quad (5.18b)$$

for  $m = 0, 1, 2, \dots$

$$\sum_{n=0}^{\infty} (A_{2n}e^{-ik_{2n}d} + B_{2n}) \left[ (S_1 + if_1) \int_0^{a_1} f_{2n}^I(y) f_{3m}(y) + (S_2 + if_2) \int_{a_1}^{a_2} f_{2n}^{II}(y) f_{3m}(y) \right]$$

$$= C_{30} (1 + e^{2ik_{30}L}) \int_0^{h_2} f_{30}(y) f_{30}(y) dy + \sum_{n=1}^{\infty} C_{3n} (1 + e^{-2k_{3n}L}) \int_0^{h_2} f_{3n}(y) f_{3m}(y) dy, \quad (5.18c)$$

for  $m = 0, 1, 2, \dots$

$$\sum_{n=0}^{\infty} -ik_{2n} (A_{2n}e^{-ik_{2n}d} - B_{2n}) \left[ \varepsilon_1 \int_0^{a_1} f_{2n}^I(y) f_{3m}(y) + \varepsilon_2 \int_{a_1}^{a_2} f_{2n}^{II}(y) f_{3m}(y) \right] \quad (5.18d)$$

$$= -ik_{3n} C_{3n} (1 - e^{-2k_{3n}L}) \langle f_{3n}(y), f_{3m}(y) \rangle \quad \text{for } m = 0, 1, 2, \dots$$

where  $\delta_{nm} = \begin{cases} 1 & \text{for } m = n = 0 \\ 0 & \text{for } m = n = 1, 2, \dots \end{cases}$  and  $d = -(b_2 - b_1)$ .

The system of linear equation as in Equation (5.18a) – (5.18d) is solved to find the reflection coefficient due to stratified porous structure given in the form of

$$K_r = \left| \frac{R_{10}}{I_{10}} \right|. \quad (5.19)$$

The system of equations as in Equation (5.18a) – (5.18d) can be used for two-layered fully-extended and submerged two-layered porous structures on considering the uniform water depth  $h_2 / h_1 = 1$  (for two-layered porous structure) and  $\varepsilon_1 = 1$ ,  $f_1 = 0$  (submerged structure).

### 5.3.3 Series of stratified structures away from the semi-infinite permeable wall

In the present subsection, the multiple stratified porous structures are placed far away from the semi-infinite permeable wall as in Figure 5.1(b). In this case, the leeward open sea region is fully occupied with a porous structure. Hence the velocity potential in the leeward porous structure region is given by

$$\phi_{2N}(x, y) = \sum_{n=0}^{\infty} C_{(2N)n} \left\{ e^{ik_{(2N)n}(x+b_{2N-1})} \right\} f_{(2N)n}(y), \quad \text{for } -\infty \leq x \leq -b_{2N-1}, 0 \leq y \leq h_{2N}. \quad (5.20)$$

where  $f_{jn}(y) = (\cosh \gamma_{j0}(h_j - y)) / (\cosh \gamma_{j0}h_j)$  for  $n = 0, 1, 2, \dots$  and  $j = 2N$ . The semi-infinite structure satisfies the dispersion relation given by

$$\omega^2 (S_3 + if_3) = g\gamma_{(2N)n} \tanh \gamma_{(2N)n} h_{2N} \quad (5.21)$$

The system of equations is obtained using the velocity potential, matching equations and mode-coupling relation as described in Section 5.3.1.

### 5.3.4 Series of stratified porous structures away from the stepped wall

In the case of stepped seawall, the multiple rigid steps are placed very near to the vertical wall as in Figure 5.1(c). It is assumed that each of the rigid steps consists of finite width and depth. Hence, there exists a velocity potential over each of the rigid step, which is similar to free spacing regions presented in Equation (5.10c). Hence, the continuity of pressure, velocity and zero-flow is considered at each of the rigid step given by

$$\phi_j(x, y) = \phi_{j+1}(x, y) \quad \text{and} \quad \frac{\partial \phi_j(x, y)}{\partial x} = \frac{\partial \phi_{j+1}(x, y)}{\partial x} \quad \text{on } x = -b_j, \quad (5.22a)$$

$$\frac{\partial \phi_j(x, y)}{\partial x} = 0 \quad \text{on } x = -b_j. \quad (5.22b)$$

The subscript  $j$  is dependent upon the number of rigid steps considered in the study.

### 5.3.5 Solution approach for finding the roots of the dispersion relation

In general, the root-finding process for the stratified porous structure is complicated due to the presence of imaginary values. The dispersion relation for the stratified porous structure is given by

$$(S_1 + if_1)\omega^2 - g\gamma_{jn} \tanh \gamma_{jn} h_j = P_n \left[ (S_1 + if_1)\omega^2 \tanh \gamma_{jn} h_j - g\gamma_{jn} \right], \quad \text{for } n = 0, 1, 2, \dots \quad (5.23a)$$

$$\text{where } P_n = \left[ \left( 1 - \frac{\varepsilon_2 (s_1 + if_1)}{\varepsilon_1 (s_2 + if_2)} \right) \tanh \gamma_{jn} a_1 \right] \left/ \left[ 1 - \frac{\varepsilon_2 (s_1 + if_1)}{\varepsilon_1 (s_2 + if_2)} \tanh^2 \gamma_{jn} a_1 \right] \right.$$

The dispersion relation for the porous structure is simplified in the form given by

$$(S_1 + if_1)\Delta - \Upsilon \tanh \beta\Upsilon = \varphi \left[ \Upsilon - (S_1 + if_1)\Delta \tanh \beta\Upsilon \right] \tanh \alpha\Upsilon, \quad (5.23b)$$

where  $\Delta = \frac{\omega^2 h_j}{g}$ ,  $\beta = \frac{a_2}{h_j}$ ,  $\alpha = \frac{a_1}{h_j}$ ,  $\Upsilon = \gamma_{jn} h_j$ ,  $\varphi = \frac{\varepsilon_2(S_1 + if_1)}{\varepsilon_1(S_2 + if_2)}$ . In the case of a single structure, the  $\varepsilon_1 = \varepsilon_2 = \varepsilon$ ,  $S_1 = S_2 = S$  and  $f_1 = f_2 = f$ . Hence, the stratified porous structure dispersion relation reduces to the complex porous structure dispersion relation given by

$$\omega^2 (S + if) = g \gamma_{jn} \tanh \gamma_{jn} h_j \quad (5.23c)$$

In the previous studies, numerous authors used various methods such as Newton-Raphson method, step approach method and contour plots (Sollit and Cross, 1972; Dalrymple et al., 1991; Yu and Chwang, 1994; Mendez and Losada, 2004; Liu et al., 2007) for finding multiple roots of the complex dispersion relation. In the present study, the Newton-Raphson method is used for finding the roots of the stratified porous structure dispersion relation and step approach technique as in Mendez and Losada (2004) is used for finding the initial values for fast convergence.

The wave force acting on the vertical wall  $K_{fw}$  is given by

$$K_{fw} = \frac{F_w}{2\rho g h_1 I_0}, \quad (5.24a)$$

$$\text{with } F_w = i\rho\omega \int_0^{h_j} \phi_{(2j+1)}(x, y) dy \quad \text{at } x = -\{(b_{2j} - b_1) + L\}, \text{ for } j = 1, 2, \dots, N \quad (5.24b)$$

where  $I_0$  is the amplitude of the incident wave potential considered to be unity.

## 5.4 RESULTS AND DISCUSSIONS

The life span of the structure can be improved by reducing the wave impact on the seaward structural interface with significant wave damping. The higher wave damping is possible with an increase in structural width or higher structural porosity. Hence, the stratification concept, considering high surface layer porosity and moderate bottom layer porosity performs well for the effective wave attenuation. The present study examines the wave trapping efficiency of multiple two-layered, three-layered and submerged two-layered porous structures in the presence of a vertical wall, stepped wall and permeable wall. The physical quantities such as wave reflection and fluid force experienced by the vertical rigid wall are reported on considering various ranges of porosity, friction factor, depth of each layer, angle of contact, free spacing, trapping

chamber, structural thickness and dimensionless wavelength. In general, high structural porosity shows the high wave transmission and maximal wave impact on the seawalls. Hence, most of the studies reported that high structural porosity with the leeward wall is a useful solution for the trapping of incident waves (Yu and Chwang, 1994; Liu et al., 2012). To achieve the moderate wave reflection and minimal wave force on the seawalls, a new type porous breakwater titled, the stratified porous structure is proposed and analysed using the matched eigenfunction expansion method. In the present study, the porous structure is divided into two/three layers, and the surface layer is considered to be of high porosity, the middle layer consists of moderate porosity and the bottom layer consists of zero porosity. The series of porous structures are placed far away from the vertical wall, stepped wall and permeable wall. A maximum number of four stratified porous structures are considered in the presence of various seawalls. In the case of two/three-layered porous structures, the bottom porous layer consisting of  $\varepsilon_2 = 0.5$  and  $f_2 = 1$  which is kept fixed throughout the study.

#### **5.4.1 Effect of the vertical wall with porous structures on wave trapping**

The evanescent wave modes are truncated for a finite number after achieving the convergence in wave reflection coefficient by multiple porous structures away from a vertical wall, stepped wall and permeable wall. Figure 5.2 shows the convergence study in  $K_r$  versus increase in evanescent wave modes  $M$  for multiple porous structures with a vertical wall, stepped wall and permeable wall. The convergence in  $K_r$  is achieved for the evanescent wave modes for  $M \geq 10$  upto four decimal places in the presence of the vertical wall, stepped wall and permeable wall.

##### **5.4.1.1 Validation with experimental results**

The efficiency of the present model is corroborated using a comparative study between present analytical results and results of notable authors for specific structures. Figure 5.3(a,b) shows the comparative study between the present study analytical results and experimental results of Dattatri et al. (1978) in Figure 5.3(a), and Twu and Chieu (2000) in Figure 5.3(b). Dattatri et al. (1978) reported the wave transmission  $K_t$  on conducting a series of experiments considering various shapes of permeable and impermeable structures. In addition, Twu and Chieu (2000) examined the scattering performance of

a vertically stratified porous structure using a set of experiments and validated using analytical results. The wave transmission  $K_t$  as in Dattatri et al. (1978) and energy damping  $K_d$  as in Twu and Chieu (2000) are computed and compared. The comparison plots show a reasonable agreement between the present study analytical results and experimental results available in the literature.

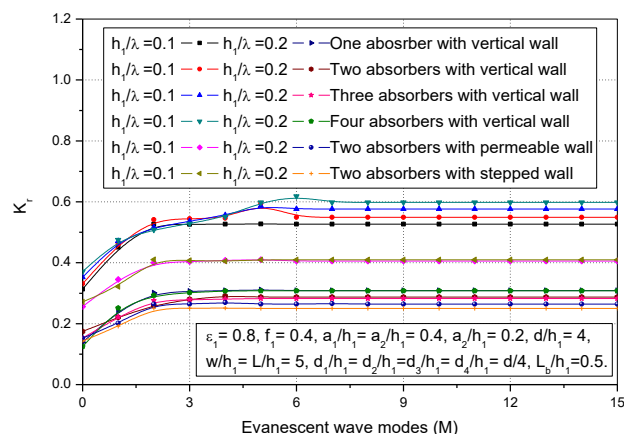


Figure 5.2: Convergence study in wave reflection coefficient  $K_r$ , due to multiple structures away from a vertical wall, permeable wall and stepped wall considering  $h_1 / \lambda = 0.1$  and  $h_1 / \lambda = 0.2$ .

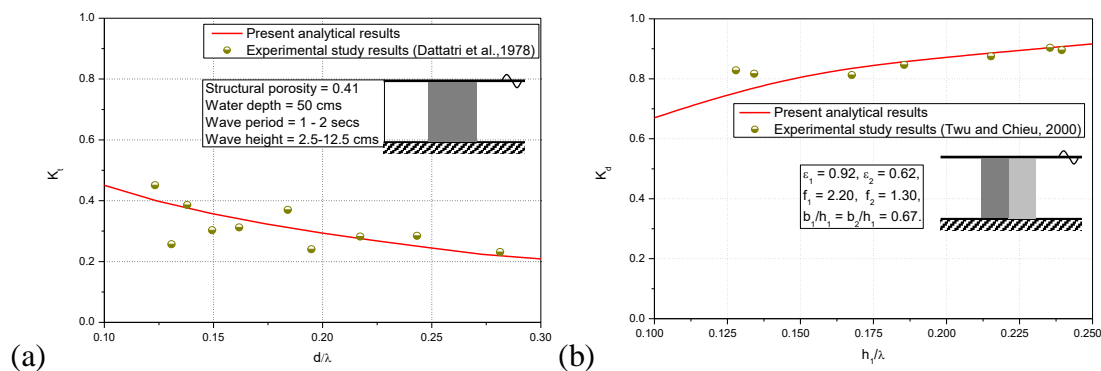


Figure 5.3: Comparative study between the present study analytical results and previous experimental results of (a) Dattatri et al. (1978) and (b) Twu and Chieu (2000).

The effect of the vertical wall with a stratified porous structure is examined with/without trapping chamber in Figure 5.4(a,b). As a special case, the single-layer porous structure is examined on considering the uniform porosity and friction factor and compared with the Mallayachari and Sundar (1994), Zhu and Chwang (2001). The present analytical results are observed to be well-agreed with the numerical/analytical results of Mallayachari and Sundar (1994), Zhu and Chwang (2001). Thereafter, the multi-layered concept is applied for the structural configurations proposed by

Mallayachari and Sundar (1994), Zhu and Chwang (2001). A significant variation in  $K_r$  is identified between the single-layer porous structure and double-layer porous structure. The stratified porous structures show minimal  $K_r$  as compared with the conventional porous structures in the presence and absence of the trapping chamber. However, a rigorous study is required to propose an ideal structural configuration for better wave trapping, which is well discussed in further sub-sections.

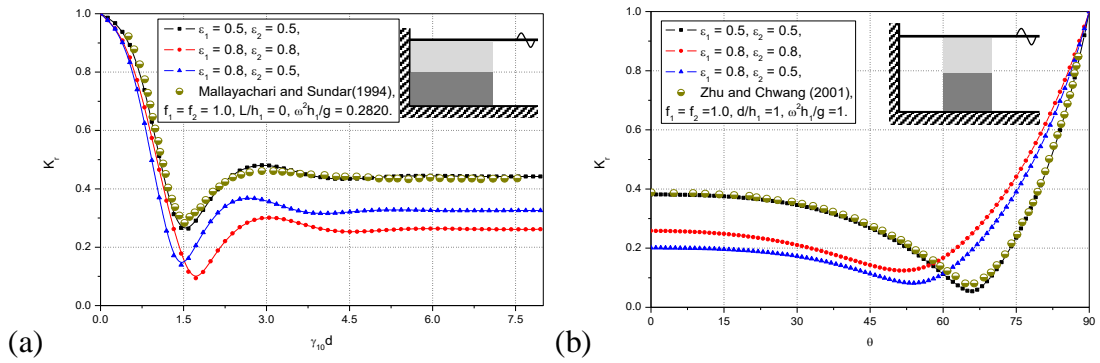


Figure 5.4: The  $K_r$  versus (a) dimensionless width  $\gamma_{10}d$  and (b) angle of contact  $\theta$  considering horizontal variable porosity  $\varepsilon_1$  for  $d/h_1 = 1$  and  $\omega^2 h_1/g = 1$ .

#### 5.4.1.2 Effect of trapping chamber spacing on wave reflection

In Figure 5.5(a-d), the reflection coefficient  $K_r$  versus trapping chamber spacing  $L/h_1$  is discussed for single porous structure considering various ranges of structure porosity  $\varepsilon_1, f_1$  in Figure 5.5(a), layer depth  $a_1/h_1, a_2/h_1$  in Figure 5.5(b), angle of contact  $\theta$  in Figure 5.5(c) and structure thickness  $d/h_1$  in Figure 5.5(d). The surge in  $L/h_1$  shows the harmonic peaks and troughs in  $K_r$  for all the combinations of  $\varepsilon_1, f_1, a_1/h_1, a_2/h_1, \theta$  and  $d/h_1$ . The difference between each of the harmonic peak and trough is observed to be reduced for higher surface layer porosity, angle of contact and structure thickness. The layer depth shows minimal impact on  $K_r$  due to the presence of a vertical wall, which reflects the total transmitted wave energy from the porous structure. Almost, uniform values of  $K_r$  is obtained for  $\theta = 60^\circ$  due to the formation of standing waves, which is also called as critical angle of incidence. Moreover, the enhance in  $d/h_1$  shows the reduction pattern in  $K_r$  due to the enhance in wave decay by the stratified porous structure. Particularly, for  $d/h_1 = 5$ , the  $K_r$  shows very minimal harmonic peaks as

compared with other  $d/h_1$  values. In fact,  $d/h_1 = 2$  also shows the minimal values of  $K_r$  at each of the harmonic trough, which is almost equal/minimal as in  $d/h_1 = 5$ . As a comparison,  $d/h_1 = 5$  requires massive capital cost as compared with  $d/h_1 = 2$  due to the higher structure thickness. However, the performance of  $d/h_1 = 2$  and  $d/h_1 = 5$  is almost uniform at each of the harmonic troughs, which is essential in the design of the trapping chamber for effective clapotis formation. Finally, the minimum value of  $K_r$  for optimal values of other physical parameters is also considered for effective wave trapping (Vijay and Sahoo, 2019).

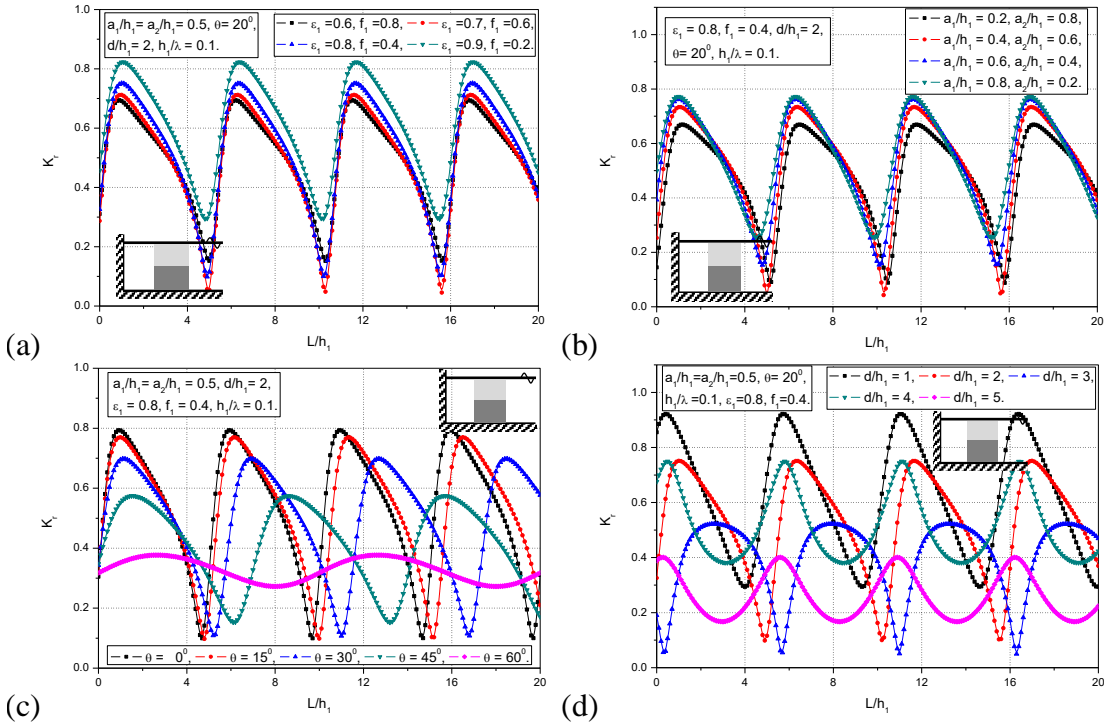


Figure 5.5: The  $K_r$  versus  $L/h_1$  for various values of (a)  $\varepsilon_1, f_1$ , (b)  $a_1/h_1, a_2/h_1$ , (c)  $\theta$  and (d)  $d/h_1$  considering  $h_1/\lambda = 0.1$  and  $N = 1$ .

In Figure 5.6(a-d), the fluid force experienced by vertical wall  $K_{fw}$  versus  $L/h_1$  is reported for single porous structure considering various ranges of structural porosity, friction factor  $\varepsilon_1, f_1$  in Figure 5.6(a), layer depth  $a_1/h_1, a_2/h_1$  in Figure 5.6(b), angle of contact  $\theta$  in Figure 5.6(c) and structural thickness  $d/h_1$  in Figure 5.6(d). The surge in structural porosity and layer depth enhances the  $K_{fw}$  (as compared with  $K_r$ ) due to more pore spaces, which allows more waves to pass through the structure. Similarly,



the surge in the angle of contact and breakwater thickness dissipate the incoming waves and reduces the wave impact on the vertical wall. However, the harmonic troughs (where the minimal  $K_{fw}$  appears) in each test suggest the effective trapping chamber. But, the comparison between  $K_r$  (Figure 5.5)  $K_{fw}$  (Figure 5.6) shows the opposite trend in wave transformation. The harmonic crest in  $K_r$  results a harmonic trough in  $K_{fw}$  for lower values of structural thickness and angle of contact, which suggests that the minimal structural thickness can control either  $K_r$  or  $K_{fw}$ . However, the surge in wave decay can reduce the harmonic crests and troughs in  $K_r$  or  $K_{fw}$  for particular values of structural thickness and angle of contact (Ramakrishnan, 2011). To strengthen the wave decay, the oblique wave contact within  $30^\circ \leq \theta \leq 60^\circ$  is useful, which can reduce the  $K_r$  or  $K_{fw}$  with minimal structural thickness.

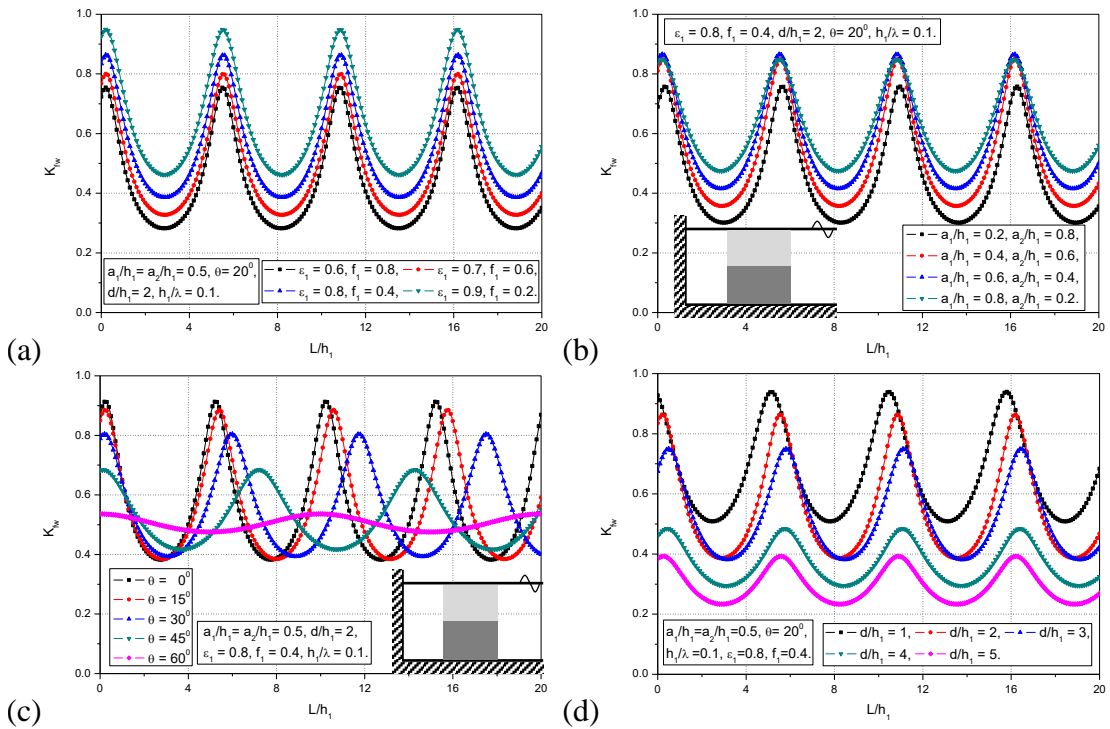


Figure 5.6: The  $K_{fw}$  versus  $L/h_1$  for various values of (a)  $\epsilon_1, f_1$ , (b)  $a_1/h_1, a_2/h_1$ , (c)  $\theta$  and (d)  $d/h_1$  considering  $h_1/\lambda = 0.1$  and  $N = 1$ .

### 5.4.1.3 Effect of confined spacing on wave trapping

In the present case, two porous structures are placed far away from the vertical wall. The effect of the confined region  $w/h_1$  available between the two porous structures is

varied to perform the variation of  $K_r$  as in Figure 5.7(a-d) and fluid force on the vertical wall  $K_{fw}$  as in Figure 5.8(a-d) considering various values of (a) porosity, friction factor (b) layer depth (c) angle of contact and (d) structural width. The higher values of breakwater porosity enhance the harmonic peaks and troughs in  $K_r$  (Figure 5.7a) and cause more wave impact on the vertical wall (Figure 5.8a). In particular,  $\varepsilon_1 = 0.9$  and  $f_1 = 0.2$  shows higher fluid oscillations between the two porous structures due to the higher porosity and very minimal friction factor, which causes more oscillations and clapotis due to multiple interactions of incident waves. As a result of high structural porosity, the corresponding  $K_{fw}$  (Figure 5.8a) is observed to be high for  $\varepsilon_1 = 0.9$  and  $f_1 = 0.2$  due to the minimal wave absorption by the breakwater. The surge in layer depth  $a_1/h_1$  shows a slight reduction in  $K_r$  (Figure 5.7b) at each of the harmonic crest and trough. But there is a significant increase in  $K_{fw}$  (Figure 5.8b) due to the change in cumulative porosity. The increase in surface layer depth enhances the volume of pore spaces and allows the more waves to pass through the structure, which results in higher  $K_{fw}$  for higher values of  $a_1/h_1 = 0.8$  as compared to lower values of  $a_1/h_1 = 0.2$ .

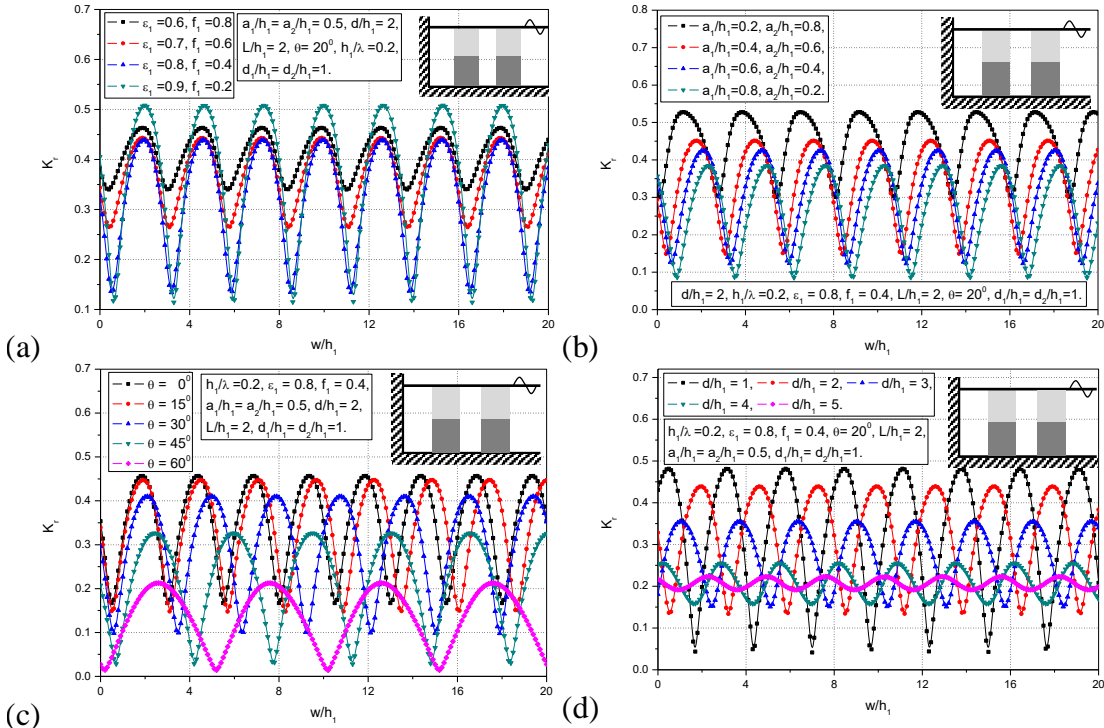


Figure 5.7: The  $K_r$  versus  $w/h_1$  for various values of (a)  $\varepsilon_1, f_1$ , (b)  $a_1/h_1, a_2/h_1$ , (c)  $\theta$  and (d)  $d/h_1$  considering  $h_1/\lambda = 0.2$  and  $N = 2$ .

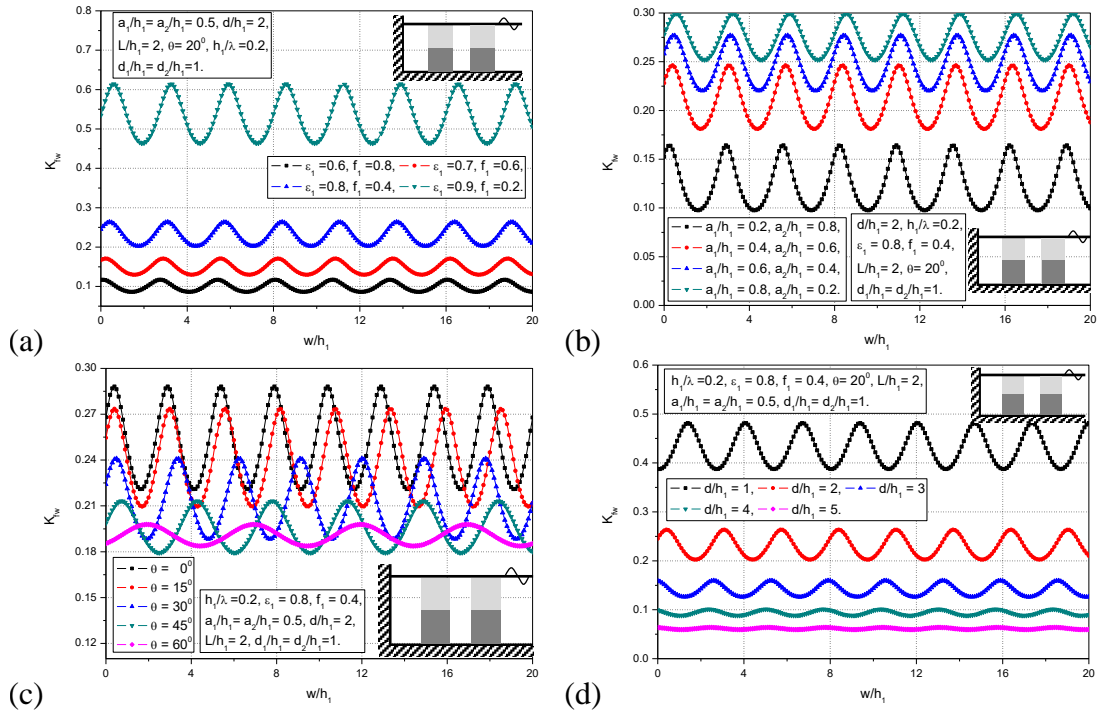


Figure 5.8: The  $K_{fw}$  versus  $w/h_1$  for various values of (a)  $\epsilon_1, f_1$ , (b)  $a_1/h_1, a_2/h_1$ , (c)  $\theta$  and (d)  $d/h_1$  considering  $h_1/\lambda = 0.2$  and  $N = 2$ .

The enhance in the angle of contact  $\theta$  reduces the harmonic peaks and troughs in  $K_r$  (Figure 5.7c) and  $K_{fw}$  (Figure 5.8c) due to the formation of standing waves. The minimal structural thickness depicts the higher fluid oscillations in  $K_r$  (Figure 5.7d) and  $K_{fw}$  (Figure 5.8d) for variable free spacing  $w/h_1$  due to minimal energy damping. Moreover, higher structural thickness shows minimal fluid oscillations due to the higher energy absorption. However, the gradual decrease in  $K_{fw}$  is obtained for various values of breakwater thickness. The structural width  $d/h_1$  shows very minimal impact on  $K_{fw}$  within  $3 \leq d/h_1 \leq 5$ . Which suggests that the  $d/h_1 = 3$  is suitable to control the incident wavelength of  $h_1/\lambda = 0.2$  using double stratified porous structures placed away from the vertical wall.

#### 5.4.1.4 Effect of structural thickness on wave trapping

The trapping of incident waves is analysed for three porous structures having double porous layers placed far away from the vertical wall. The wave reflection  $K_r$  versus  $d/h_1$  is presented for variable layer depth  $a_1/h_1$  and trapping chamber  $L/h_1$  in Figure

5.9(a,b). The increase in layer depth reduces  $K_r$  due to enhance in wave decay and all the combinations of  $a_1/h_1$  shows almost zero  $K_r$  at  $d/h_1 = 2.7$  which is termed as effective structural width. Thereafter, uniform values in  $K_r$  is noted with the minimal oscillatory pattern. However, the gradual decrease in  $K_r$  is obtained for a gradual increase in  $a_1/h_1$  due to the enhance in pore spaces in the surface porous layer. On the other hand, the enhance in trapping chamber  $L/h_1$  shows the high oscillations in  $K_r$  for variable structural thickness within  $0.01 \leq d/h_1 \leq 8$ . Moreover,  $d/h_1 = 8$  is observed to be first converging point and, the full convergence in  $K_r$  for all the values of  $L/h_1$  is observed at  $d/h_1 = 11$ . This suggests that the structural thickness  $d/h_1 = 11$  exceeding the incident wavelength  $h_1/\lambda = 0.1$  (where  $d/\lambda = 1.1$ ) and the present breakwater can be referred as semi-infinite structure, which absorbs the whole incident waves and allows very minimal wave transmission. Hence, the role of the trapping chamber  $L/h_1$  is very minimal on the wave reflection in the case of a semi-infinite porous structure.

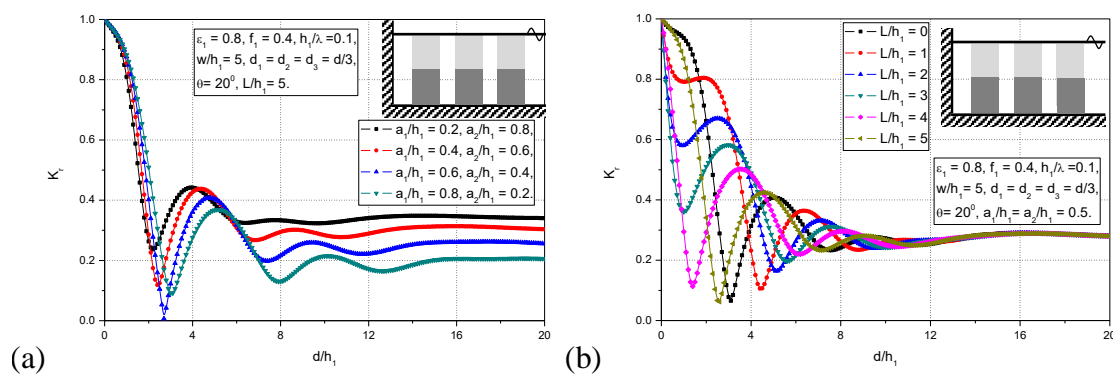


Figure 5.9: The  $K_r$  versus  $d/h_1$  for various values of (a)  $a_1/h_1, a_2/h_1$  and (b)  $L/h_1$  considering  $h_1/\lambda = 0.1$  and  $N = 3$ .

#### 5.4.1.5 Effect of angle of contact on wave trapping

The wave reflection  $K_r$  versus  $\theta$  due to four stratified porous structures consisting of two-porous layers placed away from the vertical wall is presented considering variable trapping chamber and structural thickness with (a)  $d/h_1 = 2$  (Figure 5.10a) and (b)  $d/h_1 = 4$  (Figure 5.10b). In the case of minimal structural thickness  $d/h_1 = 2$ , an

oscillating pattern in  $K_r$  is obtained and  $d/h_1 = 4$  shows a considerable decrease in  $K_r$  with the increase in  $L/h_1$ . However, in the present case two critical angles are obtained in  $K_r$  for irrespective values of the trapping chamber. However, the primary critical angle (Figure 5.10b) is observed to be moving towards the left and secondary critical angle is observed at  $\theta = 70^\circ$  due to the dominance of standing waves.

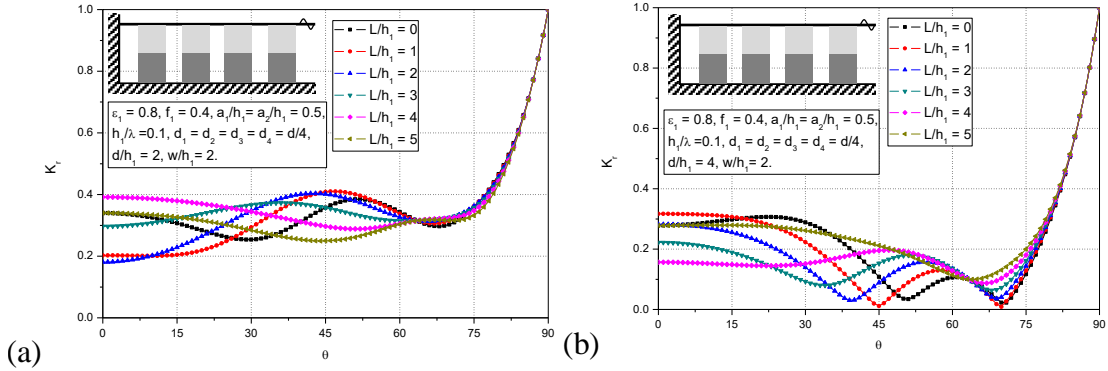


Figure 5.10: The  $K_r$  versus  $\theta$  for various values of  $L/h_1$ , (a)  $d/h_1 = 2$  and (b)  $d/h_1 = 4$  considering  $h_1/\lambda = 0.1$  and  $N = 4$ .

#### 5.4.1.6 Comparative study between the multiple porous structures of uniform width

The comparative study is performed between the single and multiple porous structures on considering the uniform thickness. The single porous structure thickness  $d/h_1$  is uniformly separated into multiple structures to study the effect of free spacing on wave trapping. Figure 5.11(a-d) shows the variation of wave reflection  $K_r$  and fluid force experienced by a vertical wall  $K_{fw}$  considering  $h_1/\lambda = 0.1$  (Figure 5.11a,b) and  $h_1/\lambda = 0.2$  (Figure 5.11c,d). The increase in the number of structures shows a very minimal role in reducing the  $K_r$  (Figure 5.11a) and  $K_{fw}$  (Figure 5.11b) due to higher wavelength and minimal structural thickness. However, in the case of  $h_1/\lambda = 0.2$ , the increase in the number of structures shows a significant enhancement in  $K_r$  and considerable reduction in  $K_{fw}$  at each of the harmonic crest and trough due to the constructive and destructive interferences and cushion effect (incident wave decay in the free spacing between the structures). The study suggests that the cushion effect plays a negligible role in the case of higher wavelength  $h_1/\lambda = 0.1$  (Figure 5.11a,b)

and effective role in the case of moderate wavelength  $h_1 / \lambda = 0.2$  (Figure 5.11c,d) for fixed structural thickness.

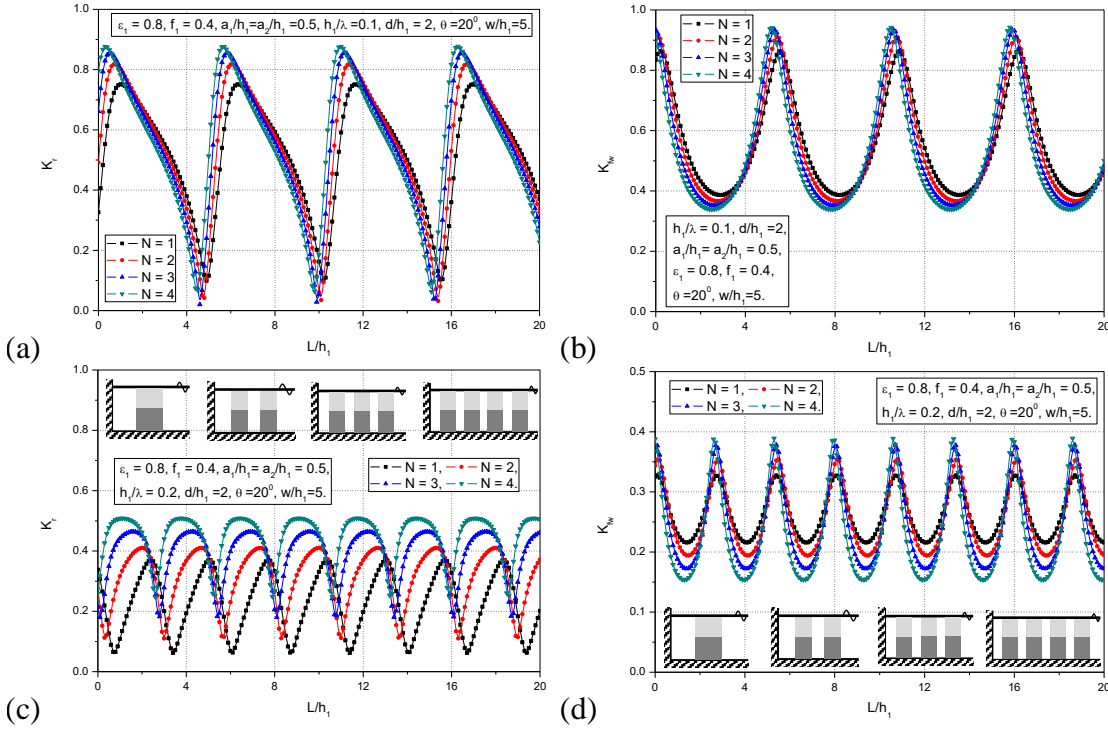


Figure 5.11: Comparative study of (a,c)  $K_r$  and (b,d)  $K_{fw}$  versus  $L/h_1$  for single and multiple structures with uniform structural width considering (a,b)  $h_1 / \lambda = 0.1$  and (c,d)  $h_1 / \lambda = 0.2$ .

Similarly, in Figure 5.12(a-d), the  $K_r$  (Figure 5.12a,c) and  $K_{fw}$  (Figure 5.12b,d) are presented considering variable thickness (adding the number of porous structures  $d_j / h_1 = 1$  for  $j=1,2,3,4$  of identical thickness). The harmonic crests and troughs are observed to be reducing with enhance in the number of structures due to the increase in wave decay and cushion effect (Somervell et al., 2017) in the multiple confined regions. The  $h_1 / \lambda = 0.1$  shows minimal oscillations in  $K_r$  (Figure 5.12a) and  $K_{fw}$  (Figure 5.12b) as compared with  $h_1 / \lambda = 0.2$  due to change in structural width. The variation between each of harmonic crest and trough is observed to be high for  $h_1 / \lambda = 0.1$  as compared with  $h_1 / \lambda = 0.2$ . In addition,  $h_1 / \lambda = 0.2$  widens the oscillations and reduces the variation between each of harmonic crest and trough. Almost uniform values of  $K_r$  (Figure 5.12c) and  $K_{fw}$  (Figure 5.12d) are obtained for three and four structures having two horizontal porous layers. The uniform values in  $K_r$  and  $K_{fw}$  are obtained due to

enhance in wave decay and cushion effect by the addition of each porous structure. (Liu et al., 2016; Vijay et al., 2020).

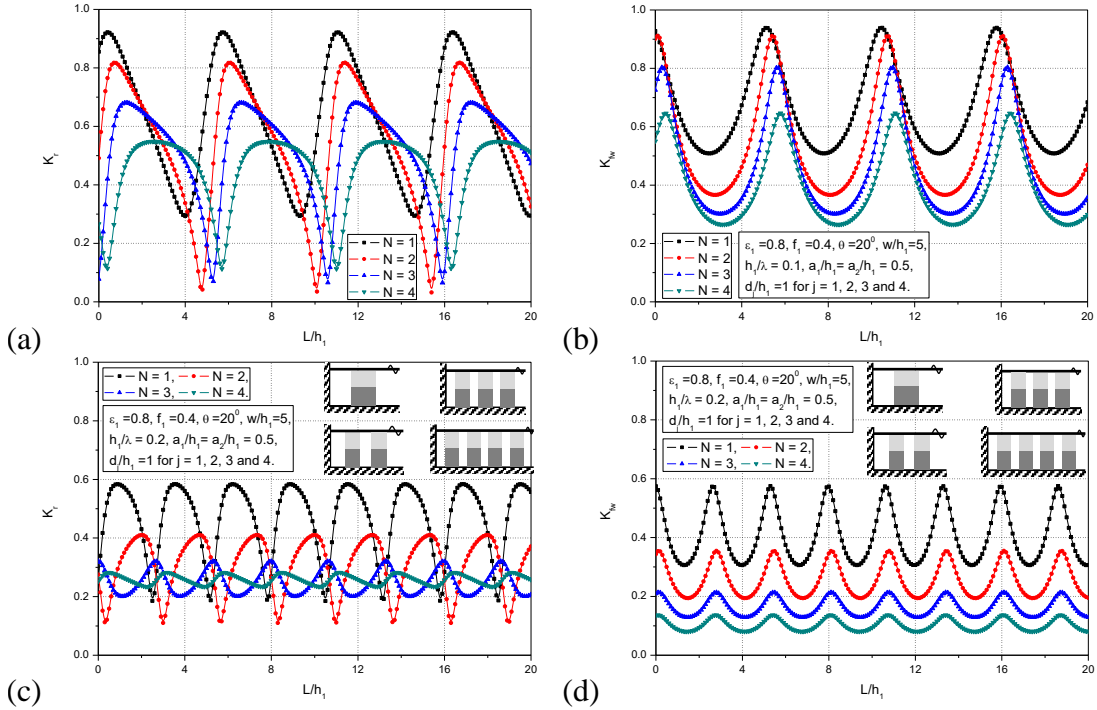


Figure 5.12: Comparative study of (a,c)  $K_r$  and (b,d)  $K_{fw}$  versus  $L/h_1$  for single and multiple structures with variable structural width considering (a,b)  $h_1/\lambda = 0.1$  and (c,d)  $h_1/\lambda = 0.2$ .

#### 5.4.1.7 Effect of bottom rigid layer on wave trapping

The wave motion over bottom rigid objects of various shapes and various positions (Manisha et al., 2019) is well reported in the literature, which is useful in regulating the deposition of sand (Kaligatla et al., 2017; Kaligatla et al., 2019). Moreover, uniform seabed is difficult to locate in the actual field. In the present study, the wave motion through two-layered porous structures placed on the rigid layer away from the various walls is studied. The porous structure is separated into two porous layers (surface and bottom layer) and a rigid bottom layer. The  $K_r$  due to the variation of the bottom rigid layer is presented in Figure 5.13(a-b) considering  $h_1/\lambda = 0.1$  (Figure 5.13a) and  $h_1/\lambda = 0.2$  (Figure 5.13b). The increase in bottom rigid layer height  $a_3/h_1$  reduces the two porous layers height due to fixed structural depth  $a_1 + a_2 + a_3 = h_1$ . The  $K_r$  is observed to be increasing with enhance in the bottom rigid layer height. The variation

between the two-layer  $a_3/h_1 = 0$  and three-layer structure  $a_3/h_1 = 0.1$  is evident in the analysis of stratified porous structures. The effective structural width is identified at  $d/h_1 = 2.2$  for  $h_1/\lambda = 0.1$  (location of almost zero wave reflection/wave trapping). In fact, the  $h_1/\lambda = 0.2$  also shows a similar trend as in  $h_1/\lambda = 0.1$ , but the surge in  $a_3/h_1$  shows the gradual increase in  $K_r$  due to reduction in wavelength. However, it is clear that the rigid bottom layer has more impact for  $h_1/\lambda = 0.2$  as compared with  $h_1/\lambda = 0.1$ . It is also observed that the consistency value of  $K_r$  is observed for variable structural thickness in the case of  $d/h_1 \geq 10$  for  $h_1/\lambda = 0.1$  and  $d/h_1 \geq 5$  for  $h_1/\lambda = 0.2$ . This is the most common phenomenon in the vicinity of wave-induced flow through porous structures. The theory behind the consistent values in  $K_r$  is that, if the structural thickness is exceeded the incident wavelength, then the porous structure will behave as a semi-infinite structure.

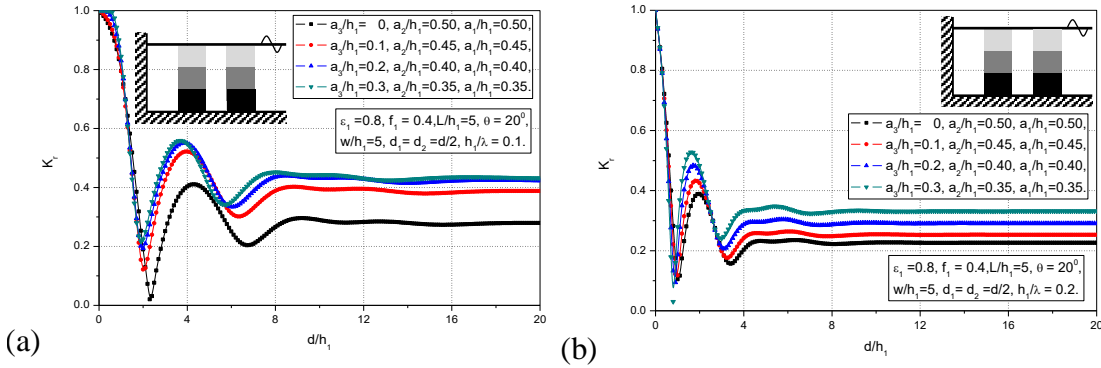


Figure 5.13: The  $K_r$  versus  $d/h_1$  for various values of  $a_1/h_1, a_2/h_1, a_3/h_1$  considering (a)  $h_1/\lambda = 0.1$ , (b)  $h_1/\lambda = 0.2$  and  $N = 2$ .

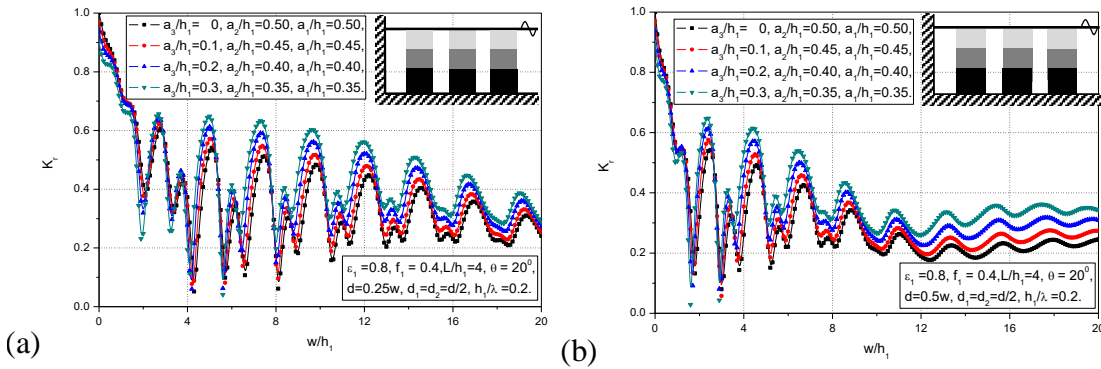


Figure 5.14: The  $K_r$  versus  $w/h_1$  for various values of  $a_1/h_1, a_2/h_1, a_3/h_1$  considering (a)  $d = 0.25w$ , (b)  $d = 0.5w$  and  $N = 3$ .



The  $K_r$  due to three porous structures having three-layers is presented for variable bottom rigid layer height in Figure 5.14(a-b). The porous structure thickness is considered to be variable such as  $d = 0.25w$  (Figure 5.14a) and  $d = 0.5w$  (Figure 5.14b). Thus, the increase in  $w/h_1$  enhances the structural thickness  $d/h_1$ , which reduces the wave impact on shoreward regions. The  $K_r$  is observed to be reducing on increasing  $w/h_1$  in terms of harmonic/ sub-harmonic peaks and troughs. The harmonic peaks are developed due to the fluid oscillations within the confined regions and  $K_r$  reduce for higher  $w/h_1$  due to the enhance in wave damping. The cushion effect may be dominant in the present structural configuration due to multiple confined/free-water regions. The harmonic peaks and troughs are observed to be minimal for higher structural width  $d = 0.5w$  as compared with minimal structural width  $d = 0.25w$ . Moreover, the increase in bottom rigid layer height  $a_3/h_1$  enhances the  $K_r$  due to zero-flow condition applied at each of the rigid interfaces. The study strongly suggests that the harmonic troughs (which are treated as effective wave trapping points) are evident in the design of offshore breakwaters for the effective life span of the structure.

#### 5.4.1.8 Comparative study between the multiple porous structures of variable width

A comparative study is performed between the four structural configurations such as breakwater with moderate porosity (Configuration C<sub>1</sub>), breakwater with higher porosity (Configuration C<sub>2</sub>), two-layered porous structure (Configuration C<sub>3</sub>) and three-layered porous structure (Configuration C<sub>4</sub>) as in Table 5.1.

Table 5.1: Various types of structural configurations for comparative study.

Model name	Surface porous layer		Middle porous layer		Rigid layer
	$\varepsilon_1$	$f_1$	$\varepsilon_2$	$f_2$	$a_3/h_1$
Configuration C <sub>1</sub>	0.5	1.0	0.5	1.0	0
Configuration C <sub>2</sub>	0.8	0.4	0.8	0.4	0
Configuration C <sub>3</sub>	0.5	1.0	0.8	0.4	0
Configuration C <sub>4</sub>	0.5	1.0	0.8	0.4	0.2

In Figure 5.15(a-d), the wave reflection  $K_r$  due to one structure (Figure 5.15a), two structures (Figure 5.15b), three structures (Figure 5.15c) and four structures (Figure

5.15d) having different structural configurations as in Table 1 are analysed. In the case of the single porous structure (Figure 5.15a), the configurations C<sub>1</sub>, C<sub>2</sub>, C<sub>3</sub> and C<sub>4</sub> show almost consistent harmonic peaks and troughs. On adding the second structure (Figure 5.15b), the significant reduction in  $K_r$  is achieved as compared with a single structure, which is due to the damping effect of wave-induced flow through permeable structures and cushion effect due to the presence of confined region. In the case of a single porous structure, the variation in  $K_r$  for four configurations is observed at each of the harmonic peaks and troughs. But, in the case of two porous structures (Figure 5.15b), the variation in  $K_r$  between the four configurations is observed to be little high as compared with a single structure (Figure 5.15a). In addition, the three (Figure 5.15c) and four structures (Figure 5.15d) shows minimum values of  $K_r$  and minor harmonic peaks and troughs as compared with the one and two porous structures due to the combined effect of wave damping and wave trapping in the multiple confined regions. However, in the case of three/four porous structures (Figure 5.15c,d), the configuration C<sub>1</sub> shows almost consistent  $K_r$  due to the destructive interferences and configuration C<sub>2</sub> shows the very high variation in  $K_r$  between the harmonic peaks and troughs due to the free fluid oscillation in the presence of high porosity. However, the Configuration C<sub>3</sub> (Figure 5.15c) and C<sub>4</sub> (Figure 5.15d) present the moderate values in  $K_r$ , which vary within C<sub>1</sub> and C<sub>2</sub> in an oscillatory manner. The Configuration C<sub>4</sub> shows little high values of  $K_r$  as compared with C<sub>3</sub> due to the presence of rigid bottom layer, which helps in on wave trapping and reduces the fluid force on the vertical wall.

On the other hand, in Figure 5.16(a-d), the wave force on a vertical wall  $K_{fw}$  in the presence of one structure (Figure 5.16a), two structures (Figure 5.16b), three structures (Figure 5.16c), and four structures (Figure 5.16d) considering various configurations as in Table 1 are analysed. An opposite trend is observed in  $K_{fw}$  as compared with  $K_r$  for all the combinations and configurations discussed above. The configuration C<sub>1</sub> shows the minimal values of  $K_{fw}$  with maximum values of  $K_r$  and configuration C<sub>2</sub> shows the maximum values of  $K_{fw}$  with minimum values of  $K_r$ . However, the stratified porous structure is able to distribute the incident wave energy in the form of  $K_r$  and

$K_{fw}$ , which is observed to be varying (configurations  $C_3$  and  $C_4$ ) within the configuration  $C_1$  (structure of moderate porosity) and  $C_2$  (structure of high porosity).

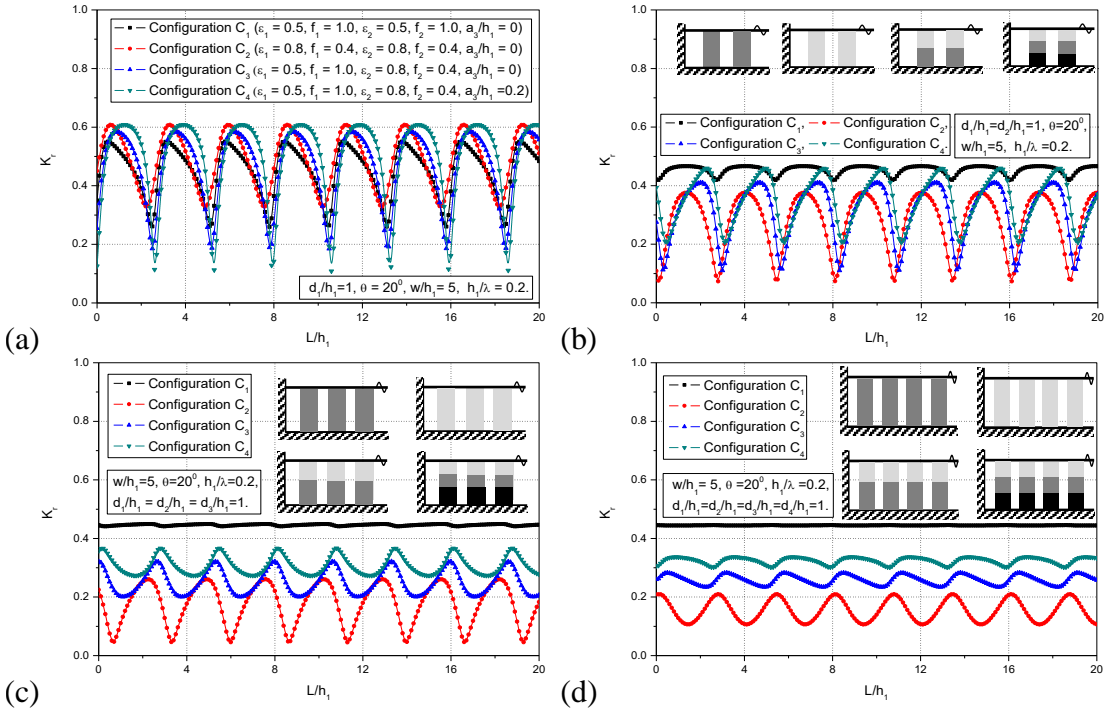


Figure 5.15: Comparative study of  $K_r$  due to various structural configurations considering (a)  $N=1$  (b)  $N=2$  (c)  $N=3$  and (d)  $N=4$ .

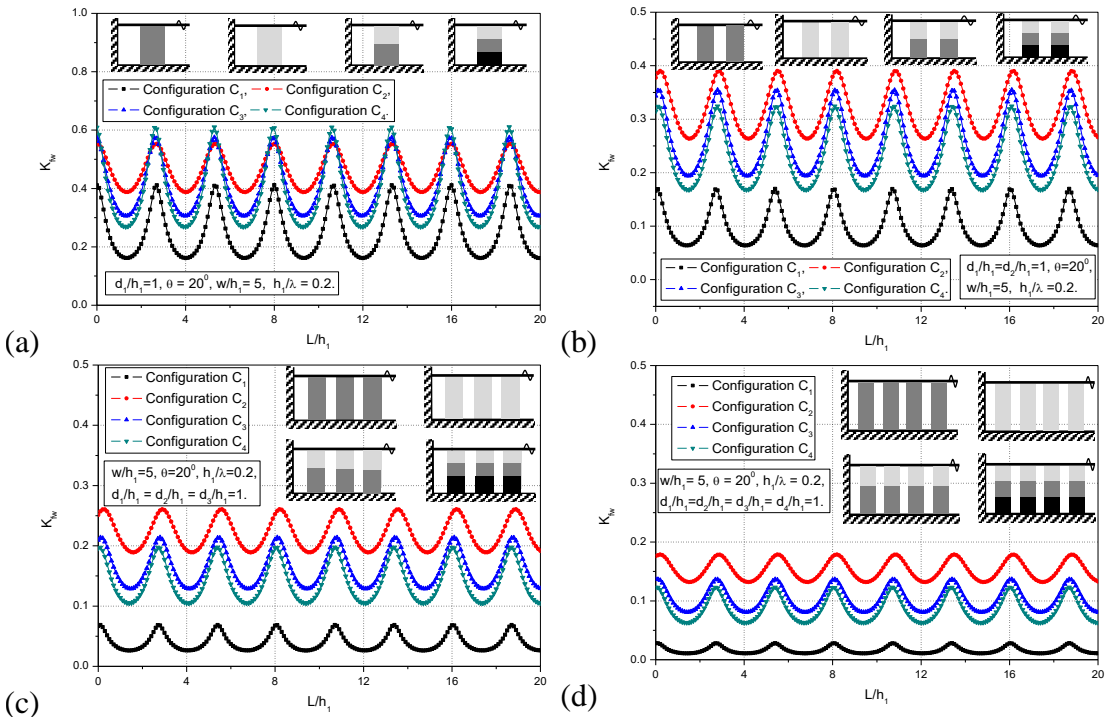


Figure 5.16: Comparative study of  $K_{fw}$  due to various structural configurations considering (a)  $N=1$  (b)  $N=2$  (c)  $N=3$  and (d)  $N=4$ .

The study suggests that, the ideal porous structure must perform minimal values of wave reflection, the fluid force on the wall for a better life span of the breakwater. Hence, the minimal  $K_r$  and  $K_{fv}$  is possible with stratified structures and series of stratified structures shows the better values in wave trapping as compared with single structure due to the effective wave trapping in the multiple confined free-water regions.

#### 5.4.1.9 Effect of submerged structures on wave trapping

In the present case, a submerged porous structure is placed on a rigid layer and kept far away from the vertical wall. The wave reflection  $K_r$  due to two submerged structures with the vertical wall is reported in Figure 5.17(a-b) on changing each layer depth (Figure 5.17a) and angle of incidence (Figure 5.17b). The  $K_r$  is observed to be high for lower values of  $d/h_1$  and the full-wave reflection  $K_r = 1$  is obtained due to the presence of a vertical wall. However, increasing the  $d/h_1$  shows a sharp reduction of  $K_r$  in an oscillatory manner. Since the structures are deeply submerged, there exists a harmonic peak, sub-harmonic peaks and troughs in  $K_r$  for variable  $d/h_1$  within  $0.01 \leq d/h_1 \leq 10$  due to the dominance of fluid oscillations in the upper region.

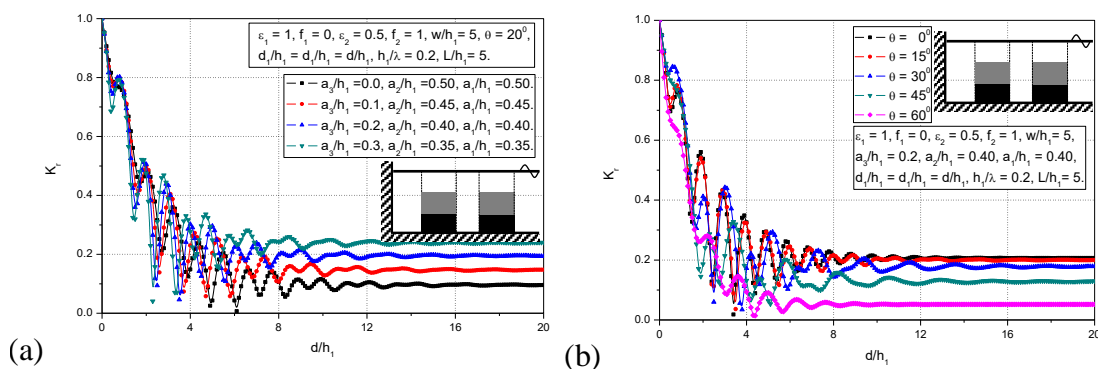


Figure 5.17: The  $K_r$  versus  $d/h_1$  for various values of (a)  $a_1/h_1, a_2/h_1, a_3/h_1$  (b)  $\theta$  considering  $h_1/\lambda = 0.2$  and  $N = 2$ .

In addition, the increase in the bottom layer changes the depth of the porous structure and lower values of  $a_3/h_1$  shows minimal  $K_r$  and higher values of  $a_3/h_1$  shows higher  $K_r$ . However, the consistent values of  $K_r$  is observed for a variable  $d/h_1$  within  $10 \leq d/h_1 \leq 20$ . On the other hand, the increase in  $\theta$  shows the gradual reduction in

$K_r$ . Particularly,  $\theta = 60^\circ$  shows very minimal values of  $K_r$  due to the effect of standing waves, which is generally termed as the critical angle. In addition, the consistent values in  $K_r$  is observed for variable  $\theta$  within  $10 \leq d/h_1 \leq 20$ , which is similar to the previous case (Figure 5.17a). Moreover, in both the situations the consistent values in  $K_r$  is observed for  $d/h_1 \geq 10$  or  $d/\lambda \geq 2$ . Similarly, in the case of two/three-layered porous structures, the consistent values in  $K_r$  is observed for  $d/\lambda \geq 1$ , which shows that the finite porous structure can be called as semi-infinite structures based on the structural position. If the structure is constructed till free surface the finite structure behaves as the semi-infinite structure for  $d/\lambda \geq 1$  and for submerged structures  $d/\lambda \geq 2$ .

#### **5.4.2 Effect of the semi-infinite permeable wall with porous structures on wave trapping**

In the present case, the porous structures are placed far away from the permeable wall and the dimensionless thickness of the permeable wall is considered to be semi-infinite, which is more than the incident wavelength  $d/\lambda \geq 1$ .

##### **5.4.2.1 Effect of the permeable wall on wave reflection**

In Figure 5.18(a-b), the wave reflection  $K_r$  due to double porous structures away from the permeable wall is presented on considering the variable angle of incidence. Two different structural configurations such as a two-layered structure (Figure 5.18a) and submerged structures (Figure 5.18b) are proposed for coastal protection. The change in the confined region  $w/h_1$  shows the harmonic peaks, sub-harmonic peaks with troughs in  $K_r$  for all the values of angle of incidence. The  $K_r$  by two-layered porous structure is minimal as compared with the submerged structures due to the energy damping. In both cases the  $\theta = 60^\circ$  shows the very minimal values of wave reflection  $K_r$  due to the formation of standing waves. However, the variation between each of the harmonic peaks and trough is higher for a two-layered structure as compared with submerged structures due to the effect of fluid oscillations in the confined region. As the study stated in the above section, the thickness of the permeable wall is infinite in nature, which absorbs whole wave energy and performs the zero-wave transmission. In the case of a two-layered structure, the effect of the permeable wall is minimal on wave

reflection  $K_r$ , as compared to the results obtained for the submerged structures under oblique wave incidence.

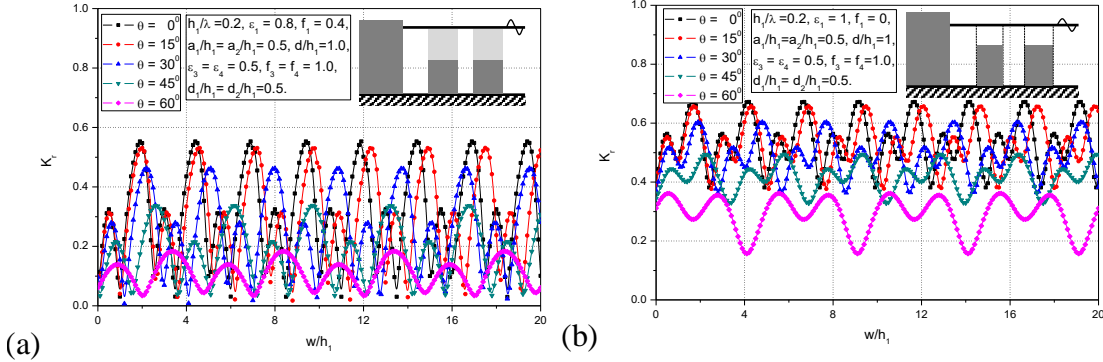


Figure 5.18: The  $K_r$  versus  $w/h_1$  for various values of  $\theta$  in the presence of (a) two-layered and (b) submerged structure away from permeable wall considering  $h_1/\lambda = 0.2$  and  $N = 2$ .

#### 5.4.2.2 Comparative study of stratified porous structures away from permeable wall

The wave trapping by various types of structural configurations as in Table 1 are analysed and compared in the presence of the permeable wall. Figure 5.19(a-b) shows the  $K_r$  due to four configurations  $C_1, C_2, C_3$  and  $C_4$  on changing the structural thickness (Figure 5.19a) and angle of incidence (Figure 5.19b).

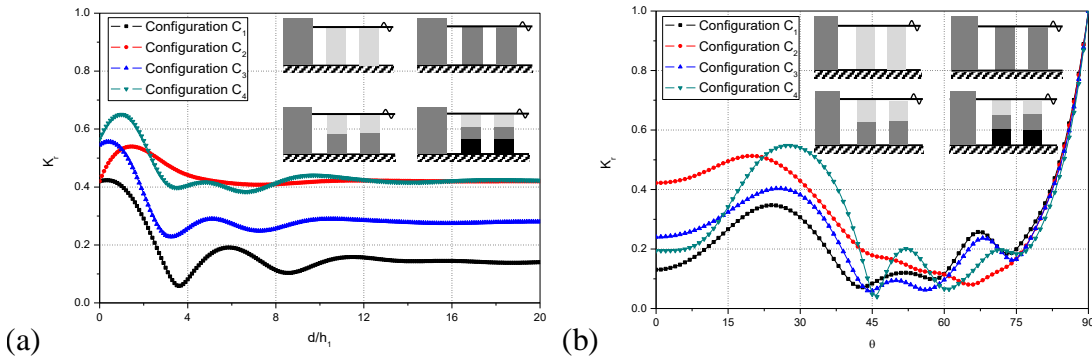


Figure 5.19: The  $K_r$  versus (a)  $d/h_1$  and (b)  $\theta$  considering various structural configurations in the presence of the permeable wall.

The minor oscillations are observed for a variable  $d/h_1$  within  $0.01 \leq d/h_1 \leq 8$ , thereafter a consistent values in  $K_r$  is obtained. In addition, the configuration  $C_1$  shows the minor variation in  $K_r$ , as compared with configuration  $C_2$  and  $C_3$ . Similarly, in the case of the variable angle of incidence, the primary critical angle is observed at  $\theta = 45^\circ$

and secondary critical angle is identified at  $\theta = 60^\circ$  which is observed to be an effective range of angle of incidence for the design and construction of stratified structures. Specifically, the variation between  $C_2$  and  $C_4$  is observed to be minimal in the case of variable  $d/h_1$  (Figure 5.19a) and  $\theta$  (Figure 5.19b). In the presence of a vertical wall (Figure 5.15 and 5.16) the configuration  $C_4$  shows minimal values of  $K_r$  as compared with configuration  $C_2$ . But in the present case, the configuration  $C_2$  and  $C_4$  show almost similar values of  $K_r$ , which may be due to the damping effect of the permeable wall.

### 5.4.3 Effect of the stepped wall with porous structures on wave trapping

The stepped walls are the most common coastal structures, which are constructed in various locations such as Wheelers bay in England, Dahanu in India. To protect the stepped wall from incident wave energy impact, a pair of stratified porous structures are placed away from the stepped wall. The two rigid steps with finite width ( $L_s/h_1$ ) and depth ( $h_{j+1}/h_j$ ) are considered. The wave reflection  $K_r$  due to stratified porous structures away from the stepped wall is studied on changing various parameters.

#### 5.4.3.1 Effect of the confined region on wave trapping

In Figure 5.20(a-d), the wave reflection  $K_r$  due to change in structural porosity  $\varepsilon_1, f_1$  (Figure 5.20a), angle of incidence  $\theta$  (Figure 5.20b), structural thickness  $d/h_1$  (Figure 5.20c) and rigid step width  $L_s/h_1$  (Figure 5.20d) are analysed. The lower values of structural porosity show the minimal variation in  $K_r$  between each harmonic peak and trough. The higher values of  $\varepsilon_1, f_1$  enlarges the oscillations in  $K_r$  and, the sub-harmonic peaks and troughs within primary peaks and troughs are noticed may be due to the presence of the stepped wall. In the case of a change in the angle of incidence  $\theta$  (Figure 5.20b), a slight reduction is noted in  $K_r$  for higher values of  $\theta$ , which may be due to the presence of submerged structures with stepped seawall. Similarly, the variation in  $d/h_1$  (Figure 5.20c) presents the multiple critical angles and very minimal  $K_r$  due to wave trapping. The lower values of  $d/h_1$  show higher oscillation as compared with higher values of  $d/h_1$  due to the combined effect of wave damping and

wave trapping. The effect of each step width available in the stepped wall is analysed on considering the variable angle of contact in Figure 5.20(d). The  $K_r$  is observed to be varying in oscillatory nature due to the full/partial clapotis. Particularly, the variable step width  $L_s/h_1$  shows the initial harmonic trough at  $\theta = 15^\circ$  then, a harmonic crest at  $\theta = 45^\circ$  and again a harmonic trough at  $\theta = 45^\circ$  due to the formation of standing waves. The increase in rigid step width  $L_s/h_1$  shows a minimal variation in  $K_r$  with a phase shift at each of the harmonic crest and trough. Thus, the study shows that the stepped wall with porous structures has a significant role in wave trapping, which is recommended for oblique wave attenuation.

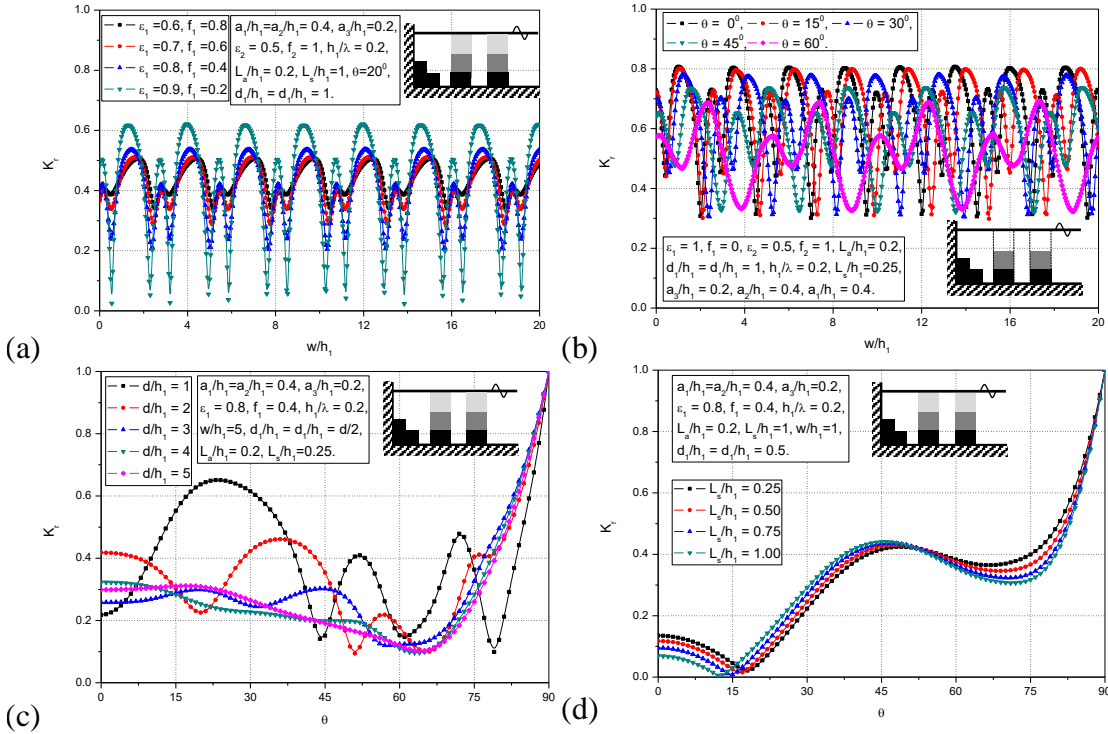


Figure 5.20: The  $K_r$  due to triple-layered porous structure with the change in (a)  $\epsilon_1, f_1$  (b)  $\theta$  (c)  $d/h_1$  and (d)  $L_s/h_1$  considering  $h_1/\lambda = 0.2$  and  $N = 2$ .

#### 5.4.4 Comparative study between vertical, permeable and stepped wall

In Figure 5.21(a-b), the comparative study is presented between the vertical wall, permeable wall and stepped wall considering a pair of three-layered porous structures (Figure 5.21a) and pair of submerged two-layered porous structures (Figure 5.21b). The  $K_r$  due to the vertical wall shows the minor oscillations as compared with the stepped wall and permeable wall in the presence of three-layered and two-layered porous



structures. However, the harmonic peaks in wave reflection  $K_r$  due to the vertical wall are almost the same as observed for stepped and permeable walls. In addition, the stepped wall and permeable walls show minimal harmonic troughs as compared with the vertical wall.

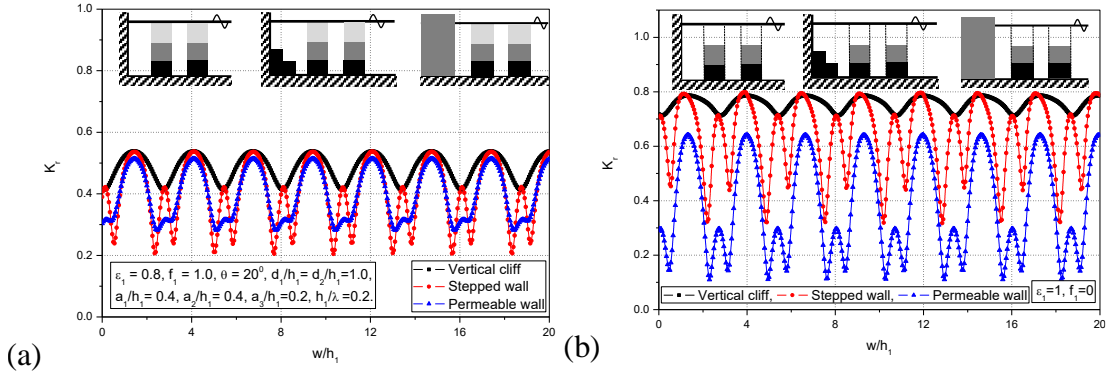


Figure 5.21: The  $K_r$  due to (a) triple-layered and (b) submerged porous structures in the presence of vertical wall, stepped wall and permeable wall considering  $h_1 / \lambda = 0.2$ .

The stepped wall encourages the sub-harmonic peaks and troughs in  $K_r$  which may be due to the effect of vortex formation (Ting and Kim., 1994; Koley et al., 2014) at the tip of each rigid step. Overall, the stepped wall shows reasonably good values in  $K_r$  as compared with the vertical wall, and the permeable wall shows minimum values of  $K_r$  as compared with the vertical wall in the presence of three-layered porous structures. In the case of two submerged porous structures, the permeable wall shows the minimal values of  $K_r$  as compared with vertical/stepped walls. From a physical point of view, the permeable wall requires a high quantity of construction material as compared with the stepped wall, and the stepped wall requires little more construction material as compared with the vertical wall. Hence, the present study suggests that the stepped wall or vertical wall with stratified porous structures consisting of three layers is the best option for the protection of mainlands from oblique incident waves.

## 5.5 CLOSURE

The oblique wave interaction with multiple stratified porous structures away from the vertical wall, permeable wall and stepped wall is analysed based on matched eigenfunction expansion method. The following conclusions are drawn from the present study:

- The analytical results obtained from the present study are well agreed with the previous experimental and numerical results by Dattatri et al. (1978), Mallayachari and Sundar (1994), Twu and Chieu (2000) and Zhu and Chwang (2001).
- The minimal  $K_r$  and  $K_{fw}$  is possible with stratified porous structures as compared with the structure of uniform porosity and friction factor and also, the multiple stratified porous structures show better values in  $K_r$  and  $K_{fw}$  as compared with a single structure due to the cushion effect.
- The little high  $K_r$  and little low  $K_{fw}$  is obtained for a three-layered structure as compared with a two-layered porous structure due to the bottom rigid layer.
- The harmonic peaks and troughs in  $K_r$  and  $K_{fw}$  are observed to be varying for the variable trapping chamber, and the magnitude of harmonic oscillations can be reduced with higher structural thickness.
- The structure of finite thickness can be called as semi-infinite structures based on the structural position. If the structure is constructed till free surface the finite structure behaves as the semi-infinite structure for  $d/\lambda \geq 1$  and submerged structures act as semi-infinite structures for  $d/\lambda \geq 2$ .
- The trapping chamber shows a very minimal role in the case of the semi-infinite structure due to the higher structural width and high wave damping.
- The effect of the permeable wall is minimal on  $K_r$  in the presence of fully-extended porous structures as compared with submerged structures.
- The increase in rigid step width  $L_s/h_1$  (available in the stepped wall) shows a minimal variation of  $K_r$  in an oscillatory manner due to the zero flow condition.
- The permeable wall requires a high quantity of construction material as compared with the vertical and stepped wall. So, the present study suggests that the stepped/vertical wall with stratified porous structures can be unique solution for the protection of mainlands from oblique incident waves.

## CHAPTER 6

# WAVE TRANSFORMATION DUE TO VERTICALLY STRATIFIED POROUS STRUCTURES

### 6.1 GENERAL INTRODUCTION

The gravity wave damping due to the presence of fully-extended structures in the offshore regions is of immense interest in the protection of offshore facilities from incoming wave attack. Different types of coastal structures have been examined widely using experimental and theoretical techniques (Rajendra et al., 2017) and still, it is a subject of great interest. Most of the studies reported that the porous structures are one of the best solutions for wave attenuation and also regulates the wave energy in the seaward and leeward open water regions. In general, the porous structures with highly dissipative media can reduce wave reflection but the high energy damping can be achieved with low dissipative media and high porosity with the large thickness of the structure (Twu et al., 2002). The wave transformation by the porous structure with uniform porosity and friction factor has been studied widely to attenuate the wave energy (Sollitt and Cross, 1972; Rojanakamthorn et al., 1989; Dalrymple et al., 1991). Numerous researchers proved that the hydrodynamic performance of the porous structure using the theoretical approach agrees well with the experimental results (Kondo and Toma, 1972; Sollitt and Cross, 1972; Sulisz, 1985; Twu and Lin, 1990; Ramakrishnan, 2011 Somervell et al., 2017). To accelerate the performance of the porous structure, various novel design techniques are considered and implemented in the offshore region. The most challenging task for coastal engineers is, a breakwater must perform minimal wave reflection, minimal wave transmission and higher wave damping using minimal construction material. It is observed that fully extended porous structures with uniform porosity are better options to enhance wave damping and the performance needs to be improved using new techniques. The high wave energy damping due to the progressive wave absorber (multiple layers) was introduced by Le Méhauté (1972) and analysis was performed using the numerical approach considering the multiple damping materials. The theoretical outcomes are validated with the

experimental results and a good agreement is obtained between both the methods. Afterward, an attempt was made by Twu and Chieu (2000) to adopt multiple porosities in a single porous structure placed on the uniform seabed to dissipate the maximum wave energy. Two-layered and three-layered porous structures are thoroughly analysed using the hydraulic tests in the presence of the multiple porosities and friction factors. The methodology as in Goda and Suzuki (1977) was used to separate the incident and reflected waves in the experimental investigation. The study reported that, for the structures allowing high wave reflection, the foundation failure might result in the process of wave damping. Afterward, Twu et al. (2001, 2002) extended the study for deeply submerged porous bars with multiple porous slices. The study revealed that the multi-layered porous structure could be constructed for partial shelter to the shores from high wave attack and the application of multiple porosities provides more emphasis on wave blocking. The previous studies by Twu et al. (2001, 2002) suggested the multi-layered concept for better wave blocking but variation in seabed characteristics and impact of the rear wall in the presence of stratified porous structure is still far from complete. The literature survey to date suggests that no studies are performed for the stratified porous structure with the varying seabed. So, the inclusion of seabed characteristics and stratified porous structure has wide application in the protection of offshore facilities by attenuating the incident wave height.

In the present study, the stratified porous structure placed on the uniform seabed is examined and further the study is extended for the analysis of elevated seabed and stepped seabed conditions. The stratified porous structure is examined in three different configurations such as (a) stratified porous structure with finite thickness (b) porous structure backed by the wall and (c) porous structure placed far away from the leeward wall. The study is performed for nine different conditions (three different structures placed on three different seabed characteristics) based on linearized wave theory using finite water depth and long-wave approximation. The closed-form solution is presented for the stratified porous structure using the eigenfunction expansion method, which is adopted for all the individual structural configurations. The direct analytical relations are presented for two-layer and three-layer stratified porous structures in the presence of the leeward wall. As a special case, the wave scattering by submerged stepped/elevated seabed in the absence of porous objects is presented. The numerical approach

used in the present study is validated with experimental results available in the literature. Finally, the significance of multiple porosities, friction factors, angle of incidence, structural width and width between the structure and back wall/confined region on wave scattering and wave trapping is investigated in the presence of stratified porous structure lying on the uniform, elevated and stepped seabed cases.

## 6.2 MATHEMATICAL FORMULATION

The porous structure is assumed to be composed of multiple layers and each layer consisting of different porosities and friction factors with finite thickness (Figure 6.1). The significance of multiple porosities and friction factors in a single porous structure is studied in the presence and absence of leeward wall with variation in rigid seabed characteristics (uniform, elevated and stepped seabed). The 3D Cartesian coordinate system is employed having  $x - z$  being the oblique wave direction towards the structure and  $y - z$  axis being vertical downward positive. It is assumed that the porous structure is divided into  $N$  number of layers considering individual porosity and friction in each of the layers. The oblique wave interacts with the stratified porous structure at  $x = -b_1$  and propagates through the structure. The fluid is assumed to occupy the region  $\bigcup_{j=1}^{N+1} I_j$  with  $I_1 \equiv (-b_1 < x < \infty, 0 < y < h_1)$ ,  $I_j \equiv (-b_{j-1} < x < -b_j, 0 < y < h_j)$  for  $j = 2, 3, \dots, N$  and  $I_{N+1} \equiv (-\infty < x < -b_N, 0 < y < h_{N+1})$  with  $z \in (-\infty, \infty)$  for all  $I_j$  in the absence of the rear wall. On the other hand, in the case of the leeward vertical wall  $I_{N+1} \equiv (-b_N - L < x < -b_N, 0 < y < h_{N+1})$  with  $z \in (-\infty, \infty)$  for all  $I_j$ . It is assumed that the fluid is inviscid, incompressible with the irrotational flow and simple harmonic in time with angular frequency  $\omega$ . So the velocity potentials  $\Phi_j(x, y, z, t)$  and the free surface deflection  $\zeta_j(x, z, t)$  are of the form of  $\Phi_j(x, y, z, t) = \text{Re}\{\phi_j(x, y)e^{ilz - i\omega t}\}$  along with  $\zeta_j(x, z, t) = \text{Re}\{\eta_j(x)e^{ilz - i\omega t}\}$ . The  $\text{Re}$  shows the real part of complex expression and  $l$  is the wavenumber component in the  $z$ -direction. Thus, the spatial velocity potential  $\phi_j(x, y)$  for  $j = 1, 2, \dots, (N + 1)$  satisfies the Helmholtz equation given by

$$\frac{\partial^2 \phi_j(x, y)}{\partial x^2} + \frac{\partial^2 \phi_j(x, y)}{\partial y^2} - l^2 \phi_j(x, y) = 0, \quad \text{for } 0 < y < h_j. \quad (6.1)$$

In addition, the velocity potential  $\phi_j$  for  $j=1,2,\dots,(N+1)$  satisfies the linearized free surface boundary condition is given by,

$$\frac{\partial \phi_j(x,y)}{\partial y} + \Gamma_j \phi_j(x,y) = 0 \quad \text{at } y=0, \quad (6.2)$$

where  $\Gamma_j = \omega^2 / g$  for  $j=1$  and  $(N+1)$  at seaward and leeward open water regions,  $\Gamma_j = \omega^2(S + if_j) / g$  for  $j=2,3,\dots,N$  at porous structures regions and  $N$  depends on the number of porous layers,  $S$  is the inertial effect,  $f_j$  is the fiction factor and  $i$  is an imaginary number.

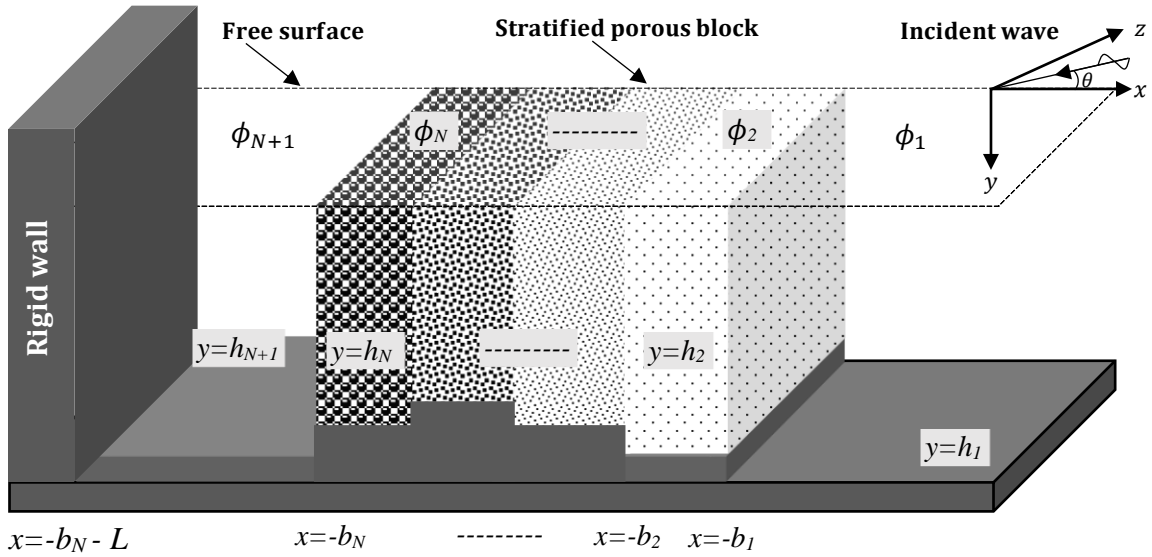


Figure 6.1: Stratified porous structure placed on the varying seabed with leeward wall.

The ocean bed is assumed to be impermeable and the no-flow condition upon impermeable seabed is given by

$$\frac{\partial \phi_j(x,y)}{\partial y} = 0 \quad \text{at } y = h_j, \quad j=1,2,\dots,(N+1). \quad (6.3a)$$

The present study deals with the relevance of uniform, elevated and stepped seabed cases on the wave transformation. The sloping seabed is approximated into multiple impermeable steps to adopt the multiple porosities, impedance of the porous medium ( $G = S - if_j$ ) and the velocity near to each impermeable step is given by

$$\frac{\partial \phi_j(x,y)}{\partial x} = 0 \quad \text{at } x = -b_j, \quad j=1,2,\dots,N. \quad (6.3b)$$

The significance of leeward wall with the confined region on wave transformation is investigated and the zero-flow condition at the impermeable wall is of the form

$$\frac{\partial \phi_j(x, y)}{\partial x} = 0 \quad \text{at } x = -(b_N + L) \quad \text{for } j = N + 1. \quad (6.4)$$

However, the dynamic pressure and velocity are continuous at the interfaces satisfying the matching equations. The fluid motion between seaward open water region, seaward porous layer, wave motion through a multi-layered porous medium and the wave propagation between leeside porous layer and leeward open water region along the horizontal  $x$  – direction is given by

$$\phi_1(x, y) = G_1 \phi_2(x, y) \quad \text{and} \quad \phi_{1x}(x, y) = \varepsilon_1 \phi_{2x}(x, y) \quad \text{at } x = -b_1, \quad (6.5a)$$

$$G_{j-1} \phi_j(x, y) = G_j \phi_{j+1}(x, y) \quad \text{and} \quad \varepsilon_{j-1} \phi_{jx}(x, y) = \varepsilon_j \phi_{(j+1)x}(x, y) \quad \text{at } x = -b_j \quad (6.5b)$$

for  $j = 2, 3, \dots, N - 1,$

$$G_{N-1} \phi_N(x, y) = \phi_{(N+1)}(x, y) \quad \text{and} \quad \varepsilon_{N-1} \phi_{Nx}(x, y) = \phi_{(N+1)x}(x, y) \quad \text{at } x = -b_N, \quad (6.5c)$$

where  $\varepsilon_j$  is the porosity of each vertical layer,  $i$  is the imaginary number and  $j = 1, 2, \dots, N$  is the number of porous layers. The inertia and friction factor (Sollitt and Cross, 1972) are determined based on the relation given by

$$S = 1 + A_m \left[ \frac{1 - \varepsilon_j}{\varepsilon_j} \right], \quad (6.6a)$$

$$f_j = \frac{1}{\omega} \frac{\int_V dV \int_t^{t+T} \varepsilon_j^2 \left( \frac{\nu q^2}{K_p} + \frac{C_f \varepsilon_j}{\sqrt{K_p}} |q|^3 \right) dt}{\int_V dV \int_t^{t+T} \varepsilon_j q^2 dt}, \quad (6.6b)$$

where  $A_m$  is virtual added mass coefficient,  $q$  is instantaneous Eulerian velocity vector at any point,  $\nu$  is kinematic viscosity,  $K_p$  is intrinsic permeability,  $C_f$  is the dimensionless turbulent resistant coefficient,  $V$  is volume and  $T$  is the wave period. The medium reactance is usually treated as unity due to a negligible added mass coefficient (Sollitt and Cross, 1972; Dalrymple et al., 1991; Liu and Li, 2013) as the structure is in a fixed position. The far-field radiation condition in the absence of the rear wall is of the form

$$\phi_j(x) = \begin{cases} (I_{10}e^{-ik_{10}x} + R_{10}e^{ik_{10}x})f_{10}(y) & \text{as } x \rightarrow \infty, \\ (T_{(N+1)0}e^{-ik_{(N+1)0}x})f_{(N+1)0}(y) & \text{as } x \rightarrow -\infty, \end{cases} \quad (6.7)$$

where  $R_{10}$  is the complex amplitude of the reflected wave and  $T_{(N+1)0}$  is complex amplitude of transmitted wave from the porous structure. The complex amplitude representing the progressive incident wave  $I_{10}$  is considered to be unity. The wavenumber  $\gamma_{j0}$  for  $j=1$  and  $(N+1)$  is the positive real roots in open water region satisfy the dispersion relation given by

$$\omega^2 = g\gamma_{j0} \tanh \gamma_{j0}h_j. \quad (6.8a)$$

The wavenumber  $\gamma_{j0}$  for  $j=2,3,\dots,N$  in the case of fully-extended porous structure satisfy the complex dispersion relation is given by

$$\omega^2(S + if_j) = g\gamma_{j0} \tanh \gamma_{j0}h_j. \quad (6.8b)$$

The dispersion relations for the case of long-wave approximation (Dalrymple et al., 1991) is of the form

$$\omega^2 = g\gamma_{j0}^2h_j \quad \text{for } j=1 \text{ and } (N+1) \quad (6.9a)$$

$$\omega^2(S + if_j) = g\gamma_{j0}^2h_j \quad \text{for } j=2,3,\dots,N \quad (6.9b)$$

where  $\omega$  is the wave frequency,  $g$  is gravitational constant,  $\gamma_{j0}$  is the wavenumber and  $h_j$  for  $j=1,2,\dots,(N+1)$  is the water depth in open water and multiple porous structure regions. The Newton-Raphson method is employed to solve the dispersion relation for the open water region. The complex dispersion relation of each of the porous structure region is solved using the perturbation method (Mendez and Losada, 2004).

### 6.3 METHOD OF SOLUTION

The present study is focused on the influence of stratified porous structures on wave transformation to increase wave damping and decrease wave reflection and transmission with multiple impedance of the porous medium. Further, the study is extended to analyse the significance of seabed characteristics (uniform seabed, elevated seabed and stepped seabed) on wave scattering in the case of finite water depth and long-wave approximations.



### 6.3.1 Porous structure in the absence of leeward wall

In this section, the general formulation along with mode-coupling relation is presented for stratified porous structure placed on various types of seabed.

#### 6.3.1.1 Finite water depth

The velocity potentials for the open water and multiple porous structure regions in the absence of the seawall is given by

$$\phi_1(x, y) = \left\{ I_{10} e^{-ik_{10}(x+b_1)} + R_{10} e^{ik_{10}(x+b_1)} \right\} f_{10}(y) + \sum_{n=1}^{\infty} \left\{ R_{1n} e^{-\kappa_{1n}(x+b_1)} \right\} f_{1n}(y), \quad (6.10a)$$

for  $-b_1 < x < \infty, 0 < y < h_1,$

$$\phi_j(x, y) = \sum_{n=0}^{\infty} \left\{ A_{jn} e^{-ik_{jn}(x+b_{j-1})} + B_{jn} e^{ik_{jn}(x+b_j)} \right\} f_{jn}(y), \quad (6.10b)$$

for  $-b_j < x < -b_{j-1}, 0 < y < h_j, j = 2, 3, \dots, N,$

$$\phi_{N+1}(x, y) = \left\{ T_{(N+1)0} e^{-ik_{(N+1)0}(x+b_N)} \right\} f_{(N+1)0}(y) + \sum_{n=1}^{\infty} \left\{ T_{(N+1)n} e^{\kappa_{(N+1)n}(x+b_N)} \right\} f_{(N+1)n}(y), \quad (6.10c)$$

for  $-\infty < x < -b_N, 0 < y < h_{N+1}.$

where  $R_{1n}, A_{jn}, B_{jn}$  and  $T_{(N+1)n}$  for  $n = 0, 1, 2, 3, \dots$  and  $j = 2, 3, \dots, N$  are the arbitrary complex unknowns to be determined.

The eigenfunctions  $f_{jn}(y)$  in each of the regions are given by

$$f_{jn}(y) = \frac{\cosh \gamma_{jn}(h_j - y)}{\cosh \gamma_{jn} h_j} \quad \text{for } n = 0, 1, 2, \dots \quad (6.11)$$

The eigenvalues  $\gamma_{jn}$  for  $j = 1, 2, 3, \dots, (N+1)$  satisfy the open water and porous structure dispersion relations given by

$$\omega^2 = g \gamma_{jn} \tanh \gamma_{jn} h_j \quad \text{for } j = 1 \text{ and } (N+1), n = 0, \quad (6.12a)$$

$$\omega^2(S + if_j) = g \gamma_{jn} \tanh \gamma_{jn} h_j \quad \text{for } j = 2, 3, \dots, N, n = 0, 1, 2, \dots, \quad (6.12b)$$

with  $\gamma_{jn} = i\gamma_{jn}$  for  $n = 1, 2, 3, \dots$  in the case of open water region,  $k_{jn}$  is wave number in  $x$ -direction,  $\gamma_{jn}$  is wave number in  $y$ -direction,  $l = \gamma_{10} \sin \theta, k_{10} = \gamma_{10} \cos \theta, \theta$  is the angle of incidence. In addition, there are purely imaginary roots  $\gamma_{jn}$  with  $\gamma_{jn}^2 = k_{jn}^2 - l^2$  for  $n = 1, 2, 3, \dots$

The eigenfunctions for the open water region and multiple porous structure regions  $f_{jn}(y)$ ,  $j = 1, 2, 3, \dots, (N+1)$  satisfy the orthogonal relation given by

$$\langle f_{jm}, f_{jn} \rangle_{j=1 \text{ and } (N+1)} = \begin{cases} 0 & \text{for } m \neq n, \\ C'_n & \text{for } m = n, \end{cases} \text{ and } \langle f_{jm}, f_{jn} \rangle_{j=2,3,\dots,N} = \begin{cases} 0 & \text{for } m \neq n, \\ C''_n & \text{for } m = n, \end{cases} \quad (6.13)$$

with respect to the orthogonal mode-coupling relation defined by

$$\langle f_{jm}, f_{jn} \rangle_{j=1 \text{ and } (N+1)} = \int_0^{h_j} f_{jm}(y) f_{jn}(y) dy, \quad (6.14a)$$

$$\langle f_{jm}, f_{jn} \rangle_{j=2,3,\dots,N} = \int_0^{h_j} f_{jm}(y) f_{jn}(y) dy, \quad (6.14b)$$

where  $C'_n|_{j=1 \text{ and } (N+1)} = \left\{ \frac{2\gamma_{jn} h_j + \sinh 2\gamma_{jn} h_j}{4\gamma_{jn} \cosh^2 \gamma_{jn} h_j} \right\}$  and  $C''_n|_{j=2,3,\dots,N} = \left\{ \frac{2\gamma_{jn} h_j + \sinh 2\gamma_{jn} h_j}{4\gamma_{jn} \cosh^2 \gamma_{jn} h_j} \right\}$   
for  $n = 0, 1, 2, \dots$  (6.15)

with  $C'_n|_{j=1 \text{ and } (N+1)}$  for  $n = 1, 2, 3, \dots$  are obtained by substituting  $\gamma_{jn} = i\gamma_{jn}$  for the open water region.

The continuity of dynamic pressure and velocity at the interface  $x = -b_j, 0 < y < h_j$  for  $j = 1$  between the open water and porous structure regions as in Equation 6.5(a,c) is employed with mode-coupling relation as in Equation 6.14(a,b) on velocity potential  $\phi_j(x, y)$  and  $\phi_{jx}(x, y)$  with the eigenfunction  $f_{jm}(y)$  to obtain

$$\langle \phi_j(x, y), f_{jm}(y) \rangle = \int_0^{h_j} \phi_j(x, y) f_{jm}(y) dy = G_j \int_0^{h_j} \phi_{(j+1)}(x, y) f_{jm}(y) dy \quad (6.16a)$$

for  $m = 0, 1, 2, \dots$  and  $j = 1$ .

$$\langle \phi_{jx}(x, y), f_{jm}(y) \rangle = \int_0^{h_j} \phi_{jx}(x, y) f_{jm}(y) dy = \varepsilon_j \int_0^{h_j} \phi_{(j+1)x}(x, y) f_{jm}(y) dy \quad (6.16b)$$

for  $m = 0, 1, 2, \dots$  and  $j = 1$ .

In addition, the continuity pressure and velocity at the interface  $x = -b_j, 0 < y < h_j$  for  $j = N$  is given by

$$\langle \phi_{j+1}(x, y), f_{(j+1)m}(y) \rangle = \int_0^{h_{j+1}} \phi_{j+1}(x, y) f_{(j+1)m}(y) dy = G_{j-1} \int_0^{h_{j+1}} \phi_j(x, y) f_{(j+1)m}(y) dy \quad (6.16c)$$

for  $m = 0, 1, 2, \dots$  and  $j = N$ .

$$\begin{aligned} \langle \phi_{(j+1)x}(x, y), f_{(j+1)m}(y) \rangle &= \int_0^{h_{j+1}} \phi_{(j+1)x}(x, y) f_{(j+1)m}(y) dy = \varepsilon_{j-1} \int_0^{h_{j+1}} \phi_{jx}(x, y) f_{(j+1)m}(y) dy \\ &\text{for } m = 0, 1, 2, \dots \text{ and } j = N. \end{aligned} \quad (6.16d)$$

Again, continuity of dynamic pressure and velocity at the interface  $x = -b_j, 0 < y < h_j$  for  $j = 2, 3, \dots, (N-1)$  between the multiple porous layers with the different impedance of the porous medium in the presence of uniform seabed as in Eq. 5(b) is employed with mode-coupling relation as in Equation 6.14(a,b) on the velocity potential  $\phi_j(x, y)$  and  $\phi_{jx}(x, y)$  with the eigenfunction  $f_{jm}(y)$  to obtain

$$\begin{aligned} G_{j-1} \langle \phi_j(x, y), f_{jm}(y) \rangle &= G_{j-1} \int_0^{h_j} \phi_j(x, y) f_{jm}(y) dy = G_j \int_0^{h_j} \phi_{j+1}(x, y) f_{jm}(y) dy \\ &\text{for } m = 0, 1, 2, \dots \text{ and } j = 2, 3, \dots, N-1. \end{aligned} \quad (6.16e)$$

$$\begin{aligned} \varepsilon_{j-1} \langle \phi_{jx}(x, y), f_{jm}(y) \rangle &= \varepsilon_{j-1} \int_0^{h_j} \phi_{jx}(x, y) f_{jm}(y) dy = \varepsilon_j \int_0^{h_j} \phi_{(j+1)x}(x, y) f_{jm}(y) dy \\ &\text{for } m = 0, 1, 2, \dots \text{ and } j = 2, 3, \dots, N-1. \end{aligned} \quad (6.16f)$$

In the presence of the elevated and the stepped seabed, the velocity near the rigid step is considered to be zero as in Equation 6.3(b). The no-flow condition at each impermeable step ( $h_j > h_{j+1}$ ) is given by

$$\int_{h_{j+1}}^{h_j} \phi_{jx}(x, y) f_{jm}(y) dy = 0, \text{ for } m = 0, 1, 2, \dots \text{ and } j = 1, 2, \dots, N. \quad (6.16g)$$

The no-flow condition at  $j = N$  in the presence of elevated seabed ( $h_{j+1} > h_j$ ) at the leeside open water and leeward porous layer regions is given by

$$\int_{h_j}^{h_{j+1}} \phi_{(j+1)x}(x, y) f_{(j+1)m}(y) dy = 0, \text{ for } m = 0, 1, 2, \dots \text{ and } j = N. \quad (6.16h)$$

However, the porous structure is separated into multiple porous layers with finite thickness considering different porosity and friction factors. In order to determine the unknown constants  $R_{1n}, A_{jn}, B_{jn}, T_{(N+1)n}$  for  $j = 2, 3, \dots, N$  infinite series sums presented as the algebraic Equation (6.16a) – (6.16f) are truncated with finite  $M$  terms and a linear system of  $2(j+1)(M+1)$  for  $j = 1, 2, \dots, N$  algebraic equations are obtained to

solve the  $2(j+1)(M+1)$  unknowns. The wave reflection and transmission due to the stratified porous structure (Behera et al., 2016; Praveen et al., 2020) is given by

$$K_r = \left| \frac{R_{10}}{I_{10}} \right| \quad \text{and} \quad K_t = \left| \frac{\gamma_{(N+1)0} \tanh \gamma_{(N+1)0} h_{(N+1)}}{\gamma_{10} \tanh \gamma_{10} h_1} \frac{T_{(N+1)0}}{I_{10}} \right|. \quad (6.17a)$$

The wave energy dissipation due to porous structure is determined based on the relation as in Chwang and Chan (1998) given by

$$K_d = 1 - K_r^2 - K_t^2. \quad (6.17b)$$

Equation (6.17a) is applicable for seabed where the depth of seaward and leeward open water regions are different. But in the case of porous structure placed on uniform depth in the seaward and leeward regions, the wave reflection and transmission are given by

$$K_r = \left| \frac{R_{10}}{I_{10}} \right| \quad \text{and} \quad K_t = \left| \frac{T_{(N+1)0}}{I_{10}} \right|. \quad (6.17c)$$

### 6.3.1.2 Long-wave approximation

The porous structure with multiple layers lying on the uniform seabed, elevated seabed and stepped seabed is analysed under the assumption of long-wave approximation. The velocity potentials in the case of porous structure in the absence of leeward wall are of the form

$$\phi_1(x) = I_{10} e^{-ik_{10}(x+b_1)} + R_{10} e^{ik_{10}(x+b_1)} \quad \text{for} \quad -b_1 < x < \infty, \quad (6.18a)$$

$$\phi_j(x) = A_{j0} e^{-ik_{j0}(x+b_{j-1})} + B_{j0} e^{ik_{j0}(x+b_j)} \quad \text{for} \quad -b_j < x < -b_{j-1}, j = 2, 3, \dots, N, \quad (6.18b)$$

$$\phi_{N+1}(x) = T_{(N+1)0} e^{-ik_{(N+1)0}(x+b_N)} \quad \text{for} \quad -\infty < x < -b_N. \quad (6.18c)$$

The wave reflection and transmission coefficients are evaluated using matched edge condition at the interface  $x = -b_j$ ,  $j = 1, 2, \dots, N$  as in Equation (6.5a) – (6.5c) to determine the unknown constants as in Equation (6.18a) – (6.18c).

### 6.3.2 Porous structure backed by a leeward wall

To protect the mainlands, various types of seawalls are suggested and examined by various coastal engineers (Madsen, 1983). In general, the porous wave absorber is one of the preferable solutions to increase the life span of the seawall by dissipating the incoming wave energy. The stratified porous structure with seawall is investigated considering different types of seabed characteristics. In this section, the spacing

between the porous absorber and seawall is considered as zero. The previous studies focused on the performance of a porous structure with uniform porosity and friction factor (Madsen, 1983; Das and Bora, 2014c). The present study deals with the stratified porous structure backed by the wall with variation in seabed characteristics.

### 6.3.2.1 Finite water depth

The fluid realm is divided into seaside open water region and multiple porous layer regions given by

$$\phi_1(x, y) = \left\{ I_{10} e^{-ik_{10}(x+b_1)} + R_{10} e^{ik_{10}(x+b_1)} \right\} f_{10}(y) + \sum_{n=1}^{\infty} \left\{ R_{1n} e^{-k_{1n}(x+b_1)} \right\} f_{1n}(y), \quad (6.19a)$$

for  $-b_1 < x < \infty, 0 < y < h_1,$

$$\phi_j(x, y) = \sum_{n=0}^{\infty} \left\{ A_{jn} e^{-ik_{jn}(x+b_{j-1})} + B_{jn} e^{ik_{jn}(x+b_j)} \right\} f_{jn}(y), \quad (6.19b)$$

for  $-b_j < x < -b_{j-1}, 0 < y < h_j, j = 2, 3, \dots, N-1,$

$$\phi_N(x, y) = \sum_{n=0}^{\infty} \left\{ C_{Nn} \cos(k_{Nn}(x+b_N)) \right\} f_{Nn}(y) \quad \text{for } -b_{N-1} < x < -b_N, 0 < y < h_N. \quad (6.19c)$$

The continuity of dynamic pressure and velocity at interfaces between open water and porous structure regions along with multiple porous layers due to change in the seabed as in Equation (6.5a) – (6.5c) is employed with mode-coupling relation as in Equation (6.14a,b) on velocity potentials as in Equation (6.19a) – (6.19c) with eigenfunction  $f_{jm}(y)$  for  $j = 1, 2, \dots, N$  to obtain the linear system of equations as in Equation (6.16a)-(6.16f).

### 6.3.2.2 Long-wave approximation

In the case of long-wave approximations for the porous structure with the leeward wall, the velocity potentials are given by

$$\phi_1(x) = I_{10} e^{-ik_{10}(x+b_1)} + R_{10} e^{ik_{10}(x+b_1)} \quad \text{for } -b_1 < x < \infty, \quad (6.20a)$$

$$\phi_j(x) = A_{j0} e^{-ik_{j0}(x+b_{j-1})} + B_{j0} e^{ik_{j0}(x+b_j)} \quad \text{for } -b_j < x < -b_{j-1}, j = 2, 3, \dots, N-1, \quad (6.20b)$$

$$\phi_N(x) = C_{N0} \cos\{k_{N0}(x+b_N)\} \quad \text{for } -b_{N-1} < x < -b_N. \quad (6.20c)$$

Using the matching edge conditions at the interface as in Equation (6.5a) – (6.5c), the  $K_r$  for a two-layered porous structure with the leeward wall is given by

$$K_r = \left| \frac{R_{10}}{I_{10}} \right| = \frac{\cos a_2 (m_1 m_3 - i \tan a_1) + i \sin a_2 (m_1 i \tan a_1 - m_3)}{\cos a_2 (m_1 m_3 + i \tan a_1) + i \sin a_2 (m_1 i \tan a_1 + m_3)}. \quad (6.21a)$$

The reflection coefficient  $K_r$  for three-layered porous structure in the presence of leeward wall is given by

$$K_r = \left| \frac{R_{10}}{I_{10}} \right| = \frac{\cos a_1 \cos a_2 (m_1 m_3 - m_2 i \tan a_3) - \sin a_1 \sin a_2 (m_1 - m_2 m_3 i \tan a_3) + i \sin a_1 \cos a_2 (m_1 m_2 m_3 i \tan a_3 - 1) + i \cos a_1 \sin a_2 (m_1 m_2 i \tan a_3 - m_3)}{\cos a_1 \cos a_2 (m_1 m_3 + m_2 i \tan a_3) - \sin a_1 \sin a_2 (m_1 + m_2 m_3 i \tan a_3) + i \sin a_1 \cos a_2 (m_1 m_2 m_3 i \tan a_3 + 1) + i \cos a_1 \sin a_2 (m_1 m_2 i \tan a_3 + m_3)} \quad (6.21b)$$

where  $a_1 = d_2 k_{30}$ ,  $a_2 = d_1 k_{20}$ ,  $a_3 = d_3 k_{40}$ ,  $m_1 = \frac{G_1 k_{10}}{\varepsilon_1 k_{20}}$ ,  $m_2 = \frac{G_2 \varepsilon_3 k_{40}}{G_3 \varepsilon_2 k_{30}}$ ,  $m_3 = \frac{G_2 \varepsilon_1 k_{20}}{G_1 \varepsilon_2 k_{30}}$ ,

$d_1$ ,  $d_2$  and  $d_3$  are the thickness  $G_1$ ,  $G_2$  and  $G_3$  are the impedance  $\varepsilon_1$ ,  $\varepsilon_2$  and  $\varepsilon_3$  are porosity of the first, second and third porous layers. The wave reflection  $K_r$  as in Equation (6.21a,b) can be validated with the previous limiting cases in the analysis of porous absorber with the leeward wall (Madsen, 1983; Dalrymple et al., 1991) by considering either  $d_1 \rightarrow 0$  or  $d_2 \rightarrow 0$  along with uniform porosity  $\varepsilon$  and friction factor  $f$  due to the presence of the porous structure.

### 6.3.3 Porous structure placed far away from the leeward wall

The hydrodynamic performance of the stratified porous structure placed far away from the vertical wall with the trapping chamber ( $L$ ) is analysed for both finite water depth and long-wave approximation.

#### 6.3.3.1 Finite water depth

The velocity potentials in each of the regions is given by,

$$\phi_1(x, y) = \left\{ I_{10} e^{-ik_{10}(x+b_1)} + R_{10} e^{ik_{10}(x+b_1)} \right\} f_{10}(y) + \sum_{n=1}^{\infty} \left\{ R_{1n} e^{-\kappa_{1n}(x+b_1)} \right\} f_{1n}(y), \quad (6.22a)$$

for  $-b_1 < x < \infty$ ,  $0 < y < h_1$ ,

$$\phi_j(x, y) = \sum_{n=0}^{\infty} \left\{ A_{jn} e^{-ik_{jn}(x+b_{j-1})} + B_{jn} e^{ik_{jn}(x+b_j)} \right\} f_{jn}(y), \quad (6.22b)$$

for  $-b_j < x < -b_{j-1}$ ,  $0 < y < h_j$ ,  $j = 2, 3, \dots, N$ ,

$$\begin{aligned} \phi_{N+1}(x, y) = & T_{(N+1)0} \left\{ e^{-ik_{(N+1)0}(x+b_j)} + e^{ik_{(N+1)0}(x+b_N+2L)} \right\} f_{(N+1)0}(y) \\ & + \sum_{n=1}^{\infty} T_{(N+1)n} \left\{ e^{K_{(N+1)n}(x+b_N)} + e^{-K_{(N+1)n}(x+b_N+2L)} \right\} f_{(N+1)n}(y), \quad (6.22c) \\ & \text{for } -(b_N + L) < x < -b_N, \quad 0 < y < h_{N+1}. \end{aligned}$$

The continuity of dynamic pressure and velocity at each of the interface as in Equation (6.5a) – (6.5c) is applied with mode-coupling relation as in Equation (6.14a,b) on velocity potentials as in Equation (6.22a-c) with eigenfunction  $f_{jm}(y)$  for  $j=1,2,\dots,N+1$  to obtain the linear system of equations as in Equation (6.16a) – (6.16f).

### 6.3.3.2 Long-wave approximation

The velocity potentials in the case of the porous structure placed far away from the leeward wall in shallow water depth are of the form

$$\phi_1(x) = I_{10} e^{-ik_{10}(x+b_1)} + R_{10} e^{ik_{10}(x+b_1)} \quad \text{for } -b_1 < x < \infty, \quad (6.23a)$$

$$\phi_j(x) = A_{j0} e^{-ik_{j0}(x+b_{j-1})} + B_{j0} e^{ik_{j0}(x+b_j)} \quad \text{for } -b_j < x < -b_{j-1}, j = 2, 3, \dots, N, \quad (6.23b)$$

$$\phi_{N+1}(x) = T_{(N+1)0} \left\{ e^{-ik_{(N+1)0}(x+b_N)} + e^{ik_{(N+1)0}(x+b_N+2L)} \right\} \quad \text{for } -(b_N + L) < x < -b_N. \quad (6.23c)$$

The wave reflection is determined on solving the system of linear equations obtained by matching the edge conditions as in Equation (6.5a) – (6.5c).

### 6.3.3.3 Wave force on the porous structure

The wave force acting on the seaside porous layer  $K_{fs}$  and leeward porous layer  $K_{fb}$  is given by

$$K_{fs} = \frac{F_s}{\rho g h_1 I_{10}} \quad \text{and} \quad K_{fb} = \frac{F_b}{\rho g h_1 I_{10}}, \quad (6.24a)$$

$$\text{with } F_s = i\rho\omega \int_0^{h_1} (\phi_1 - \phi_2) dy \text{ at } x = -b_1 \text{ and } F_b = i\rho\omega \int_0^{h_{N+1}} (\phi_N - \phi_{N+1}) dy \text{ at } x = -b_N.$$

The wave force acting on the vertical wall  $K_{fw}$  is given by

$$K_{fw} = \frac{F_w}{\rho g h_1 I_{10}}, \quad (6.24b)$$

with  $F_w = i\rho\omega \int_0^{h_N} \phi_N(x, y)dy$  at  $x = -b_N$  in the absence of trapping chamber and

$F_w = i\rho\omega \int_0^{h_{N+1}} \phi_{N+1}(x, y)dy$  at  $x = -(b_N + L)$  in the presence of trapping chamber,  $\rho$  is the

density of seawater and  $I_{10}$  is the amplitude of incident wave potential considered to be unity.

## 6.4 RESULTS AND DISCUSSION

The multi-layered porous structure placed on the flat seabed is considered to be efficient in enhancing the wave damping and reducing the wave reflection and transmission (Twu and Chieu, 2000; Twu et al., 2001, 2002). However, the seabed is uneven and it is a difficult task to identify the uniform seabed for the construction of coastal structures. The studies on multi-layered porous structure placed of the varying seabed is still under investigation and need to be analysed in detail. To study the efficiency of the present model, the current study outcomes are validated with experimental results reported by Twu and Chieu (2000) in the case of energy damping for two-layered and three-layered porous structures in the absence of leeward wall placed on the uniform seabed.

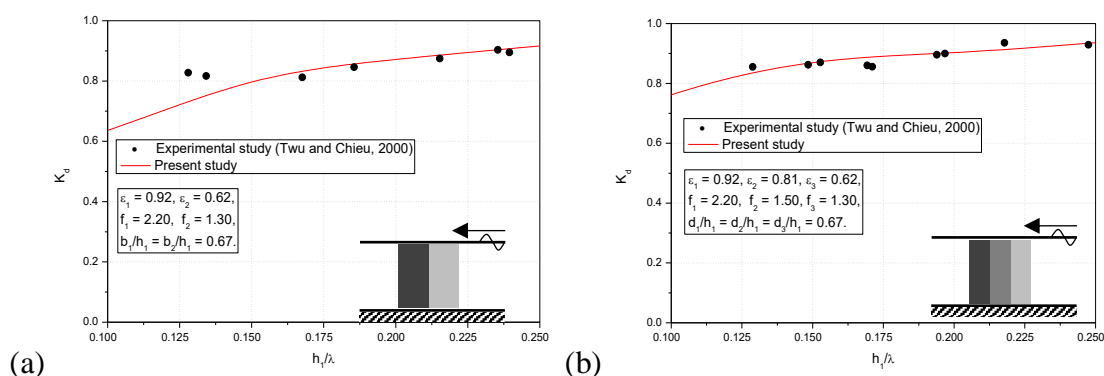


Figure 6.2: Comparison of the experimental data (Twu and Chieu, 2000) and the present study for the wave energy damping due to (a) two-layered porous structure and (b) three-layered porous structure in the absence of seawall.

Figure 6.2(a,b) shows the comparison between the present study and hydraulic test results due to the porous structure placed on the uniform seabed as in Twu and Chieu (2000). The correlation between the theoretical and experimental results shows a good agreement. Thus, the present study is extended for the analysis of variation in seabed



characteristics, the impact of the leeward wall and confined region in the presence of the stratified porous structure. In the case of the uniform seabed, the depth of the structure is occupied by the only porous material. In the case of elevated/stepped seabed, the depth of the structure is divided into permeable and impermeable structures. However, if the seabed variation is natural, the construction material required for developing the stratified porous structure placed on elevated/stepped seabed is pretty minimal as compared with the other condition (uniform seabed). The comparative study is performed between the uniform, elevated and stepped seabed conditions in the presence of stratified porous structure for identical structural width and structural depth throughout the study.

#### 6.4.1 Porous structure in the absence of leeward wall with variation in seabed

In the present study, the convergence of  $K_r$  and  $K_t$  is obtained with the increase in the evanescent wave modes and these evanescent waves are truncated for  $M = 20$ . The percentage of convergence in the  $K_r$  and  $K_t$  is observed to be more than 99.5% (or less than 0.5% deviation) with its previous truncated number for each of the condition. Twu et al. (2001, 2002) reported that less than 1% deviation in the wave reflection  $K_r$  and transmission  $K_t$  is achieved for the evanescent wave modes within  $6 \leq M \leq 10$ . Table 6.1 shows the convergence of  $K_r$  and  $K_t$  with an increase in the truncated number of evanescent wave modes  $M$  for the stratified porous structure.

Table 6.1: Convergence in  $K_r$  and  $K_t$  of a multi-layered porous structure considering  $\omega = 0.3367$ ,  $\theta = 30^\circ$ ,  $d/h_1 = 2$ ,  $f_j = 0.5$   $\varepsilon_j = 0.5$  for  $j=1,2$  and 3.

Evanescent waves (M)	Uniform seabed		Elevated seabed		Stepped seabed	
	$K_r$	$K_t$	$K_r$	$K_t$	$K_r$	$K_t$
0	0.41974	0.66015	0.42109	0.60469	0.41889	0.65912
1	0.41855	0.66038	0.42172	0.60091	0.41963	0.65848
3	0.41852	0.66041	0.42547	0.60859	0.41998	0.65740
5	0.41852	0.66042	0.43199	0.60312	0.42055	0.65773
10	0.41852	0.66042	0.44037	0.60632	0.42047	0.65820
15	0.41852	0.66042	0.44035	0.60636	0.42047	0.65820
20	0.41852	0.66042	0.44036	0.60634	0.42047	0.65820

The reflection  $K_r$ , transmission  $K_t$ , energy damping  $K_d$ , wave force impact on the seaward layer  $K_{fs}$  and wave force impact on the leeward wall  $K_{fw}$  are computed. The importance in analysing the hydrodynamic performance of the stratified porous structure is to explore a better configuration of a porous structure for its better performance as a breakwater. The parameters  $\rho = 1000 \text{ kg/m}^3$ ,  $g = 9.81 \text{ m/s}^2$  and  $S = 1$  are kept constant throughout the study. The cumulative width of the porous structure ( $d$ ) is subdivided into equal multiple porous layers  $d = \sum_{j=1}^N d_j$  for  $j = 1, 2, 3, \dots$

considering different porosities and friction factors. In the case of finite water depth, the porous structure is divided into three layers. The elevated step height is considered to be 20% and 40% ( $h_2 / h_1 = 0.8, 0.6$ ) in the open water region. In the case of the stepped seabed, the sloping bottom is approximated into the equal number of multiple steps and the seabed variation between the seaside and leeside open water region is considered to be  $h_5 / h_1 = 0.6$  (where  $h_2 / h_1 = 0.9$ ,  $h_3 / h_1 = 0.8$ ,  $h_4 / h_1 = 0.7$ ) for triple-layered structure.

#### **6.4.1.1 Effect of seabed characteristics**

In Figure 6.3(a-c), the variation in  $K_r$  between uniform seabed, elevated seabed ( $h_2 / h_1 = 0.8$ ) and stepped seabed ( $h_5 / h_1 = 0.6$ ) is performed in the presence of porous structure and the deviation is considerable in the wave reflection and transmission characteristics. The 18% increase in wave reflection  $K_r$  is observed for the case of the elevated seabed as compared with the uniform seabed within  $0^\circ < \theta < 66^\circ$  due to the presence of the impermeable elevated step height. The variation in  $K_r$  is minimum for the case of the stepped seabed as compared with uniform seabed within  $0^\circ < \theta < 62^\circ$ . Afterwards, a little increase in  $K_r$  is observed due to the presence of impermeable steps. The minimum  $K_r$  is observed at  $\theta = 74^\circ, 84^\circ$  and  $66^\circ$  for uniform, elevated and stepped seabed as in Figure 6.3(a) due to the formation of standing waves and it is termed as the critical angle (where the minimum reflection occurs). The wave transmission  $K_t$  (Figure 6.3b) is examined with variation in the angle of incidence  $\theta$  for uniform, elevated and stepped seabed. The variation between the uniform, elevated

and stepped seabed is minimum within  $0^\circ < \theta < 48^\circ$ . Afterwards, minimum  $K_t$  is observed for the case of the stepped seabed as compared with uniform and elevated seabed. However, the incident wave is subjected to wave trapping due to the wave motion upon multiple steps. The energy damping  $K_d$  versus angle of incidence is presented in Figure 6.3(c). It is observed that the uniform seabed performs better energy damping as compared with elevated and stepped seabed within  $0^\circ < \theta < 50^\circ$  but the increase in  $\theta$  shows the increase in energy damping in the case of the stepped seabed, which may occur due to trapping of waves inside the porous structure. However, in the case of oblique wave impinging, it is better to prefer stepped seabed for the best outcomes.

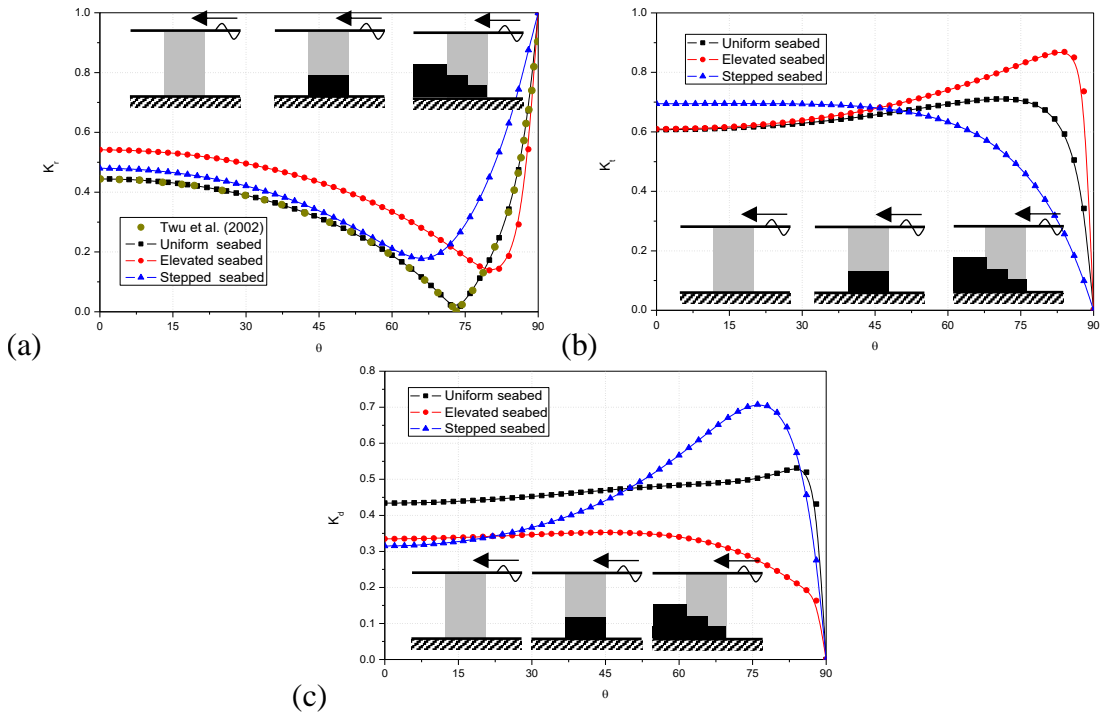


Figure 6.3: Effect of the seabed variation on (a)  $K_r$ , (b)  $K_t$  and (c)  $K_d$  versus  $\theta$  for  $f = 1$ ,  $\varepsilon = 0.4$ ,  $d / h_1 = 1$  and  $\omega^2 h_1 / g = 0.2012$ .

Thereafter, the wave reflection and transmission for various types of seabed conditions versus angle of incidence are analysed based on long-wave approximation. In the case of the uniform seabed, the depth of the structure is similar in all the open water and porous structure regions. The sloping bottom is approximated into multiple steps to achieve accurate values in the analysis of the sloping bottom with multiple porosities. Total ten steps are modelled and each step height is considered to be  $0.05h_1$  and the

variation between the seaside and leeside open water regions is  $h_{11} / h_1 = 0.5$ . In the case of the elevated seabed  $h_1 = h_{11} = 0.5h_j$  for  $j = 2, 3, \dots, 10$  (50% elevated step height). Figure 6.4(a,b) shows the  $K_r$  and  $K_t$  versus  $\theta$  for  $f = 0.5$  (Figure 6.4a) and  $f = 1.0$  (Figure 6.4b). The  $K_r$  (Figure 6.4a) with variation in seabed condition shows the minor change within  $0^\circ < \theta < 50^\circ$ , afterward the increase in  $\theta$  presents the significant variation between the outcomes and minimum  $K_r$  is observed for uniform seabed and maximum  $K_r$  is observed for stepped seabed within  $50^\circ < \theta < 90^\circ$ . In the case of  $K_t$  (Figure 6.4a), variation between uniform, elevated and stepped seabed is considerable and it is noted that the stepped seabed presents minor estimation in  $K_t$  compared with uniform and elevated seabed with the increase in  $\theta$ . The reason may be due to the uniform seabed consisting of complete porous material which allows minimum reflection and high wave transmission as compared with elevated and stepped seabed. But the stepped seabed has high reflection and less transmission coefficient with an increase in the  $\theta$ , which may be due to the addition of wave reflection due to the each of the impermeable steps.

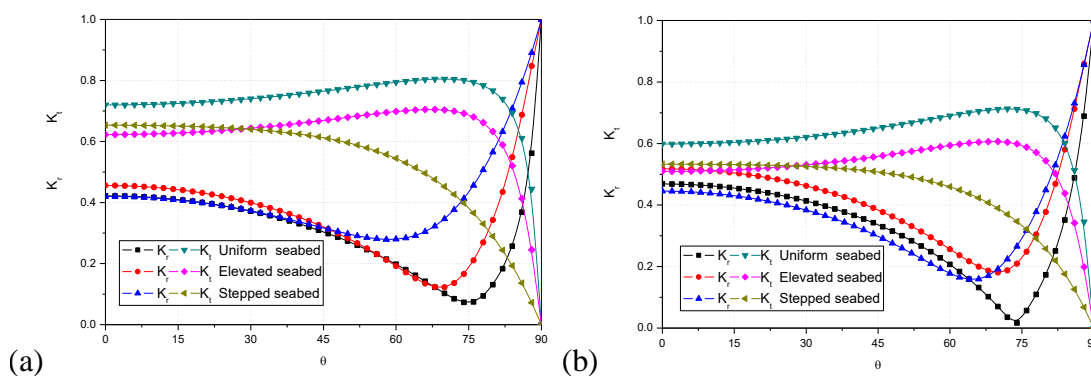


Figure 6.4: Variation in  $K_r$  and  $K_t$  due to multi-layered porous structure for (a)  $f = 0.5$  and (b)  $f = 1.0$  in the presence of different types of seabed considering  $\gamma_{10}h_1 = 1.0$ ,  $\varepsilon = 0.4$  and  $d / h_1 = 0.5$ .

Afterward, a similar study is performed by considering the friction factor  $f = 1.0$  as illustrated in Figure 6.4(b). It is noted that the variation in the seabed characteristic shows similar outcomes as aforementioned. But in this case, the stepped seabed performance is acceptable as compared with uniform and elevated seabed. The  $K_r$  due to the stepped seabed and uniform seabed is almost the same within  $0^\circ < \theta < 60^\circ$  and

the critical angle is observed within  $64^\circ < \theta < 70^\circ$  where the minimum  $K_r$  is noted. In the case of the stepped seabed, the  $K_r$  (Figure 6.4b) is minimum as compared with the uniform and elevated seabed within  $50^\circ < \theta < 90^\circ$  for the friction factor  $f = 1.0$  and  $\gamma_{10}h_1 = 1.0$ . Overall, the change in the seabed shows the significant impact in reducing the wave transmission in the case of finite water depth and long-wave approximation.

#### 6.4.1.2 Effect of multiple porosities

The effect of multiple porosities in a single porous structure is studied and compared for a fixed average porosity. Figure 6.5(a) shows  $K_r$  versus  $\gamma_{10}d$  with variation in structural porosity. Initially, the structural configuration as in Liu and Li (2013) is analysed using the multi-layered concept and the comparison between both the present and previous results are observed to be quite acceptable. Further, the study shows the significance of multiple porosities and variation between different structural configurations for wave transformation. Table 6.2 shows different model configurations consisting of different porosities and friction factors used in the present study. The four configurations C<sub>1</sub>, C<sub>2</sub>, C<sub>3</sub> and C<sub>4</sub> as in Table 2 are studied with variation in structural width. It is observed that the configuration C<sub>1</sub>, C<sub>2</sub> and C<sub>3</sub> is having fixed average porosity but configuration C<sub>4</sub> has high average porosity.

Table 6.2: Multiple porosities and friction factors with different model configurations.

Model notations	Multiple porosities and friction factors	Model notations	Multiple porosities and friction factors
C <sub>1</sub>	$\varepsilon_1 = 0.45, \varepsilon_2 = 0.45, \varepsilon_3 = 0.45$	C <sub>8</sub>	$\varepsilon_1 = 0.90, \varepsilon_2 = 0.50, \varepsilon_3 = 0.10$
C <sub>2</sub>	$\varepsilon_1 = 0.55, \varepsilon_2 = 0.45, \varepsilon_3 = 0.35$	C <sub>9</sub>	$\varepsilon_1 = 0.80, \varepsilon_2 = 0.60, \varepsilon_3 = 0.40$
C <sub>3</sub>	$\varepsilon_1 = 0.65, \varepsilon_2 = 0.45, \varepsilon_3 = 0.25$	C <sub>10</sub>	$f_1 = 0.50, f_2 = 0.50, f_3 = 0.50$
C <sub>4</sub>	$\varepsilon_1 = 0.85, \varepsilon_2 = 0.65, \varepsilon_3 = 0.45$	C <sub>11</sub>	$f_1 = 0.70, f_2 = 0.50, f_3 = 0.30$
C <sub>5</sub>	$\varepsilon_1 = 0.50, \varepsilon_2 = 0.50, \varepsilon_3 = 0.50$	C <sub>12</sub>	$f_1 = 0.90, f_2 = 0.50, f_3 = 0.10$
C <sub>6</sub>	$\varepsilon_1 = 0.60, \varepsilon_2 = 0.50, \varepsilon_3 = 0.40$	C <sub>13</sub>	$\varepsilon_1 = 0.92, \varepsilon_2 = 0.81, \varepsilon_3 = 0.62$
C <sub>7</sub>	$\varepsilon_1 = 0.70, \varepsilon_2 = 0.50, \varepsilon_3 = 0.30$		$f_1 = 2.20, f_2 = 1.50, f_3 = 1.30$

The difference between all the structural configurations C<sub>1</sub>, C<sub>2</sub>, C<sub>3</sub> and C<sub>4</sub> is minimum in  $K_r$  for the case of minimum dimensionless width  $\gamma_{10}d$  within  $0.01 < \gamma_{10}d < 1$ . The

configuration  $C_1$  shows the similar result as in Liu and Li (2013) and the 20%, 34% and 55% decrease in the  $K_r$  is observed for configurations  $C_2$ ,  $C_3$  and  $C_4$  respectively as compared with the Liu and Li (2013). The reduction in  $K_r$  is mainly due to high porosity in seaside porous layer allowing high wave energy through a porous medium and encouraging the wave trapping. Afterward, the correlation between the present study and Liu and Li (2013) is observed to be acceptable in the case of  $K_r$  presented in Figure 6.5(b). The variation between the configurations  $C_2$  and  $C_3$  is minimum in the  $K_r$  as compared with Liu and Li (2013). A little increase in  $K_r$  is noticed for configuration  $C_4$  as compared with Liu and Li (2013) due to the high structural porosity in the seaside and leeside porous layers.

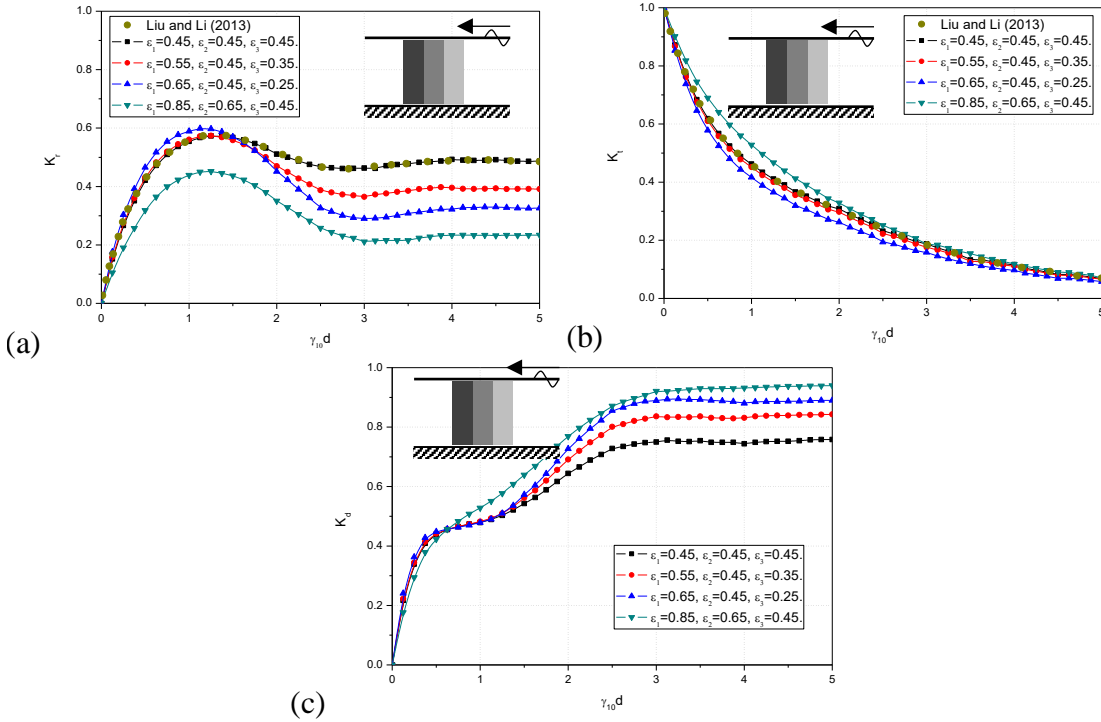


Figure 6.5: Effect of structural porosity on (a)  $K_r$  (b)  $K_t$  and (c)  $K_d$  versus  $\gamma_{10}d$  in the presence of uniform seabed for  $f = 1$ ,  $\theta = 0^0$  and  $\gamma_{10}h_1 = 0.5$ .

Figure 6.5(c) shows the energy damping  $K_d$  due to the presence of multiple porosities and it is observed that the variation between all the configurations is minimum within  $0.1 < \gamma_{10}d < 2$ . Afterwards the configurations  $C_2$  and  $C_3$  show more than 90% wave energy damping and configuration  $C_4$  shows around 96% energy damping  $K_d$  within the  $3 < \gamma_{10}d < 5$ . From the above computational results, the porous structure with three

layers consisting of high porosity in the seaside allows maximum wave energy inside the structure and the low porosity in the leeside shows better wave blocking. Thus the 95% energy damping is obtained and also the multi-layered concept can effectively work, if the width of the structure is within  $3 < \gamma_{10}d < 5$  for normal wave incidence.

### 6.4.1.3 Effect of angle of incidence

In Figure 6.6(a,b), the multi-layered porous structure is analysed for various ranges of friction factors within  $0.25 < f < 2$  and dimensionless structural width within  $0.5 < d/h_1 < 3$ . It is noted that high porosity is considered in the seaside porous layer for better wave energy penetration and porosity of each layer decreases with the increase in the number of steps. Afterward, the incoming wave energy may be arrested within the multiple porous layers and wave trapping can be achieved inside the porous structure.

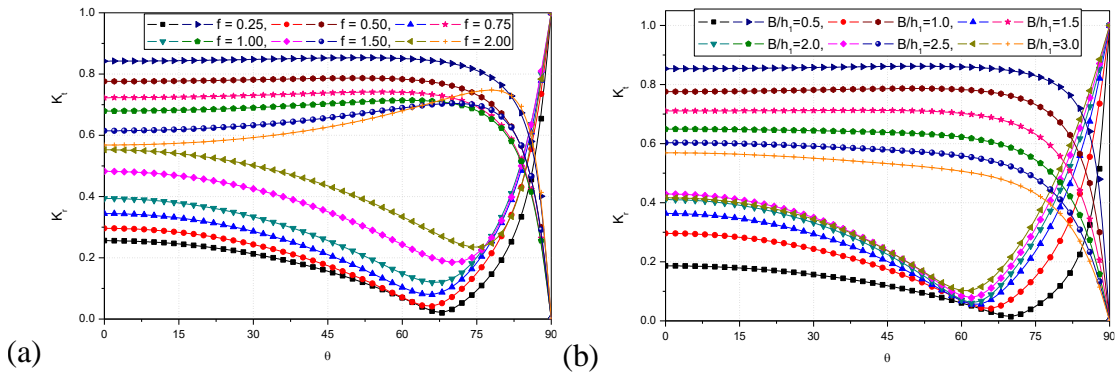


Figure 6.6: Variation in  $K_r$  and  $K_t$  due to multi-layered porous structure placed on the elevated seabed for various values of (a) friction factor with  $d/h_1 = 1$  and (b) structural width with  $f = 0.5$  considering  $\gamma_{10}h_1 = 0.5$ .

The seaside porous layer consists of  $\varepsilon_1 = 0.85$ , the second layer consists of  $\varepsilon_2 = 0.65$ , and the leeside porous layer consists of  $\varepsilon_3 = 0.45$  as in configuration C<sub>4</sub>. It may be noted that each porous layer consists of uniform width and structure is placed on elevated seabed considering 20% rigid step height  $h_j/h_1 = 0.8$  for  $j = 2, 3, 4$ . The variation in the wave reflection  $K_r$  and transmission  $K_t$  versus angle of incidence  $\theta$  is analysed for various values of friction factor within  $0.25 \leq f \leq 2$  (Figure 6.6a) along with dimensionless width of the structure within  $0.5 \leq d/h_1 \leq 3$  (Figure 6.6b). The

increase in  $f$  (uniform friction in each layer) shows the oscillating trend in the  $K_r$  within  $0^\circ \leq \theta \leq 68^\circ$ , afterward, a sharp rise in  $K_r$  is noted. However, variation is considerable in  $K_r$  and critical angle is observed for  $\theta = 68^\circ$ . On the other hand, the wave transmission coefficient  $K_t$  is plotted in Figure 6.6(a) and it is noted that the periodic increase in the friction shows the periodic decrease in  $K_t$ . However, variation in  $K_t$  is considerable with variation in the friction factor. The increase in friction factor gives the increase in energy damping, which may be due to the fact that the  $K_t$  is decreasing with an increase in friction factor. The study suggested that the friction factor within  $1 \leq f \leq 2$  is suitable to construct a stratified/multi-layered porous structure upon the elevated seabed to control the incoming wave of  $\gamma_{10}h_1 = 0.5$ . On the other hand the  $K_r$  and  $K_t$  versus angle of incidence  $\theta$  is plotted for  $0.5 \leq d/h_1 \leq 2.5$  in the presence of multiple porosities upon elevated seabed (Figure 6.6b). Increase in the  $d/h_1$  shows the oscillatory pattern in  $K_r$  within  $0^\circ \leq \theta \leq 65^\circ$  and afterward a sharp increase in  $K_r$  is noted for all the  $d/h_1$ . The increase in  $d/h_1$  shows the increase in  $K_r$  within  $0.5 \leq d/h_1 \leq 2$ , thereafter the rise in  $d/h_1$  shows the uniform estimation in  $K_r$  within  $2 \leq d/h_1 \leq 3$  due to the rise in energy damping and structural width. Similarly, the increase in  $d/h_1$  shows the gradual decrease in  $K_t$ , which suggests that the energy damping is higher for high structural width  $d/h_1$ . Thus, the study suggests that the structural width within  $2 \leq d/h_1 \leq 2.5$  is preferable to regulate incoming waves using a multi-layered porosity concept.

#### **6.4.2 Porous structure backed by the leeward wall with variation in seabed**

In general, the mainlands near beaches are protected with the seawalls. Usually, the full-wave reflection takes place at the seawall (due to zero porosity), which affects the life span of seawall due to high wave force acting on the wall. To reduce the wave force on seawall, seaside wave energy absorber is introduced (Madsen, 1983; Mallayachari and Sundar, 1994; Das and Bora, 2014c). But the porous absorber consisting of uniform porosity occupies more space and reflects more incoming waves (Milgram, 1970; Twu et al., 2001). To reduce the wave reflection, the force acting on the seawall and to



increase the energy damping, an attempt is made in the present study using the stratified or multi-layered porous structure concept with variation in the seabed characteristics. In the present section, the width between the seawall and multi-layered porous structure is considered to be zero.

#### 6.4.2.1 Effect of structural width

In this section, the stratified porous structure with the leeward wall is analysed using the assumption of linearized water wave theory. Similar to the earlier condition, the structure is separated into three layers for the simplicity of the problem. Numerical computation is performed for finding the  $K_r$  for the single-layer porous structure as in Mallyachari and Sundar (1994). The results obtained using the present study agree well with the available results as in Mallyachari and Sundar (1994) in Figure 6.7(a). Further, the multi-layer technique in a single porous structure is employed considering the three configurations  $C_5$ ,  $C_6$  and  $C_7$  as in Table 2. The configuration  $C_5$  is similar to the Mallyachari and Sundar (1994) and, the variation between the  $C_5$ ,  $C_6$  and  $C_7$  configurations is discussed in detail. It is observed that the decrease in  $K_r$  is achieved for  $C_6$  and  $C_7$  configurations as compared with Mallyachari and Sundar (1994) due to the multi-layered concept. The configuration  $C_6$  and  $C_7$  show the 18% and 34% reduction in  $K_r$  at  $\gamma_{10}d = 5$  as compared with Mallyachari and Sundar (1994) for the fixed average structural porosity.

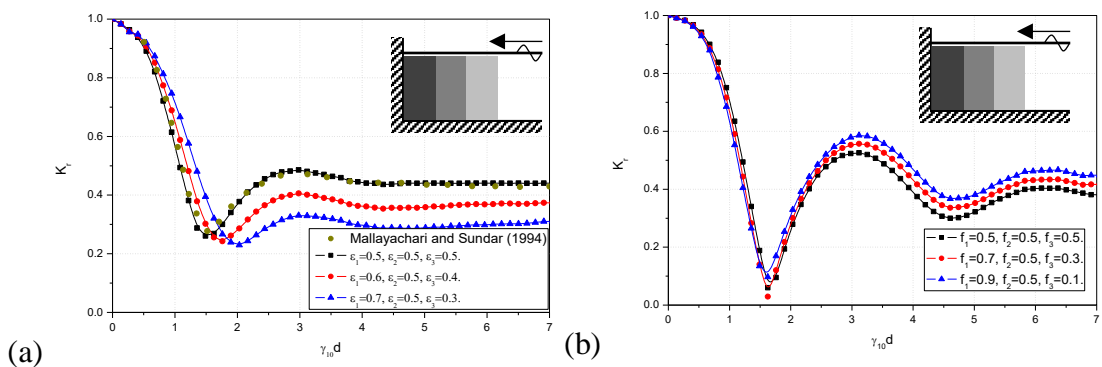


Figure 6.7: The  $K_r$  versus  $\gamma_{10}d$  for different (a) porosity with  $f = 1$  and (b) friction factor with  $\epsilon = 0.5$  considering  $\omega = 0.3630$ .

The minimum  $K_r$  is noted for all the configurations within  $1.2 \leq \gamma_{10}d \leq 2.2$  which may be due to the formation of standing waves in that particular range. On the other hand, the significance of multiple friction factors in a single porous structure is revealed by

considering a porous structure with three layers lying on the uniform seabed as in Figure 6.7(b). The three configurations  $C_{10}$ ,  $C_{11}$  and  $C_{12}$  as in Table 2 are compared and the global minima in  $K_r$  for all the configurations are observed at  $\gamma_{10}d = 1.6$ . Afterwards, the resonating pattern is noted for the three configurations with the increase in  $\gamma_{10}d$ . A little increase in  $K_r$  is observed in the presence of multiple friction factors as compared with the porous structure having uniform friction factor and the variation is minimum in  $K_r$  in the presence of multiple friction factors (Figure 6.7b) compared with multiple porosities (Figure 6.7a). But, porous structure with multiple porosities and uniform friction factor shows the significant variation in  $K_r$  as compared with porous structure with uniform porosity and multiple friction factors. In the absence of the leeward wall, the wave reflection for lower values of  $\gamma_{10}d$  is minimum but in the presence of leeward wall, the wave reflection is maximum for lower values of  $\gamma_{10}d$  due to the consideration of zero velocity near the wall. The study suggests that the waves with higher wavelengths can be completely reflected with the seawalls and the porous structure composed of multiple vertical porous layers is useful for reducing the wave impact on the vertical wall.

#### **6.4.2.2 Effect of multiple porosities**

In Figure 6.8(a,b), the wave reflection  $K_r$  and wave force acting on the seaside porous layer  $K_{fs}$  versus dimensionless structural width  $d/\lambda$  is analysed for the case of uniform seabed in the presence of three-layer porous media under oblique wave impinging. Figure 6.8(a) illustrates  $K_r$  and  $K_{fs}$  versus  $d/\lambda$  for  $\gamma_{10}h_1 = 1$  considering three different configurations such as  $C_5$ ,  $C_6$  and  $C_7$  as in Table 2. The configuration  $C_5$  shows the high reflection  $K_r$  and configuration  $C_6$  and  $C_7$  shows minimum  $K_r$  compared with configuration  $C_5$ . It may be noted that the local optima are observed, which may be due to the minimum friction factor and the destructive structural interference. More oscillations are observed due to the consideration of multiple porosities for configuration  $C_6$  and  $C_7$  as compared with configuration  $C_5$ , which shows that the fluid-voids mechanism inside the porous medium. It may be due to the transmitted wave from the first layer getting reflected back by the second layer towards

the open water region due to the less porosity in the second layer as depicted in Figure 6.8(a). A similar trend is observed in the case of wave force on the seaside porous layer  $K_{fs}$ . The decrease in  $K_{fs}$  is observed with an increase in porosity of the seaside porous layer and  $K_{fs} > 1$  for the configuration C<sub>5</sub> due to the higher wavelength and minimum porosity compared with configuration C<sub>6</sub> and C<sub>7</sub>. Figure 6.8(b) shows the  $K_r$  and  $K_{fs}$  versus  $d/\lambda$  for  $\gamma_{10}h_1 = 1.5$  in the presence of multiple porosities. The increase in  $\gamma_{10}h_1$  from  $\gamma_{10}h_1 = 1$  to  $\gamma_{10}h_1 = 1.5$  shows the minimal decrease in  $K_r$  and high variation in  $K_{fs}$  as compared with Figure 6.8(a). In Figure 6.8(b) the occurrences of local optima is limited and observed within  $0.1 < d/\lambda < 1.5$ . Afterwards, the uniform values in  $K_r$  and  $K_{fs}$  is observed within  $1.5 < d/\lambda < 2$  which may be due to the decrease in wavelength as compared with previous case (Figure 6.8a).

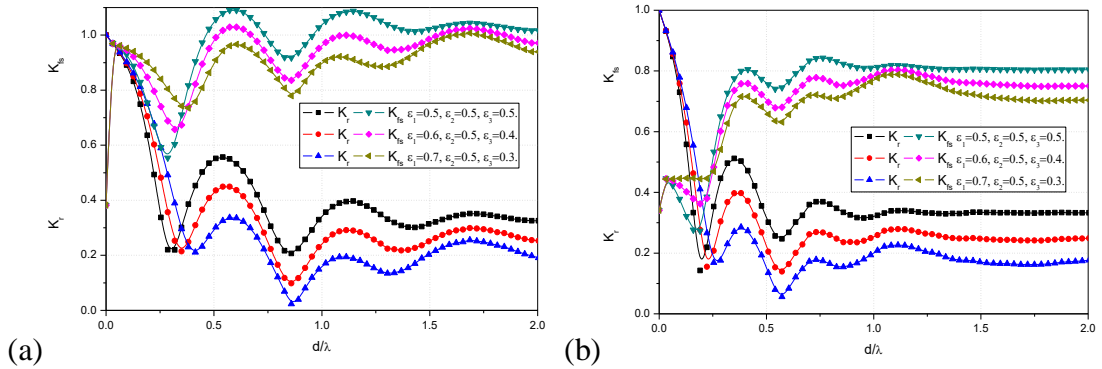


Figure 6.8: The  $K_r$  and  $K_{fs}$  versus  $d/\lambda$  for varying structural porosity on the uniform seabed for (a)  $\gamma_{10}h_1 = 1.0$  and (b)  $\gamma_{10}h_1 = 1.5$  considering  $f = 0.25$  and  $\theta = 30^\circ$ .

#### 6.4.2.3 Effect of seabed characteristics

The influence of seabed variation (uniform, elevated and stepped seabed) on the wave transformation is analysed for the variable angle of incidence. In the case of the uniform seabed, water depth in each of the regions ( $h_j/h_1 = 1$  for  $j = 2, 3, 4$ ) is assumed to be the same but in the case of the elevated seabed, the elevated seabed height is considered as 20% ( $h_j/h_1 = 0.8$  for  $j = 2, 3, 4$ ) in the open water depth. In the case of the stepped seabed, each step height is considered to be 10% in open water depth given by  $h_2/h_1 = 0.9$ ,  $h_3/h_1 = 0.8$  and  $h_4/h_1 = 0.7$ . The Figure 6.9(a,b) shows the  $K_r$  versus  $\theta$

for the various dimensionless thickness of multi-layered structure  $d/h_1 = 2$  (Figure 6.9a) and  $d/h_1 = 4$  (Figure 6.9b) with variation in seabed characteristics. The three-layered porous structure due to variation in seabed characteristics is analysed considering individual porosity and friction factor in each layer as in configuration C<sub>13</sub>. In the case of  $d/h_1 = 2$  (Figure 6.9a) and  $d/h_1 = 4$  (Figure 6.9b), the local minima are observed at  $58^\circ$ ,  $60^\circ$  and  $66^\circ$  for uniform, elevated and stepped seabed and it is termed as critical angle where the minimum reflection occurs. The variation in  $K_r$  due to uniform, elevated and stepped seabed is predominant with  $0^\circ \leq \theta \leq 70^\circ$  as in Figure 6.9(a,b). The uniform seabed shows the minimum estimation in  $K_r$ , compared with elevated and stepped seabed characteristics due to trapping of more wave energy inside the porous structure, which causes high wave force on the seawall and the elevated seabed shows the high estimation in  $K_r$  due to the constructive interferences. But the stepped seabed shows high  $K_r$  compared with the uniform seabed and low  $K_r$  compared with the elevated seabed, which suggests that the stepped seabed will be useful to achieve the better values in  $K_r$  due to the destructive interferences in the presence of the multi-layered porous structure.

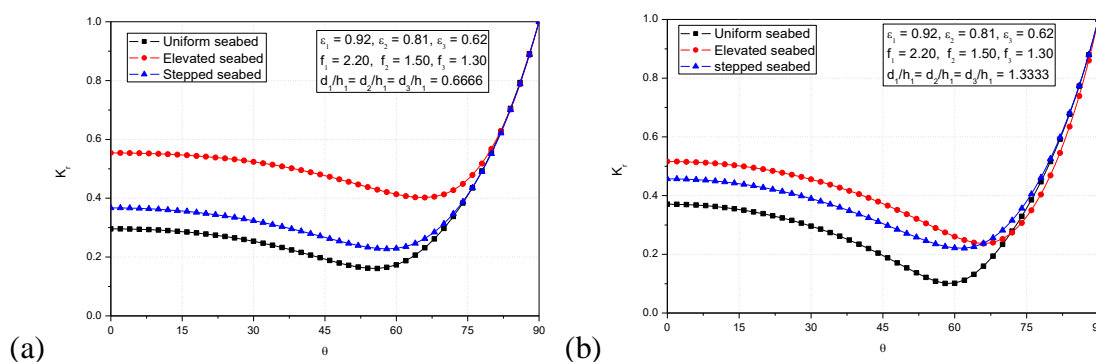


Figure 6.9: The  $K_r$  versus  $\theta$  for varying seabed characteristics in the case of (a)  $d/h_1 = 2$  and (b)  $d/h_1 = 4$  considering  $\gamma_{10}h_1 = 0.75$ .

The porous structures and seawalls are constructed very close to the shoreline, where the depth of the water is shallow. However, it is important to study and evaluate the porous structure with the leeward wall under the assumption of the shallow water-wave theory. The study is performed by considering various types of seabed characteristics, friction factors in the presence of uniform porosity. Total nine steps are modelled and

each step height is considered to be  $0.05h_1$  and the variation between seaside and leeside open water regions is  $h_{10}/h_1 = 0.5$  for stepped seabed condition. In the case of the elevated seabed, the step height is considered to be 50% ( $h_{10}/h_1 = 0.5$ ) in the open water depth. Figure 6.10(a,b) shows the variation in  $K_r$  with variation in  $\gamma_{10}h_1$  for the various types of seabed characteristics for long-wave approximation.

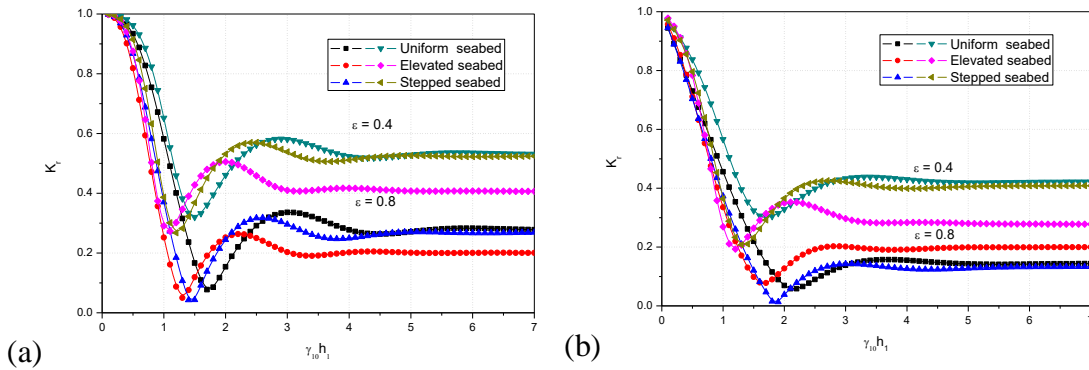


Figure 6.10: The  $K_r$  versus  $\gamma_{10}h_1$  for varying seabed characteristics in the case of (a)  $\theta = 0^\circ$  and (b)  $\theta = 45^\circ$  considering  $f = 1$  and  $d/h_1 = 1$ .

Figure 6.10(a) presents the sharp decrease in  $K_r$  for three types of the seabed and the global minima are observed within  $1 < \gamma_{10}h_1 < 2$  which may be due to the formation of standing waves at that particular range. It is observed that the elevated seabed shows the minimum reflection in the presence of normal wave incidence  $\theta = 0^\circ$  for  $\varepsilon = 0.4$  and  $\varepsilon = 0.8$ . The uniform seabed shows high wave reflection as compared with elevated and stepped seabed as in Figure 6.10(a). But in the case of oblique wave impinging  $\theta = 45^\circ$  (Figure 6.10b) the minimum reflection is observed for elevated seabed considering  $\varepsilon = 0.4$ . However, high reflection due to the presence of elevated seabed is obtained for  $\varepsilon = 0.4$  as compared with the uniform seabed and stepped seabed. From all the cases, it is noted that the uniform seabed shows a higher reflection coefficient and stepped seabed shows moderate reflection as compared with the elevated seabed. This may be due to the wave blocking when the incident wave interacts with the rigid bodies (elevated and multiple rigid steps). This suggests that the seabed characteristics, porosity and angle of incidence play a key role in the wave trapping in the case of the shallow water depth.

### 6.4.3 Porous structure away from the leeward wall with variation in seabed

As a special case, the offshore breakwater away from the seawall is studied in the presence of multiple porous layers. The gap between the multi-layered porous structure and seawall is termed as trapping chamber  $L/h_1$  and the role of the trapping chamber  $L/h_1$  in the wave trapping is examined.

#### 6.4.3.1 Effect of trapping chamber length

In Figure 6.11(a,b), the wave reflection  $K_r$  versus non-dimensional trapping chamber  $L/h_1$  is plotted in the presence of multiple porosities. Three configurations such as C<sub>5</sub>, C<sub>7</sub> and C<sub>8</sub> are analysed for  $\gamma_{10}h_1 = 0.5$  (Figure 6.11a) and  $\gamma_{10}h_1 = 1.0$  (Figure 6.11b).

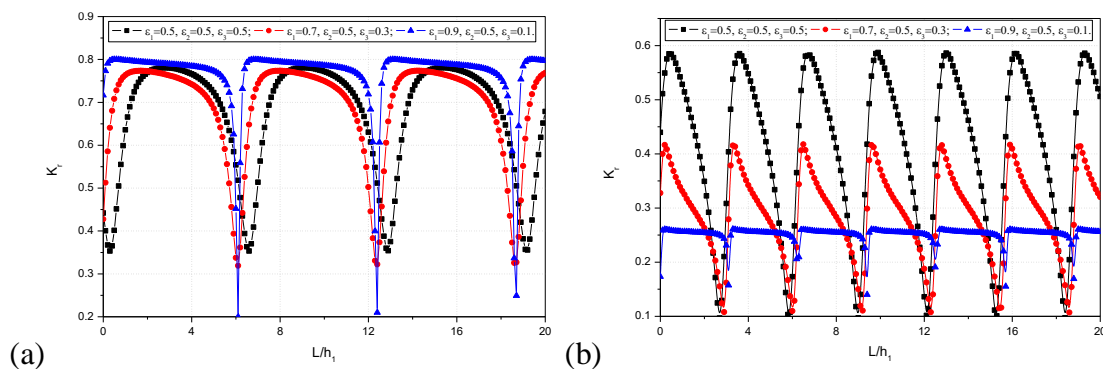


Figure 6.11: The  $K_r$  versus  $L/h_1$  for various values of structural porosity placed on uniform seabed for (a)  $\gamma_{10}h_1 = 0.5$  and (b)  $\gamma_{10}h_1 = 1.0$  considering  $f = 0.25$ ,  $d/h_1 = 4$  and  $\theta = 0^\circ$ .

The increase in  $L/h_1$  shows the periodic crests and troughs in  $K_r$  in periodic intervals. It may be due to the formation of standing waves at particular intervals where the  $K_r$  is minimum. The influence of multiple porosities is considerable in the wave trapping for  $\gamma_{10}h_1 = 0.5$  (Figure 6.11a) and the variation of  $K_r$  is clearly noted for different structural configurations. In the case of  $\gamma_{10}h_1 = 1$  (Figure 6.11b) the multiple porosities play a significant role in reducing the  $K_r$  due to high energy damping by the multi-layered porous structure. The three configurations present the periodic peaks and troughs in the  $K_r$  with the increase in  $L/h_1$ . The configuration C<sub>5</sub> shows the higher values in wave reflection  $K_r$  as compared with the remaining two configurations. But

the third configuration  $C_8$  shows an almost 58% decrease in wave reflection  $K_r$  at every resonating peak. This is due to the enhance in wave damping and high wave interaction between the porous structure and incident wave due to the high porosity  $\varepsilon_1 = 0.9$  in the seaside porous layer and the low porosity in the leeside porous layer  $\varepsilon_3 = 0.1$  for  $\gamma_{10}h_1 = 1$ .

#### 6.4.3.2 Effect of structural width

In Figure 6.12(a,b), the effect of structural width  $d/h_1$  on wave reflection  $K_r$  is studied considering three structural configurations such as  $C_5$ ,  $C_7$  and  $C_8$  as in Table 2 in the presence of the uniform seabed for a stratified porous structure placed far away from the wall. The average porosity of the three configurations  $C_5$ ,  $C_7$  and  $C_8$  are similar and configuration  $C_8$  shows the minimum values in the wave reflection  $K_r$  compared with the configuration  $C_5$  and  $C_7$  with minor oscillations due to the increase in energy damping. Eventually, the wave reflection  $K_r$  pattern is unchanged and observed similar as in Section 6.4.2. (Figure 6.8a,b). The high seaward porosity shows little oscillations in the wave reflection  $K_r$  but low seaward porosity shows the uniform estimation in wave reflection  $K_r$  after the resonating trough. The present study suggests that the high porosity in the seaside porous layer and lower porosity in the leeside porous layer is a preferable option for the high energy damping and low wave reflection by the stratified porous structure.

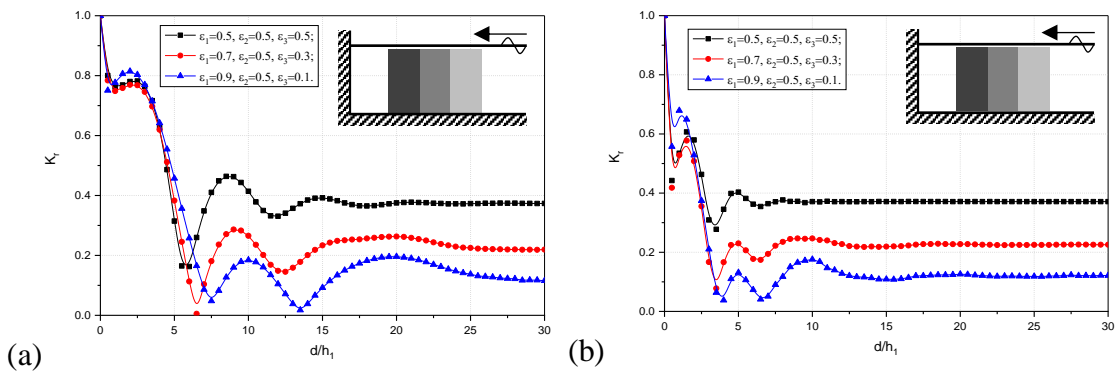


Figure 6.12: The  $K_r$  versus  $d/h_1$  for various values of structural porosity placed on uniform seabed for (a)  $\gamma_{10}h_1 = 0.5$  and (b)  $\gamma_{10}h_1 = 1.0$  considering  $f = 0.5$ ,  $L/h_1 = 1$  and  $\theta = 0^\circ$ .

### 6.4.3.3 Effect of seabed characteristics

The wave reflection  $K_r$ , due to the variation in seabed characteristics (uniform, elevated and stepped seabed) in the presence of multiple porosities as in configuration C<sub>8</sub> is examined with variation in trapping chamber  $L/h_1$  for finite water depth. The elevated step height is considered to be 40% in the open water region ( $h_2/h_1 = 0.6$ ) and stepped seabed between the two open water regions are considered as  $h_5/h_1 = 0.6$  (where  $h_2/h_1 = 0.9$ ,  $h_3/h_1 = 0.8$ ,  $h_4/h_1 = 0.7$ ).

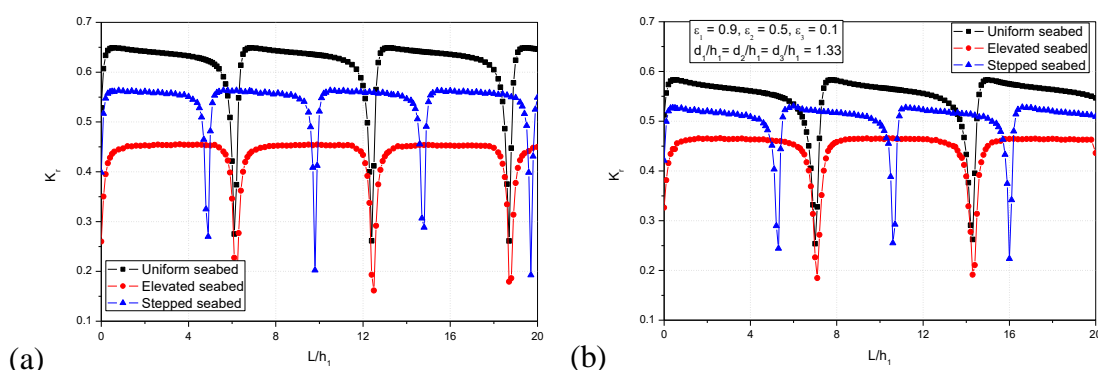


Figure 6.13: The  $K_r$  versus  $L/h_1$  for various seabed cases with multiple porosities in the case of (a)  $\theta = 0^\circ$  and (b)  $\theta = 30^\circ$  considering  $f = 0.5$ ,  $\gamma_{10}h_1 = 0.5$  and  $d/h_1 = 4$ .

The normal wave incidence  $\theta = 0^\circ$  (Figure 6.13a) and oblique wave incidence  $\theta = 30^\circ$  (Figure 6.13b) are studied considering stratified porous structure away from the leeward wall. The resonating peaks and troughs are obtained with increase in  $L/h_1$  and, the uniform seabed shows high  $K_r$ , as compared with elevated and stepped seabed characteristics as in Figure 6.13(a,b). In the previous cases, it is observed that the elevated seabed shows high  $K_r$ , but in the presence of stratified structure away from the wall, the elevated seabed shows the minimum  $K_r$ , for normal wave incidence  $\theta = 0^\circ$  (Figure 6.13a) and oblique wave incidence  $\theta = 30^\circ$  (Figure 6.13b) which is due to more wave trapping within the confined region  $L/h_1$  in the presence of rigid elevated step. But in the case of uniform and stepped seabed, the incident wave freely propagates between the confined region and structure region. But in the case of the elevated seabed, seabed variation in the leeward region ( $h_4/h_5 = 0.6$ ) shows more impact on wave trapping due to the presence of leeward confined region. However, the significant



decrease in  $K_r$  is obtained for oblique wave impinging  $\theta = 30^\circ$  (Figure 6.13b) compared with normal wave impinging  $\theta = 0^\circ$  (Figure 6.13a) in the case of the uniform, elevated and stepped seabed due to the increase in the energy damping by the stratified porous structure.

In Figure 6.14(a,b) the wave reflection  $K_r$  and wave force acting on the seawall  $K_{fw}$  is studied considering the change in seabed condition for the full solution (Figure 6.14a) and long-wave approximation (Figure 6.14b) with variation in the angle of incidence  $\theta$ . The comparative study is presented between full solution and long-wave approximation considering multiple porosities for configuration C<sub>9</sub> in Table 2. Three seabed conditions such as uniform seabed, elevated seabed (50% elevated step height) and stepped seabed (wherein  $h_2/h_1 = 0.875$ ,  $h_3/h_1 = 0.75$ ,  $h_4/h_1 = 0.625$  and  $h_5/h_1 = 0.5$ ) are examined for the stratified porous structure. The minor values in  $K_r$  and  $K_{fw}$  is obtained for stepped seabed case as compared with uniform and elevated seabed conditions in the case of finite water depth (Figure 6.14a) and long-wave approximation (Figure 6.14b).

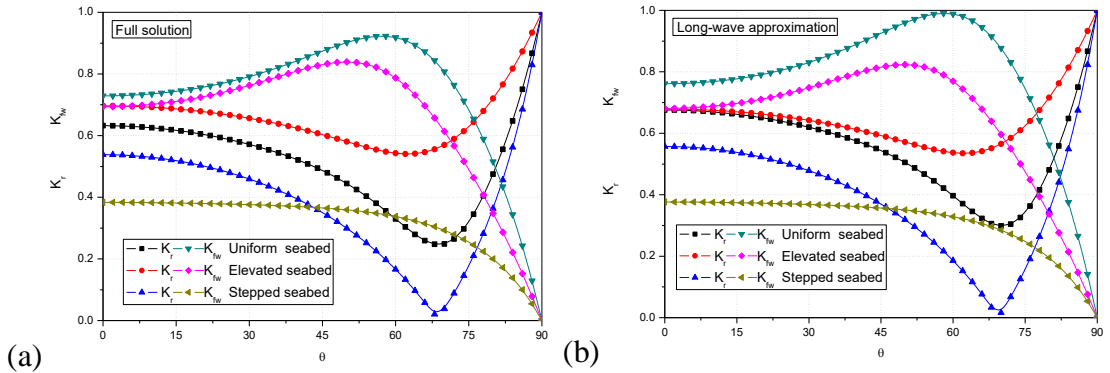


Figure 6.14: The  $K_r$  and  $K_{fw}$  versus  $\theta$  for varying seabed condition with multiple porosities for (a) finite water depth and (b) long-wave approximation considering  $d/h_1 = 2$ ,  $L/h_1 = 2$ ,  $\gamma_{10}h_1 = 0.5$  and  $f = 1$ .

In general, the uniform seabed allows the maximum waves to interact with seawall but the elevated and stepped seabed usually destruct the incident waves and reduces the wave force acting on the seawall. Especially, the minimum values of  $K_{fw}$  in the presence of stepped seabed are achieved only due to the interaction between incident waves and each impermeable step. Further, the structure in finite water depth (Figure

6.14a) shows the minor estimation in  $K_r$  and  $K_{fw}$  as compared with the long-wave approximation and variation is evident in the critical angle range within  $60^\circ < \theta < 75^\circ$  due to the least damping offered by the structure for long-wave approximation (Dalrymple et al., 1991). Hence, it is concluded that the seabed characteristics show a significant variation in wave transformation and minimum values in  $K_r$  and  $K_{fw}$  is achieved with variation in the angle of incidence in the presence of multiple porosities for finite water depth as compared with long-wave approximation.

#### 6.4.4 Wave motion over elevated and stepped bottom

In the present section, the wave motion over elevated/stepped seabed is studied without considering stratified porous structure to understand the wave scattering phenomenon. The problem formulation remains the same as defined in the previous section and the study is performed considering each structure porosity  $\varepsilon_j = 1$  and friction factor  $f_j = 0$ .

##### 6.4.4.1 Effect of elevated rigid bar height

In Figure 6.15(a,b) the wave reflection  $K_r$  and transmission coefficients  $K_t$  versus structural width  $d/h_1$  is presented for change in rigid bar height. The periodic crests and minimal wave reflection is observed for certain values of  $d/h_1$ .

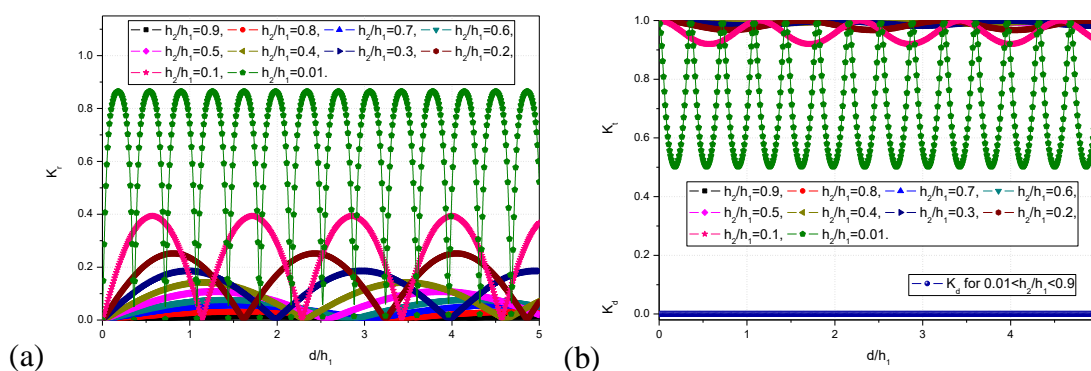


Figure 6.15: (a)  $K_r$  and (b)  $K_t$  and  $K_d$  versus  $d/h_1$  for varying bottom rigid bar height in the absence of the porous structure considering  $f_1 = 0$ ,  $\varepsilon_1 = 1$ ,  $\gamma_{10}h_1 = 1$  and  $\theta = 30^\circ$ . On the other hand, in Figure 6.15(b), the periodic troughs and almost unity in wave transmission are noticed with the increase in dimensionless width of the rigid bar. The periodic crests and troughs in  $K_r$  and  $K_t$  are observed for the same intervals, which suggest that the submerged rigid bar can perform either minimal  $K_r$  or minimal  $K_t$

due to the zero-energy damping. The  $K_d$  is observed to be zero for all the combination of the rigid bar height within  $0.01 \leq h_2 / h_1 \leq 0.9$ . This is a common phenomenon in the vicinity of wave interaction with rigid structures (Chwang and Chan, 1998; Wang et al., 2006; Praveen et al., 2020). However, the increase in rigid bar height enhances the  $K_r$  and reduces the  $K_t$  and also increases the number of peaks/troughs in the wave transformation. The variation in  $K_r$  and  $K_t$  is minimal for minimal rigid bar height and increase in rigid bar height is evident in the wave reflection. In general, the wave potential is very high near the free surface and, if the oblique wave interacts with the rigid bodies, there exists either reflection or transmission. Particularly, the step height within  $0.01 \leq h_2 / h_1 \leq 0.3$  shows an effective role in reflecting the incident waves. Specifically, in the case of rigid rectangular/vertical structures, the vortex formation develops at the edge/tip of the rigid bars and effectively reduces the  $K_t$  (Ting and Kim, 1994; Yip et al., 2002). In the case of  $h_2 / h_1 = 0.01$ , the rigid bar height reaches very near to the free surface and the oscillations in  $K_r$  and  $K_t$  is observed increasing and is very significant for the design of rigid structures. However, in all the cases, the wave damping is observed to be zero and satisfies the energy balance relation  $K_r^2 + K_t^2 = 1$ . It is also noted that the variation between elevated and stepped seabed in the absence of porous structure is very minimal for fixed width and depth of the structure but there exists a small variation in resonating peaks and troughs. In the presence of the porous structure, the elevated step height within  $0.7 \leq h_2 / h_1 \leq 1$  shows a significant impact on wave scattering as compared with the uniform seabed, but in the absence of porous structure, the step height within  $0.7 \leq h_2 / h_1 \leq 1$  shows minimal impact on  $K_r$  and  $K_t$ . In the presence of porous structure placed on elevated step within  $0.7 \leq h_2 / h_1 \leq 1$  shows significant role in enhancing the  $K_r$  as compared with uniform seabed due to the additional wave reflection in the presence of impermeable elevated seabed.

#### **6.4.4.2 Effect of leeward rigid bar height**

The wave reflection due to stepped seabed in the absence of a stratified porous structure is examined for variable leeward rigid bar height in Figure 6.16(a). Three rigid steps are considered having  $h_2 / h_1 = 0.5$  and  $h_3 / h_1 = 0.25$  with the rigid leeward bar  $h_4 / h_1$

varied within  $0.01 \leq h_4 / h_1 \leq 0.2$ . The lower values of leeward rigid bar height (Figure 6.16a) shows the moderate values in  $K_r$  and the increase in  $h_4 / h_1$  enhances the  $K_r$  along with resonating peaks. Especially, for  $h_4 / h_1 = 0.01$  the rigid bar height almost reaches the free surface and the number of resonating peaks and troughs are observed to be high, as the rigid leeward bar behaves like a sea wall and reflects the incident waves towards the seaward regions. However, the resonating troughs in the  $K_r$  are also evident, which may be due to the overtopping of incident waves.

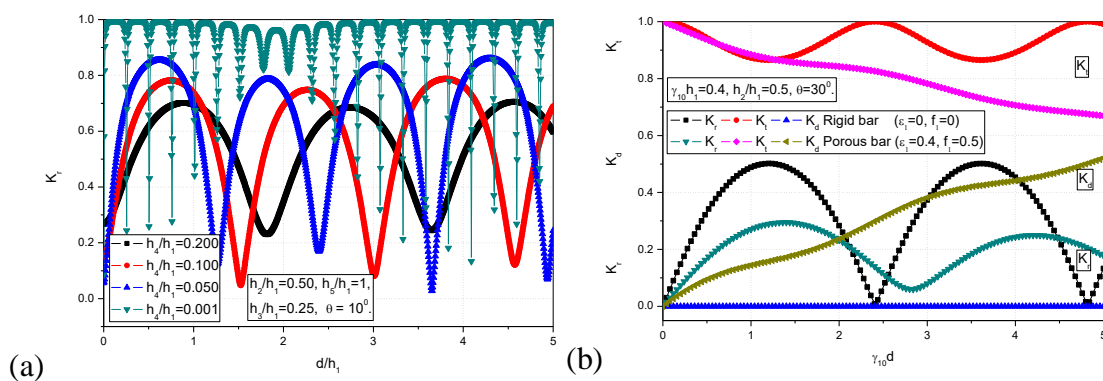


Figure 6.16: (a)  $K_r$  versus  $d / h_1$  for varying bottom leeward step height without porous structure considering  $\gamma_{10}h_1 = 1.5$ , (b) the  $K_r$ ,  $K_t$  and  $K_d$  versus  $\gamma_{10}d$  for permeable and impermeable submerged bars considering  $\gamma_{10}h_1 = 0.4$  and  $\theta = 30^\circ$ .

#### 6.4.4.3 Comparative study between the elevated porous and impermeable bar

In Figure 6.16(b), the  $K_r$ ,  $K_t$  and  $K_d$  versus  $\gamma_{10}d$  is examined for an elevated rigid bar and elevated porous bar. The elevated porous bar is deeply submerged and the porous bar is examined using the classical formulation presented in Losada et al. (1996). The width and height of the rigid/porous bar are considered identical for the purpose of comparison. The elevated rigid bed and stepped bed shows an almost similar pattern in the wave scattering, and a minimal change along with a forward shift in the  $K_r$  and  $K_t$  is observed between the elevated and stepped bed. Thus, for the sake of clarity in the comparative study, the elevated rigid bar and porous bar effect on wave transformation is reported (Figure 6.16b). The rigid bar shows high  $K_r$  as compared with a porous bar and, the  $K_t$  is varying very near to the unity for the rigid bar, but a decreasing pattern is obtained in the  $K_t$  for the porous bar. Similarly, the zero values of  $K_d$  is obtained

for a rigid bar (which satisfies the relation for wave motion over rigid bodies  $K_r^2 + K_t^2 = 1$  or  $K_d = 0$ ), but an increasing pattern in  $K_d$  is achieved for the porous bar. It is well known that the rigid bodies are effective in reflecting the incident waves and the porous structures are effective in wave damping. Hence, it is clear that the porous structures can perform a significant energy damping and the natural rigid elevated bed can reflect the incident waves. On comparing with the previous case (Figure 6.15a,b), the  $K_r$  and  $K_t$  is observed minimal for the elevated rigid bar, but in the present case (Figure 6.16b), the  $K_r$  is significant which is due to the reduction in the  $\gamma_{10}h_1$  from  $\gamma_{10}h_1 = 1$  (Figure 6.15a,b) to  $\gamma_{10}h_1 = 0.4$  (Figure 6.16b).

## 6.5 CLOSURE

The hydrodynamic performance of a stratified porous structure in the absence and presence of a leeward wall is studied under the assumption of linearized water wave theory. The matched eigenfunction expansion technique is employed to examine the significance of the multi-layered porous structure in wave blocking. The following conclusions are drawn from the present analysis:

- The theoretical outcomes for the two-layered and three-layered porous structure agree well with the experimental results presented by Twu and Chieu (2000) placed on the uniform seabed.
- High wave energy damping  $K_d > 95\%$  is achieved for multi-layered porous structure concept and the stratified porous structures can effectively perform as wave dampers if the width of the structure is of the order  $\gamma_{10}d \geq 2$ .
- The 20%, 34% and 55% decrease in  $K_r$  is obtained for the stratified porous structure as compared with Liu and Li (2013) and a 34% decrease in the wave transmission is achieved in the presence of elevated bottom with the increase in the friction factor from 0.25 to 2.
- The 18% and 34% reduction in the  $K_r$  is obtained for the stratified porous structure backed by an impermeable wall as compared with Mallayachari and Sundar (1994).

- The performance of a porous structure with multiple porous layers placed on stepped seabed shows better results in  $K_r$ , as compared with uniform and elevated seabed backed by the wall.
- The 58% reduction in  $K_r$  is obtained with variation in  $L/h_1$  at every resonating peak for multi-layered porous structure away from the leeward wall as compared with the porous structure of uniform porosity.
- The minor values of wave reflection are observed for a stratified porous structure placed away from the vertical wall for normal wave incidence.
- The construction of a seawall in the presence of a stratified porous structure will be useful for reflecting the waves of higher wavelengths.
- The stepped seabed away from the leeward wall shows the minor values in the wave reflection and wave force within  $60^\circ < \theta < 75^\circ$  for finite water depth and long-wave approximation.
- The minimum values in  $K_r$  and  $K_{fw}$  are achieved for finite water depth as compared with long-wave approximation due to the least damping by the stratified porous structure.
- The increase in rigid bar height (in the absence of porous structure) encourages the periodic crests and troughs in  $K_r$  and  $K_t$ . However, the  $K_d$  is observed to be zero for all the combinations of rigid bar height without porous structure.
- The leeward rigid step height shows a significant impact on enhancing the wave reflection. The elevated seabed and stepped seabed presents almost uniform estimation in the absence of a porous structure.
- Overall, the energy damping can be achieved with the porous structures and, the stratified porous structure can perform high energy damping and wave blocking due to the presence of multiple porosities.

# CONCLUDING REMARKS AND FUTURE WORK

### 7.1 GENERAL INTRODUCTION

The wave scattering by various types of structures such as multiple porous structures placed on the uniform seabed, elevated seabed in the presence and absence of seawall, barrier-rock porous structures, multiple horizontally and vertically stratified porous structures in the absence and presence of various seawalls (vertical wall, permeable wall and stepped seawall) are analysed using eigenfunction expansion method. The matching equations and mode-coupling relation are used to analyse the various types of porous structures. The wave reflection, transmission, energy damping, wave force experienced by seaward, leeward structural interfaces and wave force acting on the seawall are reported. The effect of structural porosity, friction factor, angle incidence, free spacing, width, dimensionless wavenumber, trapping chamber and number of porous structures on wave scattering and wave trapping is presented. In the preliminary stage, the analytical results obtained from the present study are validated with the experimental, analytical and numerical results reported by several authors.

### 7.2 SUMMARY OF THE RESEARCH WORK

The summary of the research work performed in the present study is discussed briefly are as follows:

#### 7.2.1 Wave damping by multiple porous structures

The 42% decrease in  $K_r$  is achieved with a pair of porous structures as compared with a single porous structure. Afterward, the uniform estimation in  $K_r$  is obtained with an increase in multiple structures within  $3 \leq N \leq 5$  for fixed structural thickness. The double porous structures show a drastic variation in reducing the wave force impact on the leeward wall compared with a single structure. The triple porous structure shows a considerable decrease in  $K_{fw}$  compared with the double structure for minimum porosity within  $0.3 \leq \varepsilon \leq 0.4$  at each resonating peak. Thereafter, the elevated seabed impact on

wave scattering is presented and the 10%-20% rigid bed height is suggested for effective wave damping by multiple porous structures.

### **7.2.2 Wave scattering by barrier-rock porous structures**

The analytical relations are derived and reported for finding the  $K_r$  and  $K_t$  by barrier-rock porous structure with finite thickness, structure away from the leeward wall, structure backed by wall and structure of semi-infinite thickness placed on step-bottom. Further, the analytical relations are also proposed for investigating the scattering performance of porous structures without vertical barriers. The barrier-rock porous structure placed on a rigid step, and the step height within  $0.8 \leq h_2 / h_1 \leq 0.9$  is suggested for effective wave damping. The finite structure with/without seawall behaves as a semi-infinite barrier-rock porous structure as the ratio of barrier-rock porous structure width and incident wavelength reaches to unity/higher (i.e  $d / \lambda \geq 1$ ).

### **7.2.3 Wave damping by horizontally stratified porous structures**

The increase in surface layer depth shows the surge in energy damping due to high surface layer porosity. The 31.9% reduction in wave reflection is obtained with the increase in the surface layer porosity at the resonating crest. The angle of contact  $\theta = 30^\circ$  shows the 16.3% reduction in  $K_r$  as compared with the normal angle of contact  $\theta = 0^\circ$  due to the increase in energy damping. Hence, it is better to construct the porous structure on determining the critical angle of contact for minimal wave reflection and high energy damping. The surface porous layer depth  $a_1 / h_2$  shows a significant impact in reducing the resonating peaks and troughs. The high resonating peak is observed for  $a_1 / h_2 = 0.2$  and 8% for  $a_1 / h_2 = 0.4$ , 21% for  $a_1 / h_2 = 0.6$ , 37% for  $a_1 / h_2 = 0.8$  the decrease in  $K_r$  is obtained as compared with  $a_1 / h_2 = 0.2$  for four porous structures. The multiple porous structures are useful if the structural width is higher. But, for fixed structural width (if one structure width is separated into with two structures), the resonating crests and troughs have a major role in reducing the  $K_r$  and  $K_t$ , thus the high values of  $K_d$  can be achieved. The double submerged two-layered structures show a significant reduction in  $K_r$  and  $K_t$  at each of the resonating troughs as compared



with the single structure for fixed width. The reduction of  $K_r$  and  $K_t$  is evident with the addition of the second structure as compared with the single structure. The addition of the second structure is effective within  $4 \leq d/h_1 \leq 12$  to obtain minimal wave transmission and high energy damping.

#### **7.2.4 Wave trapping by horizontally stratified porous structures**

The wave trapping performance of multiple horizontally stratified porous structures placed far away from the vertical wall, stepped wall and permeable wall are analysed. The trapping chamber shows a very minimal role in the case of the semi-infinite structure due to the higher structural width and high wave damping. The effect of the permeable wall is minimal on  $K_r$  in the presence of fully-extended porous structures as compared with submerged structures. The increase in rigid step width  $L_s/h_1$  (available in the stepped wall) shows a minimal variation in  $K_r$  in an oscillatory manner due to the zero flow condition. The permeable wall requires a high quantity of construction material as compared with the vertical and stepped wall. So, the present study suggests the stepped/vertical wall with stratified porous structures for the protection of the mainlands from oblique incident waves.

#### **7.2.5 Wave damping and wave trapping by vertically stratified porous structures**

The wave motion through a single porous structure consisting of multiple vertical porous layers is examined in the presence of uniform seabed, elevated seabed and stepped seabed. The theoretical outcomes for the two-layered and three-layered porous structure agree well with the experimental results presented by Twu and Chieu (2000) placed on the uniform seabed. High wave energy damping  $K_d > 95\%$  is achieved for multi-layered porous structure concept and the stratified porous blocks can effectively perform as wave dampers if the width of the structure is of the order  $d/h_1 \geq 2$ . The 20%, 34% and 55% decrease in  $K_r$  is obtained for the stratified porous block as compared with Liu and Li (2013), and 34% decrease in the wave transmission is achieved in the presence of elevated bottom with the increase in the friction factor from 0.25 to 2. Minimal porosity in the leeside porous layer is a preferable option for the better wave blocking and mainland protection. The 18% and 34% reduction in the  $K_r$ ,

is obtained for the stratified porous block backed by the impermeable wall as compared with Mallayachari and Sundar (1994). The significant wave trapping is obtained by vertically stratified porous structure placed on the elevated seabed as compared with the uniform seabed.

### **7.3 SIGNIFICANT CONTRIBUTION FROM THE RESEARCH WORK**

The present analytical study focused on wave scattering and wave trapping performance of several types of breakwaters which are of recent interest in Coastal Engineering. The major contribution from the present work reported in the thesis are as follows:

- The present study mainly focused on wave scattering and trapping performance of various types of breakwaters, which are existing in several locations.
- The direct analytical relations for finding wave reflection and transmission coefficients by various porous structures are reported and validated with the available solutions.
- The wave reflection, transmission, wave damping, wave force on the seaside, leeside of breakwater and wave force experienced by the vertical rigid wall in the presence of single/multiple porous structures are reported.
- The 42% reduction in wave transmission is achieved with double porous structures as compared with single porous structure for fixed structural width.
- The width of the semi-infinite porous structure is defined using the comparative study with the finite porous structure in the presence/absence of seawall. The ratio of incident wavelength to structural width approaches to unity  $d / \lambda = 1$ , then the conventional porous structure can be regarded as a semi-infinite structure.
- The seaward and leeward thin barriers with rockfill are proposed and investigated. The thin barriers are suggested for the protection of breakwaters, which is already constructed in Dongying bay breakwater China.
- The resonating peaks and troughs are obtained in the reflection coefficient with the change in the free spacing/trapping chamber. The resonating trough in  $K_r$  shows high fluid force on the rigid wall and resonating crest in  $K_r$  shows the minimal force on the rigid seawall.

- The horizontally multi-layered breakwater is effectively distributing the incident wave energy in the form of wave reflection and wave force experienced by seawall as compared with a conventional porous structure consisting of high/moderate structural porosity.
- The comparative study is performed between a vertical rigid wall, stepped wall and permeable wall in the presence of multiple porous structures. The study shows that the peak values of  $K_r$  are almost similar by each of the seawalls, but stepped seawall shows minor values of  $K_r$  in each of the resonating troughs.
- In the case of the vertically stratified porous structure, the tranquil zone is possible with the structure of high thickness.

#### **7.4 FUTURE SCOPE OF RESEARCH**

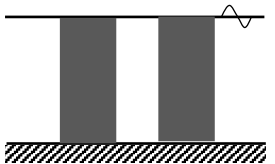
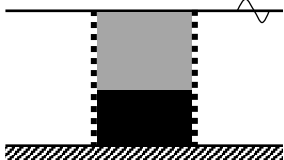
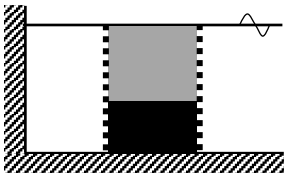
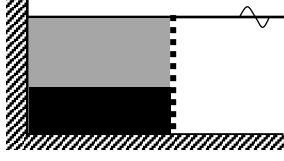
The possible extensions of the present study are as follows:

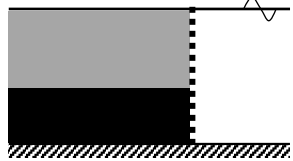
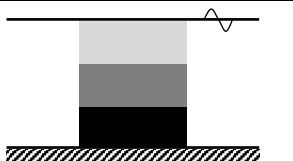
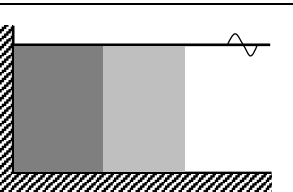
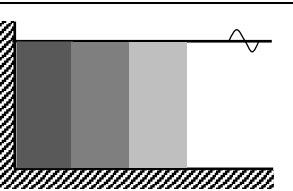
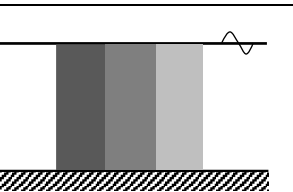
- The study can be extended for wave interaction with multiple porous structures in the presence of undulating bottom in both single and two-layer fluid.
- In the case of the horizontally stratified porous structure, two/three number of porous layers are analysed. More number of porous layers can be analysed for effective wave blocking.
- In all the cases, porous structures are placed on the rigid seabed. The porous seabed with multiple structures is recommended.
- Porous structures of various shapes in the presence of various seawalls, such as the curved wall, porous front wall and the sloping wall is recommended for future investigations.



## ANNEXURE

The direct analytical relations and significant conclusions from the Ph.D. Thesis are reported for further development of the marine structures.

Sl. No	Type of structure	Schematic diagram	Direct analytical equations/ Remarks
1.	Two porous structures		The 42% reduction of wave transmission is obtained for double porous structures as compared with single porous structure for identical structural width considering $f = 1$ , $\varepsilon = 0.4$ , $\gamma_{10}h = 1$ , $w/h = 1$ and $d/h = 2$ .
2.	Barrier-rock porous structure of finite thickness		$K_r = \left  \frac{R_{10}}{I_{10}} \right  = \frac{i \tan k_{20}d (X^2 - M_b^2 Q_L Q_L) + M_b X (Q_L - Q_L)}{i \tan k_{20}d (X^2 + M_b^2 Q_S Q_L) + M_b X (Q_L + Q_S)}$ $K_t = \left  \frac{T_{30}}{I_{10}} \right  = \frac{2EM_b \{ (1 - R_{10})(X - ik_{10}) - i\gamma_{10}G_1(1 + R_{10}) \}}{(M_b Q_L + X)(M_b - i\gamma_{10}G_1) - (M_b Q_L - X)(M_b + i\gamma_{10}G_1) E^2}$
3.	Barrier-rock porous structure placed far away from rigid wall		$K_r = \left  \frac{R_{10}}{I_{10}} \right  = \frac{i \tan k_{20}d (X^2 - M_b^2 Q_L Z_L) + M_b X (Z_L - Q_L)}{i \tan k_{20}d (X^2 + M_b^2 Q_S Z_L) + M_b X (Z_L + Q_S)}$
4.	Barrier-rock porous structure backed by a rigid wall		$K_r = \left  \frac{R_{10}}{I_{10}} \right  = \frac{X - (i\gamma_{10}G_1 - ik_{10})M_b \tan k_{20}d}{X + (i\gamma_{10}G_1 + ik_{10})M_b \tan k_{20}d}$

5.	Semi-infinite porous structures with seaward barrier		$K_r = \left  \frac{R_{10}}{I_{10}} \right  = \frac{X - (i\gamma_{10}G_1 - ik_{10})M_b}{X + (i\gamma_{10}G_1 + ik_{10})M_b}$
6.	Horizontally stratified porous structure		<p>The higher porosity in the surface porous layer, moderate porosity in the middle layer and zero porosity in the bottom layer is suggested for the optimal wave damping and wave blocking by the horizontally stratified porous structures.</p>
7.	Two-layered vertically stratified porous structure backed by wall		$K_r = \left  \frac{R_{10}}{I_{10}} \right  = \frac{\cos a_2 (m_1 m_3 - i \tan a_1) + i \sin a_2 (m_1 i \tan a_1 - m_3)}{\cos a_2 (m_1 m_3 + i \tan a_1) + i \sin a_2 (m_1 i \tan a_1 + m_3)}$
8.	Three-layered vertically stratified porous structure backed by wall		$K_r = \left  \frac{R_{10}}{I_{10}} \right  = \frac{\cos a_1 \cos a_2 (m_1 m_3 - m_2 i \tan a_3) - \sin a_1 \sin a_2 (m_1 - m_2 m_3 i \tan a_3) + i \sin a_1 \cos a_2 (m_1 m_2 m_3 i \tan a_3 - 1) + i \cos a_1 \sin a_2 (m_1 m_2 i \tan a_3 - m_3)}{\cos a_1 \cos a_2 (m_1 m_3 + m_2 i \tan a_3) - \sin a_1 \sin a_2 (m_1 + m_2 m_3 i \tan a_3) + i \sin a_1 \cos a_2 (m_1 m_2 m_3 i \tan a_3 + 1) + i \cos a_1 \sin a_2 (m_1 m_2 i \tan a_3 + m_3)}$
9.	Vertically stratified porous structure		<p>The stratified porous structures can effectively perform as wave dampers if the width of the structure is of the order <math>\gamma_{10}d \geq 2</math> in the presence of uniform seabed for <math>\varepsilon_1 = 0.85</math>, <math>\varepsilon_2 = 0.65</math>, <math>\varepsilon_3 = 0.45</math>, <math>f_1 = f_2 = f_3 = 1</math>, <math>\theta = 0^\circ</math> and <math>\gamma_{10}h_1 = 0.5</math>.</p>

## REFERENCES

- Abbott, M.B., McCowan, A. and Warren, I.R. (1981). Numerical modelling of free-surface flows that are two-dimensional in plan. In: Transport models for inland and Coastal Water. *Proc. Symposium on Predictive Ability. Academic Press.*
- Bayram, A. (2000). Experimental study of a sloping float breakwater. *Ocean Engineering*, 27(4), 445-453.
- Behera, H. and Khan, M.B. (2019). Numerical modeling for wave attenuation in double trapezoidal porous structures. *Ocean Engineering*, 184, 91-106.
- Behera, H. and Ng. C.O. (2017). Interaction between oblique waves and multiple bottom standing flexible porous barriers near a rigid wall. *Meccanica*, 53(4-5), 871-885.
- Behera, H. and Sahoo, T. (2014). Gravity wave interaction with porous structures in two-layer fluid. *Journal of Engineering Mathematics*, 87(1), 73-97.
- Behera, H., Sahoo, T. and Ng, C.O. (2016). Wave scattering by a partial flexible porous barrier in the presence of a step-type bottom topography. *Coastal Engineering Journal*, 58(03), 1650008.
- Belorgey, M., Rousset, J.M. and Carpentier, G. (2003). Perforated breakwaters, Dieppe harbour Jarlan Caisson: general schedule and acquired experience. *Proceedings of 13th International Offshore and Polar Engineering Conference. ISOPE, Honolulu, USA, 850-857.*
- Chen, H.B, Tsai, C.P. and Chiu, J.R. (2006). Wave reflection from vertical breakwater with porous structure. *Ocean Engineering*, 13, 1705-1717.
- Cheng, Y., Ji, C., Zhai, G. and Gaidai, O. (2016). Hydroelastic analysis of oblique irregular waves with a pontoon-type VLFS edged with dual inclined perforated plates. *Marine Structures*, 49, 31-57.
- Cho, I. H. and Kim, M. H. (2000). Interactions of horizontal porous flexible membrane with waves. *Journal of Waterway, Port, Coastal, and Ocean Engineering*, 126(5), 245-253.
- Cho, I. H. and Kim, M. H. (2008). Wave absorbing system using inclined perforated plates. *Journal of Fluid Mechanics*, 608, 1-20.
- Cho, I. H., Koh, H. J., Kim, J. R. and Kim, M. H. (2013). Wave scattering by dual submerged horizontal porous plates. *Ocean Engineering*, 73, 149-158.

Chwang, A.T. and Chan, A.T. (1998). Interaction between porous media and wave motion. *Annual Review of Fluid Mechanics*, 30(1), 53-84.

Cox, J.C. and Clark, G.R. (1992). Design development of a tandem breakwater system for Hammond Indiana. In Coastal structures and breakwaters: *Proceedings of Institution of Civil Engineers*, London, 6-8 November 1991, pp. 111-121.

Dalrymple, R.A., Losada, M.A. and Martin, P.A. (1991). Reflection and transmission from porous structures under oblique wave attack. *Journal of Fluid Mechanics*, 224, 625-644.

Das, S. and Bora, S.N. (2014a). Reflection of oblique ocean water waves by a vertical porous structure placed on a multi-step impermeable bottom. *Applied Ocean Research*, 47, 373-385.

Das, S. and Bora, S.N. (2014b). Wave damping by a vertical porous structure placed near and away from a rigid vertical wall. *Geophysical and Astrophysical Fluid Dynamics*, 108(2), 147-167.

Das, S. and Bora, S.N. (2014c). Reflection of oblique ocean water waves by a vertical rectangular porous structure placed on an elevated horizontal bottom. *Ocean Engineering*, 82, 135-143.

Das, S. and Bora, S.N. (2014d). Damping of oblique ocean waves by a vertical porous structure placed on a multi-step bottom. *Journal of Marine Science and Application*, 13(4), 362-376.

Dattatri, J., Raman, H. and Shankar, N.J. (1978). Performance characteristics of submerged breakwaters. *Coastal Engineering Proceedings*, 2153-2171.

Davies, A.G. (1982). The reflection of wave energy by undulations on the sea bed. *Dynamics of Atmospheres and Oceans*, 6, 207-232.

Elchahal, G., Younes, R. and Lafon, P. (2008). The effects of reflection coefficient of the harbour sidewall on the performance of floating breakwaters. *Ocean Engineering*, 35(11), 1102-1112.

Essoglou, M., Seymour, D. and Berkley, J. (1975). TFB: A transportable open ocean breakwater. *OCEAN 75 Conference*, IEEE, 723-725.

Fang, Z., Xiao, L., Kou, Y. and Li, J. (2018). Experimental study of the wave-dissipating performance of a four-layer horizontal porous-plate breakwater. *Ocean Engineering*, 151, 222-233.

Franco, L. (1994). Vertical breakwaters: the Italian experience. *Coastal Engineering*, 22(1-2), 31-55.



- 
- Goda, Y. and Suzuki, Y. (1977). Estimation of incident and reflected waves in random wave experiments. *Proceedings of 15<sup>th</sup> International conference on Coastal Engineering*, 828-845.
- Hu, J., Zhao, Y. and Liu, P. L. F. (2019). A model for obliquely incident wave interacting with a multi-layered object. *Applied Ocean Research*, 87, 211-222.
- Huang, B. L. and Wang, S. C. (2017). Wave attenuation mechanism of cross-plates applied in landslide-induced tsunami in river course. *Journal of Mountain Science*, 14(4), 649-661.
- Huang, Z., Li, Y. and Liu, Y. (2011). Hydraulic performance and wave loadings of perforated/slotted coastal structures: A review. *Ocean Engineering*, 38(10), 1031-1053.
- Isaacson, M., Baldwin, J., Allyn, N. and Cowdell, S. (2000). Wave interactions with perforated breakwater. *Journal of Waterway, Port, Coastal, and Ocean Engineering*, 126(5), 229-235.
- Isaacson, M. and Byres, R. (1988). Floating breakwater response to wave action. *Coastal Engineering Proceedings*, 2189-2200.
- Isaacson, M., and Qu, S. (1990). Waves in a harbour with partially reflecting boundaries. *Coastal Engineering*, 14(3), 193-214.
- Kaligatla, R.B., Manisha and Sahoo, T. (2017). Wave trapping by dual porous barriers near a wall in the presence of bottom undulation. *Journal of Marine Science and Application*, 16(3), 286-297.
- Kaligatla, R.B., Prasad, N.M. and Tabssum, S. (2019). Oblique interaction between water waves and a partially submerged rectangular breakwater. *Proceedings of the Institution of Mechanical Engineers, Part M: Journal of Engineering for the Maritime Environment*. 234(1), 154-169.
- Kaligatla, R.B., Tabssum, S. and Sahoo, T. (2018). Effect of bottom topography on wave scattering by multiple porous barriers. *Meccanica*, 53(4-5), 887-903.
- Karmakar, D., Bhattacharjee, J. and Guedes Soares, C. (2013). Scattering of gravity waves by multiple surface-piercing floating membrane. *Applied Ocean Research*, 39, 40-52.
- Karmakar, D. and Guedes Soares, C. (2014). Wave transformation due to multiple bottom-standing porous barriers. *Ocean Engineering*, 80, 50-63.
- Karmakar, D. and Guedes Soares, C. (2015). Propagation of gravity waves past multiple bottom-standing barriers. *Journal of Offshore Mechanics and Arctic Engineering*, 137(1), 011101-10.
-

Kharaghani, S. and Lee, J. J. (1986). Wave interaction with moored sloping breakwater. *Coastal Engineering Proceedings*, 2559-2568.

Kim, M. H. and Kee, S. T. (1996). Flexible-membrane wave barrier. I: Analytic and numerical solutions. *Journal of Waterway, Port, Coastal, and Ocean Engineering*, 122(1), 46-53.

Koley, S., Behera, H. and Sahoo, T. (2015). Oblique wave trapping by porous structures near a wall. *Journal of Engineering Mechanics*, 141(3), 04014122.

Koley, S., Kaligatla, R. B. and Sahoo, T. (2014). Oblique wave scattering by a vertical flexible porous plate. *Studies in Applied Mathematics*, 135(1), 1-34.

Koley, S. and Sahoo, T. (2017). Wave interaction with a submerged semi-circular porous breakwater placed on a porous seabed. *Engineering Analysis with Boundary Elements*, 80, 18-37.

Kondo, H. and Toma, S. (1972). Reflection and transmission for a porous structure. *Coastal Engineering Proceedings*, 1847-1866.

Le Méhauté, B. (1972). Progressive wave absorber. *Journal of Hydraulic Research*, 10(2), 153-169.

Li, A.J., Li, H.J. and Liu, Y. (2019). Analytical study of oblique wave scattering by a submerged pile–rock breakwater. *IMechE Part M: Journal of Engineering for the Maritime Environment*, 233(1), 41-54.

Lin, Q., Meng, Q.R. and Lu, D.Q. (2018). Waves propagating over a two-layer porous barrier on a seabed. *Journal of Hydrodynamics*, 30(3), 453-462.

Liu, Y. and Li, H.J. (2013). Analysis of oblique wave interaction with a submerged perforated semi-circular breakwater. *Journal of Engineering Mathematics*, 83(1), 23-36.

Liu, Y. and Li, H.J. (2013). Wave reflection and transmission by porous breakwaters: A new analytical solution. *Coastal Engineering*, 78, 46-52.

Liu, Y. and Li, H.J. (2014). Analysis of wave performance through pile–rock breakwaters. *Proceedings of the Institution of Mechanical Engineers, Part M: Journal of Engineering for the Maritime Environment*, 228(3), 284-292.

Liu, Y., Li, Y. and Teng, B. (2007). Wave interaction with a new type perforated breakwater. *Acta Mechanica Sinica*, 23(4), 351-358.

Liu, Y., Li, Y. C. and Teng, B. (2012). Interaction between obliquely incident waves and an infinite array of multi-chamber perforated caissons. *Journal of Engineering Mathematics*, 74(1), 1-18.

- 
- Liu, Y., Li, H.J. and Zhu, L. (2016). Bragg reflection of water waves by multiple submerged semi-circular breakwaters. *Applied Ocean Research*, 56, 67-78.
- Losada, I. J., Losada, M. A. and Baquerizo, A. (1993). An analytical method to evaluate the efficiency of porous screens as wave dampers. *Applied Ocean Research*, 15(4), 207-215.
- Losada, I.J., Silva, R. and Losada, M.A. (1996). 3-D non-breaking regular wave interaction with submerged breakwaters. *Coastal Engineering*, 28(1-4), 229-248.
- Madsen, P.A. (1983). Wave reflection from a vertical permeable wave absorber. *Coastal Engineering*, 7(4), 381-396.
- Mallayachari, V. and Sundar, V. (1994). Reflection characteristics of permeable seawalls. *Coastal Engineering*, 23(1-2), 135-150.
- Mani, J.S. (2009). Experimental and numerical investigations on zigzag porous screen breakwater. *Natural Hazards*, 49, 401–409.
- Manisha, Kaligatla, R.B. and Sahoo, T. (2019). Effect of bottom undulation for mitigating wave-induced forces on a floating bridge. *Wave Motion*, 89, 166-184.
- Mendez, F.J. and Losada, I.J. (2004). A perturbation method to solve dispersion equations for water waves over dissipative media. *Coastal Engineering*, 51(1), 81-89.
- Milgram, J.H. (1970). Active water-wave absorbers. *Journal of Fluid Mechanics*, 42(4), 845-859.
- Murakami, H., Itoh, S., Hosoi, Y. and Sawamura, Y. (1994). Wave induced flow around submerged sloping plates. *Coastal Engineering Proceedings*, 1454-1468.
- Nallayarasu, S., Cheong, H. F. and Shankar, N. J. (1994). Wave induced pressures and forces on a fixed submerged inclined plate. *Finite Elements in Analysis and Design*, 18(1-3), 289-299.
- Neelamani, S., Al-Salem, K. and Taqi, A. (2017). Experimental investigation on wave reflection characteristics of slotted vertical barriers with an impermeable back wall in random wave fields. *Journal of Waterway, Port, Coastal, and Ocean Engineering*, 143(4), 06017002-1-10.
- Newman, J.N. (1965a). Propagation of water waves past long two-dimensional obstacles. *Journal of Fluid Mechanics*, 23 (1) 23 - 29.
- Newman, J.N. (1965b). Propagation of water waves over an infinite step. *Journal of Fluid Mechanics*, 23 (2) 399 - 415.
- Patrick, D. A. (1951). Model study of amphibious breakwaters. *California Univ Berkeley Inst of Engineering Research*.
-

Pontoon Breakwater (1948), U.S Navy Civil Engineer Corps Bulletin, Vol. 2, No. 14 , 10-13.

Praveen, K.M., Karmakar, D. and Guedes Soares, C. (2020). Wave interaction with floating elastic plate based on the timoshenko–mindlin plate theory. *Journal of Offshore Mechanics and Arctic Engineering*, 142(1), 011601-1-15.

Rajendra, K., Balaji, R. and Mukul, P. (2017). Review on Indian research on innovative breakwaters. *Indian Journal of Geo Marine Sciences*, 46(3), 431-452.

Ramakrishnan, B. (2011). Characteristics of wave oscillations between two porous barriers. *ISH Journal of Hydraulic Engineering*, 17(2), 50-61.

Rambabu, C.A. and Mani, J.S (2005). Numerical prediction of performance of submerged breakwaters. *Ocean Engineering*. 32, 1235–1246.

Reddy, M.G. and Neelamani, S. (2004). Hydrodynamic studies on vertical seawall defended by low-crested breakwater. *Ocean Engineering*, 32, 747–64.

Rojanakamthorn, S., Isobe, M. and Watanabe, A. (1989). A mathematical model of wave transformation over a submerged breakwater. *Coastal Engineering in Japan*, 32(2), 209-234.

Sahoo, T., Lee, M.M. and Chwang, A.T. (2000). Trapping and generation of waves by vertical porous structures. *Journal of Engineering Mechanics*, 126(10), 1074-1082.

Sankarbabu, K., Sannasiraj, S.A. and Sundar, V. (2007). Interaction of regular waves with a group of dual porous circular cylinders. *Applied Ocean Research*, 29(4), 180-190.

Sankarbabu, K., Sannasiraj, S.A. and Sundar, V. (2008). Hydrodynamic performance of a dual cylindrical caisson breakwater. *Coastal Engineering*, 55(6), 431-446.

Sollitt, C.K. and Cross, R.H. (1972). Wave transmission through permeable breakwaters. *Coastal Engineering Proceeding*, 1827-1846.

Somervell, L.T., Thampi, S.G. and Shashikala, A.P. (2017). A novel approach for the optimal design of a vertical cellular breakwater based on multi-objective optimization. *Coastal Engineering Journal*, 59(04), 1750019.

Stoker J.J. (1958). “Water waves.” New York: Interscience.

Suh, K.D., Kim, Y.W. and Ji, C.H. (2011). An empirical formula for friction coefficient of a perforated wall with vertical slits. *Coastal Engineering*, 58(1), 85-93.

Sulisz, W. (1985). Wave reflection and transmission at permeable breakwaters of arbitrary cross-section. *Coastal Engineering*, 9(4), 371-386.

- 
- Ting, F.C. and Kim, Y.K. (1994). Vortex generation in water waves propagating over a submerged obstacle. *Coastal Engineering*, 24(1-2), 23-49.
- Twu, S.W. and Chieu, C.C. (2000). A highly wave dissipation offshore breakwater. *Ocean Engineering*, 27(3), 315-330.
- Twu, S.W. and Lin, D.T. (1990). Wave reflection by a number of thin porous plates fixed in a semi-infinitely long flume. *Coastal Engineering Proceedings*, 1046-1059.
- Twu, S.W. and Liu, C.C. (2004). Interaction of non-breaking regular waves with a periodic array of artificial porous bars. *Coastal Engineering*, 51(3), 223-236.
- Twu, S.W., Liu, C.C. and Hsu, W.H. (2001). Wave damping characteristics of deeply submerged breakwaters. *Journal of Waterway, Port, Coastal, and Ocean Engineering*, 127(2), 97-105.
- Twu, S.W., Liu, C.C. and Twu, C.W. (2002). Wave damping characteristics of vertically stratified porous structures under oblique wave action. *Ocean Engineering*, 29(11), 1295-1311.
- Vijay, K.G. and Sahoo, T. (2019). Scattering of surface gravity waves by a pair of floating porous boxes. *Journal of Offshore Mechanics and Arctic Engineering*, 141(5), 051803-1-10.
- Vijay, K.G., Neelamani, S. and Sahoo, T. (2019). Wave interaction with multiple slotted barriers inside harbour: Physical and numerical modelling. *Ocean Engineering*, 1-10.
- Vijay, K.G., Sahoo, T. and Datta, R. (2020). Wave-induced responses of a floating structure near a wall in the presence of permeable plates. *Coastal Engineering Journal*, 62(1), 35-52.
- Wang, Y., Wang, G. and Li, G. (2006). Experimental study on the performance of the multiple-layer breakwater. *Ocean Engineering*, 33(13), 1829-1839.
- Yip, T. L., Sahoo, T., and Chwang, A.T. (2002). Trapping of surface waves by porous and flexible structures. *Wave Motion*, 35(1), 41-54.
- Yu, X. (1995). Diffraction of water waves by porous breakwaters. *Journal of Waterway, Port, Coastal, and Ocean Engineering*, 121(6), 275-282.
- Yu, X. and Chwang, A.T. (1994). Wave motion through porous structures. *Journal of Engineering Mechanics*, 120(5), 989-1008.
- Zhao, Y., Li, H.J. and Liu, Y. (2017). Oblique wave scattering by a submerged porous breakwater with a partially reflecting sidewall. *Journal of Marine Science and Technology*, 25(4), 383-392.

Zhao, Y., Liu, H.J. Li and Chang, A. (2017). Oblique wave motion over multiple submerged porous bars near a vertical wall. *Journal of Ocean University of China*, 16(4), 568-574.

Zhu, S. and Chwang, A. T. (2001). Analytical study of porous wave absorber. *Journal of Engineering Mechanics*, 127(4), 326-332.

Zhu, S. (2001). Water waves within a porous medium on an undulating bed. *Coastal Engineering*, 42(1), 87-101.

## AUTHOR'S RESUME

Name: Valliboina Venkateswarlu

Ph.D. Research Scholar

Department of Water Resources and Ocean Engineering,  
National Institute of Technology Karnataka, Surathkal,  
Mangalore – 575025.

Contact No: +91 807 457 77 95 and +91 850 001 84 00

Email ID: venki.venkat117@gmail.com



The author was born on 7<sup>th</sup> June, 1992 in Nellore District, Andhra Pradesh, India. Having passed Board of Secondary Education from Z.P.P. High School, Atmakur West, Andhra Pradesh in 2007 and completed intermediate from Sri Siddardha Junior College, Buchireddy Palem, Nellore, Andhra Pradesh in 2009, he graduated with Bachelor in Civil Engineering from G. Pulla Reddy Engineering College, Sri Krishna Devaraya University, Kurnool in 2013. Thereafter, he obtained Masters in Hydraulic and Water Resources specialization from Sri Venkateswara University College of Engineering, S V University, Tirupati in 2016. After completing his master's degree, he joined the doctoral research programme in the Department of Applied Mechanics and Hydraulics, National Institute of Technology, Karnataka, Surathkal in the year 2016. The author's interest lies in the field of porous media flow and wave structure interaction. During the period of his research, he communicated and published his work in various reputed international journals and conference proceedings. The detail list of publications are presented below:

### (a) List of publications in Journals:

1. **V. Venkateswarlu** and D. Karmakar, (2019). Wave scattering by vertical porous block placed over flat and elevated seabed. *Marine Systems and Ocean Technology*, 14(2-3), 85-109, Springer, (Scopus indexed Journal). DOI: [10.1007/s40868-019-00058-z](https://doi.org/10.1007/s40868-019-00058-z)
2. **V. Venkateswarlu** and D. Karmakar, (2019). Numerical investigation on the wave dissipating performance due to multiple porous structures. *ISH Journal of Hydraulic Engineering*, 1-18, Taylor and Francis, (Scopus indexed Journal). DOI: [10.1080/09715010.2019.1615393](https://doi.org/10.1080/09715010.2019.1615393)
3. **V. Venkateswarlu** and D. Karmakar, (2020). Influence of impermeable elevated bottom on the wave scattering due to multiple porous structures. *Journal of Applied Fluid Mechanics*, 13(1), 371-385. (Scopus and SCIE indexed Journal, IF = 0.918). DOI: [10.29252/jafm.13.01.29890](https://doi.org/10.29252/jafm.13.01.29890)

4. **V. Venkateswarlu** and D. Karmakar, (2020). “Significance of seabed characteristics on wave transformation in the presence of stratified porous block”. *Coastal Engineering Journal*, Taylor and Francis, (Scopus and SCIE indexed Journal, IF = 2.016). DOI: [10.1080/21664250.2019.1676366](https://doi.org/10.1080/21664250.2019.1676366)
5. **V. Venkateswarlu** and D. Karmakar, (2020). “Wave transport through barrier-rock porous structures placed on step-bottom”, *Ships and Offshore structures*, Taylor and Francis, (Scopus and SCIE indexed Journal, IF = 1.763). DOI: [10.1080/17445302.2019.1694296](https://doi.org/10.1080/17445302.2019.1694296)
6. **V. Venkateswarlu** and D. Karmakar, (2020). “Wave motion over stratified porous absorber combined with seaward vertical barrier”. *Proceedings of the Institution of Mechanical Engineers, Part M: Journal for Engineering and Maritime Environment*, SAGE Publications, DOI: [10.1177/1475090220912643](https://doi.org/10.1177/1475090220912643) (Accepted for publication), (Scopus and SCIE indexed Journal, IF = 1.241).
7. **V. Venkateswarlu**, K.M. Praveen and D. Karmakar (2019). “Surface gravity wave scattering by multiple energy absorbing structures of variable horizontal porosity”, *Coastal Engineering Journal*, Taylor and Francis, (Scopus and SCIE indexed Journal, IF = 2.016). DOI: [10.1080/21664250.2020.1794274](https://doi.org/10.1080/21664250.2020.1794274)
8. **V. Venkateswarlu** and D. Karmakar, (2020). “Gravity wave trapping by series of horizontally-stratified wave absorbers away from various seawall”, *Journal of Offshore Mechanics and Arctic Engineering*, Transactions of ASME (Scopus and SCIE indexed Journal, IF = 1.186). DOI: [10.1115/1.4047104](https://doi.org/10.1115/1.4047104)
9. K.G. Vijay, **V. Venkateswarlu** and D. Karmakar (2020). Scattering of gravity waves by multiple submerged rubble-mound breakwaters, *Arabian Journal for Science and Engineering*, Springer, (Scopus and SCIE indexed Journal, IF = 1.711). DOI: [10.1007/s13369-020-04767-1](https://doi.org/10.1007/s13369-020-04767-1)
10. **V. Venkateswarlu**, K. M. Praveen, K.G. Vijay and D. Karmakar (2020). “Oblique water wave motion through two-layer barrier-rock breakwater placed on elevated bottom”, *Ships and Offshore structures*, Taylor and Francis, (In first revision).

**(b) List of publications in Book Chapters:**

11. **V. Venkateswarlu** and D. Karmakar (2019). “Wave interaction with multiple submerged porous structures”. *Proceedings of the International Conference on Ocean Engineering*, 265-279, Springer, DOI: [10.1007/978-981-13-3134-3\\_20](https://doi.org/10.1007/978-981-13-3134-3_20) (Scopus indexed).



**(c) List of publications in Conference Proceedings:**

12. V. Venkateswarlu and D. Karmakar (2017). “Wave interaction with submerged rectangular porous structure in the presence of impermeable wall”. 3rd Indian Conference on Applied Mechanics (INCAM 5th – 7th July 2017). MNNIT Allahabad, 449 – 450.
13. V. Venkateswarlu and D. Karmakar (2017). “Gravity wave interaction with multiple submerged porous structures on impermeable multi-step bottom”. International Conference on Theoretical, Applied, Computational and Experimental Mechanics, (ICTACEM 28th - 30th December 2017), IIT Kharagpur.
14. V. Venkateswarlu and D. Karmakar (2018). “Numerical study on the performance of multiple porous structures under oblique wave attack”. 6th Indian National Conference on Coastal Harbour and Ocean Engineering (INCHOE 26th - 28th September 2018), CWPRS Pune, Vol. 1, 446 – 456.
15. V. Venkateswarlu and D. Karmakar (2018). “Wave interaction with multi-layered porous structure in the presence of porous front sea wall”. 6th Indian National Conference on Coastal Harbour and Ocean Engineering (INCHOE 26th – 28th September 2018), CWPRS Pune, Vol. 2: 588 – 598.
16. V. Venkateswarlu, K.M. Praveen and D. Karmakar (2018). “Wave reflection due to the presence of porous structure with stepped seawall”. 7th International and 45th National Conference on Fluid Mechanics and Fluid Power (FMFP 10th - 12th December 2018), IIT Bombay.
17. V. Venkateswarlu, K.R. Athul Krishna and D. Karmakar (2018). “Wave force control on seawall using seaside porous blocks”. Conference on next frontiers in civil engineering, (NFICE 30th Nov – 1st Dec 2018), IIT Bombay.
18. V. Venkateswarlu, K. M. Praveen and D. Karmakar (2019). “Analytical study on the wave trapping performance of horizontal triple-layered porous absorber away from the vertical cliff.” HYDRO-2019, 18th – 20th December 2019, Osmania University, Hyderabad, India.

